Hybrid Seismic Retrofit Systems Using TMD and Soft-first Story Principle

(同調マスダンパーとソフトファーストストーリーを用いた制振改修法に関する研究)

程　春

Abstract

Steel buildings have exhibited considerable response during recent earthquakes. The response was so large that people could directly observe with their naked eyes and take it to video images. In most of the cases the structural damages were very small, but the large response of skeletons had caused lots of non-structural damages and severely influenced the living quality of the buildings. In order to improve this, some measures to reduce the seismic response of the existing steel buildings should be proposed and realized urgently. To this end a new hybrid retrofit system using TMD and Soft-first story principle is proposed and its applicability is investigated in this thesis.

The followings are the main works described in this thesis.

Firstly, the basic theory of optimization methods for TMD was reviewed and some popular optimum methods were summarized and analyzed. An example of traditional TMD was selected and numerically calculated for 60 earthquake waves. Then, a non-traditional TMD was proposed and studied to derive an optimum expression, for two kinds of dampers, viscous damper and friction damper. Finally, the hybrid TMD, which combined with traditional TMD and non-traditional TMD, was proposed.

Secondly, a numerical simulation, including frequency response analysis and earthquake response analysis, has been carried out to explore the dynamic property and vibration mitigation effect of this proposed retrofit system. The parameter variations used for the numerical studies include 6 kinds of number of floors, 5 types of TMD mass ratios, 4 stiffness soften ratios and 9 stiffness harden ratios. The result of frequency response analysis shows that the TMD combined system can reduce the resonance of the structure significantly. Finally, the earthquake response analysis has been carried out using 60 types of earthquake records. The acceleration of the top floor and the drift from the first floor to the top floor were compared to study about the effectiveness.

Then, a shaking table test was carried out to explore the feasibility and effectiveness of the proposed retrofit system. For the shaking table test a three-story steel frame Benchmark model was used, and two kinds of retrofit patterns, TMD1 and TMD2, were applied. With these two patterns, 7 cases of structures were prepared; the original structure, the SFS structure, the SFS_HUS structure, the SFS with TMD 1 structure, the SFS_HUS with TMD 1 structure, the SFS with TMD 2 structure and the SFS_HUS with TMD 2 structure. Each model has been tested by loading of Sweep wave, Whitenoise wave, and other 5 earthquake records.

Furthermore, some practical problems were considered for practical application. First, the effect of additional stiffness due to the TMD was considered and analyzed. Then, the double adjustment procedure was proposed when make use of the additional stiffness. The system robustness has been also considered for various mass ratio and additional stiffness. Finally, an initial displacement method was introduced, which was often considered to obtain more effectiveness especially when the system is mainly subjected to impulse excitations.

Finally, a new vision based method for displacement measuring was proposed and studied. It may be used to the structures with large displacement response such as high-rise building, structures with soft story or isolated story. A shaking table test has been carried out to see the feasibility for obtaining an historical displacement response. Then the theory was applied to a video record from a surveillance camera of the high-rise buildings at Shinjuku during the Great East Japan Earthquake.

In brief, a hybrid seismic retrofit systems using TMD and soft-first story principle is proposed in this thesis in order to reduce the large seismic response of existing steel buildings. Its applicability is investigated through numerical simulations with 6 types of models and a shaking table test using Benchmark model. The results showed that the proposed retrofit system can significantly reduce the response of the original structure especially the acceleration response of the top floor.

Contents

Chapter 1

Introduction

1.1 Background

During the recent big earthquakes (The Hyogoken-Nanbu Earthquake in 1995, Mid Niigata Prefecture Earthquake in 2004, Off the Pacific Coast of Tohoku Earthquake in 2011), there were rarely serious damages such as structure collapse occurred in steel structures. But there were structural damages occurred in low-rise steel structures and lots of damages of non-structural components in medium and low-rise steel structures. A large earthquake response has been considered as a characteristic of steel structures which has also been realized by more and more researchers to be a problem that influences structural safety and people's living quality, especially in earthquake-prone countries such as Japan [1-1]~[1-6] .

1.1.1 Damages of steel structures during past earthquakes

Southern Hyogo Prefecture Earthquake happened on 17th, Jan. 1995 in Japan with magnitude of 7.3. There were over 6,000 innocent people killed and over 40,000 people injured during this earthquake. Civil engineers, researchers were all shocked at the devastation of the earthquake site from TV broadcasting. There were both lots of serious structural damages including collapsed and also non-structural damages including glass fail and decoration broken of steel structures [1-1][1-7] . Among surveyed 993 damaged steel buildings by Committee of Steel Structure of Kinki Branch of Architectural Institute of Japan, there were about 9.1% buildings collapsed ,33.5% buildings suffered a severer damage and 30.2 % buildings had a slight damage such as nonstructural damages [1-8] .

Mid Niigata Prefecture Earthquake happened on 23th Oct. 2004 in Japan with magnitude of 6.8. There were 68 innocent people killed and over 4,000 people injured during this Earthquake. Damages of steel structures were not that so much, but there were still several cases been reported including the damages of steel gymnasiums [1-2].

From the earthquake record of the Great East Japan Earthquake, it could be found that there are mainly two characteristics of the main shock comparing to the recent large earthquakes: 1) Multiple destruction regions could be observed from wave shape; 2) Relatively long duration [1-1][1-4][1-5].

Furthermore, the record at the distant field from epicenter showed that the duration was extremely long, and the long-period motion with natural period of 2.0s~3.5s repeated after the main shock was also reported [1-4][1-5].

Fig. 1.1 shows the damage distribution for different structural heights. An important phenomenon could be found that most of the damages occurred at the top floor of the structure within 60m. Fig. 1.2 shows the relationship of the damage cases and the type of structures. In which, another phenomenon could be found that most of damages happened in steel structures. Furthermore, the most happened damages were about non-structural components, Fig. 1.3 and Fig. 1.4 showed the falling of ceiling and decorating, respectively.

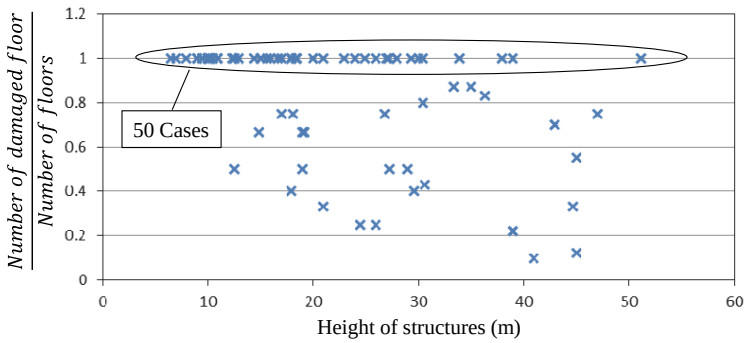

Figure 1.1 Ratio of the number of damaged floor to the number of floors [1-9]

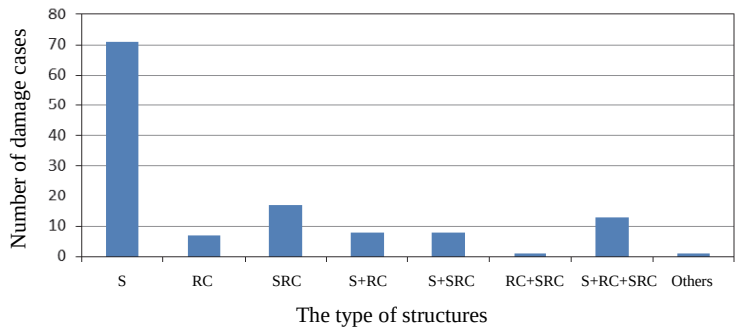

Figure 1.2 The relationship of the damage cases and the type of structures [1-9]

Figure 1.3 The falling of ceilings [1-4]

Figure 1.4 The falling of decorating [1-10]

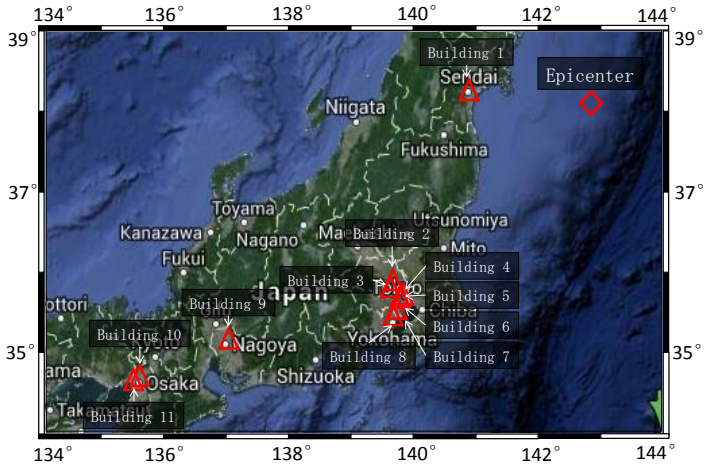

Figure 1.5 The locations of Epicenter and measured buildings
(Modified from google map: https://maps.google.com)

Table 1.1 Earthquake response record (From Reference [1-6])

Name	Building Location	Floors	Distance from Epicenter(km)	Sensor Floors	PGA(gal)	
					X	Y
Building 1	Sendai	15 B2	174	B2F	163	259
				15F	358	346
Building 2	Saitama	27 B3	377	B3F	74	62
				27FS	248	398
				27FC	257	686
Building 3	Tokyo	20 B1	380	B1F	69	66
				20F	385	290
Building 4	Tokyo	21B4	386	B4F	74	71
				21F	121	130
Building 5	Tokyo	20	386	01F	91	83
				20F	209	150
Building 6	Tokyo	8	387	01F	118	—
				08F	277	—
Building 7	Kawasaki	7	401	01F	107	77
				07F	360	303
Building 8	Yokohama	23 B2	411	B2F	60	—
				23F	162	—
Building 9	Nagoya	10	620	01F	18	16
				10F	102	86
Building 10	Osaka	18 B3	758	B3F	11	9
				18F	65	38
Building 11	Osaka	55 B3	769	01F	34	24
				52FN	126	88
				52FS	130	85

There are several buildings in Japan being monitored, the earthquake response would be recorded and opened on the website by Building Research Institute, Independent Administrative Corporation. The locations of Epicenter and measured buildings are showed in Fig. 1.5. The peak acceleration of earthquake response of 11 steel buildings of the main shock from Sendai to Osaka is summarized in Table 1. Where, the information of Building 6 and Building 9 came from reference [1-7] and [1-8]. In Table 1, X and Y direction represents the two structural directions of each building.

There was still damage report even for steel buildings with vibration control devices. For example, the Shinjuku Center Building which has been retrofitted by so called T-RESPO Constitution [1-11] with oil dampers (Fig. 1.6), was reported that it had been vibrated for over 13 minutes and had a large peak displacement response of 1.08m of the top floor [1-12], and even had some nonstructural damages occurred like pipe leaking [1-13].

a) Oil damper

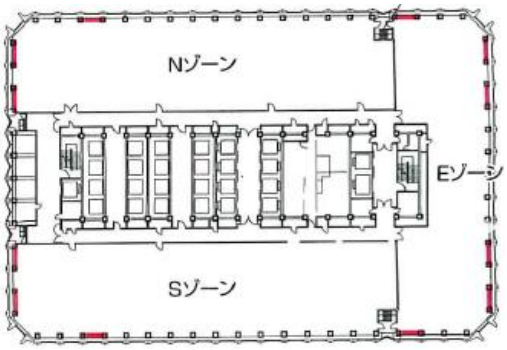

b) Plan view

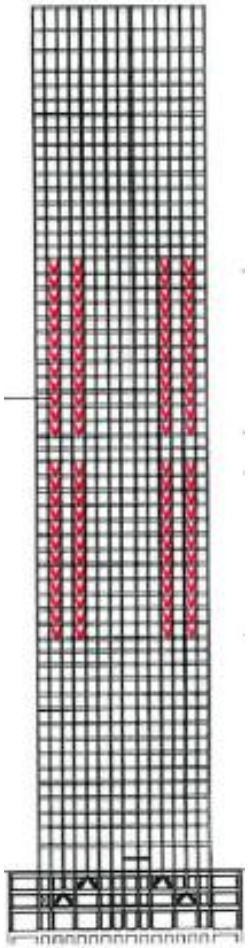

c) Front view

Figure 1.6 Oil damper and its distribution in Shinjuku Center Building [1-11]

1.1.2 Soft-first Story Method

As one of the earliest seismic mitigation methods, the concept of Soft-first story has been proposed since 60s by Fintel and Khan [1-14] by absorbing earthquake energy through the concentrated large deformation at the soft first story. Because of the aesthetic attraction and the advantages of the open first floor, the soft first story is very frequently adopted by urban designers and will still be popular in the foreseeable future [1-15].

A reinforced concrete building built at the Science University of Tokyo in 1981 using the concept of soft first story by double columns method putting steel column into a hollow concrete to keep a space between them. The damper is installed at the top of the concrete column in order to absorb the energy and restrict the displacement of the inner steel column [1-16]. A 12 story building named Union House which is supported at hinged piles is built in Auckland, New Zealand. Damper is placed between the column and the ground to absorb the energy [1-17]. Using the same theory, the Wellington Central Police Station with 10-story is built on hinged piles in New Zealand, and furthermore, upper structures is strengthened by braces [1-18].

In 2000, a 10-story steel building, showed in Fig. 1.7, has been built at Tokyo, Japan by Taisei Corporation whose column is made of high strength steel which can provide a low horizontal stiffness and a high vertical stiffness to let the story deflection angle within linear stage at most 1/100. Oil damper was placed at the first floor to absorb energy using this large deflection of the first floor when the structure suffered wind or earthquake excitations [1-19].

In 2010, a 9-story steel building with 2 floors underground has been built at Shinjuku, Tokyo. The first story has been set as an energy absorption story. Pin connections were used between the column and the ground. An earthquake resisting wall was constructed at the center of the first story; dampers were placed between the wall and the structure. According to the numerical simulation under rare occurrence earthquake, the maximum response of displacement angle of the energy absorbing story is about 1/70, which is still within linear stage, and 1/150 for upper stories. It is emphasized that enough safety margin could be guaranteed for this building with soft-first story. [1-20]

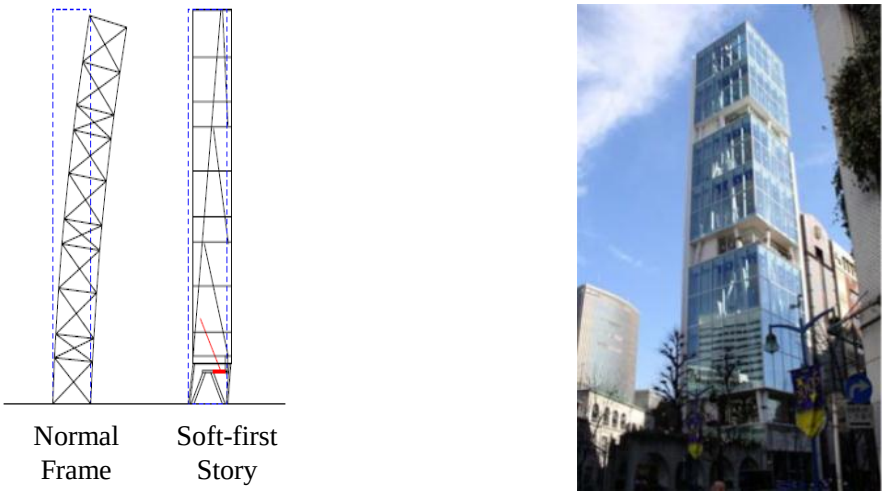

Figure 1.6 Juichikai Building at Ginza, Tokyo, 2000 [1-19]

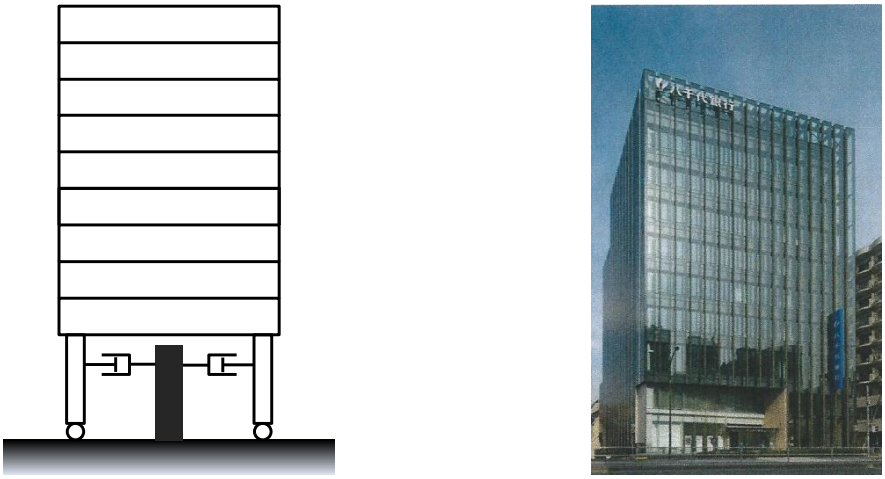

Figure 1.7 Yachiyo Bank at Shinjuku, Tokyo, 2010 [1-20]

With the progress of science and technology, especially the improvement of the damping properties of the dashpot and the mechanical properties of steel, the idea of Soft-first story from early age becomes into reality in nowadays. It is heard that the two buildings mentioned before performed well during the 3.11 Great East Japan Earthquakes. But this kind of system has the disadvantages that the reaction frame or wall is necessary for the connection of the dashpot thus will let the design more complicate.

So, instead of the dashpot, a tuned mass damper (TMD) might be a better choice for this kind of system, which does not need any reaction systems for counter forces and

let the design more free. Furthermore, TMD will be designed to suffer a resonant vibration to absorb more energy thus could have a better vibration mitigation effect [1-21].

1.1.3 Tuned Mass Damper

The concept of the tuned mass damper (TMD) is first proposed by Frahm [1-22], who first obtained the patent of TMD at 1911 which was used to reduce the ship vibration subjected to wave excitation. However, the system he proposed doesn't include a viscous damper which is seemed as one of the three basic components of TMD. The basic concept as to use an attached mass doing resonant vibration instead of the primary mass is the basic theory of TMD.

Tuned mass damper (TMD) basically has three basic components: mass, spring and viscous damper. The TMD, which has three basic components, is attached to a primary structure normally at the top floor. Along with the coefficient of the spring and viscous damper be set to the optimum value, TMD can significantly reduce the resonant vibration of the primary structure as the tuned TMD will resonate instead of the primary structure. Especially, the theory and application of this system for wind and earthquake excited vibration control has been well established so far [1-23]. And it has already been installed in tall buildings and towers to control wind-excited vibrations [1-24]. Such as the Citicorp Center Office Building in New York City [1-25], the Centrepoint Tower in Sydney [1-26], the Chiba Port Tower [1-27] in Japan, the Shanghai World Financial Center in China [1-28], the Taipei 101 Tower in Taiwan [1-29], the Milad Tower in Iran [1-30] and so on. The application of TMD to real structures in Japan is summarized in [1-31], Table 1.2 shows the bridges applied with TMD and Table 1.3 shows the buildings applied with TMD.

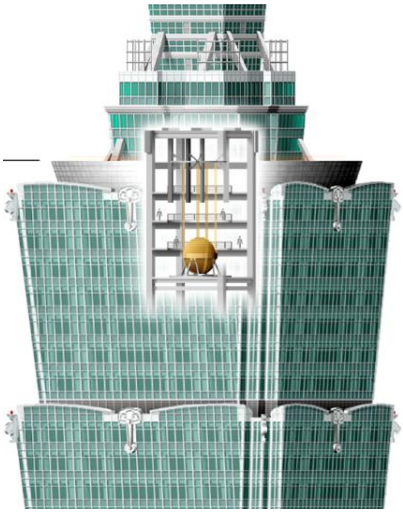

Figure 1.8 TMD in Taipei 101
[http://en.wikipedia.org/wiki/Tuned_mass_damper]

Table 1.2 Bridges applied with TMD in Japan [1-31]

Years	Name	Height(m)	Frequency(Hz)
1980	Chichibu Bridge (秩父橋)	40	―
1985	Meikonishi Bridge (名港西大橋)	122	―
	Aratsu Bridge (荒津大橋)	60	―
	Hituishijima Bridge (櫃石島橋)	139	0.75
	Iwakurojima Bridge (岩黒島橋)	148	―
1990	Bannaguro Bridge (花畔大橋)	45	―
	Higashikoube Bridge (東神戸大橋)	147	0.256
	Sun Bridge (サンブリッジ)	―	―
	Yokohamabei Bridge (横浜ベイブリッジ)	172	―
	Yuge Bridge (弓削大橋)	―	0.584
1995	Okutama Bridge (奥多摩大橋)	―	0.595
	Tsurumikoro Bridge (鶴見航路橋)	180	0.76

Table 1.3 Buildings and Towers applied with TMD in Japan [1-31]

Name	No. of floors	Height (m)	Completion Year
MHS Building	8	26.8	1988
Higashiyama Sky Tower	7	134.0	1989
Fukuoka Tower	5	148.1	1989
Huis Ten Bosch Dome Thorn	5	85.55	1992
P&G Technical Center of Japan Branch	31	131.4	1993
Akida Port Tower	5	109.7	1994
Kofuku Building	9	—	—
Hakada Sea Hork	36	—	—
Ebisu Building of Ishizai Shop	9	—	—
Zai Kaihatu Building	24	—	—
Sendai AER	33	—	—
Edogawaku Prospects Tower	11	—	—
Fukushima Keikaku Kyotu Building	24	—	—
Ashiya Prospects Tower	5	—	—
Umeda DT Tower	27	—	—

1.2 Proposal of Hybrid Seismic Retrofit Systems

In the previous section, it is clearly presented that most of damages happened in steel buildings especially within the height of 60m during Great East Japan Earthquake. And most of those damages were about non-structural components and occurred at the top floor. This large earthquake response at the top floor influences structural safety and people's living quality, especially in earthquake-prone countries such as Japan.

In order to reduce the large earthquake response especially at the top floor for existing steel buildings, a retrofit method which has a low cost, is easy to construction and has a good effectiveness is preferred (Fig.1.9). Among some retrofit methods, such as structural strength reinforcement method, which has a low cost and is easy to construction but doesn't have a good effectiveness to reduce the earthquake response such as acceleration, velocity of the top floor, base isolation method, which has a good effectiveness but its cost is high and hard to construction, passive control is seemed has all these three requirements.

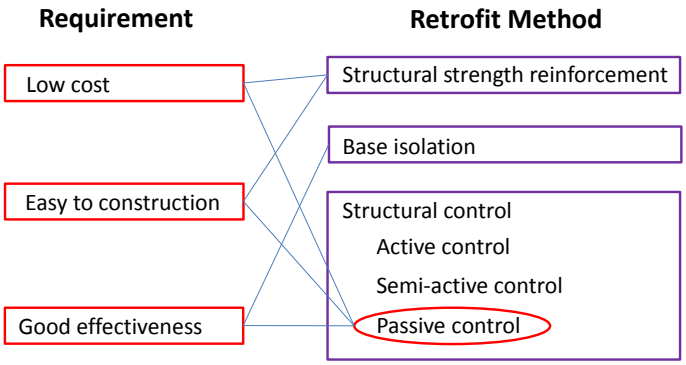

Figure 1.9 Consideration among retrofit methods

Two methods in structural passive control, Soft-first story and Tuned mass damper, is chosen to be combined as a new retrofit method which is proposed in this thesis. As we known, soft first story is vulnerable to P-δ effect, the restriction of the displacement of the first story should be considered. Normally, viscous damper is adopted as the energy absorber placed at the first floor. But this kind of system needs a reaction frame to support the damper, and also the cost of damper is high and the design is not easy [1-32].

On the other hand, base isolated structure, which is the extreme case of the soft-first story, has been applied very frequently, especially in medium and low-rise buildings because of the good seismic mitigation effect. But when the base isolated structure suffered from a big earthquake, the isolation bearing should provide a large horizontal displacement without reducing its vertical capacity. Because using better bearing materials or installing viscous dampers into the isolation floor will increase the cost quickly, Melkumyan supposed a new system which adopted Tuned Mass Damper (TMD) to reduce the displacement for the base isolated structures [1-33][1-34] .

Based on the previous statement, we proposed a hybrid retrofit system (Fig. 1.10) used for existing steel structures which adopt TMD as the energy absorber at the soft-first story. TMD, which is composed by three components, mass, spring and viscous damper, is easy to design and install at a low cost. TMD is normally placed at the top of the structure, at which the equivalent mass is small, to obtain a large mass ratio in order to play the best effect. Although, the equivalent mass at the first floor is bigger than the top floor, it can be reduced by reducing the horizontal stiffness of the first floor. Furthermore, in order to ensure safety of the soft story which is vulnerable to P-δ effect,

the TMD mass will be supported from ground which will not add mass gravity to the column of primary system.

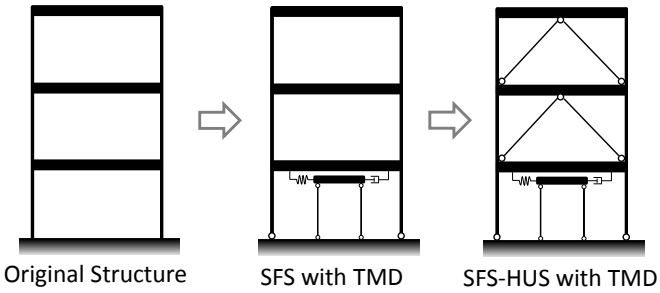

a) Using pin connections

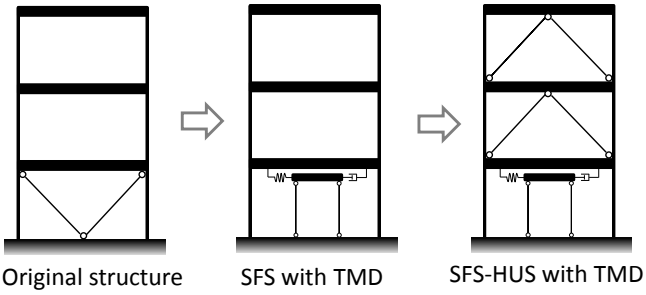

b) Taking off braces

Figure 1.10 The concept of the proposed seismic retrofit systems

Once the TMD mass can be supported from ground, there is no need to retrofit the column of primary structure, and also a relatively large mass ratio could be realized. The seismic mitigation effect of proposed system is expected because of the increased mass ratio by reducing the horizontal stiffness of the first floor and adopting a relatively large TMD mass.

In the following studies to validate the effectiveness of this proposed hybrid seismic retrofit method in Chapter 4 and 5, the acceleration and velocity response of the top floor, the drift from the first floor to the top floor are adopted as the effect index of response reduction. And the displacement response of the first floor is taken into limitation consideration.

1.3 Objective and Approach

From the previous statement, we know that steel buildings experienced larger responses during earthquakes, even if there were rarely structural damages, but the

large responses had caused lots of non-structural damages and severely influenced the living quality of the buildings. The work to reduce the seismic response of the existing steel buildings has been realized necessary and urgently.

But the existing structural retrofit method has problems as follows

1) A normal structural resistant reinforcement method could improve the strength of the structure, but could not obtain a good effectiveness on vibration reducing.
2) The active structural control method, such as adding AMD could improve the structural anti-seismic capabilities significantly, but it costs a lot and has a low reliability.
3) The normal structural passive control, such as adding dashpot into some stories, could improve the structural anti-seismic ability, but it still costs much and its design is complicate, and sometimes needs to retrofit the structural components.

The main purpose of this thesis is, firstly, to propose the hybrid seismic retrofit system for medium and low-rise existing steel buildings in order to solve the problems above. Secondly, propose the hybrid TMD which is suitable to be applied on the proposed hybrid seismic retrofit system. And finally, find an optimum design strategy for the hybrid TMD and explore the dynamic properties and vibration mitigation effectiveness of this proposed hybrid seismic retrofit systems.

In order to achieve these, there are mainly three parts of work has been done in this thesis. Firstly, the basic theory of optimization methods for TMD was studied and some popular optimum methods were summarized and analyzed. The Fixed point method has been considered suitable for the TMD subjected to seismic excitations. Then, a hybrid TMD was proposed, which makes the TMD at the first floor be more realistic. Secondly, a numerical simulation, including frequency response analysis and earthquake response analysis, has been carried out to explore the dynamic property and vibration mitigation effect of this proposed retrofit system. Finally, a shaking table test was complemented to explore the feasibility and effectiveness of the proposed retrofit system.

1.4 Overview of This Thesis

Chapter 2 describes the concept of this proposed seismic retrofit system using TMD and soft-first story principle. It has been demonstrated theoretically that, the softening of the lateral stiffness of the first floor and the hardening of the upper floors could enlarge the TMD virtual mass ratio, using a 2DOF shearing model. Then, the basic approach was discussed for soften the stiffness of the first floor and harden the stiffness of the upper floor.

Chapter 3 mainly discussed the various optimization methods and various types of TMD. Some popular optimization methods were summarized here, and one of them has been chosen for the using when subjected to seismic excitations through a comparison analysis using 60 earthquake waves. Then, a non-traditional TMD is studied here, and the optimum expression has been deduced when subjected to ground acceleration excitations for two kinds of combinations with viscous damper and friction damper. Finally, a hybrid TMD which combined with traditional TMD and non-traditional TMD was proposed here, and it is considered appropriate for the proposed system.

Chapter 4 illustrates the dynamic properties and effectiveness of the proposed retrofit system through numerical simulations. The changing parameters of the numerical model include 6 kinds of number of floors, 5 types of TMD mass ratios, 4 stiffness soften ratios and 9 stiffness harden ratios. The result of frequency response analysis shows that the TMD combined system can reduce the resonant vibrations significantly. Finally, the earthquake response analysis has been carried out using 60 earthquake records. The acceleration of the top floor and the drift from the first floor to the top floor has been taken into the effectiveness comparison.

Chapter 5 describes a shaking table test applying with the proposed retrofit system. A three-story steel frame Benchmark model was used, and two kinds of retrofit patterns were considered. Each pattern has 7 kinds of structures, the original structure, the SFS structure, the SFS_HUS structure, the SFS with TMD 1 structure, the SFS_HUS with TMD 1 structure, the SFS with TMD 2 structure and the SFS_HUS with TMD 2 structure. And each model has been tested by loading of Sweep wave, Whitenoise wave, and other 5 earthquake records.

Chapter 6 considered some practical problems when it is applied for a real use. First, the additional stiffness from the TMD supporting frame has been considered and analyzed. Then, a Double adjustment method is proposed when make use of the additional stiffness. The system robustness has been introduced with various mass ratio and additional stiffness. Finally, an initial displacement method is introduced which is considered to be more effective especially when subjected to impulse excitations.

Chapter 7 describes a new vision based method for displacement measuring which could be used in the earthquake field. It is appropriate to structures with large displacement response such as high-rise building, structures with soft story or isolated story. A shaking table test has been carried out to test the feasibility for obtaining an historical displacement response. Finally, an application has been implemented into a video from a surveillance camera which recorded the response of the high-rise buildings at Shinjuku during the Great East Japan Earthquake.

Finally, Chapter 8 describes the main conclusions of this thesis and the future work of the proposed retrofit system.

Chapter 2

Introduction of the Proposed Hybrid Seismic Retrofit Systems

2.1 Background

As mentioned before, in order to decrease the large response of existing steel structures, we proposed a new hybrid retrofit system which adopted Tuned Mass Damper (TMD) and soft-first story principle.

For the promotion of seismic resistant capacity of existing structures, there are mainly two methods including structural strength reinforcement and structural control. While structural control is considered has a better earthquake resisting performance, and it is also easier to be applied as a retrofit method for the less influence to the existing structures, which also has variant types, such as active control, passive control, semi-active control, etc. Among these, passive control is widely considered has a high cost performance [2-1].

Based on these advantages, to adopt passive control as the retrofit method would be a good choice for both considering cost and performance. Furthermore, structural passive control basically has two groups including base isolation and energy dissipation strategy, such as tuned mass damper, displacement dependence damper or velocity dependence damper, etc. While, base isolation is considered as the most effective one, however, it is also almost the most expensive one among passive control methods [2-2].

Tuned mass damper has been pointed out that has a better effective than other kinds of

dampers and also is easier to be installed with a lower cost [2-3]. However, the effect of TMD is directly related to the mass ratio, when the mass ratio of TMD is larger, a better effect could be obtained. It is known that TMD placed at the top floor could obtained a best vibration control performance because of the virtual mass ratio is bigger than the case if it is placed at the under floors. Note that, virtual mass ratio is defined as the ratio of TMD mass to the equivalent mass of the controlled mode (normally the fundamental mode) when TMD is applied to MDOF primary structure. But a large TMD mass will also increase the burden of the column of the existing structures especially for a structure with low redundancy. So, we supposed to place TMD mass to the ground floor to avoid this problem as showed in Fig. 2.1.

Once the TMD mass be supported from ground, there is no need to strengthen the column of primary structure, and also a relatively large TMD mass could be realized. In order to keep the effective of TMD when it is placed at the ground floor, we supposed to decrease the horizontal stiffness of the first floor to make the structure be a soft-first story structure. When the horizontal stiffness was reduced, the virtual mass ratio will increase and this is the reason for the improving of the TMD effect using soft-first story principle. Furthermore, the effect could be even more improved by increasing the horizontal stiffness of the upper floors. Which is considered be effective for reducing the drift of the first floor to the top floor.

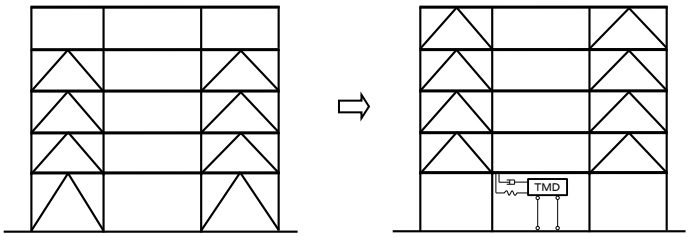

Figure 2.1 Concept of proposed seismic retrofit systems

The seismic mitigation effect of proposed system is expected because of the increased mass ratio by reducing the horizontal stiffness of the first floor, increasing the horizontal stiffness of the upper floor and adopting a relatively large TMD mass.

2.2 The TMD Virtual Mass Ratio

In order to reduce the big seismic response of steel structures, we proposed a hybrid retrofit system used for medium and low rise steel buildings, which adopted Tuned

Mass Damper (TMD) and soft-first story principle. TMD, which is composed by three components, mass, spring and viscous damper, is easy to design and install at a low cost. Because of the TMD effect directly related with the mass ratio, TMD is normally placed at the top of the structure, where the equivalent mass of the system is small, to obtain a large virtual mass ratio.

But here, in order to ensure safety of the soft story which is vulnerable to P-δ effect, the TMD mass is placed at the first floor supported from ground thus will not add mass gravity to the column of primary system. Once the TMD mass can be supported from ground, it is also no need to retrofit the column of primary structure. Although, the equivalent mass of the primary system at the first floor, normally the fundamental mode, is bigger than the top floor, it can be reduced by reducing the horizontal stiffness of the first floor. Furthermore, to adopt a large TMD mass could also directly enlarge the virtual mass ratio.

Since the TMD virtual mass ratio increased by reducing the horizontal stiffness of the first floor and adopting a relatively larger TMD mass, the seismic mitigation effect of proposed system could be expected even if the TMD is placed at the ground floor.

For MDOF primary systems, the TMD virtual mass ratio is defined as Eq. 2.1.

$$\mu = \frac{m_T}{M_i^*} \qquad 2.1$$

Where, m_T means TMD mass; M_i^* means the equivalent mass of *i*th mode which is aimed to be controlled and its obtaining method could be found in the book *Dynamic Vibration Absorbers and its application* written by Seto. K. [2-4]. The detailed derivation process of the formula can be found in Appendix A.

Here, we use a 2DOF primary system, showed in Fig.2.2, to illustrate the virtual TMD mass ratio could be increased indeed through reducing the stiffness of the first floor.

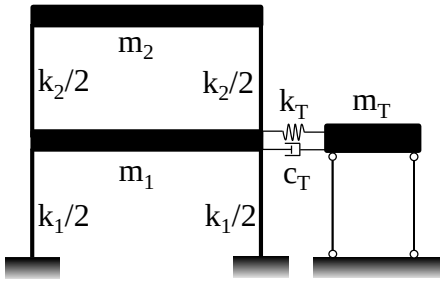

Figure 2.2: 2DOF primary system

The motion equilibrium equation of this 2DOF primary system is showed as follows.

$$\begin{bmatrix} m_1 & \\ & m_2 \end{bmatrix} \begin{Bmatrix} \ddot{x}_1 \\ \ddot{x}_2 \end{Bmatrix} + \begin{bmatrix} k_1 + k_2 & -k_2 \\ -k_2 & k_2 \end{bmatrix} \begin{Bmatrix} x_1 \\ x_2 \end{Bmatrix} = \begin{Bmatrix} 0 \\ 0 \end{Bmatrix} \qquad 2.2$$

The natural circular frequencies could be obtained.

$$\omega_{1,2}{}^2 = \frac{A \mp \sqrt{A^2 - B}}{2m_1 m_2} \qquad 2.3$$

Where, A and B is defined as

$$\begin{aligned} A &= k_1 m_2 + k_2 m_1 + k_2 m_2 \\ B &= 4k_1 k_2 m_1 m_2 \end{aligned} \qquad 2.4$$

The mode shape normalized by dividing the amplitude at the first DOF can be obtained. Note that, the normalization adopted here is suitable for the TMD which placed at the first floor.

$$\Phi_{1,2} = \begin{Bmatrix} 1 \\ 1 \\ \hline 1 - \dfrac{A \mp \sqrt{A^2 - B}}{2k_2 m_1} \end{Bmatrix} \qquad 2.5$$

So, the equivalent mass of the first mode could be obtained as follows

$$M_1{}^* = \Phi_1{}^T M \Phi_1 = m_1 + \frac{m_2}{\left(1 - \frac{A - \sqrt{A^2 - B}}{2k_2 m_1}\right)^2} \qquad 2.6$$

The partial differential of $M_1{}^*$ for k_1 and k_2 could be obtained and whether it is positive or negative is showed here, the detailed deduce process could be found in Appendix A. The partial differential of $M_1{}^*$ for k_1 is positive, so the equivalent mass of fundamental mode is a monotone increasing function of k_1. However, the partial differential of $M_1{}^*$ for k_2 is negative, so the equivalent mass of fundamental mode is a monotone decreasing function of k_1.

$$\frac{\partial \mathrm{M}_1{}^*}{\partial \mathrm{k}_1} > 0 \qquad 2.7$$

$$\frac{\partial \mathrm{M}_1{}^*}{\partial \mathrm{k}_2} < 0 \qquad 2.8$$

Furthermore, if we adopted k_1/k_2 as an independent variable, the partial differential of $M_1{}^*$ for k_1/k_2 could be also obtained, showed in Appendix A. Because it is positive, the equivalent mass of fundamental mode $M_1{}^*$ is also a monotone increasing function of k_1/k_2 .

$$\frac{\partial M_1{}^*}{\partial (\frac{k_1}{k_2})} > 0 \qquad 2.9$$

As mentioned above, the decreasing of k_1, increasing of k_2 or decreasing of the ratio of k_1 to k_2 could decrease the equivalent mass of fundamental mode. Then, we can get the limit of $M_1{}^*$ as $m_1 + m_2$, when the ratio of k_1 to k_2 tends to zero.

$$\lim_{\frac{k_1}{k_2} \to 0} M_1{}^* = m_1 + m_2 \qquad 2.10$$

The virtual mass ratio is defined as the ratio of the TMD mass to the equivalent mass of fundamental mode (usually, we take the fundamental mode as the objective control mode). So, the decreasing of k_1, increasing of k_2 or decreasing of the ratio of k_1 to k_2 could increase the TMD virtual mass ratio. And, similarly, the limit of $M_1{}^*$ could

be obtained as $m_T/(m_1+m_2)$, when the ratio of k_1 to k_2 tends to zero.

$$\mu = \frac{m_T}{{M_1}^*} \tag{2.11}$$

$$\lim_{\frac{k_1}{k_2}\to 0} \mu = \frac{m_T}{m_1+m_2} \tag{2.12}$$

As we know, the vibration control effective of TMD is directly related to the mass ratio. So, the decreasing of k_1, which means decreasing of the horizontal stiffness of the first floor, will increase the TMD effect for proposed system. Similarly, the increasing of k_2, which means the increasing of the horizontal stiffness of the second floor, will also increase the TMD effect for proposed retrofit system.

2.3 Approaches for Stiffness Change

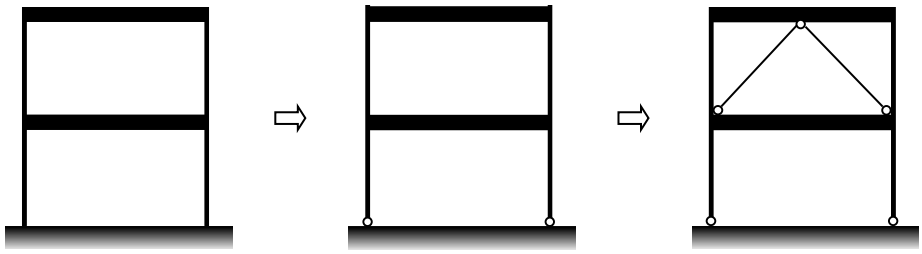

Original frame | SFS (Softened by changing with hinge) | SFS_HUS (Hardened by adding braces)

Figure 2.3 Concept of the method for stiffness changing 1

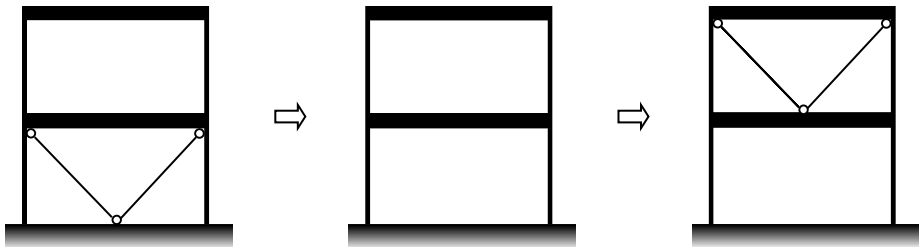

Original braced frame | SFS (Softened by taking off braces) | SFS_HUS (Hardened by adding braces)

Figure 2.4 Concept of the method for stiffness changing 2

In this study, the named ‘Soft-first story (SFS)’ or ‘Hard-upper story (HUS)’ is not an absolute meaning. It means the horizontal stiffness relatively smaller or larger than the

structure before changed.

For example, showed in Fig. 2.3, the horizontal stiffness of the first floor could be reduced by replacing the fixed boundary at the bottom of the column with pinned boundary. As we know, the lateral stiffness of a column with both two ends fixed is $12\mathrm{EI}/l^3$. While, when the fixed one end changed to pinned boundary, its lateral stiffness becomes to $3\mathrm{EI}/l^3$. So, the horizontal stiffness of the Soft-first story of method 1, could be reduced to 25% of the original one.

Normally, the method for stiffen the lateral stiffness of the upper stories is adding braces. It is showed in Fig. 2.5, four types of braced systems. Either of them has the function that can stiffen the lateral stiffness of changed stories [2-5][2-6]. And, it is also pointed out that, the maximum story drifts of moment braced frames are 70% lower than moment resisting frames [2-5]. Here, we assume the lateral stiffness of moment braced frame is 3.3 times stiffer than that of moment resisting frame.

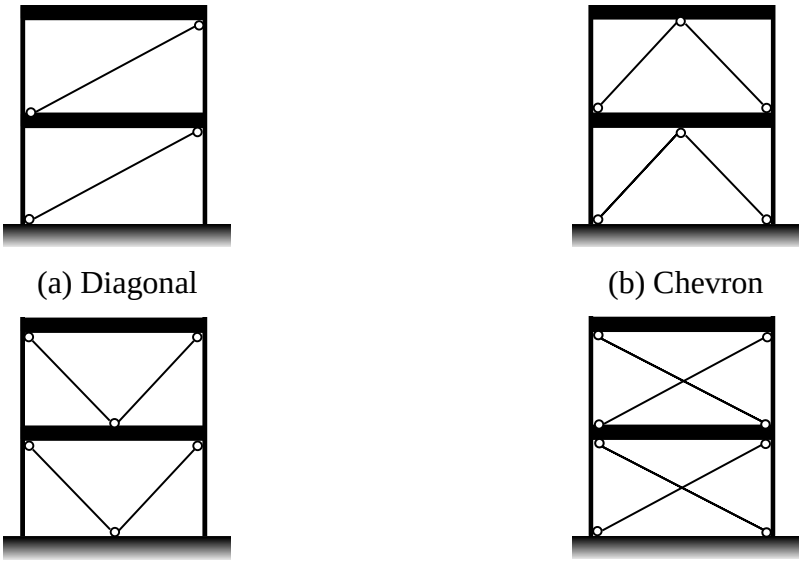

(a) Diagonal (b) Chevron

(c) V-braced (d) X-braced

Figure 2-5 Bracing systems

2.4 Conclusion

In this chapter, first we explained the theoretical rationality of proposed retrofit system using a 2DOF primary system. For a certain TMD mass ratio, the softening of

the lateral stiffness of the first floor or the hardening of the lateral stiffness of the upper floor will increase the virtual mass ratio of the combined system.

Theoretically, when the ratio of the lateral stiffness of the first floor to that of the upper floor decreased, the TMD virtual mass ratio will also increase. As we known that, the seismic control effect of TMD is controlled by the TMD mass ratio, and the above result could demonstrate the rationality of proposed retrofit system.

Then the realization approach for the stiffness change for the existing structures is discussed here. We proposed basically two ways to realize the Soft-first story based on a convenient construction principle.

The first approach is for a non-braced frame structure, a hinge connection can be used to decrease the lateral stiffness of the first floor and adding braces to increase the lateral stiffness of the upper floors.

The second approach is for a braced frame structure, taking off the brace of the first floor will help to setup a relative soft-first story. If there are no brace on the upper floor, then adding braces into the upper floors can increase the lateral stiffness of the upper floors.

Chapter 3

Studies on Tuned Mass Damper

3.1 Introduction

The optimum expression of tuning ratio and damping ratio of TMD was derived firstly by Brock [3-1]. The theory of TMD is detained established in the well-known book written by Den Hartog at 1947 [3-2].

Tuned mass damper (TMD) basically has three basic components: mass, spring and viscous damper. This system can significantly reduce the resonant vibration of the primary structure as the tuned TMD will resonate instead of the primary structure. Especially, the theory and application of this system for wind-excited vibration control has been well established so far [3-3].

Recently, more and more researches have been carried out to explore the effectiveness of the TMD for the vibration control of structural seismic response. Villaverde [3-4] implemented a numerical and experimental study of a 2D 10-story shear building and a 3D cable-stayed bridge. Nine different kinds of earthquake records have been adopted as the ground excitation. The results showed that the vibration mitigation effectiveness were significantly different of different structures under the same earthquake or the same structures under the different earthquakes. The vibration mitigation effectiveness is the best when the predominant frequency of the input wave close to that of the controlled structure. But when the predominant frequency of the input wave is far away from that of structure, the effectiveness will decreased rapidly. Gupta and Chandrasekaren's [3-5] study also showed that TMD is not as effective in reducing the response of structures to seismic excitations as that they are for sinusoidal excitations. Kaynia [3-6] used 48 earthquake waves to explore the

effectiveness of TMD for the vibration control of structural fundamental mode. The result showed that the best effectiveness could be obtained when the tuning ratio equals to 1, and the increasing of the structural period and damping will loss the vibration control effect. Sladek and Klingner [3-7] applied TMD on the top floor of a 25-story structure using the optimum parameters from Den Hartog's method. Two earthquake waves were adopted as the input excitation and the result showed that the TMD was not as effective as expected.

The effectiveness of TMD for seismic excitation was first introduced by Wirsching and Yao [3-8]. Five-story and ten-story structures with 2% damping were adopted as the primary structures. The TMD mass was decided as the half of the mass of a typical floor. The tuning ratios and damping ratio was 1 and 0.2, respectively. Furthermore, a study of three structures with 1, 5, and 10 story, respectively, by Wirsching and Campbell [3-9] showed that TMD were quite effective in reducing the structural response induced by a stationary white noise base acceleration. Dong [3-10] pointed out that the light wing of a structure could reduce its seismic response significantly because it can work as a vibration absorber and the wing itself will have a large response. Ohno [3-11] proposed a method for TMD in order to let the mean square acceleration response be minimized.

Jagadish [3-12] studied a two-story building using the top floor as the vibration absorber with a bilinear material behavior. It is concluded that, up to 50% reduction in the ductility demand could be obtained when the tuning ratio stayed within 0.8~1.0. Sadek [3-13] pointed out that TMD can be effective in controlling the seismic-induced structural vibration. The rest of problem is to find the optimum TMD parameters in order to achieve the best vibration control effectiveness.

In this study, we compared the existing typical optimum method including the Fixed point method, Minimal variance method and Equal damping method for seismic excitation under 60 different earthquake waves. The result shows that the vibration reduction effectiveness of Fixed point method and Minimal variance has not so much difference, but they both are better than Equal damping method.

Then we studied the effectiveness of non-traditional TMD which is barely adopted into a real application because of the unusual damper connection issue. The theoretical and numerical results all showed that the vibration reduction effectiveness

of non-traditional TMD is better than that of traditional TMD. And, the difference of effectiveness will be larger when the mass ratio becomes larger. Then a shaking table test of a SDOF steel frame with and without TMD is carried out to demonstrate the effectiveness of the non-traditional TMD subjected to seismic excitation. The results showed that the earthquake response of with TMD system is smaller than that of without TMD system.

Finally, we proposed a hybrid type of TMD, which combined the concept of traditional TMD and non-traditional TMD, in order to make the design more flexible and more practical. Then we introduced the optimum process of this hybrid TMD. The theoretical result showed that placing the non-traditional type of damping into the traditional TMD will improve the vibration reduction effectiveness.

3.2 Background of TMD Optimization Methods

3.2.1 Fixed point method

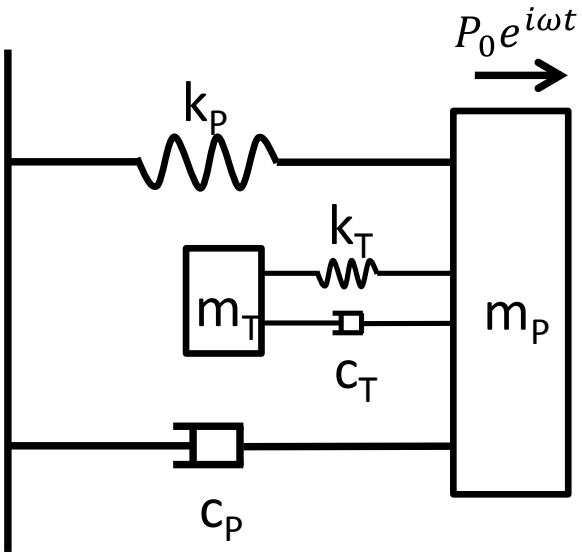

Figure 3.1 TMD system

Showed in Fig. 3.1, TMD is consisted by mass, spring and a viscous damper. TMD, the secondary system, is applied on one degree of freedom system which be named as primary system to show the optimum strategy. If a harmonic force with amplitude of

P_0 applied on the main mass, the motion equilibrium equation could be obtained as Eq. 3.1.

$$\begin{bmatrix} m_P & \\ & m_T \end{bmatrix}\begin{Bmatrix} \ddot{x_p} \\ \ddot{x_T} \end{Bmatrix} + \begin{bmatrix} c_P + c_T & -c_T \\ -c_T & c_T \end{bmatrix}\begin{Bmatrix} \dot{x_p} \\ \dot{x_T} \end{Bmatrix} + \begin{bmatrix} k_P + k_T & -k_T \\ -k_T & k_T \end{bmatrix}\begin{Bmatrix} x_P \\ x_T \end{Bmatrix} = \begin{Bmatrix} P_0 e^{i\omega t} \\ 0 \end{Bmatrix} \qquad 3.1$$

Where, m_P, c_P and k_P is mass, damping and stiffness of the primary system, respectively. m_T, c_T and k_T is mass, damping and stiffness of the secondary system, respectively. $\ddot{x_P}$, $\dot{x_P}$ and x_P is acceleration, velocity and displacement response of the primary system, respectively. $\ddot{x_T}$, $\dot{x_T}$ and x_T is acceleration, velocity and displacement response of the secondary system, respectively.

If we assumed the solution as $x_P = x_1 e^{i\omega t}$, $x_T = x_2 e^{i\omega t}$, and ignored the damping of the primary system, the transfer function could be obtained.

$$H(\beta) = \frac{A + iB}{C + iD} \qquad 3.2$$

Where, the excitation frequency ratio $\beta = \omega/\omega_P$, where the circular frequency of the primary system $\omega_P = \sqrt{k_P/m_P}$. And, A, B, C and D are functions of the excitation frequency ratio β, the tuning ratio γ ($\gamma = \omega_T/\omega_P$, $\omega_T = \sqrt{k_T/m_T}$), the TMD mass ratio μ ($\mu = m_T/m_P$), and the TMD damping ratio ξ_T ($\xi_T = c_T/(2m_T\omega_T)$) . Then, the amplitude of the transfer function can be obtained as follows.

$$D(\beta) = |H(\beta)| = \sqrt{\frac{A^2 + B^2}{C^2 + D^2}} \qquad 3.3$$

If the damping of the primary system is ignored, the following formula of response function could be obtained.

$$H(\omega) = P_0 \frac{\left(k_T - m_T\,\omega^2\right) + i\omega c_T}{\begin{array}{c}[(-m_P\omega^2 + k_P)(-m_T\omega^2 + k_T) - m_T\omega^2 k_T] \\ +i\omega c_T(-m_P\omega^2 + k_P - m_T\omega^2)\end{array}} \qquad 3.3$$

$$H(\omega)^2 = {P_0}^2 \frac{\left(k_T - m_T\,\omega^2\right)^2 + \omega^2 {c_T}^2}{\begin{array}{c}[(-m_P\omega^2 + k_P)(-m_T\omega^2 + k_T) - m_T\omega^2 k_T]^2 \\ +\omega^2 {c_T}^2(-m_P\omega^2 + k_P - m_T\omega^2)^2\end{array}} \qquad 3.4$$

$$D = |H(\beta)| = P_0 \sqrt{\frac{(2\xi_T\beta\gamma)^2 + (\beta^2 - \gamma^2)^2}{(2\xi_T\beta\gamma)^2(\beta^2 - 1 + \mu\beta^2)^2 + [\mu\gamma^2\beta^2 - (\beta^2 - 1)(\beta^2 - \gamma^2)]^2}} \qquad 3.5$$

Where, D is the response amplitude of the primary system. If we set the TMD mass ratio μ as a certain value, the excitation frequency ratio β as the independent variable, the maximum formula of transfer function amplitude would be a function of only tuning ratio γ and damping ratio ξ_T .

Fig. 3-2 shows the relationship between D and β under variant damping ratio ξ_T, which equals 0, 0.05, 0.1, 0.3 and 1, respectively, under the condition of mass ratio μ of 0.05 and tuning ratio γ of 1. Fig. 3-3 shows the relationship between D and β under variant tuning ratio γ, which equals0.93, 0.95 and 1.02, respectively, under the condition of mass ratio μ of 0.05 and damping ratio of 0.1336 ξ_T.

From, Fig. 3-2, it can be found that the response curse would through two fixed point P and Q independent from the damping ratio, when mass ratio μ and tuning ratio γ is constant. Based on this property, the so called Fixed point method was summarized in Den Hartog's [3-2] book, which is seemed as the most typical optimization method for TMD.

There are two basic steps for this method in the optimization process. Firstly, choose the optimal tuning ratio γ^{opt} in order to let the two fixed point P and Q have the same height. Secondly, choose the optimal damping ratio ${\xi_T}^{opt}$ in order to let the two peaks horizontally pass through the two points P and Q, respectively. Actually, ${\xi_{T,1}}^{opt}$ from the condition of horizontally pass through point P and ${\xi_{T,2}}^{opt}$ from the condition of horizontally pass through point Q are different from each other. Usually, an average value showed in Eq. 3.6 is adopted as the optimum damping ratio ${\xi_T}^{opt}$. The obtained optimum formulas are listed in Table 3.1 as the achievement of the former studies.

$$\xi_T{}^{opt^2} = \frac{1}{2}(\xi_{T,1}{}^{opt^2} + \xi_{T,2}{}^{opt^2}) \qquad 3.6$$

If we consider the damping of the primary system, a closed-form expression of solution is impossible to be obtained. Basically, the numerical method is used to find the optimum value [3-17] [3-18].

The basic numerical solving process is introduced here as follows. As showed in Eq. 3.7, we adopted $f(\gamma, \xi_T)$ as the function of the maximum of D. Then, from the optimum condition of Eq. 3.7a and Eq. 3.7b, respectively, the optimal numerical solution of tuning ratio and damping ratio could be obtained.

$$Maximum(D) = f(\gamma, \xi_T) \qquad 3.7$$

$$\begin{cases} \dfrac{\partial f(\gamma, \xi_T)}{\partial \gamma} = 0 \\ \dfrac{\partial^2 f(\gamma, \xi_T)}{\partial \gamma^2} > 0 \end{cases} \qquad 3.7a$$

$$\begin{cases} \dfrac{\partial f(\gamma, \xi_T)}{\partial \xi_T} = 0 \\ \dfrac{\partial^2 f(\gamma, \xi_T)}{\partial \xi_T{}^2} > 0 \end{cases} \qquad 3.7b$$

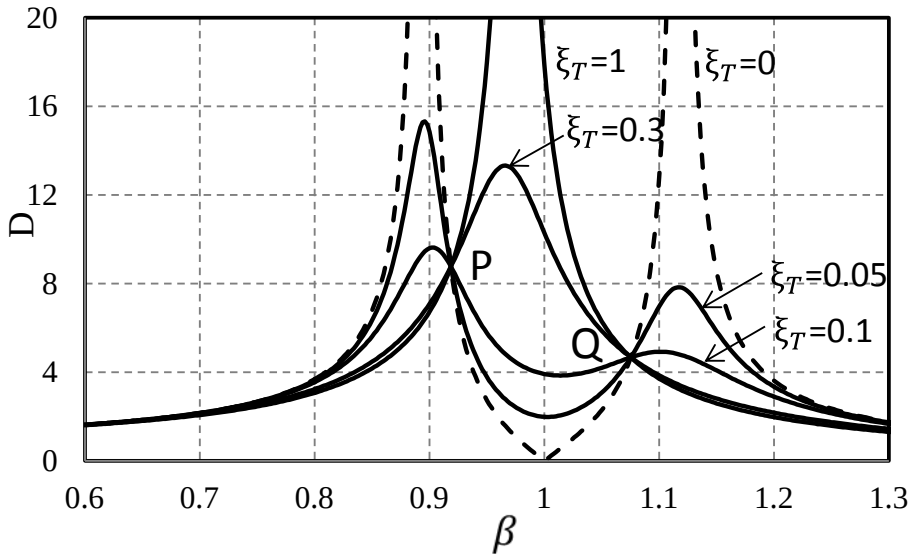

Figure 3.2 The influence of damping ratio ($\mu = 0.05,\ \gamma = 1$)

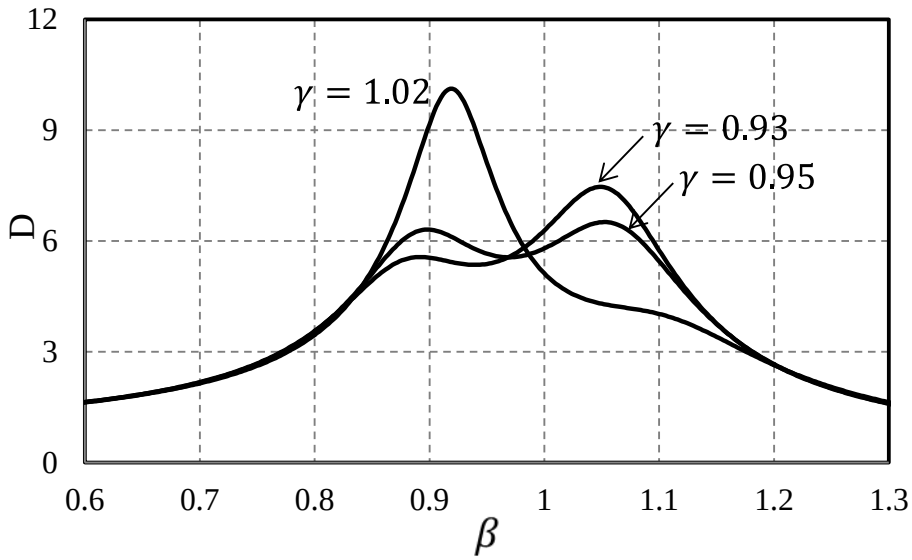

Figure 3.3 The influence of tuning ratio ($\mu = 0.05,\ \xi_T = 0.1336$)

Table 3.1 Optimum parameters for TMD attached to undamped primary system using Fixed point method under various harmonic excitations [3-14]

No.	Excitation		Optimized response			Optimized parameters	
	Type	Applied to	Parameter optimized	Definition of D	D^{opt}	γ^{opt}	${\xi_T}^{opt^2}$
1 [3-2]	Force $P_0 e^{i\omega t}$	Primary mass	X_P	$\frac{k_P X_P}{P_0}$	$\sqrt{\frac{2+\mu}{\mu}}$	$\frac{1}{1+\mu}$	$\frac{3\mu}{8(1+\mu)}$
2 [3-15]	Force $P_0 e^{i\omega t}$	Primary mass	$\dot{X}_P$	$\frac{k_P \dot{X}_P}{P_0 \omega_P}$	$\sqrt{\frac{2+\mu}{\mu(1+\mu)}}$	$\frac{\sqrt{1+\mu/2}}{1+\mu}$	$\frac{3\mu(1+\mu+\frac{5\mu^2}{24})}{8(1+\mu)(1+\frac{\mu}{2})^2}$
3	Force $P_0 e^{i\omega t}$	Primary mass	$\ddot{X}_P$	$\frac{m_P \ddot{X}_P}{P_0}$	$\sqrt{\frac{2}{\mu(1+\mu)}}$	$\frac{1}{\sqrt{1+\mu}}$	$\frac{3\mu}{8(1+\mu/2)}$
4	Force $P_0 e^{i\omega t}$	Primary mass	Frame force	$\frac{k_P X_P}{P_0}$	$\sqrt{\frac{2+\mu}{\mu}}$	$\frac{1}{1+\mu}$	$\frac{3\mu}{8(1+\mu)}$
5	Acceleration $\ddot{X}_0 e^{i\omega t}$	Frame	$y_P = x_P - x_0$	$\frac{{\omega_P}^2 Y_P}{\ddot{X}_0}$	$\sqrt{\frac{2}{\mu}}(1+\mu)$	$\frac{\sqrt{1-\mu/2}}{1+\mu}$	$\frac{3\mu}{8(1+\mu)(1-\frac{\mu}{2})}$
6	Acceleration $\ddot{X}_0 e^{i\omega t}$	Frame	$\ddot{X}_P$	$\frac{\ddot{X}_P}{\ddot{X}_0}$	$\sqrt{\frac{2+\mu}{\mu}}$	$\frac{1}{1+\mu}$	$\frac{3\mu}{8(1+\mu)}$
7	Acceleration $\ddot{X}_0 e^{i\omega t}$	Frame	X_P	$\frac{{\omega_P}^2 X_P}{\ddot{X}_0}$	$\sqrt{\frac{2}{\mu}}(1+2\mu+2.125\mu^2+3.375\mu^3+\cdots)$	$\frac{\sqrt{1-\mu/2+\sqrt{(1-3\mu-\frac{7}{4}\mu^2)^{1/2}}}}{2(1+\mu)^2}$	$\frac{3\mu(1-3\mu+1.5\mu^2-2.833\mu^3\ldots)}{8(1-3.5\mu-2\mu^2-0.5\mu^3\ldots)}$
8 [3-16]	Force $b\omega^2 e^{i\omega t}$	Primary mass	X_P	$\frac{m_P X_P}{b}$	$\sqrt{\frac{2}{\mu(1+\mu)}}$	$\frac{1}{\sqrt{1+\mu}}$	$\frac{3\mu}{8(1+\mu/2)}$
9	Force $b\omega^2 e^{i\omega t}$	Primary mass	Frame force	$\frac{k_P X_P}{b{\omega_P}^2}$	$\sqrt{\frac{2}{\mu(1+\mu)}}$	$\frac{1}{\sqrt{1+\mu}}$	$\frac{3\mu}{8(1+\mu/2)}$

3.2.2 Minimal variance method

If we assume the external force as a random excitation which has a spectral density S_0 of white noise process, then the variance of the response quantity σ_x^2 is as Eq. 3.8. The closed-expression of σ_x^2 could be obtained using integrals from Crandall and Mark [3-19].

$$\sigma_x^2 = \int_{-\infty}^{\infty} S_0 \, |H(\omega)|^2 \mathrm{d}\omega \qquad 3.8$$

And, the optimization conditions are:

$$\frac{\partial(\sigma_x^2)}{\partial\gamma}=0 \qquad 3.9$$

$$\frac{\partial(\sigma_x^2)}{\partial\xi_T}=0 \qquad 3.10$$

The obtained optimum formulas are listed in Table 3.2 from the former studies.

Table 3.2 Optimum parameters for TMD attached to undamped primary system using Minimal variance method

No.	Excitation		Optimized response			Optimized parameters	
	Type	Applied to	Parameter optimized	Definition of N	N^{opt}	γ^{opt}	${\xi_T}^{opt2}$
1 [3-20]	Force	Primary mass	X_P	$\frac{\sigma_x^2 k_P^2}{2\pi S_0 \omega_P}$	$\sqrt{\frac{1+3\mu/4}{\mu(1+\mu)}}$	$\frac{\sqrt{1+\mu/2}}{1+\mu}$	$\frac{\mu(1+\frac{3\mu}{4})}{4(1+\mu)(1+\mu/2)}$
2 [3-14]	Force	Primary mass	$\dot{X}_P$	$\frac{\sigma_x^2 k_P^2}{2\pi S_0 \omega_P^3}$	$\sqrt{\frac{1}{\mu(1+\mu)}}$	$\frac{1}{\sqrt{1+\mu}}$	$\frac{\mu}{4}$
3 [3-20]	Acceleration	Frame	$y_P = x_P - x_0$	$\frac{\sigma_y^2 \omega_P^3}{2\pi S_0}$	$\sqrt{\frac{(4-\mu)(1+\mu)^3}{4\mu}}$	$\frac{\sqrt{1-\mu/2}}{1+\mu}$	$\frac{\mu(1-\mu/4)}{4(1+\mu)(1-\frac{\mu}{2})}$

Similarly, for the damped primary system, the optimum parameters could be solved numerically using the optimum conditions of Eq. 3.9 and Eq. 3.10.

3.2.3 Equal damping method

Furthermore, the optimization of TMD subject to seismic excitations has also been studied by some researchers, such as Villaverde [3-21] [3-22], Villaverde and Koyoama [3-23], Villaverde and Martin [3-24], etc. They found that TMD works best when the damping ratios of the first two complex modes of the combined system approximately equals to the average of the damping ratios of the primary structure and TMD. In order to achieve this, Villaverde [3-21] suggested that the tuning ratio and damping ratio of TMD should be as follows.

$$\gamma^{opt} = 1 \tag{3.11}$$

$$\xi_T{}^{opt} = \xi_P + \Phi\sqrt{\mu} \tag{3.12}$$

Where ξ_P is the damping ratio of the primary structure, Φ is the amplitude of the mode shape at the TMD location, μ is TMD mass ratio which is the ratio of the TMD mass to the generalized mass of the primary system (usually the fundamental mode).

However, the optimum value provided by Villaverde has a good approximation for keeping the first two complex modes of the combined system equals to the average of the damping ratios of the primary structure and TMD, only for a small TMD mass ratio less than 0.005. So, Sadek [3-25] suggest a modified formula for SDOF primary system as follows.

$$\gamma^{opt} = \frac{1}{1+\mu}\left(1 - \xi_P\sqrt{\frac{\mu}{1+\mu}}\right) \tag{3.13}$$

$$\xi_T{}^{opt} = \frac{\xi_P}{1+\mu} + \sqrt{\frac{\mu}{1+\mu}} \tag{3.14}$$

If TMD is applied to MDOF primary system, the virtual mass ratio is defined as the ratio of the TMD mass to the generalized mass of the fundamental mode, which is normalized to have a unit modal participation factor, formulated as follows.

$$\mu = \frac{m_T}{\emptyset(1)^T[M]\emptyset(1)} \tag{3.15}$$

Then, Sadek's formula for MDOF primary system should be modified as follows.

$$\gamma^{opt} = \frac{1}{1+\Phi\mu}\left(1 - \xi_P\sqrt{\frac{\Phi\mu}{1+\Phi\mu}}\right) \tag{3.16}$$

$$\xi_T{}^{opt} = \Phi\left(\frac{\xi_P}{1+\mu} + \sqrt{\frac{\mu}{1+\mu}}\right) \tag{3.17}$$

Where, M is the mass matrix of the combined system, $\emptyset(1)$ is the fundamental mode shape normalized to have a unit modal participation factor. The nominal mass ratio is constant for a given TMD mass value and primary system, while, the virtual TMD mass ratio will change when TMD mass attached at different floors. It can be approximated that adopting $\Phi\mu$ as the virtual TMD mass ratio when TMD is attached to MDOF primary system.

3.2.4 Numerical simulation for the comparison

30 SDOF structures, whose natural periods start from 0.1s to 3.0s with increments of 0.1s, were adopted in earthquake response analysis with and without TMD to evaluate the three types of optimization methods mentioned above in determining TMD parameters for seismic excitation. Damping ratio ξ_P of primary structures is assumed as 0.02. Four kinds of TMD mass ratio μ is selected to vary from 0.05 to 0.2 with increments of 0.05. Three types of optimum methods, Fixed point method, Minimal variance method and Equal damping method, are adopted to implement this comparison analysis. Where, the optimum value in No. 5 and No. 3 of Fixed point method and Minimal variance method, respectively, are selected for this numerical simulation. And, Sadek's formula Eq. 3.16 and Eq. 3.17 of Equal damping method are used in this study. A set of 60 horizontal components of earthquake records (Appendix E) from stations in the western U.S. and Japan were adopted to implement this comparison analysis. These records a wide range of earthquake magnitudes (5.7~7.3), Epicentral distances (1.2~107km), peak ground acceleration (109.45~1304.10gal). Fig. 3.4 ~Fig. 3.8 shows the average and coefficient value of the displacement and acceleration response subjected to those 60 earthquake excitations.

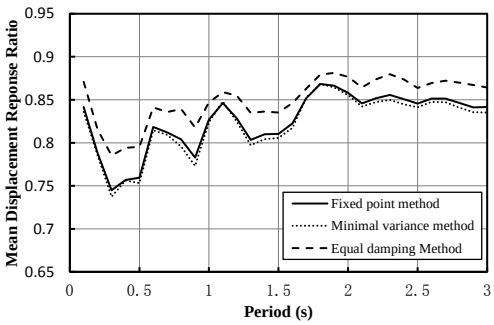

Figure 3.4(a) Mean displacement response ratio (mass ratio $\mu = 0.05$)

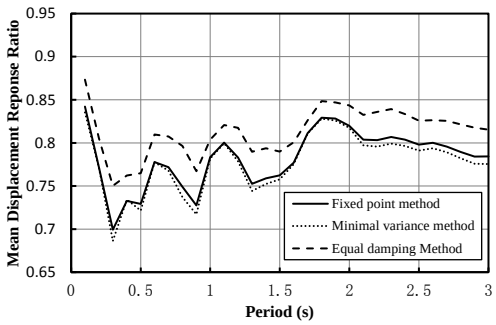

Figure 3.4(b) Mean displacement response ratio (mass ratio $\mu = 0.1$)

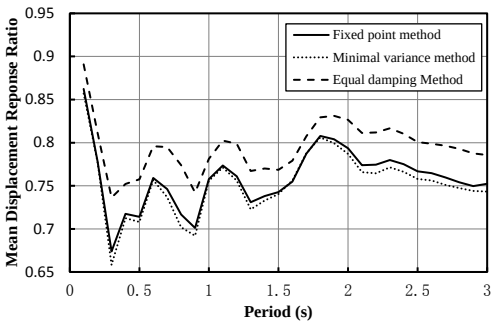

Figure 3.4(c) Mean displacement response ratio (mass ratio $\mu = 0.15$)

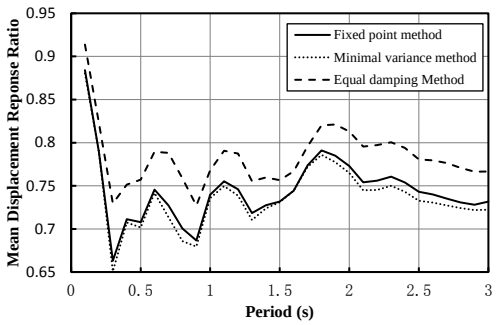

Figure 3.4(d) Mean displacement response ratio (mass ratio $\mu = 0.2$)

From the result of displacement response ratio, showed in Fig.3.4, we can conclude that, the displacement mitigation effectiveness of Minimal variance method is a little better than Fixed point method. But these two methods are much better than Equal damping method in reducing displacement response. When the TMD mass ratio becomes larger, this difference also goes larger.

From the result of acceleration response ratio, showed in Fig. 3.5, it can be concluded that the effectiveness of Fixed point method and Minimal variance method is almost the same. But the acceleration mitigation effect of these two methods is obviously better than Equal damping method. When TMD mass ratio becomes larger, the difference of these three methods becomes smaller.

From the result of TMD stroke ratio, showed in Fig. 3.6, the same as expected, it can be found that the Minimal variance method has the largest TMD stroke the Equal damping method has the smallest TMD stroke. It is interesting to find that the TMD stroke of Fixed point method is smaller than Minimal variance method as they two has the almost same displacement and acceleration response.

From the result of the Coefficient of Variations (COV) of displacement response ratio, showed in Fig. 3.7, and the Coefficient of Variations of acceleration response ratio, showed in Fig. 3.8, we can find the same tendency that, COV of the Fixed point method is smaller than the Minimal variance method, larger than the Equal damping method. Which means the response stability of the Fixed point method is better than the Minimal variance method. The Equal damping method has the best response stability.

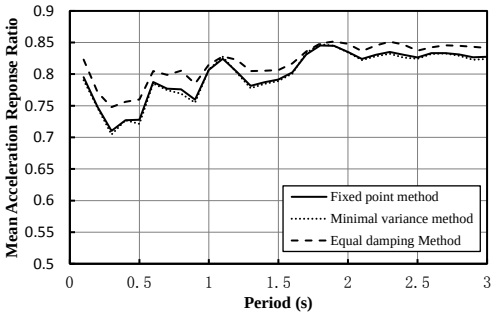

a) mass ratio $\mu = 0.05$

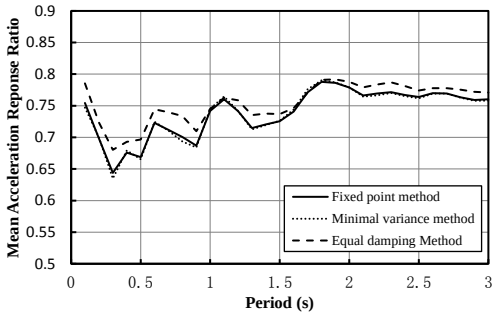

b) mass ratio $\mu = 0.1$

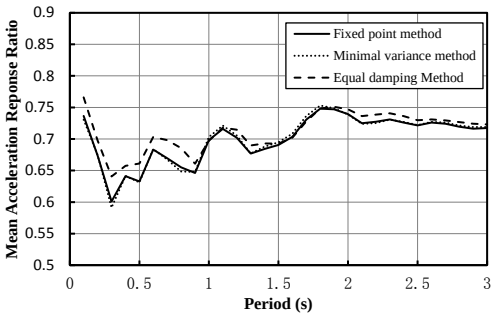

c) mass ratio $\mu = 0.15$

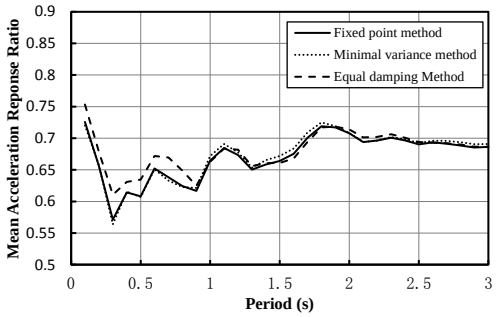

d) mass ratio $\mu = 0.2$

Figure 3.5 Mean acceleration response ratio

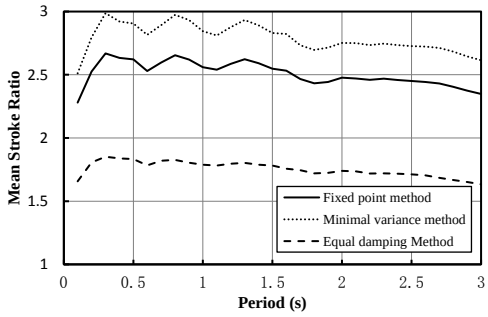

Figure 3.6 a) Mean TMD stroke response ratio (mass ratio $\mu = 0.05$)

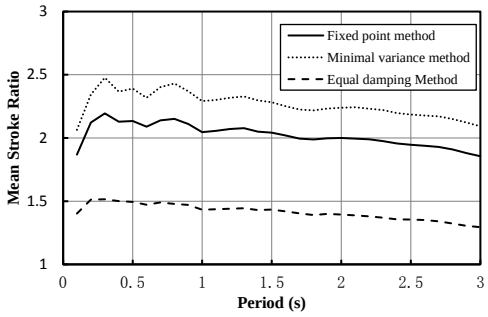

b) mass ratio $\mu = 0.1$

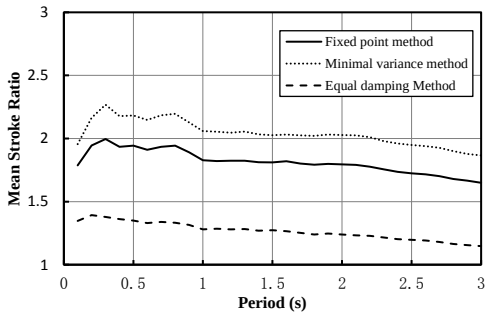

c) mass ratio $\mu = 0.15$

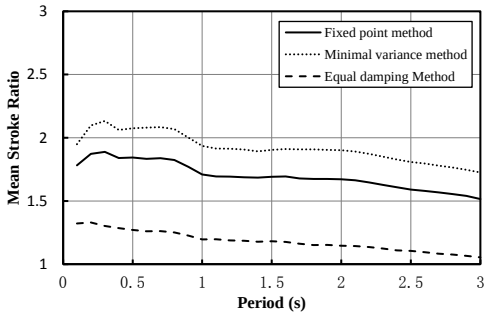

d) mass ratio $\mu = 0.2$

Figure 3.6 Mean TMD stroke response ratio

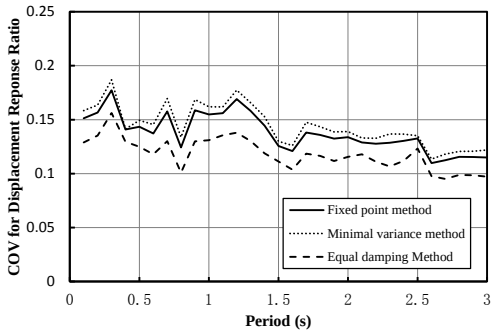

a) mass ratio $\mu = 0.05$

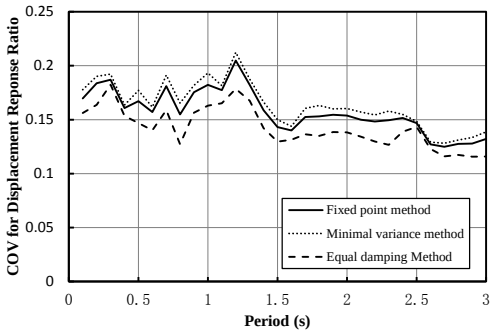

b) mass ratio $\mu = 0.1$

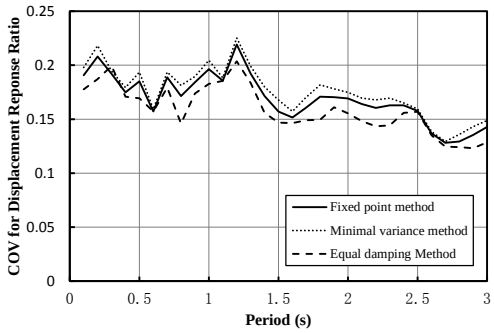

c) mass ratio $\mu = 0.15$

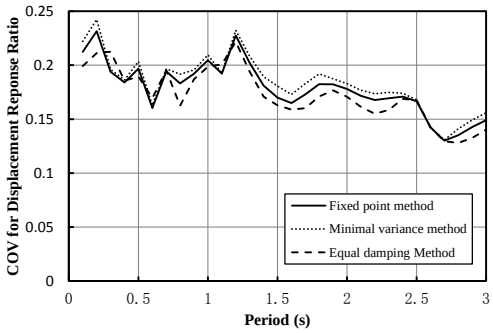

d) mass ratio $\mu = 0.2$

Figure 3.7 Coefficient of variations of displacement response ratio

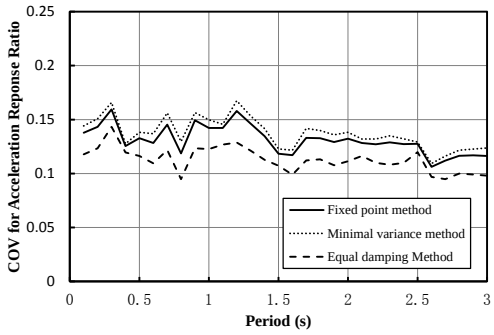

a) mass ratio $\mu = 0.05$

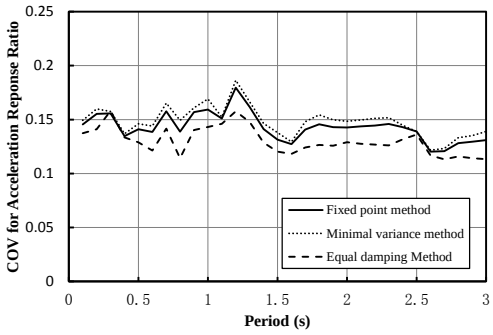

b) mass ratio $\mu = 0.1$

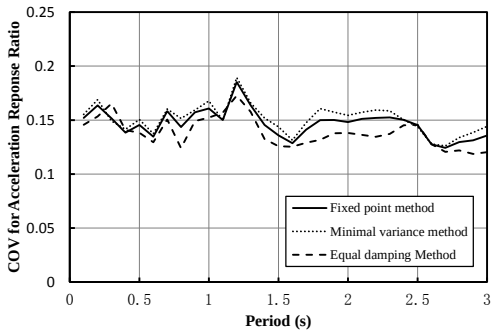

c) mass ratio $\mu = 0.15$

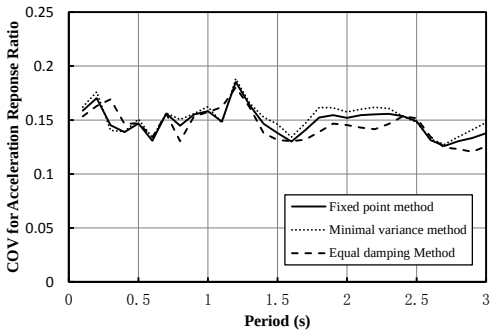

d) mass ratio $\mu = 0.2$

Figure 3.8 Coefficient of variations of acceleration response ratio

From the findings mentioned above from the numerical simulation result, the Fixed point method is chose as the basic optimum method in this study based on the reasons listed below:

1) The displacement response and the acceleration response of Fixed point method is almost the same as the Minimal variance method and much smaller than the Equal damping method. This means the Fixed point method is one of the two has the best vibration mitigation effectiveness.

2) Within the best two effective methods, the TMD stroke of the Fixed point method is smaller than the Minimal variance method. This means that the Fixed point method take less space than the Minimal variance method, which make the practicability of the Fixed point method better than the Minimal variance method.

3) The Fixed point method also has a better stability than the Minimal variance method.

3.3 Study on Non-traditional TMD

3.3.1 Research background

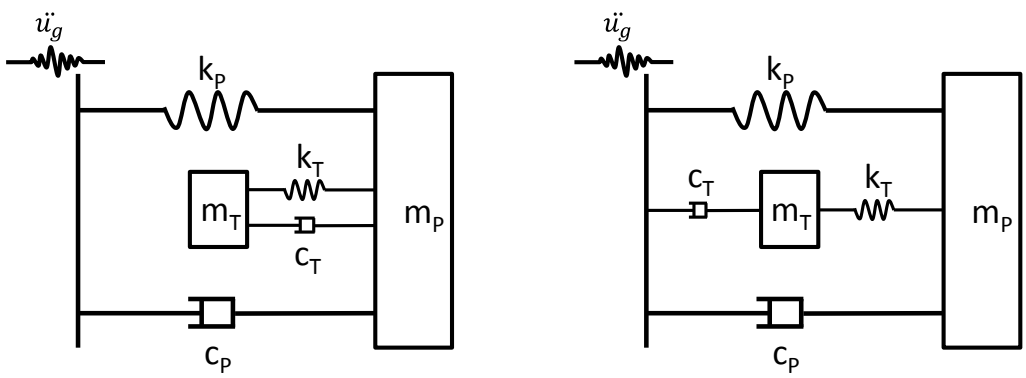

a) Traditional TMD **b)** Non-traditional TMD

Figure 3.9 The concept of Traditional and Non-traditional TMD

As showed in Fig. 3.9, another type of TMD named Non-traditional TMD, whose damper is connected directly to the ground which is different from the Traditional TMD, has been pointed out more effective than traditional TMD [3-26]~[3-30] . Especially, in [3-31], a study on exploring the vibration mitigation effectiveness of the non-traditional TMD when combined with a base-isolated structure showed that the non-traditional TMD could provide a wider frequency suppression range and achieve

a larger suppression of the maximum magnitude of the frequency transfer function with a relatively smaller stroke.

Wong and Cheung [3-28] derived the optimum formulae of the non-traditional TMD for ground displacement excitation. They also showed the property that non-traditional TMD has larger vibration suppression than the traditional TMD. Liu and Coppola [3-29] studied the optimum parameters when it is attached to a damped primary system subjected to harmonious force excitation using two numerical methods, Chebyshev's equioscillation theorem [3-32] and Nelder-Mead or sequential simplex method [3-33].

Here, we first derived the optimum parameters of non-traditional TMD for ground acceleration excitation using the typical Fixed point method. Then we use a friction damper instead of viscous damper and derived the optimum damping and tuning ratio subjected to both force and ground excitations using the method suggested by Ricciardelli and Vickery [3-34].

Finally, a shaking table test of a steel 1DOF model with non-traditional TMD is carried out to test its vibration control effectiveness. Two different kinds of dampers, a viscous damper and a friction damper, were adopted to perform as the energy dissipation components.

3.3.2 Optimization for ground excitation

In this study, the parameter optimization for non-traditional TMD has been carried out using Fixed point method when the structure subjected to ground excitations.

$$\begin{bmatrix} m_P & \\ & m_T \end{bmatrix} \begin{Bmatrix} \ddot{x_p} \\ \ddot{x_T} \end{Bmatrix} + \begin{bmatrix} c_P & \\ & c_T \end{bmatrix} \begin{Bmatrix} \dot{x_p} \\ \dot{x_T} \end{Bmatrix} + \begin{bmatrix} k_P + k_T & -k_T \\ -k_T & k_T \end{bmatrix} \begin{Bmatrix} x_P \\ x_T \end{Bmatrix} = \begin{Bmatrix} -m_P \ddot{u_g} \\ -m_T \ddot{u_g} \end{Bmatrix} \qquad 3.18$$

If we ignore the damping of the primary system, a closed-form exact solution of optimum tuning ratio and damping ratio could be obtained. First, assume that $\ddot{u_g} = A_0 e^{i\omega t}$, the response function could be obtained as

$$|H(\beta)| = \frac{1}{\omega_P{}^2}\sqrt{\frac{(\beta^2-\gamma^2-\mu\gamma^2)^2+(2\xi_T\beta\gamma)^2}{[(-\beta^2+1+\mu\gamma^2)(-\beta^2+\gamma^2)-\mu\gamma^4]^2+(-\beta^2+1+\mu\gamma^2)^2(2\xi_T\beta\gamma)^2}} \qquad 3.19$$

It can be found that the property of the response function of non-traditional TMD is the same as the conventional TMD that the response curve will pass through two fixed points whatever the damping ratio is. So the Fixed point method firstly proposed by Den Hartog can be used here to obtain the optimum parameters with closed-form expression.

The response function R is defined as

$$R = \left|\frac{X_P}{A_0}\right|\omega_P{}^2 = \sqrt{\frac{(\beta^2-\gamma^2-\mu\gamma^2)^2+\left(2\xi_T\beta\gamma\right)^2}{[(-\beta^2+1+\mu\gamma^2)(-\beta^2+\gamma^2)-\mu\gamma^4]^2+(-\beta^2+1+\mu\gamma^2)^2\left(2\xi_T\beta\gamma\right)^2}} \qquad 3.20$$

Firstly, the optimum tuning parameters can be obtained which will make the heights of the fixed point P be the same as the fixed point Q.

$$\gamma^{opt} = \frac{1}{\sqrt{1-\frac{\mu}{2}}} \qquad 3.21$$

Then, let the differential equation $\partial R/\partial\beta$ equals to zero at the point P, which means the curve pass through point P horizontally with slope of zero, the damping ratio can be solved as

$$\xi_{T,1}{}^2 = \frac{6\mu\sqrt{2\mu}-\mu^2\sqrt{2\mu}+4\mu^2}{16\sqrt{2\mu}+8\mu\sqrt{2\mu}-16\mu} \qquad 3.22$$

Similarly, let the differential equation $\partial R/\partial\beta$ equals to zero at the point Q, the damping ratio can be solved as

$$\xi_{T,2}{}^2 = \frac{6\mu\sqrt{2\mu}-\mu^2\sqrt{2\mu}-4\mu^2}{16\sqrt{2\mu}+8\mu\sqrt{2\mu}+16\mu} \qquad 3.23$$

Finally, the optimum damping ratio is decided as the average of the two values showed in Eq. 3.21 and Eq. 3.22, of the different points which leads to

$$\xi_T{}^{opt} = \sqrt{\mu \frac{12 + 8\mu - \mu^2}{32 + 16\mu + 8\mu^2}} \qquad 3.24$$

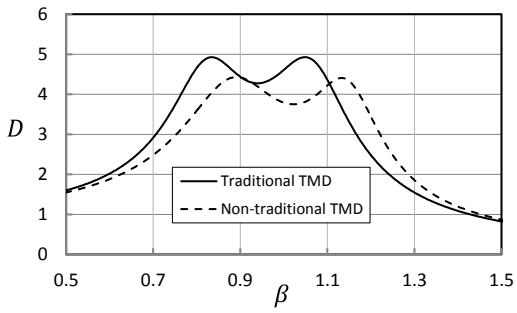

Figure 3.10 The response comparison of Traditional and Non-traditional TMD (Mass ratio $\mu = 0.1$)

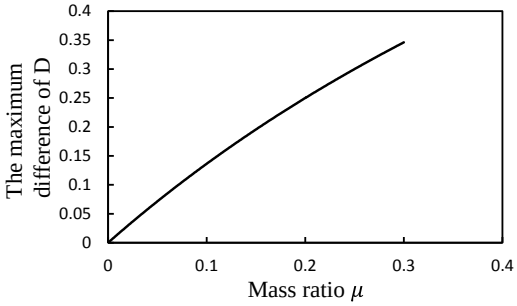

Figure 3.11 The Max difference of D between Traditional and Non-traditional TMD

Table 3.3 Result comparison ($\mu = 0.1$)

	Traditional TMD	Non-traditional TMD
γ^{opt}	0.886	1.026
ξ^{opt}	0.189	0.195
$D(\beta_1,\ \beta_2)$	4.919	4.249
D_{max}	4.928	4.430
$D(\beta = \gamma^{opt})$	4.561	3.752
$\overline{D}$	2.939	2.816

Note: $\overline{D} = \frac{1}{1.5-0.5}\int_{0.5}^{1.5} D d\beta$

Fig. 3.10 shows the response of Traditional TMD and Non-traditional TMD with mass ratio as 0.1. It can be found that the peak value of Non-traditional TMD is smaller than that of Traditional TMD. This means that the Non-traditional TMD has a better effect in reducing the resonant vibrations than Traditional TMD. Furthermore, Fig. 3.11 shows the relationship between the difference of the peak value and the mass ratio. It can be found that the difference becomes larger when the mass ratio becomes larger

The optimum parameters and some other values are listed in Table 3.3. It can be found that the optimum value of tuning ratio and damping ratio of Non-traditional TMD is larger than that of Traditional TMD. The height of fixed points of Non-traditional TMD is smaller than that of Traditional TMD. The peak value D_{max} of Non-traditional TMD is smaller than that of Traditional TMD. The response value when the excitation frequency equals to the optimum tuning ratio of the Non-traditional TMD is smaller than that of Traditional TMD. Finally, the integration from 5 to 1.5 of the Non-traditional TMD is also smaller than that of Traditional TMD.

3.3.3 Optimization for friction damper

The Tuned Mass Damper (TMD) or Tuned Vibration Absorber is widely recognized to be an effective means to reduce the structural dynamic response in both Civil and Mechanical Engineering applications. There are also more and more researchers extend the theory of TMD, either considering more complicated mechanical systems or various forms of excitations. On the other hand, a non-linear behavior has to be taken into consideration. Because some of the times, the primary or TMD system has stepped into non-linear stage and which cannot be ignored, or the non-linear behavior results in a better performance of the vibration mitigation or let the construction or maintenance simpler. [3-34]

Inaudi and Kelly has proposed a TMD with two friction devices providing damping force by acting at a right angle with the direction of motion of the TMD mass [3-35]. Ricciardelli and Vickery proposed an optimization method for TMD parameters when having linear stiffness dry friction damping. The numerical analysis showed that a friction TMD is more effective than a viscous TMD. [3-34]

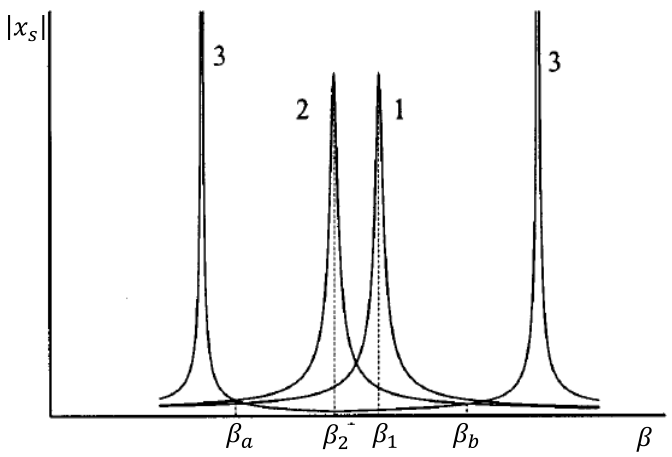

Figure 3.12 Response of the system with and without TMD [3-34]

In this study, the optimum parameters of friction non-traditional TMD is deduced using the optimization strategies mentioned above proposed by Ricciardelli and Vickery. This method is based on three ranges of different cases of: 1) response of the plain SDOF system, 2) the response of the system with friction TMD but no relative motion occurs between the TMD mass and the primary structure, 3) the response of the system with friction TMD but the ratio of friction force and the excitation amplitude equals to zero. [3-34]

First, it can be found that a range of excitation exists in which the response of Case 2 is larger than Case3. And this range could be calculated by equating the response of Case with that of Case 3. Then, the TMD parameters (tuning and friction force) was decided to make the friction damper effective only inside this range, within β_a and β_b showed in Fig. 3.12.

The optimization result of friction non-traditional TMD subjected to force and ground excitation, respectively, is listed below and the details can be found in Appendix.

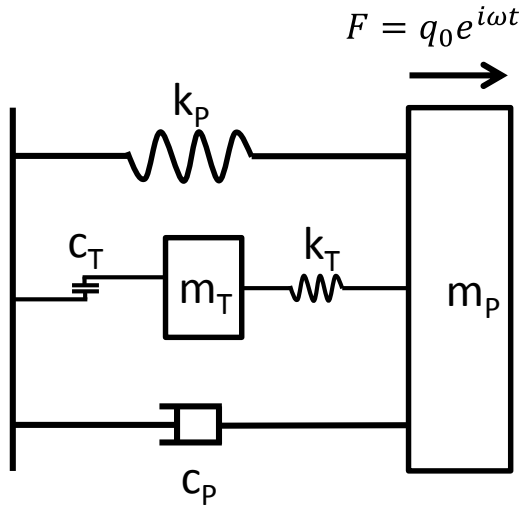

Figure 3.13 Friction Non-traditional TMD subjected to force excitation

First, as showed in Fig. 3.13, the optimization of friction non-traditional TMD subjected to force excitation is introduced. Eq. 3.25 shows the motion equilibrium equation of this combined system.

$$\begin{bmatrix} m_P & \\ & m_T \end{bmatrix} \begin{Bmatrix} \ddot{x_P} \\ \ddot{x_T} \end{Bmatrix} + \begin{bmatrix} c_P & \\ & c_T \end{bmatrix} \begin{Bmatrix} \dot{x_P} \\ sgn(\dot{x_T}) \end{Bmatrix} + \begin{bmatrix} k_P + k_T & -k_T \\ -k_T & k_T \end{bmatrix} \begin{Bmatrix} x_P \\ x_T \end{Bmatrix} = \begin{Bmatrix} q_0 e^{i\omega t} \\ 0 \end{Bmatrix} \qquad 3.25$$

First, $|x_P|$ is calculated in the case of no relative motion

$$|x_P| = \frac{q_0}{k_P} \frac{1}{\sqrt{(-\beta^2 + 1 + \mu\gamma^2)^2 + (2\xi_1\beta)^2}} \qquad 3.26$$

If Eq.3.27 reached, relative motion will occur

$$k_T x_1 = c_0 \qquad 3.27$$

From the above two equation, Eq. 3.28 can be obtained

$$\beta^2{}_{lim} = 1 + \mu\gamma^2 \pm \frac{q_0 \mu \gamma^2}{c_0} \qquad 3.28$$

If the ratio of friction force with excitation amplitude equals to zero, then

$$|x_P| = \frac{q_0}{k_P} \frac{|-\beta^2 + \gamma^2|}{|(-\beta^2 + \gamma^2)(1 - \beta^2 + \mu\gamma^2) - \mu\gamma^4|} \qquad 3.29$$

Then, Eq. 3.30 can be obtained

$$c_0 = q_0 \frac{\mu\gamma^2}{\pm \frac{B \pm \sqrt{B^2 - 8C}}{4} \mp (1 + \mu\gamma^2)} \qquad 3.30$$

Let the two values in Eq. 3.30 equals to each other, the optimum values can be obtained as showed in Eq. 3.31 and Eq. 3.32.

$$\gamma^{opt} = \frac{1}{\sqrt{1 - \mu}} \qquad 3.31$$

$$c_0{}^{opt} = \sqrt{2\mu} q_0 \qquad 3.32$$

Then, the optimization of friction non-traditional TMD subjected to ground excitation is introduced (Fig. 3.14). Eq. 3.33 shows the motion equilibrium equation of this combined system.

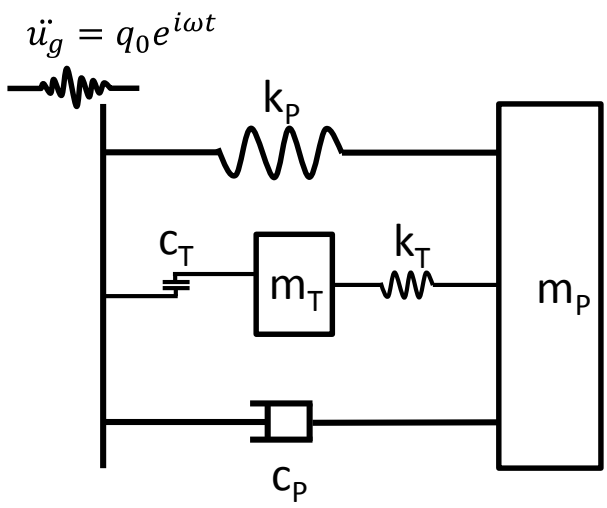

Figure 3.14 Friction Non-traditional TMD subjected to ground excitation

$$\begin{bmatrix} m_P & \\ & m_T \end{bmatrix}\begin{Bmatrix} \ddot{x_P} \\ \ddot{x_T} \end{Bmatrix} + \begin{bmatrix} c_P & \\ & c_T \end{bmatrix}\begin{Bmatrix} \dot{x_P} \\ sgn(\dot{x_T}) \end{Bmatrix} + \begin{bmatrix} k_P + k_T & -k_T \\ -k_T & k_T \end{bmatrix}\begin{Bmatrix} x_P \\ x_T \end{Bmatrix} = \begin{Bmatrix} -m_P \ddot{u_g} \\ -m_T \ddot{u_g} \end{Bmatrix} \quad 3.33$$

First, the response is calculated in the case of no relative motion

$$|x_P| = \frac{q_0}{k_P} \frac{m_P}{\sqrt{(-\beta^2 + 1 + \mu\gamma^2)^2 + (2\xi_P\, \beta)^2}} \quad 3.34$$

The relative motion occurred condition is showed in Eq. 3.35

$$k_T x_P = c_T \quad 3.35$$

From the above two equation, β_{lim} can be obtained

$${\beta_{lim}}^2 = 1 + \mu\gamma^2 \pm \frac{q_0}{c_T} \mu\gamma^2 m_P \quad 3.36$$

If the ratio of friction force with excitation amplitude equals to zero, then

$$|x_P| = \frac{q_0}{k_P} \left| \frac{-m_P(-\beta^2+\gamma^2) - m_T\gamma^2}{(-\beta^2+1+\mu\gamma^2)(-\beta^2+\gamma^2) - \mu\gamma^4} \right| \quad 3.37$$

Then, Eq. 3.38 can be obtained

$$c_0 = q_0 \frac{\mu\gamma^2 m_P}{\pm \frac{B \pm \sqrt{B^2 - 8C}}{4} \mp (1 + \mu\gamma^2)} \quad 3.38$$

Finally, let the two values in Eq. 3.38 equals to each other, the optimum values can be obtained as showed in Eq. 3.39 and Eq. 3.40.

$$\gamma^{opt} = \frac{1}{\sqrt{1 - \frac{\mu}{2}}} \quad 3.39$$

$${c_0}^{opt} = \sqrt{2\mu} m_P q_0 \quad 3.40$$

3.3.4 Shaking table test for non-traditional TMD

In order to explore the feasibility and effectiveness of the non-traditional TMD system, whose mass is supported from ground, a shaking table test is carried out using a simplified SDOF frame seemed as the objective structure. As shown in Fig. 3.15, TMD mass is supported by two columns with 3 hinge joint at each end. And the left one joint will be installed a rotary damper or friction damper as shown in Fig. 3.16 and Fig. 3.17. Two springs are used to connect the TMD mass and the frame. The mass of the frame is 6.7kg; the natural period is 0.29s. There are two kinds of TMD mass and the mass ratio of each is 3.6% and 5.5%, respectively.

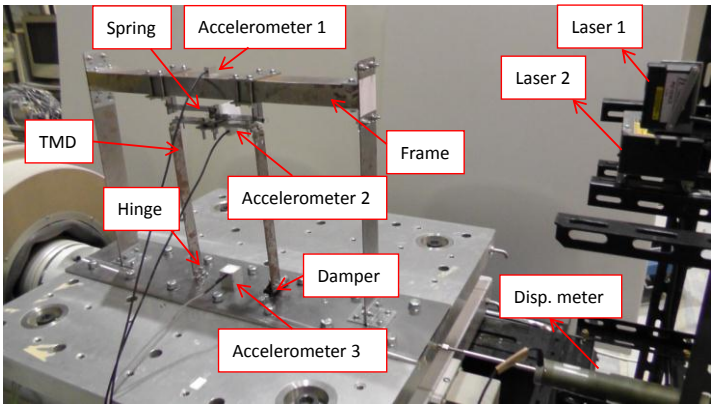

Figure 3.15 Model setup

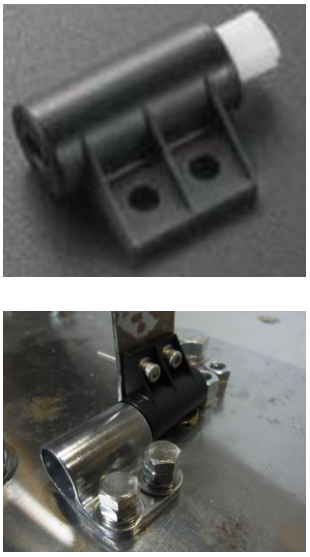

Figure 3.16 The rotary damper

Figure 3.17 The friction damper

Table 3.4 shows the information of the specimen, there are two types of TMD mass with mass ratio of 3.6% and 5.5%, and two types and dampers, rotary damper and friction damper.

Table 3.4 Model Information

Type of TMD	Mass ratio	Damping
T1+Rotary	3.6%	Rotary damper, 3.08N/m/s
T1+Friction	3.6%	Friction damper, 0.10Nm
T2+Rotary	5.5%	Rotary damper, 4.27N/m/s
T2+Friction	5.5%	Friction damper, 0.12Nm

Firstly, a frequency sweep wave is adopted as the input wave, whose frequency changes from 1Hz to 5Hz to 1Hz at the speed of 1Hz/min with the acceleration amplitude of 0.02g. Then 5 waves whose PGA is adjusted to 0.1g and 0.2g are adopted, which is Whitenoise (0Hz~6Hz), El Centro-NS(1940), Taft-EW(1952), Kobe(1995) and Hachinohe-NS(1968) , into this test.

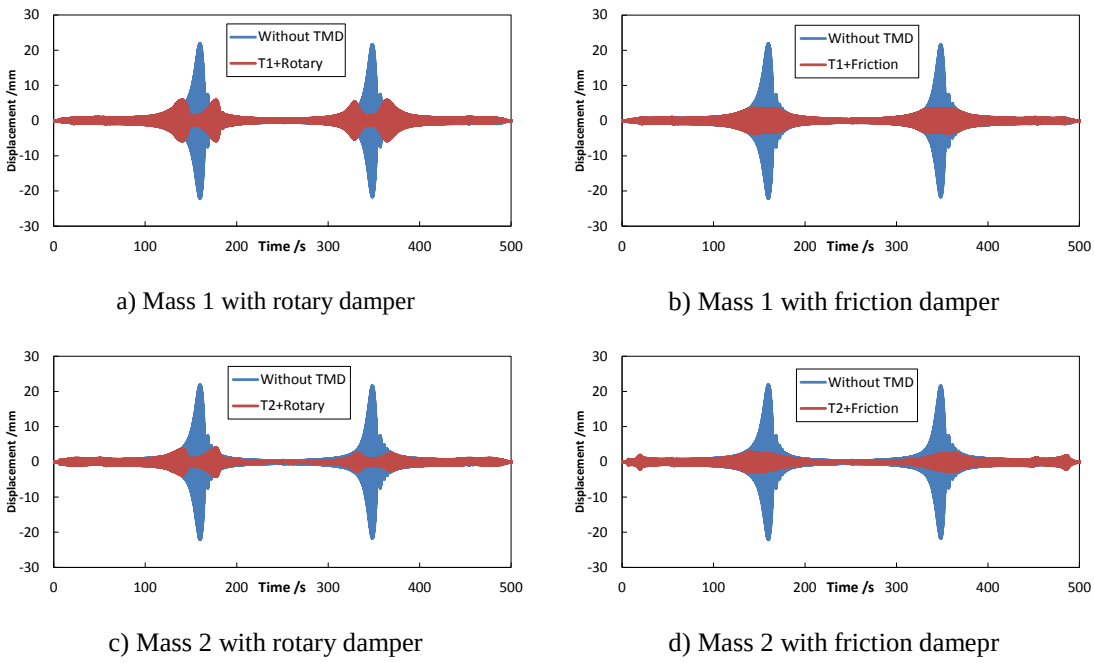

a) Mass 1 with rotary damper

b) Mass 1 with friction damper

c) Mass 2 with rotary damper

d) Mass 2 with friction damepr

Figure 3.18 Relative displacement response

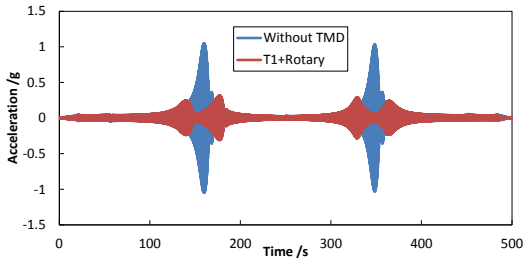

a) Mass 1 with rotary damper

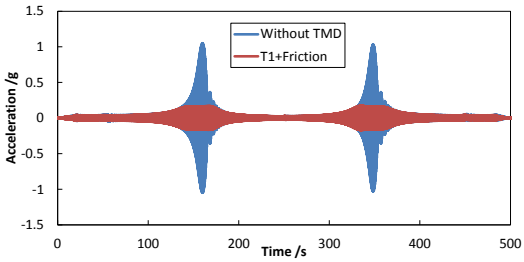

b) Mass 1 with friction damper

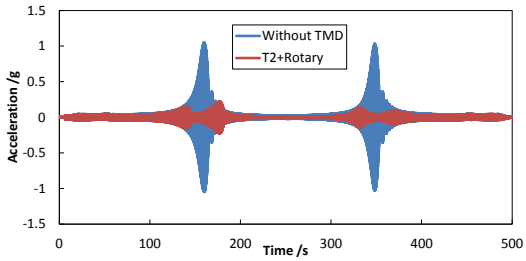

c) Mass 2 with rotary damper

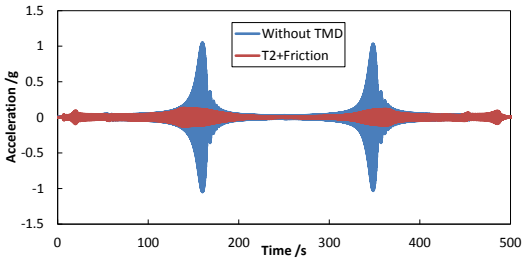

d) Mass 2 with friction damepr

Figure 3.19 Accleration response

From the result of sweep wave, listed in Fig. 3.18 and Fig. 3.19, it is clear that the system performed very well to mitigate the resonant vibration. The response of the two basic modes of the combined system is the same which demonstrated the tuned property of TMD. It is interest to find that the two peaks of two modes of the friction TMD are not as clear as that of viscous TMD. This phenomenon might be caused by the non-linear behavior of the friction damper, which is not discussed here.

From the response value listed in Table 3.5 of relative displacement, it can be found that the viscous TMD system can reduce the maximum resonant displacement response to about 26.6% and 19.4% of the original one when the mass ratio is 3.6% and 5.5%. However, the friction TMD system can reduce the maximum resonant displacement response to about 16.2% and 13.5% of the original one, respectively for different mass ratios. And for earthquake input, at most cases, the response of the system combined with friction TMD is about 10% lower than that of viscous damper for mass ratio of 3.6%. For viscous TMD, the maximum response of the primary system with TMD mass ratio of 5.5% is about 3%~14% lower than that of the primary system with TMD mass ratio of 3.6%.

Table 3.5 The maximum and RMS value of relative displacement response (mm)

Input wave		Without TMD		T1+Rotary		T1+Friction		T2+Rotary		T2+Friction	
Name	PGA(gal)	Max	RMS	Max	RMS	Max	RMS	Max	RMS	Max	RMS
Sweep	20	22.2	3.1	5.9	1.5	3.6	1.2	4.3	0.9	3.0	0.9
Whitenoise	100	14.0	3.6	6.9	1.9	6.9	1.7	6.7	1.7	7.2	1.7
	200	27.7	7.6	13.4	3.7	13.8	3.4	12.8	3.4	15.6	4.0
El Centro	100	8.5	1.9	5.8	0.9	5.4	0.9	5.3	0.8	5.6	0.9
	200	15.7	3.4	11.8	1.9	10.7	1.7	11.5	1.8	10.6	1.8
Taft	100	11.0	2.2	8.4	1.3	6.1	1.1	6.9	1.1	6.0	1.1
	200	20.8	4.1	14.9	2.5	13.5	2.2	13.7	2.3	14.1	2.3
Kobe	100	6.4	1.3	7.1	1.0	6.4	0.8	6.8	0.9	6.1	0.8
	200	13.8	2.4	14.4	2.0	13.1	1.8	14.0	1.8	13.6	1.9
Hachinohe	100	8.5	1.6	8.3	1.0	7.2	0.9	7.6	0.8	6.8	0.9
	200	17.7	2.9	16.6	2.0	14.7	1.8	14.7	1.6	11.9	1.6
Tohoku	100	16.9	2.3	8.9	0.8	7.4	0.8	7.9	0.7	8.7	0.8

Table 3.6 The maximum and RMS value of acceleration response (gal)

Input wave		Without TMD		T1+Rotary		T1+Friction		T2+Rotary		T2+Friction	
Name	PGA(gal)	Max	RMS	Max	RMS	Max	RMS	Max	RMS	Max	RMS
Sweep	20	1051	147	315	67	173	56	226	43	130	39
Whitenoise	100	657	203	318	83	320	81	309	80	335	81
	200	1286	361	630	168	636	161	623	164	774	201
El Centro	100	403	90	269	43	256	40	253	40	266	40
	200	749	162	551	87	510	78	542	86	522	87
Taft	100	524	104	374	58	277	50	323	52	281	50
	200	989	195	665	111	613	100	629	107	680	112
Kobe	100	299	59	322	44	290	37	307	38	281	36
	200	644	119	662	92	593	86	646	89	637	95
Hachinohe	100	410	73	361	43	333	42	332	35	325	42
	200	845	139	741	87	661	81	668	75	543	73
Tohoku	100	811	110	405	36	357	38	388	36	421	39

From the response value listed in Table 3.6 of maximum acceleration response, it can be conclude that the viscous TMD system can reduce the maximum resonant displacement response to about 29.9% and 21.5% of the original one when the mass ratio is 3.6% and 5.5%. However, the friction TMD system can reduce the maximum resonant displacement response to about 16.5% and 12.4% of the original one, respectively for different mass ratios. And for earthquake input, at most cases, the

response of the system combined with friction TMD is about 2%~26% lower than that of viscous damper for mass ratio of 3.6%. For viscous TMD, the maximum relative displacement response of the primary system with TMD mass ratio of 5.5% is about 4%~11% lower than that of the primary system with TMD mass ratio of 3.6%.

But it could be found that the maximum acceleration and displacement response of primary structure have not been reduced under Kobe wave excitation from Table 3.5 and 3.6. Fig. 3.20 showed the acceleration spectrum of Kobe wave which may explain it. As showed in Fig. 3.20, the spectrum value at the period of 0.29 for original frame is right at the valley of the curve.

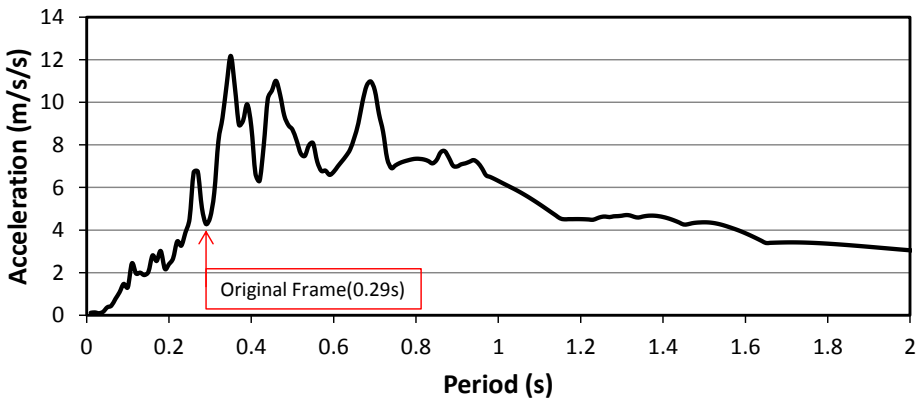

Figure 3.20 Acceleration spectrum of Kobe wave

Based on the results listed above of this steel frame specimen, we can conclude that:

a) The non-traditional TMD either using viscous damper or friction damper can reduce the resonant response of primary structure significantly. For the mass ratio of 5.5%, the resonant relative displacement response amplitude could be reduced to 19.4% and 13.5% of that of original structure.

b) The non-traditional TMD either using viscous damper or friction damper can also reduce the earthquake response of primary structure effectively, especially, when the predominant period of the input earthquake close to that of the structure. For the mass ratio of 5.5%, the maximum relative displacement response amplitude could be reduced up to 53.2% of that of original structure.

c) The friction non-traditional TMD is more effective than the viscous non-traditional TMD. For the mass ratio of 3.6%, the maximum relative displacement and

acceleration response of the system combined with friction TMD is about 7%~13%and 2%~26% lower than that of viscous damper, respectively.

3.4 Proposal of Hybrid TMD

3.4.1 Introduction

As mentioned above, there are basically two types of TMD, the traditional TMD and non-traditional TMD. The difference between them is just the connecting pattern of the dash pot; the damper of traditional TMD connects the TMD mass with primary structure while the damper of non-traditional TMD connects the TMD mass with the ground.

Normally, the traditional TMD is widely used in real projects because TMD is usually placed to the top of the structure. While, in the proposed retrofit system, because of the TMD is placed at the ground floor, the application of non-traditional TMD becomes possible. As we know, non-traditional TMD is more effective than traditional TMD [3-38] [3-39], so the possibility to use the non-traditional TMD for the proposed retrofit system is welcomed for engineers.

But the reality is that, even for the TMD placed at the ground floor, the traditional damper for connecting TMD mass with primary structure is still more convenient than the non-traditional damper connecting TMD mass with ground, because the distance from the TMD mass to the primary structure is much closer than that from the TMD mass to ground. In this study, a hybrid TMD is considered with both traditional damper and non-traditional damper. This kind of system is considered to let the TMD design more freely, thus promote the feasibility of proposed retrofit system.

3.4.2 Optimization of TMD parameters

As showed in Fig. 3.21, Hybrid TMD has four basic components, a mass, a spring connecting mass and primary structure, a traditional damper connecting mass and primary structure and a non-traditional damper connecting mass and ground. The Fixed point Method is adopted here to implement the optimization for the hybrid TMD.

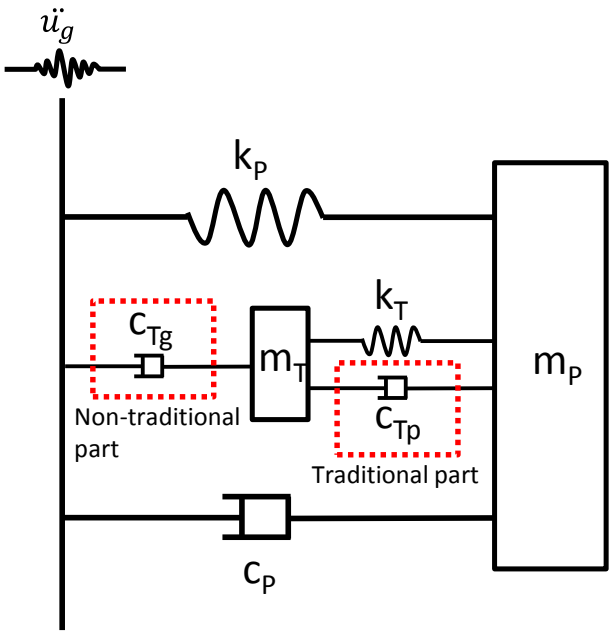

Figure 3.21 Hybrid TMD

Eq. 3.41 is the motion equilibrium of the Hybrid TMD system.

$$\begin{bmatrix} m_P & \\ & m_T \end{bmatrix}\begin{Bmatrix} \ddot{x}_P \\ \ddot{x}_T \end{Bmatrix} + \begin{bmatrix} c_P + c_{Tp} & -c_{Tp} \\ -c_{Tp} & c_{Tp} + c_{Tg} \end{bmatrix}\begin{Bmatrix} \dot{x}_P \\ \dot{x}_T \end{Bmatrix} + \begin{bmatrix} k_P + k_T & -k_T \\ -k_T & k_T \end{bmatrix}\begin{Bmatrix} x_P \\ x_T \end{Bmatrix} = \begin{Bmatrix} -m_P\ddot{u}_g \\ -m_T\ddot{u}_g \end{Bmatrix} \qquad 3.41$$

If it is assumed that $\ddot{u}_g = X_0 e^{i\omega t}$,

The response amplitude could be obtained as follows

$$D = \left|\frac{x_1 {\omega_P}^2}{X_0}\right|$$

$$= \sqrt{\frac{(\beta^2 - \gamma^2 - \mu\gamma^2)^2 + \left[2\beta\gamma\left(\xi_{Tg} + \xi_{Tp} + \mu\xi_{Tp}\right)\right]^2}{\begin{array}{c}\left[(-\beta^2 + 1 + \mu\gamma^2)(-\beta^2 + \gamma^2) - \mu\gamma^4 - 4\mu\xi_{Tp}\xi_{Tg}\gamma^2\beta^2 - 4\xi_P(\xi_{Tp} + \xi_{Tg})\beta^2\gamma\right]^2 + \\ \left\{\left[(-\beta^2 - \mu\beta^2 + 1)\xi_{Tp}\gamma + (-\beta^2 + 1 + \mu\gamma^2)\xi_{Tg}\gamma + (-\beta^2 + \gamma^2)\xi_P\right]2\beta\right\}^2\end{array}}} \qquad 3.42$$

Where $\xi_{Tp} = c_{Tp}/2m_T\,\omega_T$, $\xi_{Tg} = c_{Tg}/2m_T\,\omega_T$, and $\xi_P = c_P/2m_P\,\omega_P$

The object function for the optimization is expressed as follows

$$f\left(\beta, \gamma, \xi_{Tp}, \xi_{Tg}\right) = \min_{\beta}\left(\max_{\beta}(D)\right) \qquad 3.43$$

Because of the two damping ratio exists in the Eq. 3.42, there is no fixed points help us to obtain a closed form of optimization. So, a numerical calculation is used here to implement this optimization.

Fig. 3.22 shows the numerical optimizing flow for searching the optimal value of tuning ratio and damping ratio. This approach is used to decide the optimal tuning ratio γ, the traditional damping ratio ξ_{Tp}, or the non-traditional damping ratio ξ_{Tg}. If these three parameters are all under decided, the optimization will lead to the calculation for a non-traditional TMD system because the traditional damping ratio ξ_{Tp} will be 0.

Here, a more general situation is considered that a certain value of the traditional damping ratio ξ_{Tp} or the non-traditional damping ratio ξ_{Tp} is given, the rest one to be determined, renamed as ξ , and the tuning ratio γ are the undetermined value. The optimization adopted two inner loops and one outer loop to obtain the optimum value. First, assign initial value of tuning ratio γ^0 for the first inner loop and then calculate the inner loop optimum damping ratio ξ_i. Then, assign the obtained value of ξ_i from the first inner loop as the initial value ξ^0 of the second inner loop to calculate the inner loop optimum tuning ratio γ_j. Then the outer loop to judge the loop condition for the value γ^k and ξ^k. Once the outer loop condition is satisfied, the optimum value will be decided as $\gamma^{opt} = \gamma^k$ and $\xi^{opt} = \xi^k$.

According to the numerical calculating flow showed in Fig. 3.22, the optimum damping ratio and tuning ratio of hybrid TMD could be obtained, and Fig 3.23 (a) and (b) showed the solved optimum damping ratio ${\xi_{Tp}}^{opt}$ under different assigned damping ratio ξ_{Tg} and the maximum response value corresponding to these optimum values. And, more detailed results for optimum damping ratio and tuning ratio under variant conditions are listed in Table 3.7~3.12.

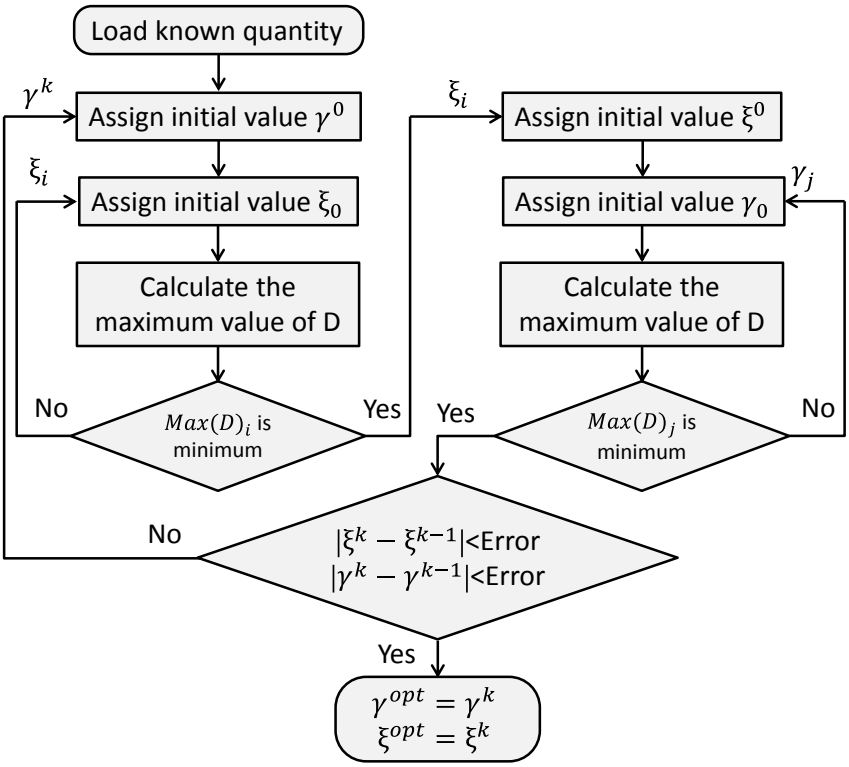

Figure 3.22 The numerical optimizing flow

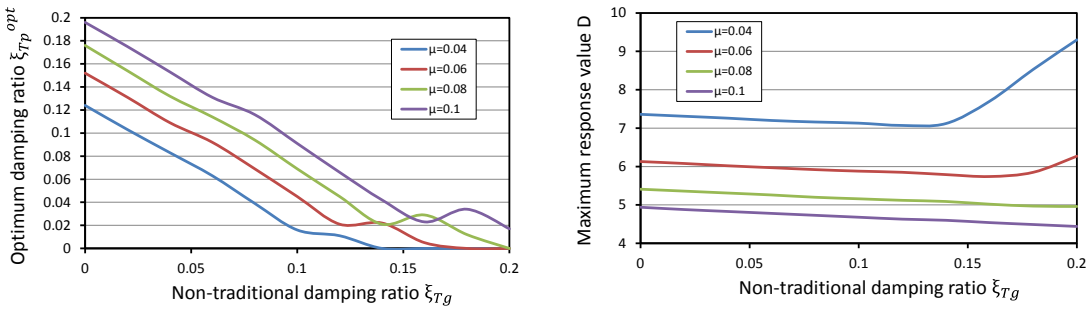

a) Optimum damping $\xi_{Tp}{}^{opt}$ ratio under assigned damping ratio ξ_{Tg}

b) Maximum response value under the optimum parameters

Figure 3.23 The optimum damping ratio and corresponding maximum response value

Table 3.7 The optimum value of ξ_{Tp} under various ξ_{Tg} and μ

μ	ξ_{Tg}										
	0	0.02	0.04	0.06	0.08	0.10	0.12	0.14	0.16	0.18	0.20
0.01	0.062	0.042	0.021	0.004	0	0	0	0	0	0	0
0.02	0.088	0.067	0.048	0.025	0.011	0	0	0	0	0	0
0.03	0.107	0.086	0.067	0.045	0.022	0.012	0	0	0	0	0
0.04	0.124	0.103	0.083	0.063	0.039	0.016	0.011	0	0	0	0
0.05	0.139	0.117	0.096	0.079	0.055	0.031	0.026	0.008	0	0	0
0.06	0.152	0.131	0.109	0.092	0.069	0.045	0.021	0.022	0.005	0	0
0.07	0.164	0.143	0.121	0.103	0.082	0.057	0.033	0.034	0.017	0	0
0.08	0.176	0.154	0.132	0.114	0.094	0.069	0.045	0.021	0.029	0.012	0
0.09	0.186	0.165	0.143	0.124	0.105	0.080	0.056	0.032	0.040	0.023	0.006
0.10	0.196	0.175	0.153	0.131	0.116	0.091	0.066	0.042	0.023	0.034	0.017

Table 3.8 The optimum value of γ under various ξ_{Tg} and μ

μ	ξ_{Tg}										
	0	0.02	0.04	0.06	0.08	0.10	0.12	0.14	0.16	0.18	0.20
0.01	0.989	0.994	0.998	1.003	1.002	1.005	1.018	1.027	1.037	1.049	1.063
0.02	0.976	0.982	0.989	0.996	1.002	1.008	1.012	1.023	1.033	1.044	1.058
0.03	0.964	0.972	0.980	0.988	0.997	1.004	1.011	1.017	1.028	1.040	1.053
0.04	0.952	0.961	0.970	0.979	0.989	1.000	1.007	1.016	1.023	1.035	1.048
0.05	0.941	0.950	0.960	0.970	0.981	0.993	1.001	1.012	1.021	1.030	1.043
0.06	0.929	0.940	0.950	0.961	0.973	0.985	0.998	1.006	1.018	1.027	1.038
0.07	0.919	0.929	0.941	0.952	0.964	0.977	0.991	1.000	1.013	1.025	1.035
0.08	0.908	0.919	0.931	0.943	0.955	0.969	0.983	0.999	1.007	1.020	1.033
0.09	0.897	0.909	0.921	0.934	0.947	0.961	0.976	0.992	1.000	1.014	1.029
0.10	0.887	0.899	0.911	0.924	0.938	0.952	0.968	0.984	1.000	1.008	1.023

Table 3.9 The maximum response value under various μ with corresponding optimum value of ξ_{Tg} and ξ_{Tp}

μ	ξ_{Tg}										
	0	0.02	0.04	0.06	0.08	0.10	0.12	0.14	0.16	0.18	0.20
0.01	13.72	13.70	13.69	13.68	15.83	19.61	23.34	26.91	30.32	33.56	36.60
0.02	10.20	10.15	10.10	10.05	10.01	10.18	11.72	13.52	15.24	16.87	18.40
0.03	8.42	8.36	8.31	8.26	8.22	8.18	8.23	9.06	10.21	11.31	12.34
0.04	7.36	7.31	7.26	7.20	7.16	7.13	7.07	7.12	7.70	8.53	9.30
0.05	6.65	6.60	6.54	6.49	6.44	6.41	6.36	6.31	6.38	6.86	7.48
0.06	6.13	6.08	6.02	5.97	5.92	5.88	5.85	5.79	5.74	5.85	6.27
0.07	5.73	5.68	5.63	5.57	5.52	5.48	5.44	5.38	5.34	5.29	5.45
0.08	5.41	5.36	5.31	5.26	5.20	5.16	5.12	5.09	5.02	4.97	4.96
0.09	5.15	5.10	5.05	5.00	4.95	4.90	4.86	4.82	4.76	4.71	4.66
0.10	4.94	4.88	4.83	4.78	4.73	4.68	4.63	4.60	4.54	4.49	4.44

Table 3.10 The optimum value of ξ_{Tg} under various ξ_{Tp} and μ

μ	ξ_{Tp}										
	0	0.02	0.04	0.06	0.08	0.10	0.12	0.14	0.16	0.18	0.20
0.01	0.059	0.048	0.029	0.010	0	0	0	0	0	0	0
0.02	0.081	0.074	0.056	0.037	0.018	0	0	0	0	0	0
0.03	0.097	0.090	0.079	0.060	0.040	0.021	0.001	0	0	0	0
0.04	0.111	0.103	0.099	0.080	0.060	0.041	0.021	0.002	0	0	0
0.05	0.122	0.114	0.117	0.098	0.078	0.059	0.039	0.020	0	0	0
0.06	0.132	0.124	0.131	0.115	0.095	0.075	0.056	0.036	0.016	0	0
0.07	0.141	0.133	0.141	0.130	0.111	0.091	0.071	0.051	0.031	0.012	0
0.08	0.150	0.142	0.151	0.145	0.125	0.105	0.085	0.066	0.046	0.026	0.006
0.09	0.157	0.150	0.159	0.160	0.139	0.119	0.099	0.079	0.059	0.039	0.019
0.10	0.164	0.158	0.168	0.172	0.153	0.133	0.112	0.092	0.072	0.052	0.032

Table 3.11 The optimum value of γ under various ξ_{Tp} and μ

μ	ξ_{Tp}										
	0	0.02	0.04	0.06	0.08	0.10	0.12	0.14	0.16	0.18	0.20
0.01	1.003	1.000	0.996	0.992	0.995	0.995	0.984	0.982	0.979	0.975	0.971
0.02	1.004	1.000	0.994	0.988	0.982	0.976	0.976	0.973	0.970	0.967	0.963
0.03	1.005	1.000	0.995	0.987	0.980	0.972	0.965	0.965	0.962	0.958	0.955
0.04	1.006	1.000	0.997	0.988	0.979	0.971	0.962	0.954	0.954	0.950	0.946
0.05	1.008	1.000	0.999	0.989	0.979	0.970	0.960	0.951	0.943	0.942	0.938
0.06	1.009	1.000	1.000	0.991	0.980	0.969	0.959	0.949	0.940	0.932	0.930
0.07	1.009	1.000	1.000	0.993	0.981	0.970	0.959	0.948	0.937	0.927	0.923
0.08	1.010	1.000	1.000	0.995	0.982	0.970	0.958	0.947	0.936	0.925	0.914
0.09	1.011	1.000	1.000	0.998	0.984	0.971	0.959	0.946	0.934	0.923	0.912
0.10	1.011	1.000	1.000	1.000	0.986	0.973	0.959	0.946	0.933	0.921	0.909

Table 3.12 The maximum response value under various μ with corresponding optimum value of ξ_{Tg} and ξ_{Tp}

μ	ξ_{Tp}										
	0	0.02	0.04	0.06	0.08	0.10	0.12	0.14	0.16	0.18	0.20
0.01	13.72	13.78	13.85	14.05	16.03	19.91	24.27	28.28	32.27	36.24	40.19
0.02	10.05	10.08	10.18	10.26	10.35	10.51	12.30	14.35	16.37	18.39	20.39
0.03	8.24	8.19	8.34	8.42	8.49	8.57	8.65	9.70	11.08	12.44	13.79
0.04	7.16	7.09	7.24	7.31	7.39	7.46	7.54	7.62	8.43	9.47	10.50
0.05	6.43	6.36	6.48	6.56	6.63	6.70	6.78	6.86	6.93	7.68	8.52
0.06	5.90	5.82	5.89	6.00	6.07	6.14	6.21	6.29	6.37	6.52	7.20
0.07	5.48	5.41	5.42	5.56	5.63	5.70	5.77	5.85	5.92	6.00	6.26
0.08	5.15	5.08	5.05	5.20	5.27	5.34	5.42	5.49	5.56	5.64	5.71
0.09	4.88	4.80	4.76	4.91	4.98	5.05	5.12	5.19	5.26	5.34	5.41
0.10	4.65	4.57	4.51	4.64	4.72	4.79	4.87	4.94	5.01	5.08	5.15

The optimum value of traditional damping ratio ξ_{Tp} and tuning ratio γ under various ξ_{Tg} and μ are listed in Table 3.7 and 3.8. The maximum response value under various μ with corresponding optimum value of ξ_{Tg} and ξ_{Tp} are listed in Table 3.9. It is clear that when the non-traditional damping ratio ξ_{Tg} increased below the optimum value for non-traditional TMD system, the maximum response will decreased. But when the non-traditional damping ratio ξ_{Tg} increased larger than the optimum value for non-traditional TMD system, the maximum response will still increase.

The optimum value of non-traditional damping ratio ξ_{Tg} and tuning ratio γ under various ξ_{Tp} and μ are listed in Table 3.10 and 3.11. The maximum response value under various μ with corresponding optimum value of ξ_{Tp} and ξ_{Tg} are listed in Table 3.12. It can be found that when the traditional damping ratio ξ_{Tp} increased, whether below or beyond the optimum value for traditional TMD system, the maximum response will increased.

In brief, hybrid TMD is the mix of non-traditional TMD and traditional TMD, when ξ_{Tp} becomes to zero, it will becomes to non-traditional TMD; when ξ_{Tg} becomes to zero, it will becomes to traditional TMD. And, the effect of non-traditional TMD is better than Hybrid TMD, and the effect of Hybrid TMD is better than traditional TMD.

3.5 Conclusion

In this chapter, we mainly introduced the basic theory of TMD, and studied the suitable optimum method for the proposed retrofit system. Then we introduced a Non-traditional TMD which is more effective than Traditional TMD and is possible to be applied into the proposed retrofit system. The parameter optimization has been carried out for the Non-traditional TMD combined with viscous damper or friction damper. Furthermore, a hybrid TMD proposed here which combined the property of Traditional TMD and Non-traditional TMD. We can get the following conclusions.

1) From the comparison analysis using 60 earthquake records among three optimum methods, Fixed point method, Minimal variance method and Equal damping method, it can be concluded that Fixed point method has the best performance among three.

2) The closed-form optimum expressions for tuning ratio and damping ratio have been deduced for Non-traditional TMD combined with viscous damper or friction damper.

3) The result from shaking table test for Non-traditional TMD illustrate that this TMD system either combined with viscous damper or friction damper can significantly reduce the resonant vibration for the controlled structure. Furthermore, based on the test result, the Non-traditional TMD combined with friction damper is more effective than that combined with viscous damper.

4) Finally, a Hybrid TMD, which can make the TMD design more freely thus promote the feasibility of the proposed retrofit system, is proposed. The Hybrid TMD combines Traditional TMD and Non-traditional TMD, is considered suitable for the application to the proposed retrofit system. A numerical optimum process was complimented for the Hybrid TMD subjected to ground excitation during various mass ratios. The result shows that the Non-traditional part of damping will help improve the vibration mitigation effect.

Chapter 4

Validation of the Soft-first Story Concept with TMD by Numerical Analysis

4.1 Introduction

First of all, the frequency response analysis is carried out to explore the effect of proposed seismic retrofit system. As mentioned above, the method of realizing soft first story structure from normal existing buildings could be removing the brace of the first floor. On the other hand, to install braces into the upper floors (here we means the floors above the second floor) as to increase the horizontal stiffness of them, can also let the first story become relatively softer. Furthermore, the removed braces of the first floor can be used as the adding materials to increase the horizontal stiffness of the upper floors. The decreasing ratio of horizontal stiffness of the first floor and the increasing ratio of horizontal stiffness of upper floors are adopted as the basic parameters to describe the structural response.

4.2 Information of the Numerical Model

The structural stiffness is idealized as the story shear model (Fig. 4.2) and the structural mass is simplified as lumped mass model (Fig. 4.1). As shown in Fig. 4.2, the shearing stiffness is assumed as distributed as $K_N = \frac{1}{N^{2/3}} K_1$ (N is the story number) [4-1]. The first natural period is assumed as T=0.03H (H is the height of buildings) [4-2] and the height of each story is assumed as 3 meters. Six kinds of models, the number of stories

are 2, 4, 8, 12, 16 and 20, respectively, had been adopted to implement this analysis. Rayleigh damping matrix is used in this analysis with damping ratio of 1% for the first and second mode.

As mentioned in Chapter 2, the horizontal stiffness of the first floor could be reduced by replacing the fixed boundary at the bottom of the column with pinned boundary. So, the horizontal stiffness of the Soft-first story of this method could be reduced to 25% of the original one. In another hand, as mentioned in Chapter 2, the method for stiffen the lateral stiffness of the upper stories is adding braces, and the lateral stiffness of moment braced frame could be about 3 times stiffer than that of moment resisting frame.

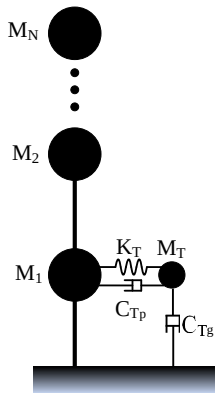

Figure 4.1 The lumped mass model

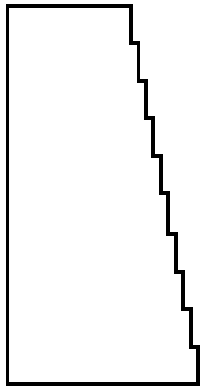

Figure 4.2 Distribution of shearing stiffness

6 kinds of structures, the number of stories are 2, 4, 8, 12, 16 and 20 are adopted in this study. As mentioned above, the lateral stiffness ratio of the first story of the retrofitted structure to the original structure $\frac{K_{after}^{1F}}{K_{before}^{1F}}$ is selected to vary from 1 to 0.25 with increments of 0.25; while, the lateral stiffness ratio of the upper story of the retrofitted structure to the original structure $\frac{K_{after}^{2F\sim topF}}{K_{before}^{2F\sim topF}}$ is selected to vary from 1 to 3 with increments of 0.25.

The hybrid TMD is adopted in this simulation and the traditional part of damping C_{Tp} is assumed as 0. Furthermore, 5 kinds of the ratio of TMD mass to the overall buildings mass, which is 0.5%, 1%, 2%, 5% and 10%, respectively, was adopted into this simulation. Once mass ratio μ ($\mu = m_T/{M_1}^*$) been decided, the optimal tuning

ratio γ^{opt} and optimal damping ratio ξ^{opt} can be obtained by numerical calculation method mentioned in Chapter 3.4, which is based on the Fixed point method proposed by Den Hartog. Here, ${M_1}^*$ means the equivalent mass of the first mode, in which the mode vector is standardized as be divided by the item at the first DOF where TMD is placed, which was explained in Chapter 2.3.

4.3 Frequency Response Analysis

4.3.1 Introduction

Laplace transformation is used in the frequency response analysis [4-3]. The motion equilibrium equation is showed as Eq. 4.1.

$$[m]\{\ddot{x}\} + [c]\{\dot{x}\} + [k]\{x\} = \{Q\} \tag{4.1}$$

Then the Laplace transformation could be obtained as Eq.4.2

$$\begin{aligned} &s^2[m]\{x(s)\} + s[c]\{x(s)\} + [k]\{x(s)\} \\ &= \{Q(s)\} + s[m]\{q(0)\} + [m]\{\dot{q}(0)\} + [c]\{q(0)\} \end{aligned} \tag{4.2}$$

Then we define $Z(s)$ as showed in Eq. 4.3

$$[Z(s)] = s^2[m] + s[c] + [k] \tag{4.3}$$

Then the response vector could be obtained as

$$\begin{aligned} \{x(s)\} = &[Z(s)]^{-1}\{Q(s)\} + s[Z(s)]^{-1}(s[m] + [c])\{q(0)\} \\ &+[Z(s)]^{-1}[m]\{\dot{q}(0)\} \end{aligned} \tag{4.4}$$

If the initial condition is 0, it leads to

$$\{x(s)\} = [Z(s)]^{-1}\{Q(s)\} \tag{4.5}$$

If the loading force is assumed as harmonic force showed in Eq. 4.6 and Eq. 4.7

$$Q_j(t) = Q_{0j} f_j(t) \tag{4.6}$$

$$f_j(t) = e^{i(\omega_j t - \varphi_j)} \quad 4.7$$

Finally, the response could be obtained

$$\{x(t)\} = \sum_{j=1}^{n} \frac{Q_{0j}}{|Z(i\omega_j)|} \{C(i\omega_j)^{(j)}\} e^{i(\omega_j t - \varphi_j)} \quad 4.8$$

4.3.2 Result

As we known, the effective of TMD is controlled by the TMD mass ratio. In MDOF systems, the virtual mass ratio is defined as the ratio of the TMD mass to the equivalent mass of the object mode (normally the fundamental mode). 5 kinds of overall mass ratios, 0.5%, 1%, 2%, 5% and 10%, defined as the ratio of TMD mass to the structural overall mass, are adopted in this numerical analysis, but the virtual mass ratio will be much smaller.

The virtual mass ratio in the various structures during the simulation is listed in Appendix F when the overall mass ratio is 0.1. We can find that, the virtual mass ratio was significantly decreased to 0.038, 0.011,0.003 or even 0.00045 for 2 story model, 4 story model, 8 story model and 20 story model, respectively, if the lateral stiffness has been not changed either for the first floor nor the upper floor. However, the good news is that the stiffness softening of the first floor or the hardening of the upper floor will significantly improve the virtual mass ratio. For example, when the soft rate is 0.25 and hard rate is 3, the virtual mass ratio was increased to 0.093, 0.080, 0.060, and 0.027 for 2 story model, 4 story model, 8 story model and 20 story model, respectively. The increasing of virtual mass ratio by changing the structural stiffness guaranteed the effectiveness of the proposed retrofit system.

Appendix G is the result collection of frequency response analysis for overall mass ratio of 0.01 and 0.1. Fig. G.1 and Fig. G.2 shows the response rate of maximum acceleration of the top floor and the response rate of the drift between the first floor and the top floor. From the result, it is clear that the softening of the lateral stiffness will donate much more than the hardening of the lateral stiffness of the upper floor in reducing acceleration response. Oppositely, the hardening of the lateral stiffness of the upper floor will donate much more than the softening of the lateral stiffness in

reducing the drift response. The same trend is that, when the lateral stiffness of the first floor gets weaker or the lateral stiffness of the upper floor gets stiffer, the acceleration and drift reduction effect will be better.

Fig. G.3 and Fig. G.4 shows the response rate of the maximum shear force and the response rate of the maximum displacement of the first floor. From the result, we can find that the displacement response of the first floor will be increased when the lateral stiffness of the first floor was softened or the lateral stiffness of the upper floors was hardened. But it will still be less than the original structures when the TMD mass is weigh enough or this is applied in a low structure. Although the response of the displacement of the first floor may become larger than that of original structure, the shear force response showed in Fig. G.3 illustrated that the maximum shear force in the first floor will still be smaller than that of original structure. When the lateral stiffness of the first floor gets softer or the lateral stiffness of upper floors gets stiffer, the shear force ratio will become smaller.

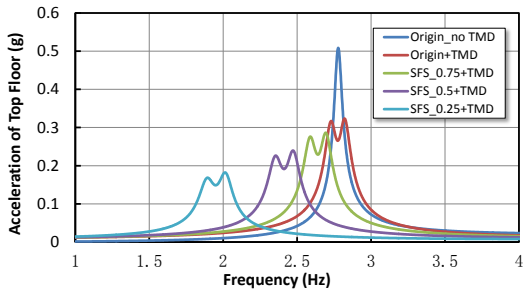

a) 4 story model, overall mass ratio: 0.01

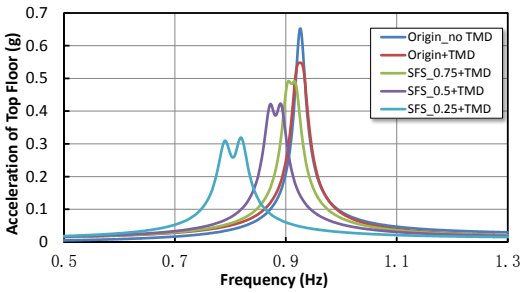

b) 12 story model, overall mass ratio: 0.01

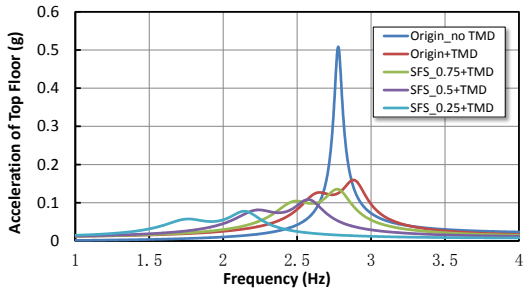

c) 4 story model, overall mass ratio: 0.1

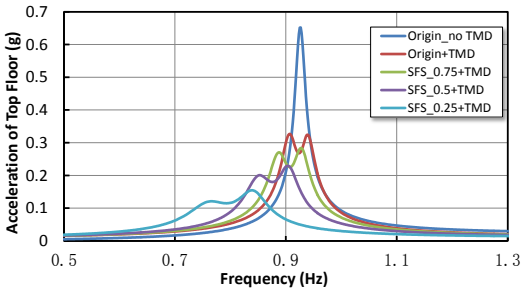

d) 12 story model, overall mass ratio: 0.1

Figure 4.3 Acceleration response of the top floor

First, the acceleration response of 4 story model and 12 story model is selected to illustrate the relationship between softening of the lateral stiffness of the first floor and the acceleration response. From Fig. 4.3, we can see that the TMD system has a

low peak acceleration response than the origin one. Under the same TMD mass, when the lateral stiffness becomes softer, the peak acceleration response becomes smaller, and the natural frequency of the structure also becomes smaller. Furthermore, when the structure becomes higher, the decreased portion of peak acceleration response, caused by the softening of the lateral stiffness of the first floor, becomes larger. Finally, when the TMD mass becomes heavier, the peak acceleration response becomes smaller. But, when the TMD mass ratio becomes larger, the decreased portion of peak acceleration response, caused by the softening of the lateral stiffness of the first floor, becomes smaller.

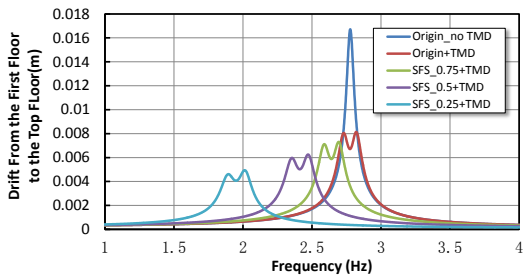

a) 4 story model, overall mass ratio: 0.01

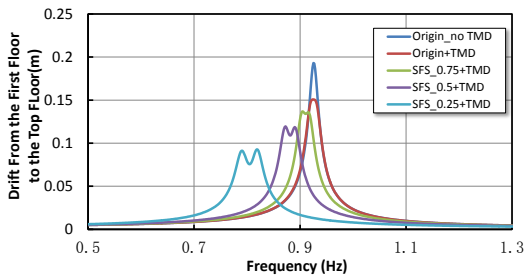

b) 12 story model, overall mass ratio: 0.01

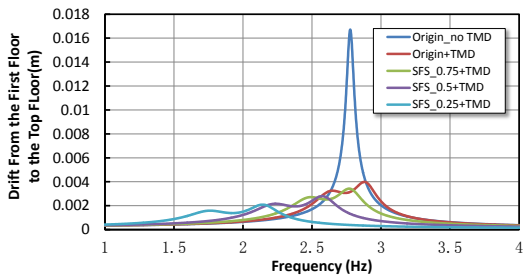

c) 4 story model, overall mass ratio: 0.1

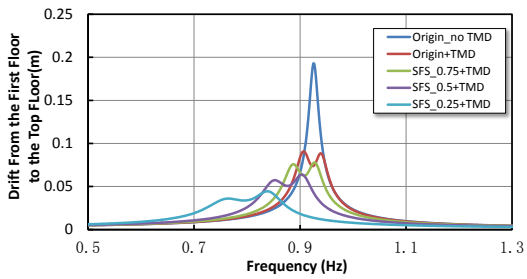

d) 12 story model, overall mass ratio: 0.1

Figure 4.4 Drift response from the first floor to the top floor

Then, the drift response from the first floor to the top floor of 4 story model and 12 story model is selected to illustrate the relationship between softening of the lateral stiffness of the first floor and the drift response. From Fig. 4.4, we can see that the TMD system has a low peak drift response than the origin one. Under the same TMD mass, when the lateral stiffness becomes softer, the peak acceleration response becomes smaller, and the natural frequency of the structure also becomes smaller. Furthermore, when the structure becomes higher, the decreased portion of peak drift response, caused by the softening of the lateral stiffness of the first floor, becomes larger. Finally, when the TMD mass becomes heavier, the peak drift response becomes smaller. But, when the TMD mass ratio becomes larger, the decreased portion of peak

drift response, caused by the softening of the lateral stiffness of the first floor, becomes smaller.

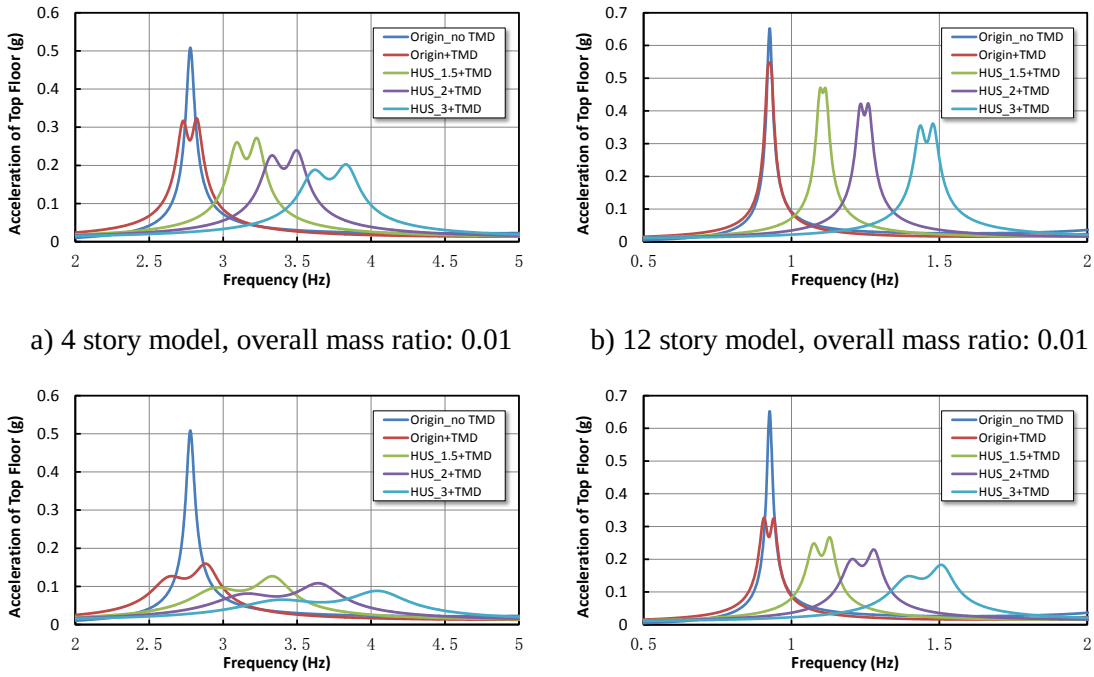

a) 4 story model, overall mass ratio: 0.01

b) 12 story model, overall mass ratio: 0.01

c) 4 story model, overall mass ratio: 0.1

d) 12 story model, overall mass ratio: 0.1

Figure 4.5 Acceleration response of the top floor

Here, the acceleration response of 4 story model and 12 story model is selected to illustrate the relationship between hardening of the lateral stiffness of the upper floor and the acceleration response. From Fig. 4.5, we can see that the TMD system has a low peak acceleration response than the origin one. Under the same TMD mass, when the lateral stiffness becomes stiffer, the peak acceleration response becomes smaller, and the natural frequency of the structure also will becomes larger. Furthermore, when the structure becomes higher, the decreased portion of peak acceleration response, caused by the hardening of the lateral stiffness of the upper floor, becomes larger. Finally, when the TMD mass becomes heavier, the peak acceleration response becomes smaller. But, when the TMD mass ratio becomes larger, the decreased portion of peak acceleration response, caused by the hardening of the lateral stiffness of the upper floor, becomes smaller.

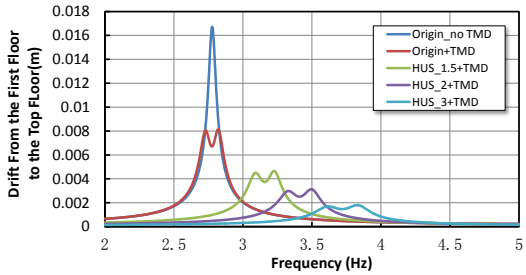

a) 4 story model, overall mass ratio: 0.01

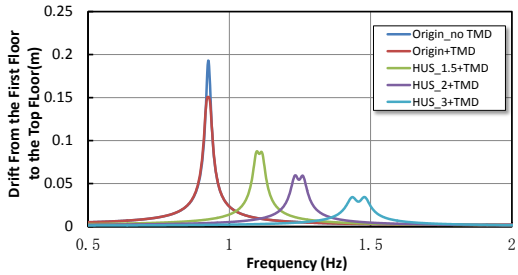

b) 12 story model, overall mass ratio: 0.01

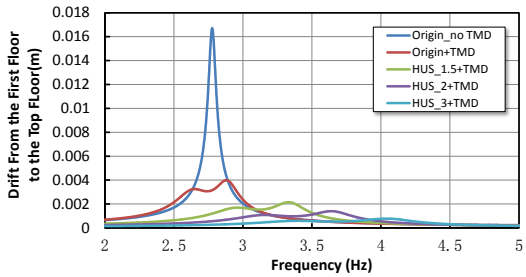

c) 4 story model, overall mass ratio: 0.1

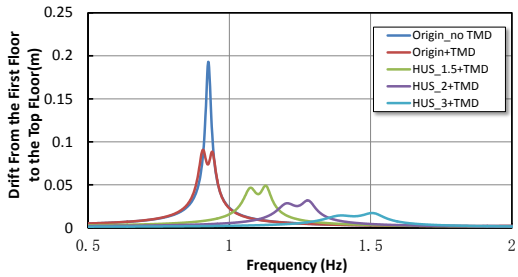

d) 12 story model, overall mass ratio: 0.1

Figure 4.6 Drift response from the first floor to the top floor

The drift response from the first floor to the top floor of 4 story model and 12 story model is selected to illustrate the relationship between hardening of the lateral stiffness of the upper floor and the drift response. From Fig. 4.6, we can see that the TMD system has a low peak drift response than the origin one. Under the same TMD mass, when the lateral stiffness becomes stiffer, the peak acceleration response becomes smaller, and the natural frequency of the structure becomes larger. Furthermore, when the structure becomes higher, the decreased portion of peak drift response, caused by the hardening of the lateral stiffness of the upper floor, becomes larger. Finally, when the TMD mass becomes heavier, the peak drift response becomes smaller. But, when the TMD mass ratio becomes larger, the decreased portion of peak drift response, caused by the hardening of the lateral stiffness of the upper floor, becomes smaller.

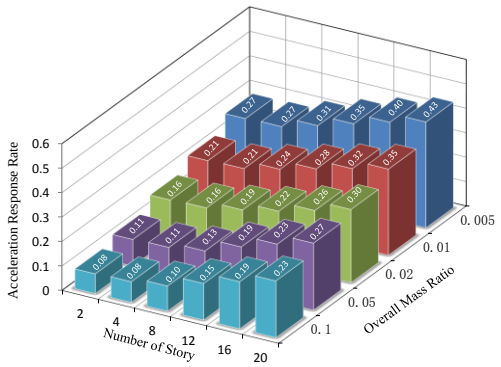

Figure 4.7 The rate of the maximum acceleration response of the top floor of the seismic retrofit structure to the original structure (Soft rate: 0.25, Hard rate: 3)

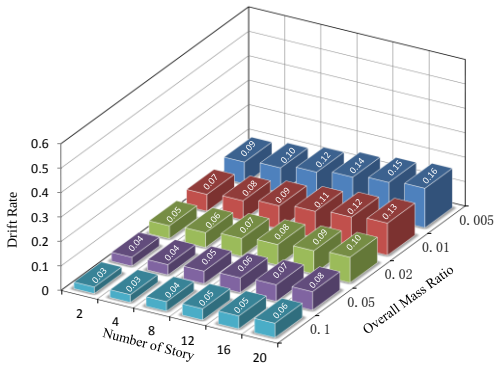

Figure 4.8 The rate of the maximum drift from the first floor to the top floor of the seismic retrofit structure to the original structure (Soft rate: 0.25, Hard rate: 3)

The number of story, the overall mass ratio are selected as the parameter, the relationship between them and the rate of the maximum acceleration response of the top floor is showed in Fig. 4.7, and the relationship between them and the rate of the maximum drift from the first floor to the top floor of the seismic retrofit structure to the original structure is showed in Fig. 4.8. It can be found that the reduction of the acceleration response or the drift response is better when the structure is lower or the TMD mass becomes larger.

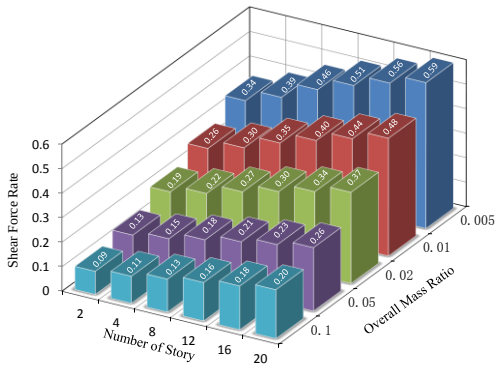

Figure 4.9 The rate of the maximum shear force of the first floor of the seismic retrofit structure to the original structure (Soft rate: 0.25, Hard rate: 3)

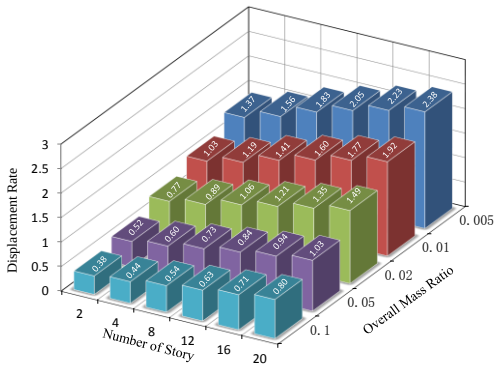

Figure 4.10 The rate of the maximum displacement response of the first floor of the seismic retrofit structure to the original structure (Soft rate: 0.25, Hard rate: 3)

Similarly, the number of story, the overall mass ratio are selected as the parameter, the relationship between them and the rate of shear force of the first floor is showed in Fig. 4.9, and the relationship between them and the rate of the maximum displacement response of the first floor is showed in Fig. 4.10. It can be found that the displacement response of the first floor will be significantly increased especially when the structure gets higher and the TMD mass is lighter. But it will still be less than the original structures when the TMD mass is weigh enough or this is applied in a low structure. Although the response of the displacement of the first floor may become larger than that of original structure, the shear force response showed in Fig. 4.9 illustrated that the maximum shear force in the first floor will still be smaller than that of original structure. When the structure is lower or the TMD mass becomes larger, the shear force ratio will become smaller.

4.4 Earthquake Response Analysis

4.4.1 Introduction

A set of 60 horizontal components of earthquake records (Appendix E) from stations in the western U.S. and Japan were adopted to implement this numerical analysis. These records have a wide range of earthquake magnitudes (5.7~7.3), Epicentral distances (1.2~107km), peak ground acceleration (109.45~1304.10gal). Newmark-β method is used to solve the motion equilibrium equation here.

6 kinds of structures, number of stories is 2, 4, 8, 12, 16 and 20, respectively, idealized as the story shear model are adopted in this study as the same as what be used in the frequency analysis. And, the lateral stiffness ratio of the first story of the retrofitted structure to the original structure is selected to vary from 1 to 0.25 with increments of 0.25; while, the lateral stiffness ratio of the upper story of the retrofitted structure to the original structure is selected to vary from 1 to 3 with increments of 0.25. Rayleigh damping matrix is used in this analysis with damping ratio of 1% for the first and second mode.

Same as the frequency analysis, 5 kinds of the ratio of TMD mass to the overall buildings mass, which is 0.5%, 1%, 2%, 5% and 10%, respectively, was adopted into

this simulation. The optimal tuning ratio γ^{opt} and optimal damping ratio ξ^{opt} are obtained by a numerical process mentioned in Chapter 3.4.

4.4.2 Result

Fig. 4.15 shows the mean rate of the maximum acceleration response of the top floor subjected to the 60 earthquake input. Fig. 4.16 shows the coefficient of the variation for the acceleration response rate of the top floor. It is clear from the result that the mean acceleration response of the retrofit system with TMD is smaller than that of the origin structure. Especially, among these 6 models, 4 story model and 8 story model has the smallest mean acceleration response rate. And also, the coefficient of variation for acceleration response rate is the smallest for 4 story and 8story model, it means that they have a relatively robust acceleration reduction effect. Obviously, when the TMD mass becomes heavier, both the mean acceleration response rate and the coefficient of variation for acceleration response rate will become smaller.

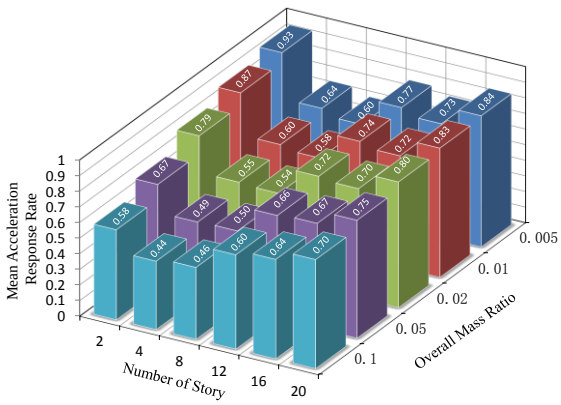

Figure 4.15 Mean acceleration response rate of the top floor (Soft rate: 0.25, Hard rate: 3)

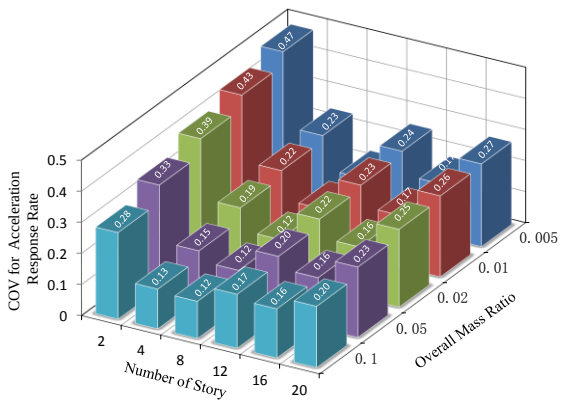

Figure 4.16 Coefficient of variation for acceleration response rate of the top floor (Soft rate: 0.25, Hard rate: 3)

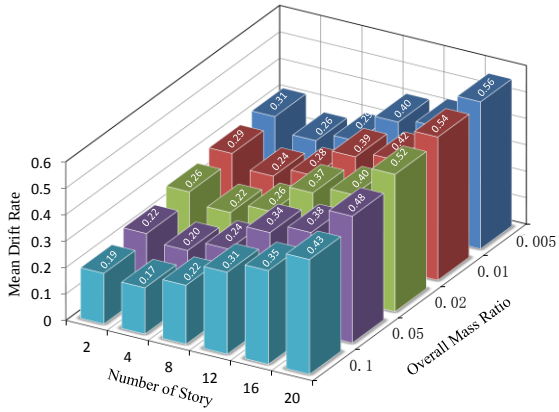

Figure 4.17 Mean drift response rate from the first floor to the top floor (Soft rate: 0.25, Hard rate: 3)

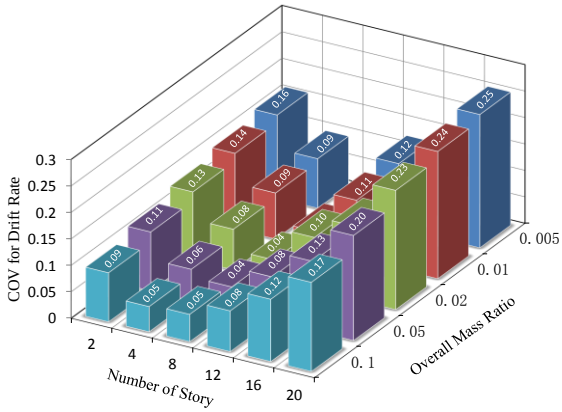

Figure 4.18 Coefficient of variation for drift response rate from the first floor to the top floor (Soft rate: 0.25, Hard rate: 3)

Fig. 4.17 shows the mean rate of the drift response from the first floor to the tip floor subjected to the 60 earthquake inputs. Fig. 4.18 shows the coefficient of the variation for the drift response rate of the top floor. It is clear from the result that the mean drift response of the retrofit system with TMD is smaller than that of the origin structure. Especially, among these 6 models, 4 story model has the smallest mean drift response rate. And, the coefficient of variation for drift response rate is the smallest for 4 story and 8story model, it means that they have a relatively robust drift reduction effect. Obviously, when the TMD mass becomes heavier, both the mean drift response rate and the coefficient of variation for drift response rate will become smaller.

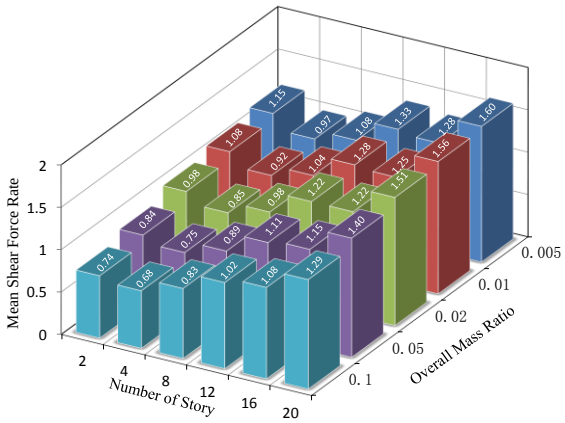

Figure 4.19 Mean shear force rate of the first floor (Soft rate: 0.25, Hard rate: 3)

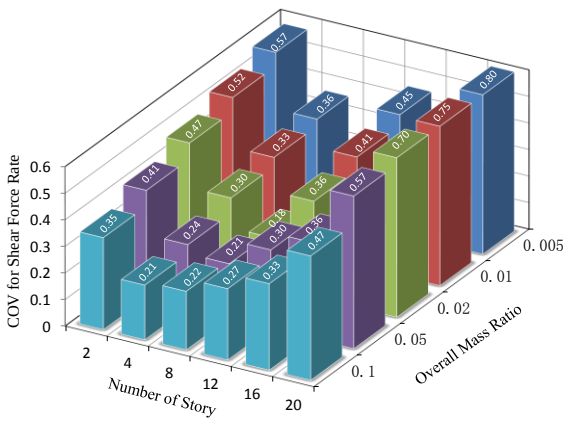

Figure 4.20 Coefficient of variation for shear force rate of the first floor (Soft rate: 0.25, Hard rate: 3)

Fig. 4.19 shows the mean rate of the shear force response of the first floor subjected to the 60 earthquake inputs. Fig. 4.20 shows the coefficient of the variation for the shear force rate of the first floor. It is clear from the result that the mean shear force response of the retrofit system with TMD for 2, 4, 8 story models is smaller than that of the original structure, but the response of higher than 12 story model will be larger than that of the original structure. Especially, among these 6 models, 4 story model has the smallest mean shear force response rate. And also, the coefficient of variation for response rate of shear force is the smallest for 4 story and 8story model, it means that they have a relatively robust effectiveness. Obviously, when the TMD mass becomes heavier, both the mean shear force response rate and the coefficient of variation for shear force response rate will become smaller.

Fig. 4.21 shows the mean rate of the displacement response of the first floor subjected to the 60 earthquake inputs. Fig. 4.22 shows the coefficient of the variation for the displacement response rate of the first floor. It is clear from the result that the mean displacement response of the retrofit system with TMD is larger than that of the original structure. Among these 6 models, 4 story model has the smallest mean displacement response rate. And also, the coefficient of variation for response rate of displacement of the first floor is the smallest for 4 story and 8story model, it means that they have a relatively stable response. Obviously, when the TMD mass becomes heavier, both the mean displacement response rate and the coefficient of variation for displacement response rate will become smaller.

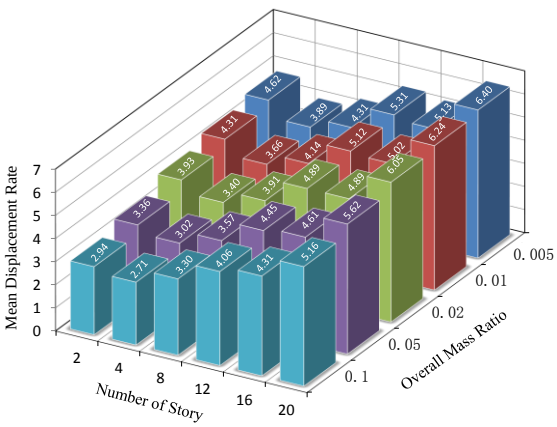

Figure 4.21 Mean displacement response rate of the first floor (Soft rate: 0.25, Hard rate: 3)

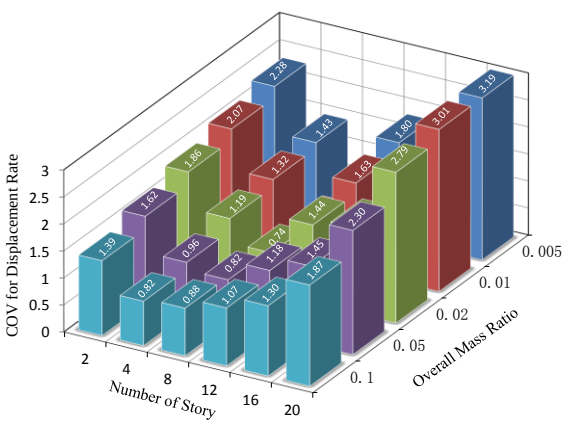

Figure 4.22 Coefficient of variation of displacement response rate of the first floor (Soft rate: 0.25, Hard rate: 3)

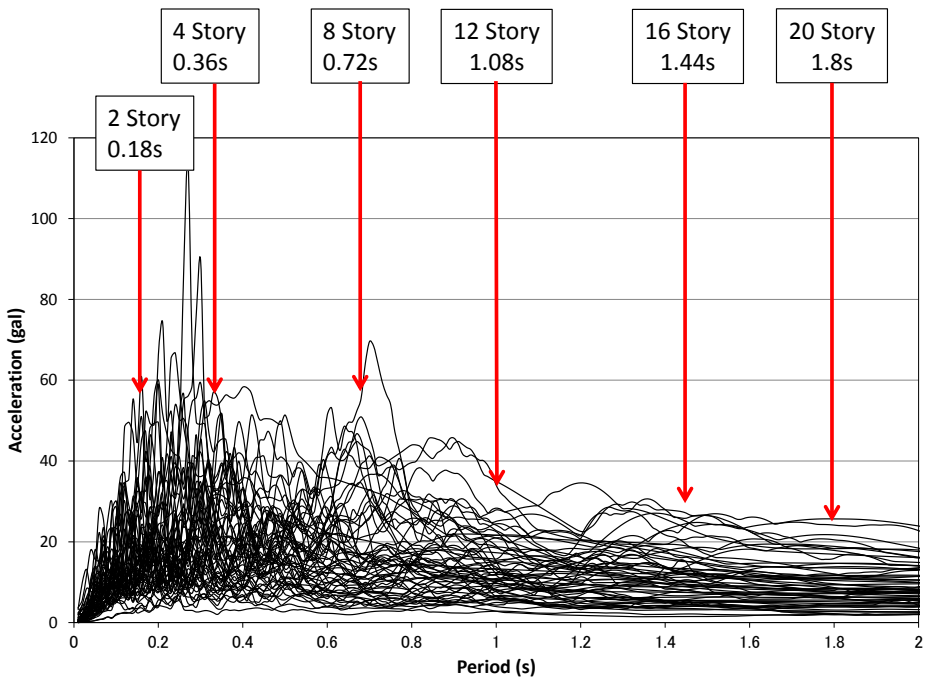

Figure 4.23 Acceleration spectrum of 60 earthquake waves

Fig. 4.23 shows the acceleration spectrum of the 60 input earthquake waves. It can be found that the natural frequencies of 4 story model and 8 story model located at a relatively high value of the spectrum. This is probably one of the reasons why the 4 and 8 story models has the best vibration reduction effect. And another conceivable reason is that, for the same overall mass ratio, when the structure has fewer numbers of stories, the TMD virtual mass ratio is larger. The virtual mass ratio is showed in Appendix F of the whole models.

Fig. 4.24 shows the maximum stroke of TMD with overall mass ratio of 0.1 under 5 input earthquake records with PGA adjusted to 0.1g for 6 types of structures with variant number of story, which has the soft-first story with the soften rate of 0.25 and harden rate of 3. It can be found that when the primary structure becomes higher, the maximum stroke of TMD will become larger.

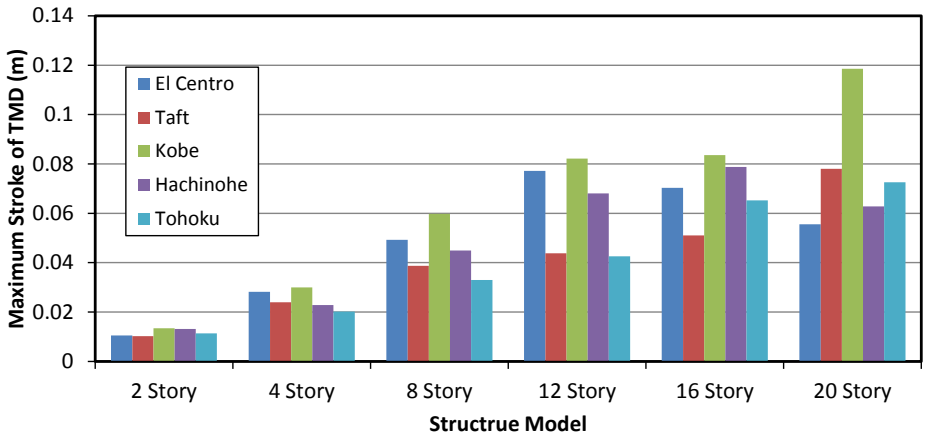

Figure 4.24 Maximum stroke of TMD under the input earthquake records with adjusted PGA of 0.1g

4.5 Comparison of the Proposed Hybrid Seismic Retrofit System with the Pure Dashpot System

Juikai building and Yachio Bank were introduced in Chapter One as the real example of Soft-first story structures, and the pure dashpot was adopted as their energy dissipation component placed at the ground floor. The comparison of Soft-first story structure with TMD (Fig. 4.23) and with pure dashpot (Fig. 4.24) is carried out in this section.

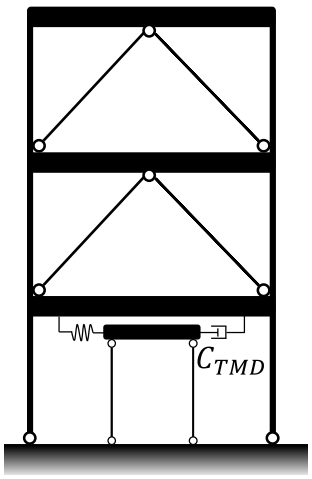

Figure 4.23 Soft-fist story structure with TMD supported from ground

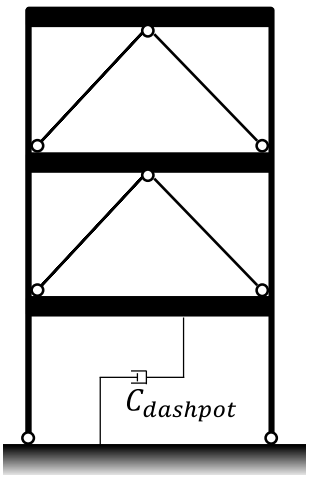

Figure 4.24 Soft-first story structure with the pure dashpot at the ground floor

6 types of model are adopted here, which is the same as used in the former section, with different number of floors: 2, 4, 8, 12, 16 and 20, respectively. The ratio of damping factor of the dashpot which used in the pure dashpot system to the damping factor of the viscous damper in TMD, $C_{dashpot}/C_{TMD}$, is adopted as the parameter.

Fig. 4.25 showed the response ratio of the maximum acceleration of the top floor of the structure with pure dashpot system to the one with TMD system. It can be found that when $C_{dashpot}/C_{TMD}$ becomes larger, the acceleration response ratio of pure dashpot system to TMD system will become smaller. And for example, in order to let them have an equal response, damping factor of pure dashpot should be about 10 times larger than that of TMD for 12 story model.

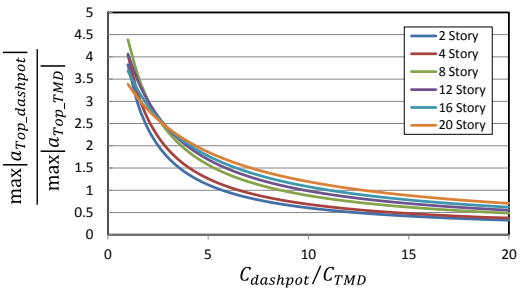

Figure 4.25 Response ratio of the maximum acceleration of the top floor

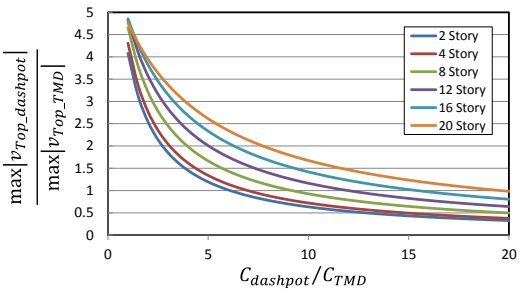

Figure 4.26 Response ratio of the maximum velocity of the top floor

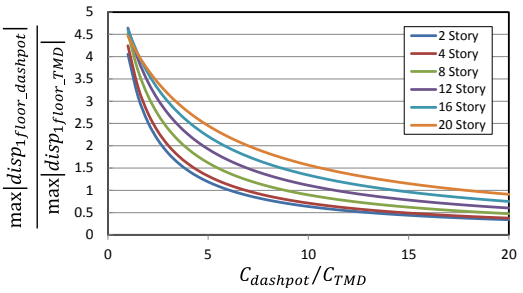

Figure 4.27 Response ratio of the maximum drift from the first floor to the top floor

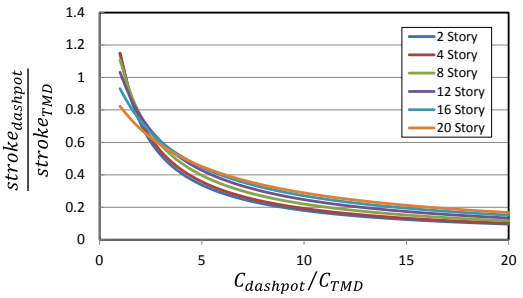

Figure 4.28 Response ratio of the maximum stroke of the pure dashpot to TMD

Fig. 4.26 showed the response ratio of the maximum velocity of the top floor of the structure with pure dashpot system to the one with TMD system. It can be found that when $C_{dashpot}/C_{TMD}$ becomes larger, the velocity response ratio of pure dashpot system to TMD system will become smaller. And for example, in order to let the two structures have an equal velocity response, damping factor of pure dashpot should be about 12 times larger than that of TMD for 12 story model.

Fig 4.27 showed the response ratio of the maximum drift from the first floor to the top floor of the structure with pure dashpot system to the one with TMD system. Similarly, it can be found that when $C_{dashpot}/C_{TMD}$ becomes larger, the drift response ratio of pure dashpot system to TMD system will become smaller. Fig 4.28 showed the response ratio of the maximum stroke of the pure dashpot to TMD. It can be found that when the damping factor of the pure dashpot is about 10 times larger than that of TMD, the maximum stroke ratio is about 0.2 of the pure dashpot to TMD.

4.6 Conclusion

In this chapter, the frequency response analysis and earthquake response analysis are carried out to explore the effect of proposed seismic retrofit system.

6 kinds of structures, number of stories are 2, 4, 8, 12, 16 and 20 are adopted in this study. The lateral stiffness ratio of the first story of the retrofitted structure to the original structure is selected to vary from 1 to 0.25 with increments of 0.25; while, the lateral stiffness ratio of the upper story of the retrofitted structure to the original structure is selected to vary from 1 to 3 with increments of 0.25.

In the frequency response analysis, Laplace transformation is used in the frequency response analysis. And in the earthquake response analysis, a set of 60 horizontal components of earthquake records were adopted, and Newmark- β method is used to solve the motion equilibrium equation here.

From the result of the frequency response analysis and earthquake response analysis, we can get the conclusion as follows.

1) The softening of the lateral stiffness of the first floor and the hardening of the lateral stiffness of the upper floors can increase the TMD virtual mass ratio. For example, when the TMD overall mass ratio is 0.1, the virtual mass ratio is 0.038, 0.011,0.003 and 0.00045 for 2 story model, 4 story model, 8 story model and 20 story model, respectively, if the lateral stiffness has been not changed either for the first floor nor the upper floor. And it can be increased to 0.093, 0.080, 0.060, and 0.027, respectively, if the lateral stiffness of the first floor was softened to 0.25 times and the stiffness of the upper floors were hardened up to 3 times.

2) The softening of the lateral stiffness of the first floor will extend the natural period of the TMD combined system and reduce the peak acceleration response of the top floor and the peak drift response from the first floor to the top floor.

3) The hardening of the lateral stiffness of the upper floors will shorten the natural period of the combined system and reduce the peak acceleration response of the top floor and the peak drift response from the first floor to the top floor.

4) As expected, the softening of the lateral stiffness will donate much more than the hardening of the lateral stiffness of the upper floors in reducing acceleration response. Oppositely, the hardening of the lateral stiffness of the upper floors will contribute much more than the softening of the lateral stiffness in reducing the drift response.

5) Although the response of the displacement of the first floor may become larger than that of original structure caused by the stiffness softening of the first floor or the stiffness hardening of the upper floors, the maximum shear force in the first floor will still be smaller than that of original structure.

6) When the other parameters (TMD mass, Stiffness soften rate, Stiffness harden rate) keep constant, when the controlled structure has less number of floors, the vibration mitigation effect will be better, including the acceleration response of the top floor, the drift from the first floor to the top floor.

7) From the average result of earthquake response analysis, 4 story model and 8 story model have the best vibration mitigation effect including the control of acceleration response of the top floor and the drift from the first floor to the top floor. According to the result of the coefficient of variation of the response rate, 4 story model and 8 story model have the best stability among those six models. This is probably because of the predominant frequencies of the input earthquakes are close to the natural frequency of the objective structure.

Chapter 5

Shaking Table Test for the Proposed Hybrid Seismic Retrofit Systems

5.1 Introduction

In order to test the effectiveness of the proposed retrofit system for steel structures, a shaking table test was carried out with a scale model. This steel frame model is based on a benchmark model for structure control [5-1] [5-2]. There are two benchmark problems using this structure, one is active mass driver system (Fig. 5.1) and another is active tendon system (Fig. 5.2). This three story benchmark structure is selected because of the widespread interest in this class of systems [5-3] [5-4] [5-5]. The prototype of this building was discussed by Chung, which was subject to one-dimensional ground motion in that study [5-6].

In this study, we choose this benchmark system for dealing with a new structural control problem: a seismic retrofit system using TMD and Soft-first story proposed here. Two types of retrofit patterns, which will be introduced in Chapter 5.3 and 5.4, were used here. Sweep wave, Whitenoise and 5 Earthquake records were adopted as the input for the shaking table. Finally, the maximum response of absolute acceleration of the top floor, the maximum response of displacement angle from the first floor to the top floor, the maximum response of displacement angle of the first floor were adopted to illustrate the effect of this retrofit system.

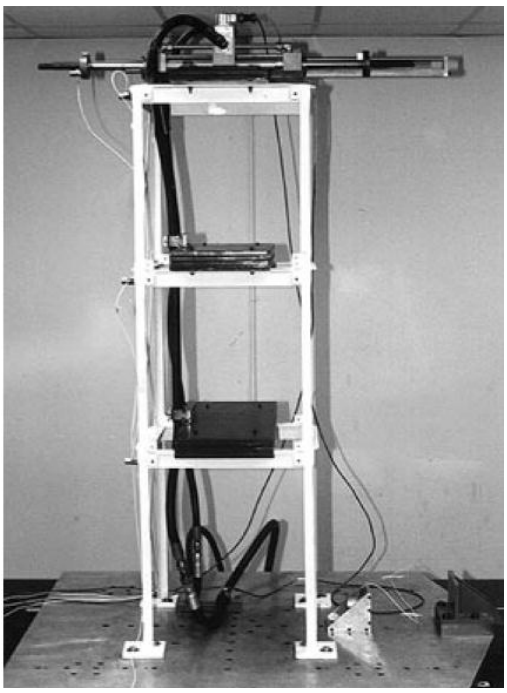

Figure 5.1 Three Degree-of-Freedom test structure with AMD system [5-1]

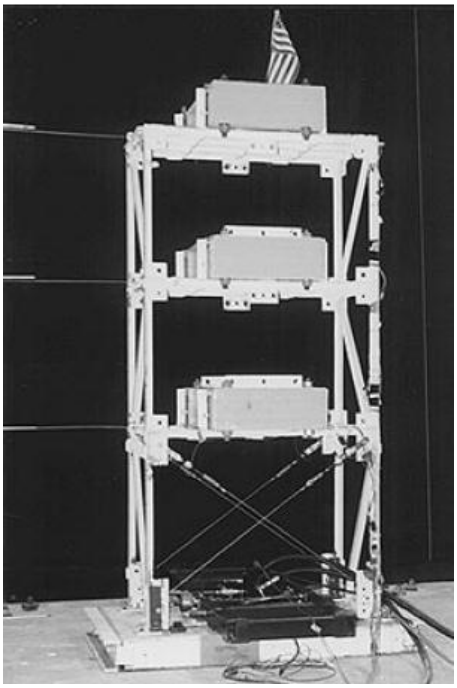

Figure 5.2 Three Degree-of-Freedom test structure with active tendon system [5-2]

5.2 Information of the Test Model

Fig. 5.3 shows the three story steel frame specimen of the shaking table test with height of 102cm and weight of 38.4kg. And the natural frequency is 5.3Hz, 14.8Hz and 22.1Hz, respectively for the three modes. The basic model information is collected in Table 5.1. While the similarity scale of this specimen to the original building is listed in Table 5.2.

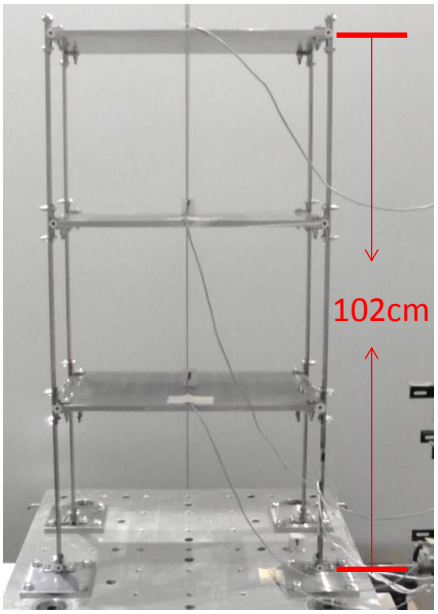

Figure 5.3 Three Degree-of-Freedom shaking table test model

Table 5.1 Model information

Mass		38.4kg
Height		102cm
Frequency	Mode1	5.3Hz
	Mode2	14.8Hz
	Mode3	22.1Hz

Table 5.2 Model similarity scale

Quantity	Rate
Force	1:500
Length	1:10
Time	1:5
Acceleration	2.5:1
Mass	1:1250

Eq. 5.1 and Eq. 5.2 shows the mass matrix and stiffness matrix, respectively, of this Three Degree-of-Freedom frame.

$$M = \begin{bmatrix} 13.0 & & \\ & 12.7 & \\ & & 12.7 \end{bmatrix} kg \qquad 5.1$$

$$K = \begin{bmatrix} 2k & -k & \\ -k & 2k & -k \\ & -k & k \end{bmatrix}, \; k = 69500N/m \qquad 5.2$$

The measuring system is showed in Fig. 5.4, 14 channels of data would be recorded during the test time. They include 5 channels of displacement, which measures the displacement of each floor of the frame, TMD mass and the shaking table, 5 channels of acceleration, which measures the acceleration of each floor of the frame, TMD mass and shaking table, and 4 channels of strain gage, which measures the strain inside and outside surface at the top and bottom of the column of the first story, respectively. And the sampling frequency was set to 1000Hz with a low pass filter of 100Hz.

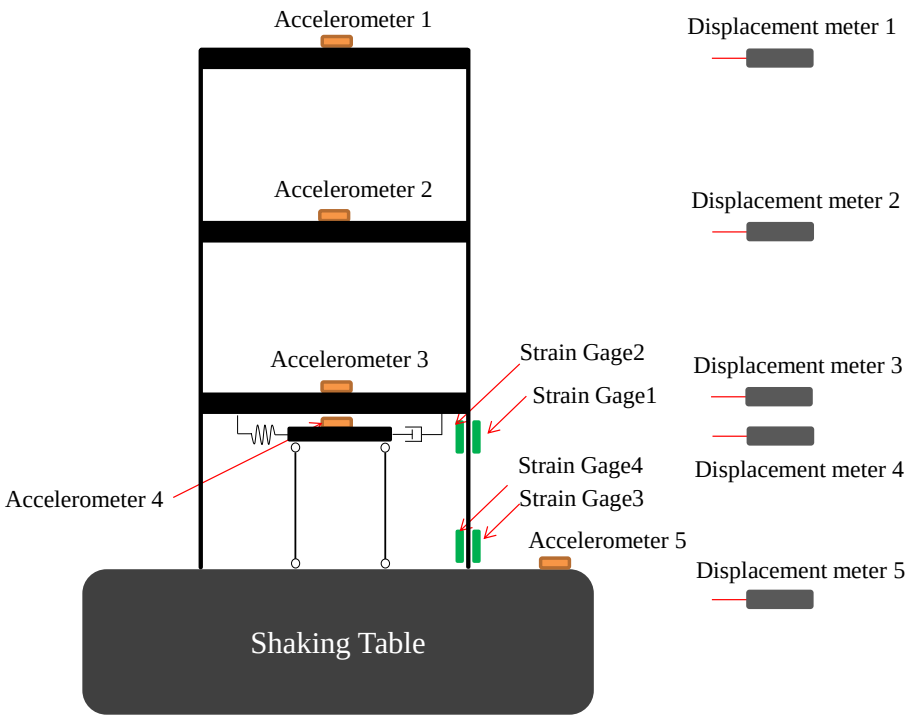

Figure 5.4 Measuring system

Before the input of earthquake wave, sweep wave was adopted to test the basic property of the specimen and also for the adjusting of the TMD tuning ratio. The frequency of this sweep wave is from 2Hz to 35Hz and return to 2Hz with a speed of

6Hz/min. After the complement of the tuning adjusting of the spring, two whitenoise waves, with a frequency from 0~8Hz (Fig. 5.5) and 0~35Hz (Fig. 5.6), respectively, and 5 earthquake waves (Fig. 5.7~Fig. 5.11) were adopted as the input of the shaking table. Note that, because of the time scale is 1:5, the time of the input earthquake waves were shorten to 5 times quicker than the real records. The information of the whole input waves is listed in Table 5.3.

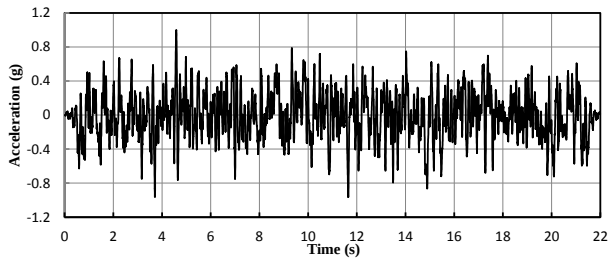

Figure 5.5 Whitenoise wave 1 (0~8Hz)

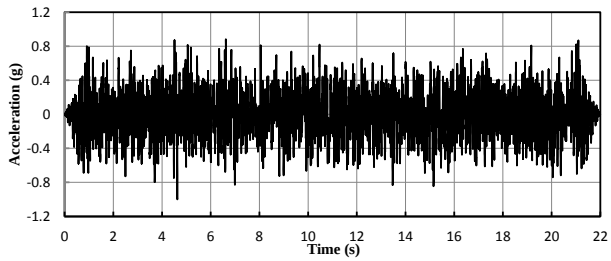

Figure 5.6 Whitenoise wave 2 (0~35Hz)

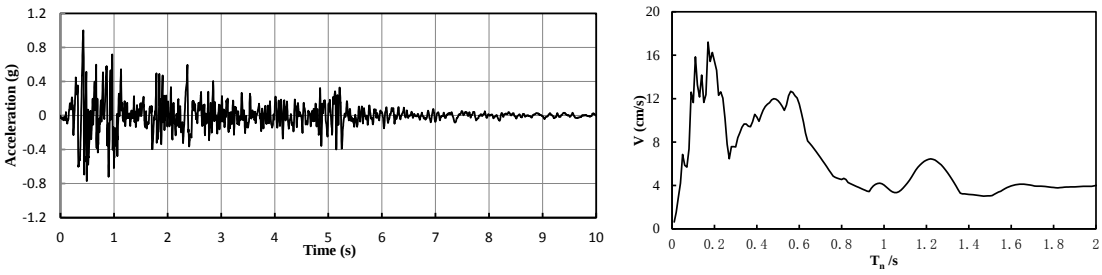

a) Time history curve b) Velocity response spectrum

Figure 5.7 El Centro_NS, 1940

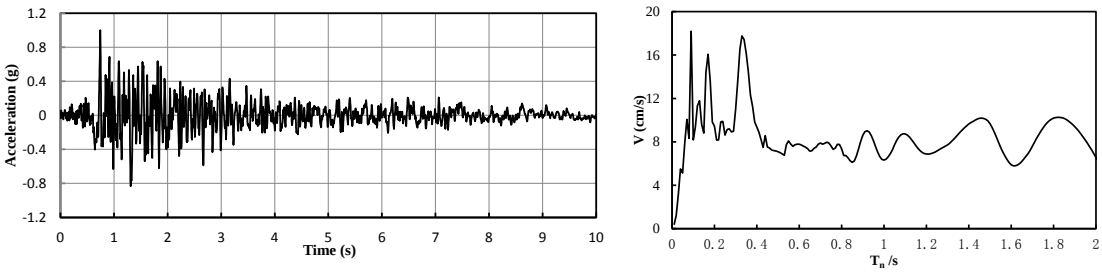

a) Time history curve b) Velocity response spectrum

Figure 5.8 Taft_EW,1952

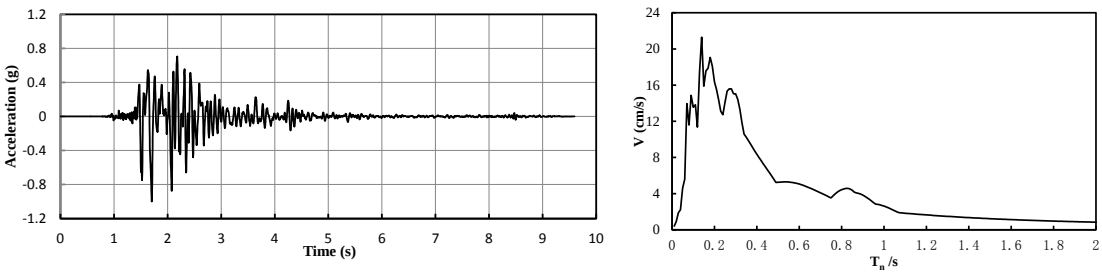

a) Time history curve b) Velocity response spectrum

Figure 5.9 Kobe_NS,1995

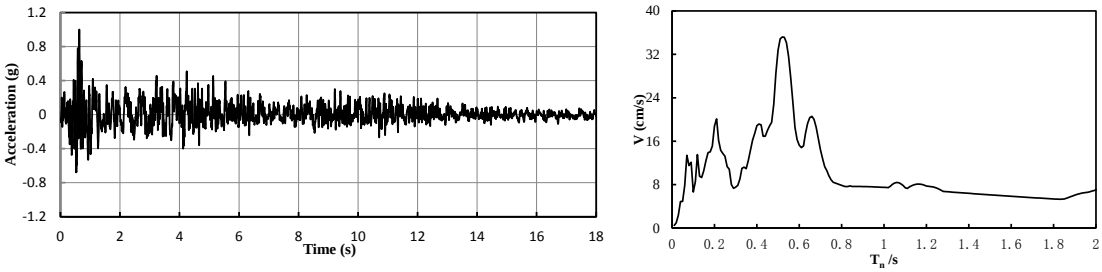

a) Time history curve b) Velocity response spectrum

Figure 5.10 Hachinohe_NS,1968

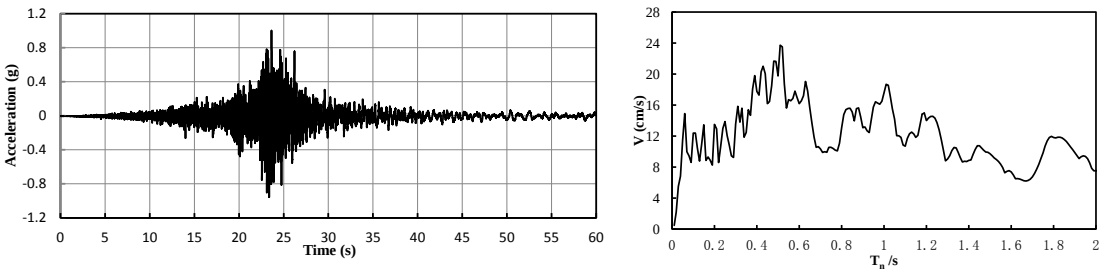

a) Time history curve b) Velocity response spectrum

Figure 5.11 Tohoku_EW,2011

Table 5.3 Input wave information

Input Wave	PGA (g)	
Sweep (2~35~2Hz)	0.02	
Whitenoise1 (0~8Hz)	0.25	
Whitenoise2 (0~35Hz)	0.25	
NS_El Centro (1940)	0.25	0.5
EW_Taft (1952)	0.25	0.5
NS_Kobe (1995)	0.25	0.5
NS_Hachinohe (1968)	0.25	0.5
NS_Tohoku (2011)	0.25	0.5

5.3 Free Vibration Test For Damping Measurement

There are two types of dampers adopted as the TMD damper here, one is rotary damper [5-7] which adopted silicone oil as the damping material, and its damping force has a linear relation with the velocity. The rotary damper is used as the non-traditional damper connects TMD mass with ground. Another one is air damper [5-8] which is made of aluminum alloy and its damping ratio could be changed continuously by an adjusting screw. The air damper is used as the traditional damper connects TMD mass with the structure.

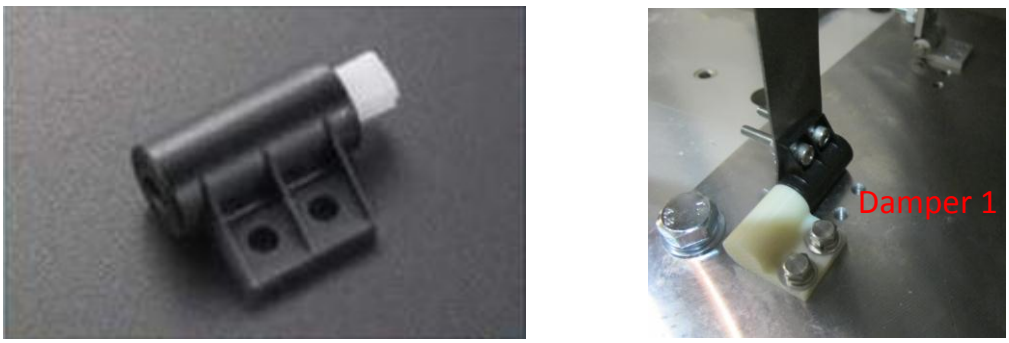

a) Picture of rotary damper [5-7] b) Damper setup

Figure 5.12 Rotary damper

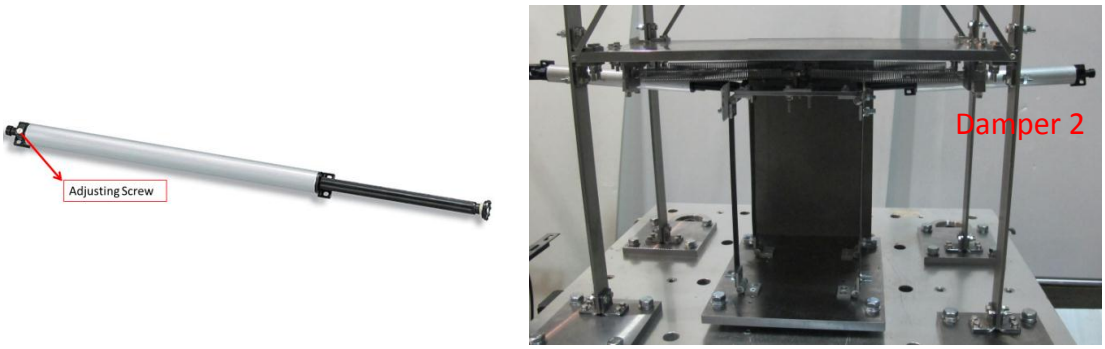

a) Picture of air damper [5-8] b) Damper setup

Figure 5.13 Air damper

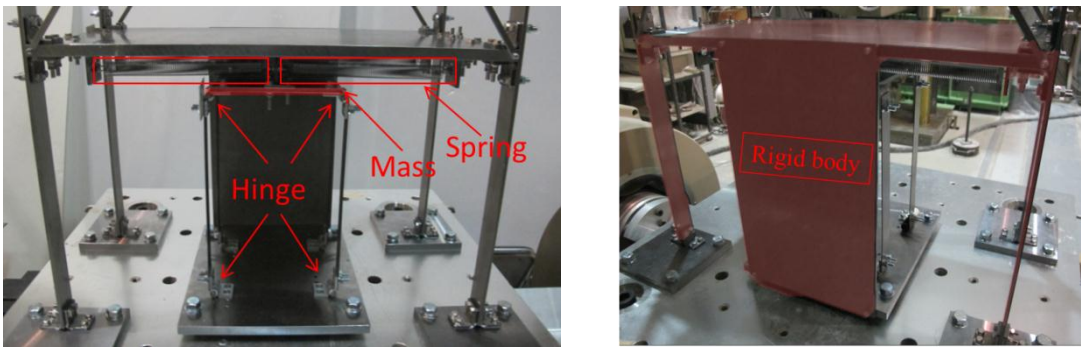

a) Front view b) Dorsal view

Figure 5.14 1DOF Test system

In order to obtain the damping ratio of the dampers used in this test, a 1DOF system is used here with mass of 1kg and spring stiffness of 296N/m. The damping ratio is assumed linearly relative with velocity, a pure viscous damping, thus a free vibration test could be used to determine the damping ratio easily. The test system is showed in Fig. 5.14, when the damper was installed to the structure, an initial displacement would be loaded and released to excite the free vibration. The displacement of the mass is recorded, and used to determine the damping ratio of the rotary damper and the air damper using Eq. 5.3 [5-9].

$$\xi = \frac{1}{2\pi j} ln \frac{u_i}{u_{i+j}} \qquad 5.3$$

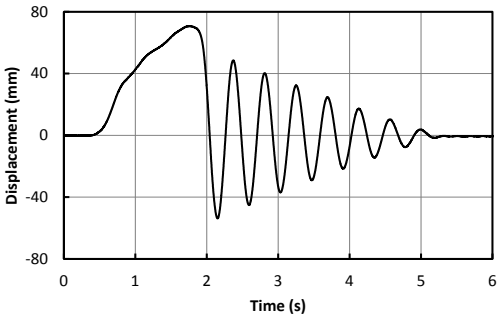

Figure 5.15 Displacement response without damper

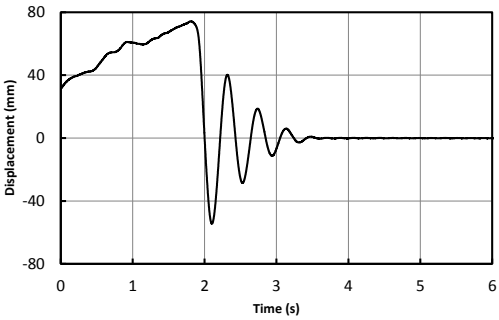

Figure 5.16 Displacement response with two rotary dampers

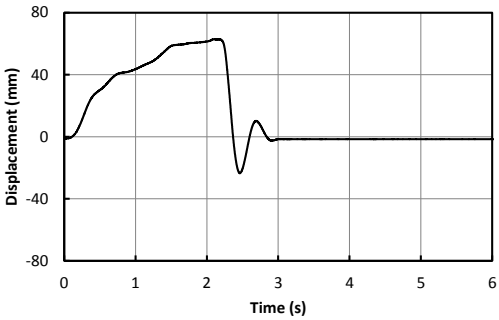

Figure 5.17 Displacement response with two air dampers

Fig. 5.15 shows the result of the displacement response for the 1DOF system without installing any damper. The damping ratio could be obtained as $\xi_0 = 0.029$.

Fig. 5.16 shows the result of the displacement response for the 1DOF system with 2 rotary dampers. The damping ratio could be obtained as $\xi_{Rotary} = 0.15$, and $C_{Rotary} = 2m\xi\omega$ =1.7N/m/s .

Fig. 5.17 shows the result of the displacement response for the 1DOF system with 2 air dampers. The damping ratio could be obtained as $\xi_{Air} = 0.36$, and $C_{Air} = 2m\xi\omega$ =4.7N/m/s .

5.4 Shaking Table Test of Retrofit Pattern 1

5.4.1 Introduction

Fig. 5.18 shows the retrofit system of pattern 1, the benchmark model of the steel frame with three stories is adopted as the original structure. For pattern 1, the way to soften the lateral stiffness of the first story is taking place the fixed boundary at the bottom of the column with pinned boundary, which is named Soft-first Story (SFS) Structure here. Then, two TMDs with different mass will be installed into the soft first story, which is named SFS with TMD1 and SFS with TMD2, respectively.

Further, the way to strengthen the lateral stiffness of the upper floors of a SFS structure is adding braces into the upper floors, which is named Soft-first Story Hard-upper Story Structures (SFS-HUS). Then, two TMDs with different mass will be installed into the soft first story, which is named SFS with TMD1 and SFS with TMD2, respectively. The concept of this method is showed in Fig. 5.18.

Fig. 5.19 shows the test specimen of each model including Original Structure, SFS Structure, SFS-HUS Structure without TMD, SFS with TMD1, SFS with TMD2, SFS-HUS with TMD1, and SFS-HUS with TMD2. Two rotary dampers were used in the model of SFS with TMD1, and three rotary dampers were used in the model of SFS-HUS with TMD1. While, in the model of SFS with TMD2, we used two air dampers without rotary dampers. In the model of SFS-HUS with TMD2, we used two air dampers and two rotary dampers. Dampers were decided based on the optimum damping ratio.

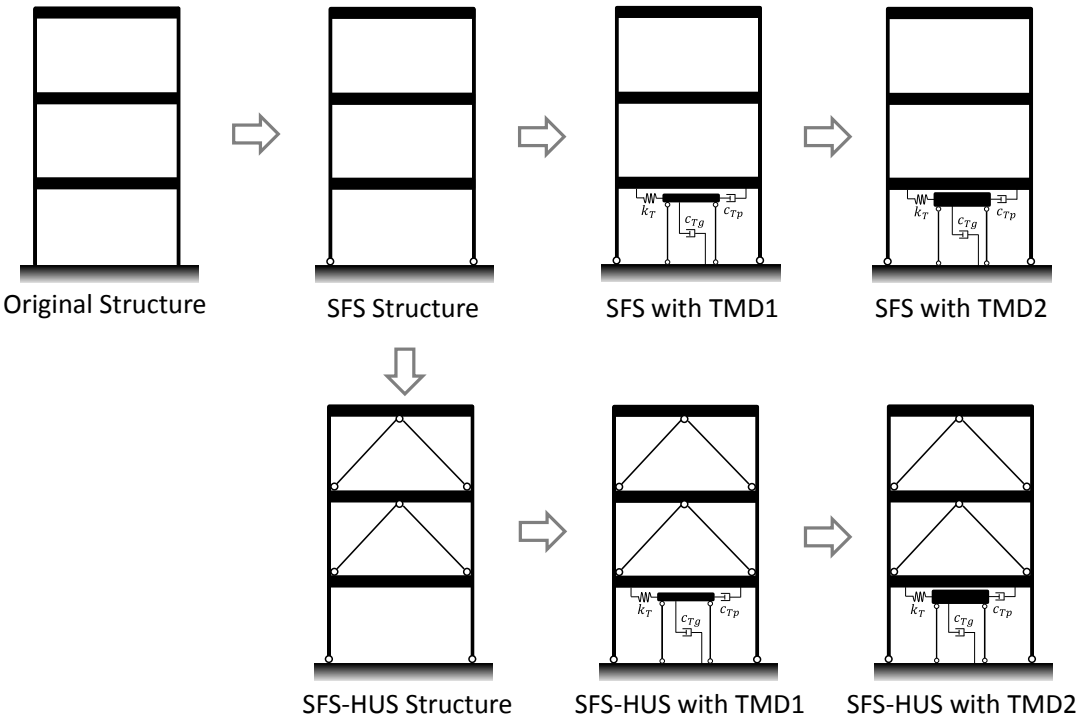

Figure 5.18 The retrofit system of pattern 1

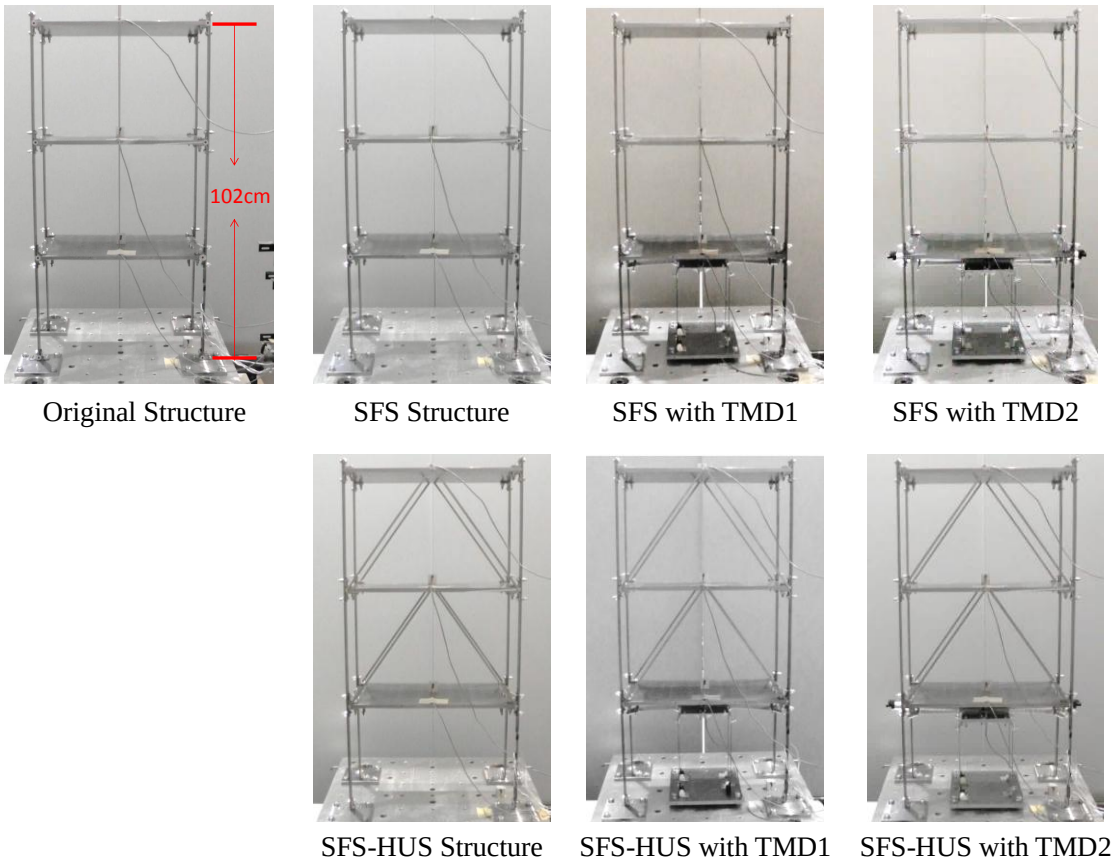

Figure 5.19 The test specimen of pattern 1

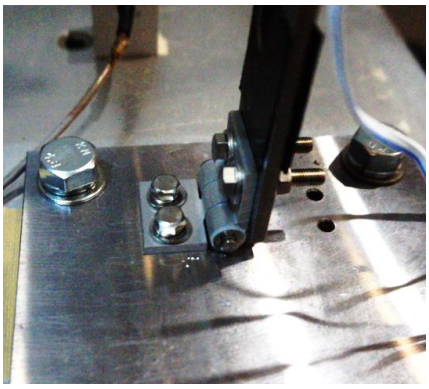

a) Pinned connection

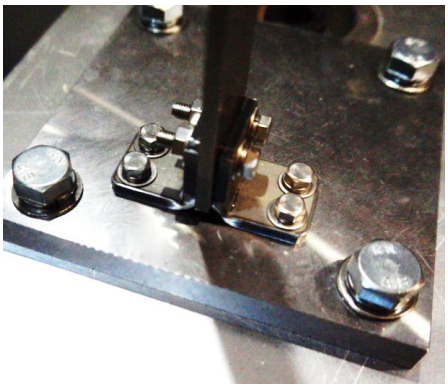

b) Fixed connection

Figure 5.20 Pinned and fixed connection of columns

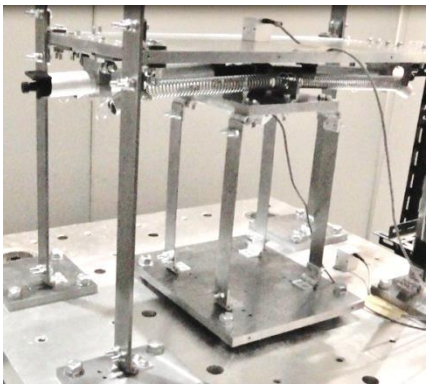

a) The front view

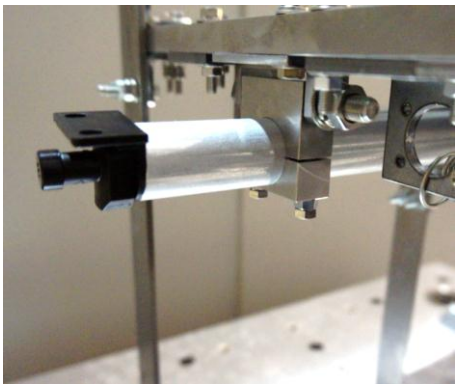

b) Pinned connection

Figure 5.21 Test setup of air dampers

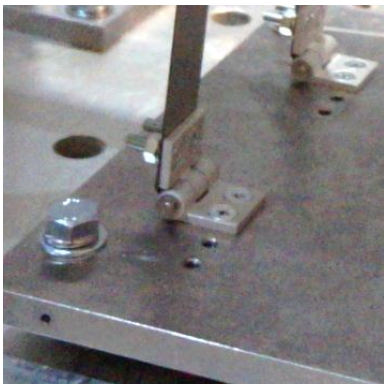

a) Original pinned connection

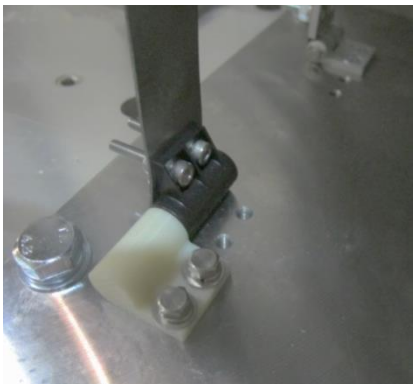

b) Setup with rotary dampers

Figure 5.22 Test setup of rotary dampers

Fig. 5.20 shows the fixed connection and pinned connection of the column which is used for the original structure and SFS structure. Fig. 5.21 shows the setting of the air damper, the end connected with the primary structure is a pinned connection which allowed the damper doing in-plane rotation. Fig. 5.22 shows the setup of the rotary dampers. When the rotary dampers are not used, a hinge will be connected on.

Table 5.4 Natural frequencies of the models without TMD

Model Type	Natural Frequency (Hz)		
	Mode 1	Mode 2	Mode 3
Original Structure	5.3	14.8	22.1
SFS Structure	2.8	12.8	21.3
SFS-HUS Structure	3.1	—	—

Table 5.5 Information of the TMD parameter of the seismic retrofit system

Model Type	Mass Ratio	Tuning Ratio	Damping Ratio	
			ξ_{Tg}	ξ_{Tp}
SFS with TMD1	0.02	1.074	0.087	0
SFS-HUS with TMD1	0.025	1.039	0.127	0
SFS with TMD2	0.046	1.052	0	0.112
SFS-HUS with TMD2	0.055	1.018	0.039	0.108

The natural frequencies of the models of Original Structures, SFS Structures and SFS_HUS Structures are listed in Table 5.4. The information of the TMD parameters of the combined system, including mass ratio, tuning ratio and damping ratio, are listed in Table 5.5.

5.4.2 Test result

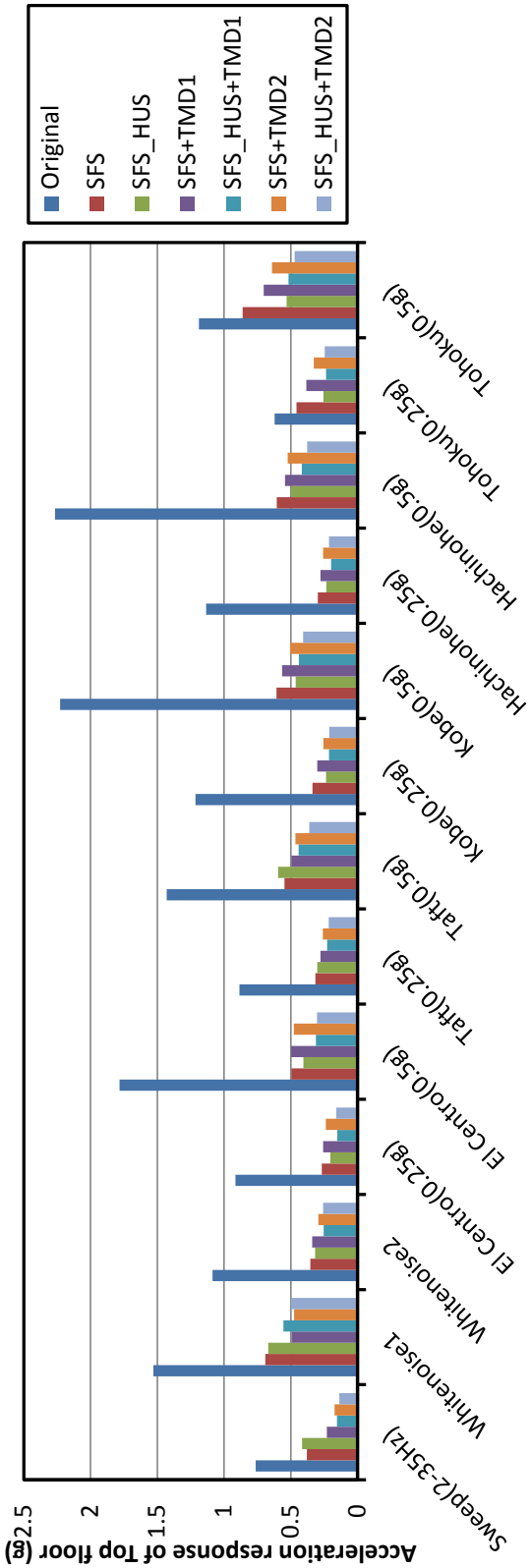

Figure 5.23 The maximum acceleration response of top floor

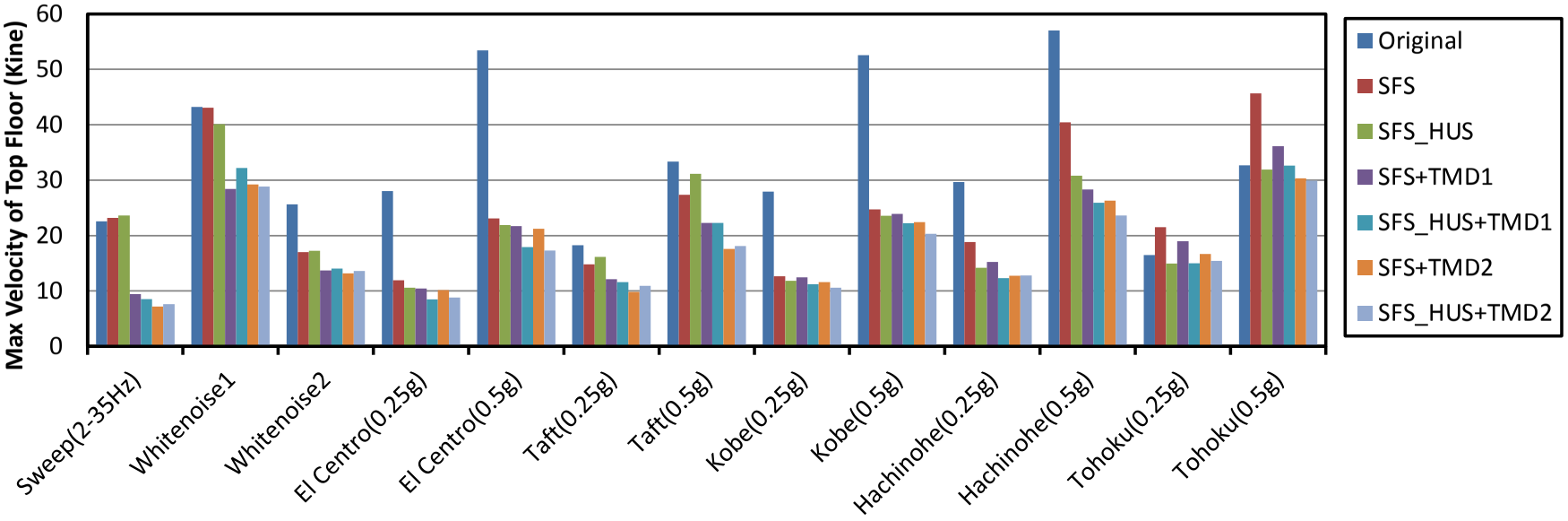

Figure 5.24 The maximum velocity response of top floor

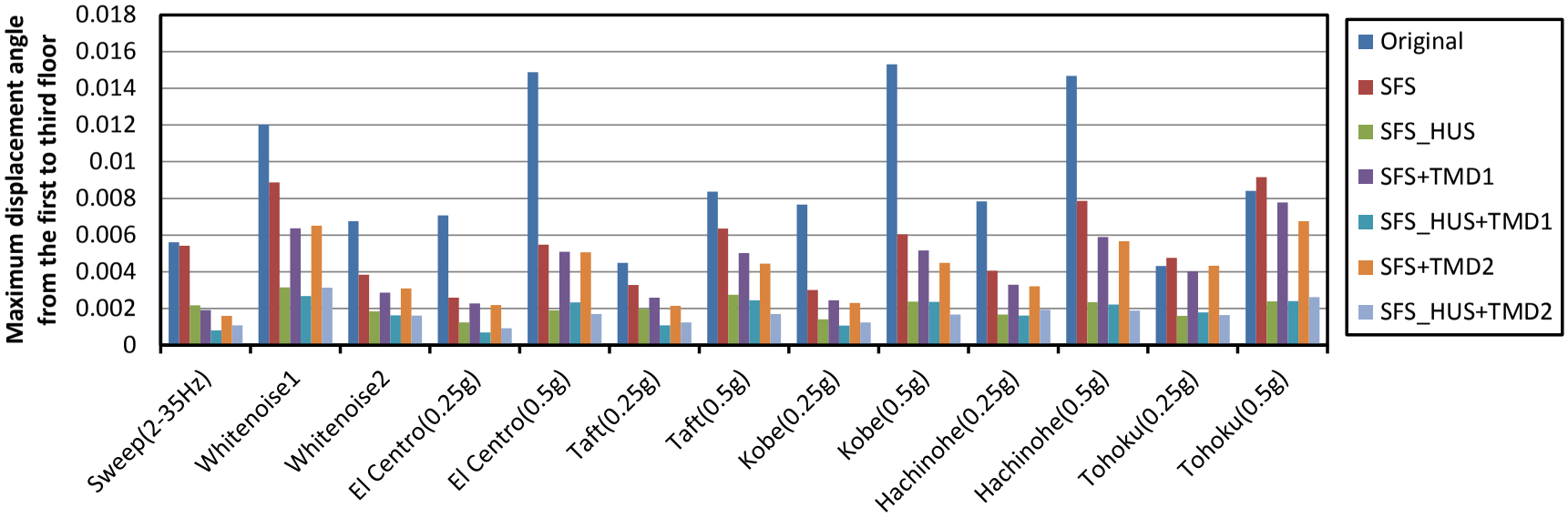

Figure 5.25 The maximum displacement angle from the first to the top floor

Fig. 5.23 shows the maximum acceleration response of top floor of the whole seven models subjected to 13 ground excitations including one sweep wave, two whitenoise and 10 earthquake inputs. From the result of the sweep input, where the peak response means the resonant response, the combined TMD system has the lowest acceleration response and the response of SFS_HUS with TMD is smaller than that of SFS with TMD. Furthermore, for the systems with the same stiffness but different TMD, for example, SFS with TMD1 and SFS with TMD2, the one with a heavier TMD has a smaller peak response.

For the whitenoise input or earthquake input, we can get the same extend that the peak acceleration response could be reduced significantly to about 0.2~0.5 times of the original structure. The response of SFS_HUS with TMD is smaller than that of SFS with TMD. Furthermore, for the systems with the same stiffness but different TMD, the one with a heavier TMD has a smaller peak response.

There is an important phenomenon that when the predominant frequencies of the input earthquake wave close to the original structure, a better vibration control effect could be obtained for the proposed retrofit system. For example, Kobe and Hachinohe both has a peak at about 0.2 Hz, which can be found from Fig. 5.11, which is very close to the structural natural frequency of the first mode. The vibration mitigation decrement of these two inputs is very high up to about 80%.

Fig. 5.24 shows the maximum velocity response of top floor of the whole seven models subjected to 13 ground excitations including one sweep wave, two whitenoise and 10 earthquake inputs. From the result of the sweep input, the combined TMD system has the lowest velocity response and the response of SFS_HUS with TMD is smaller than that of SFS with TMD. Furthermore, for the systems with the same stiffness but different TMD, for example, SFS with TMD1 and SFS with TMD2, the one with a heavier TMD had a smaller peak response.

For the whitenoise input or earthquake input, we can get the same extend that the peak velocity response could be reduced significantly down to about half of the original structure. The response of SFS_HUS with TMD is smaller than that of SFS with TMD. Furthermore, for the systems with the same stiffness but different TMD, the one with a heavier TMD has a smaller peak response.

In order to confirm whether the frame especially the damper is still in a linear stage or not, two-stage GPA of earthquake was adopted in the shaking table test. The response of acceleration and velocity demonstrated that the system was still in a linear stage.

Fig. 5.25 shows the maximum displacement angle from the first to the top floor. From the result of the sweep input, we can see that the combined TMD system has the lowest acceleration response and the response of SFS_HUS with TMD is smaller than that of SFS with TMD. Furthermore, for the systems with the same stiffness but different TMD, the one with a heavier TMD has a smaller peak response.

For the whitenoise input or earthquake inputs, we can get the same extend that the peak displacement angle of the SFS with TMD systems could be reduced to about 0.4~0.8 times of the original structure. The response of SFS_HUS with TMD is much smaller about 50% of that of SFS with TMD. Furthermore, for the systems with the same stiffness but different TMD, the one with a heavier TMD has a smaller peak response. The phenomenon that when the predominant frequencies of the input earthquake wave close to the original structure, a better vibration control effect could be obtained, can also be found here.

The acceleration spectrum of the input earthquake is showed in Fig. 5.26. This could be an important reference to explain why there are differences among vibration reduction effects for different input earthquake waves in the test result. For example, the reduction effect of acceleration response showed in Fig.5.24 is better for El Centro (1940) than Tohoku (2011). It may be explained that the spectrum value at the period for original structure is much larger for El Centro than Tohoku, and it's almost the same for SFS structure and SFS_HUS structure.

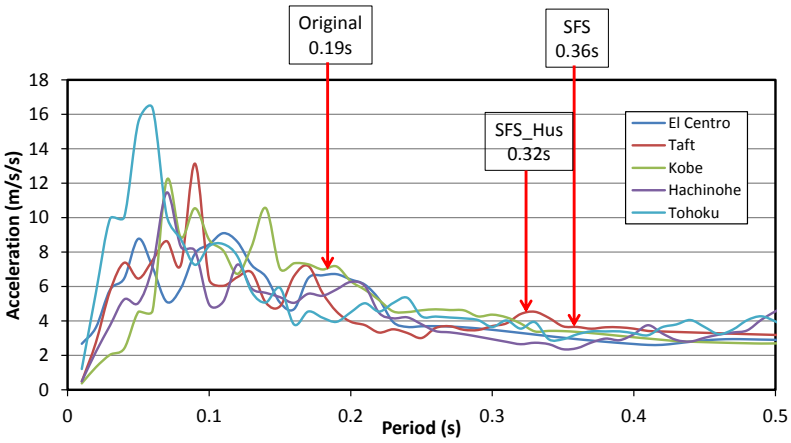

Figure 5.26 Acceleration spectrum of the input earthquake

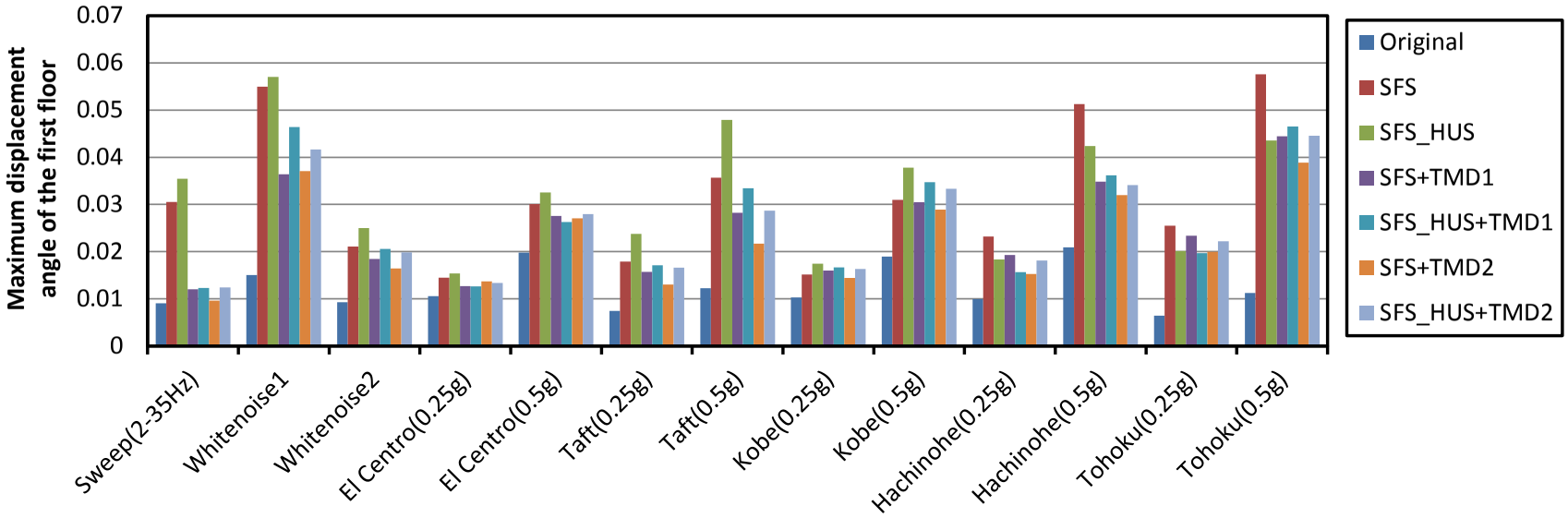

Figure 5.27 The maximum displacement angle of the first floor

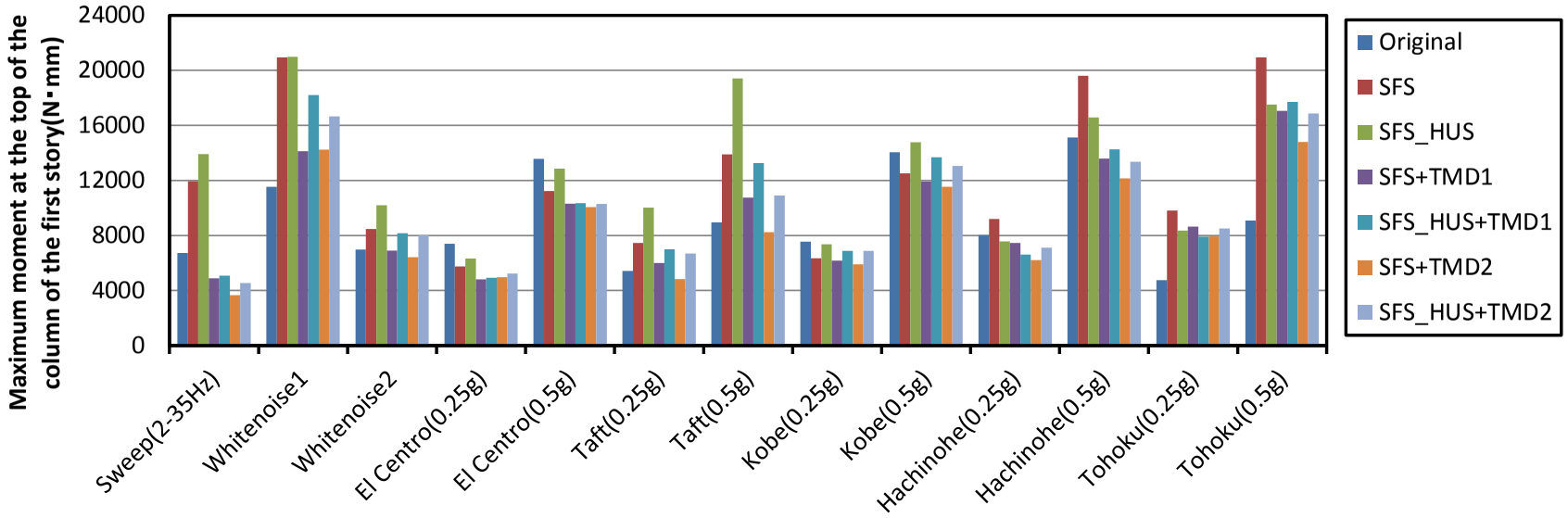

Figure 5.28 The maximum moment at the top of the column of the first floor

Because the stiffness of the first floor is softened, it is necessary to pay attention to the response of the first floor. Fig. 5.27 shows the maximum displacement angle of the first floor. Fig. 5.28 shows the maximum moment at the top of the column of the first floor. From the result of the sweep input, we can see that the displacement of the first floor of the combined TMD system is larger than that of the original structure, while the maximum moment at the top of the column of the first floor of the combined TMD system is still smaller than that of the original structure.

For the whitenoise input or earthquake inputs, we can get the same extend that the peak displacement of the first floor of the combined TMD systems will be normally larger than that of the original structure. When the predominant frequencies of the input earthquake wave close to the original structure, which will cause a better vibration control effect mentioned above, the maximum moment at the top of the column of the first floor will still be smaller than that of the original structure.

From the result of the acceleration and velocity response of the top floor of Fig. 5.23, 5.24, it could be found that the retrofitted system only with the stiffness softening without TMD still reduced the response greatly. This probably because of the prolonged natural period of the retrofitted structure is distant from the predominant period of the input earthquake wave. But without TMD, the displacement response of the first floor of SFS structure will become much larger than that of the original one. If the TMD is placed at the ground floor, even if the reduced displacement response of the first floor was still larger than that of the original structure, the moment at the top of the column could be reduced to almost the same as the original structure. Furthermore, there is another important reason for using TMD is that, only stiffness softening or hardening could not reduce the resonant response of the structure.

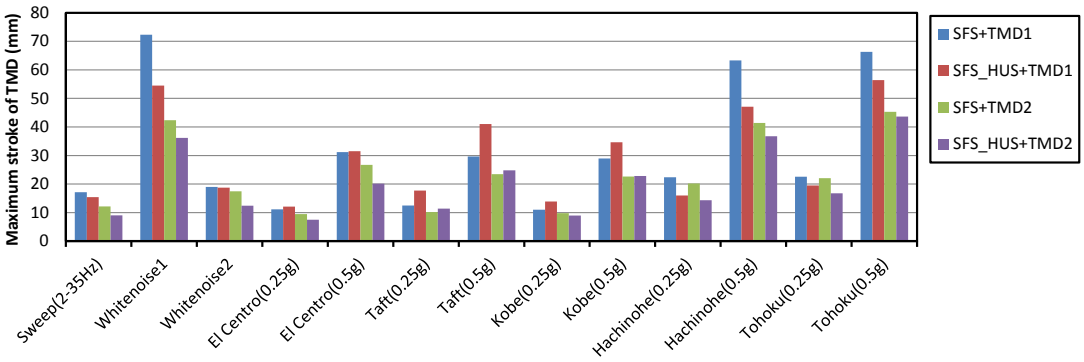

Figure 5.29 The maximum stroke length of the TMD

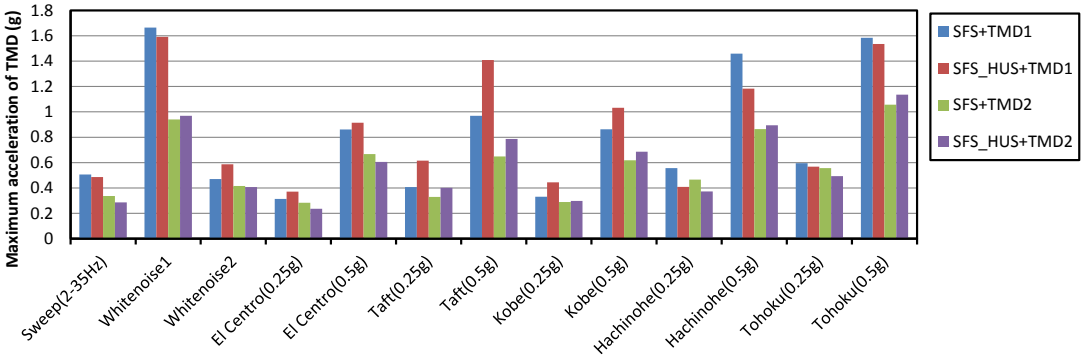

Figure 5.30 The maximum acceleration response of the TMD

Fig. 5.29 shows the maximum stroke of the TMD, and Fig. 5.30 shows the maximum acceleration of the TMD. From the result, we can conclude that, when a heavier TMD mass is adopted, the stroke length and the acceleration response of the TMD mass will become smaller.

5.4.3 Numerical simulation

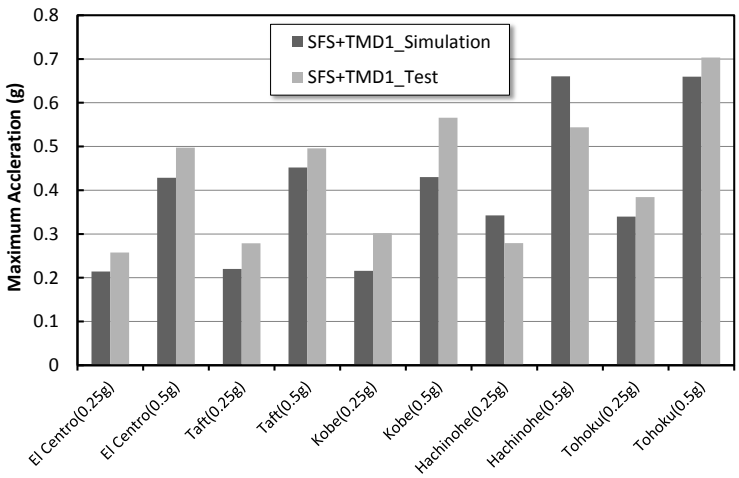

Figure 5.31 Maximum acceleration response for SFS with TMD1

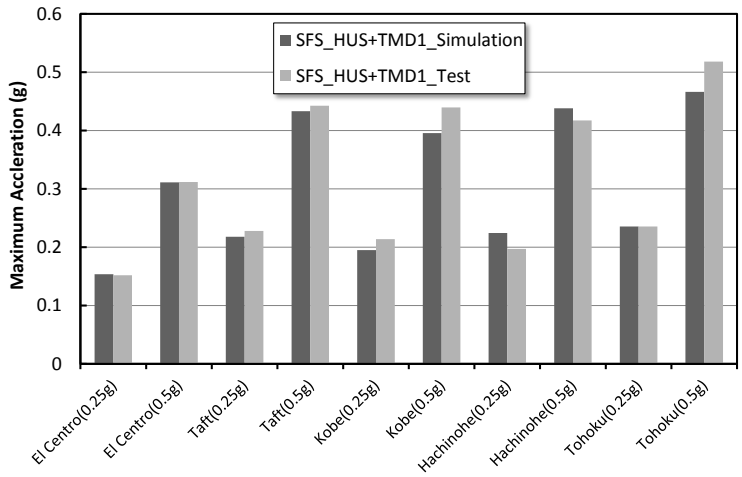

Figure 5.32 Maximum acceleration response for SFS_HUS with TMD1

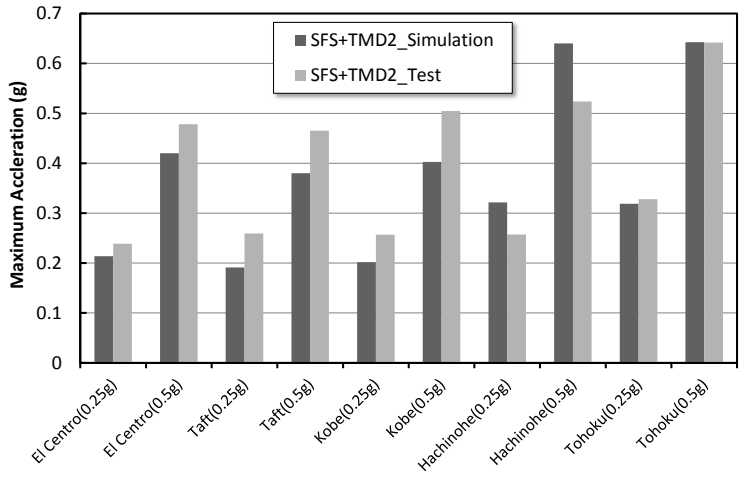

Figure 5.33 Maximum acceleration response for SFS with TMD2

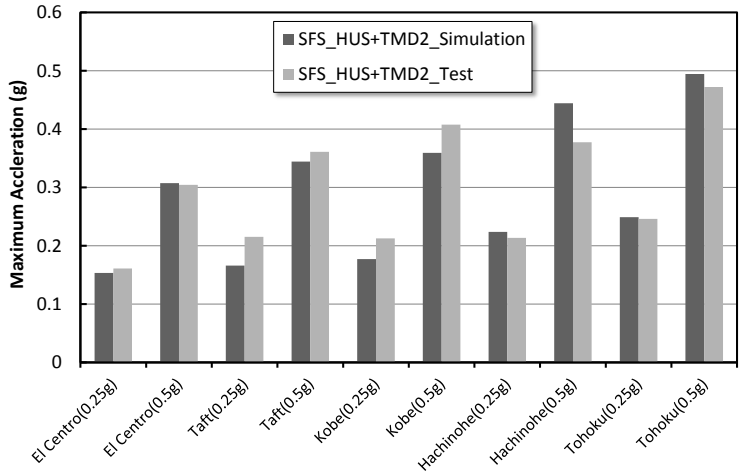

Figure 5.34 Maximum acceleration response for SFS_HUS with TMD2

A numerical simulation using the parameters totally from the test specimen, including the mass matrix (Eq.5.1), stiffness matrix (Eq. 5.2) and TMD parameters (Table 5.5), is carried out to comparing with the result from the shaking table test.

Maximum acceleration response for SFS with TMD1, SFS_HUS with TMD1, SFS with TMD2 and SFS_HUS with TMD2 is showed in Fig. 5.31~5.34, respectively. The result shows that the difference between numerical analysis and the test result is within an acceptable range.

5.5 Shaking Table Test of Retrofit Pattern 2

5.5.1 Introduction

Fig. 5.35 shows the retrofit system of pattern 2, the benchmark model of the steel frame with three stories with brace at the first floor is adopted as the original structure. For pattern 2, the way to soften the lateral stiffness of the first story is taking off the brace at the first floor, which is named Soft-first Story (SFS) Structure here. Then, two TMDs with different mass will be installed into the soft first story, which is named SFS with TMD1 and SFS with TMD2, respectively.

Further, the way to strengthen the lateral stiffness of the upper floors of a SFS structure is adding braces into the upper floors, which is named Soft-first Story Hard-upper Story Structures (SFS-HUS). Then, two TMDs with different mass will be installed into the soft first story, which is named SFS with TMD1 and SFS with TMD2, respectively.

Fig. 5.36 shows the test specimen of each model including Original Structure, SFS Structure, SFS-HUS Structure without TMD, SFS with TMD1, SFS with TMD2, SFS-HUS with TMD1, and SFS-HUS with TMD2. In the model of SFS with TMD1, we used three rotary dampers and in the model of SFS-HUS with TMD1, we used two air dampers. While, in the model of SFS with TMD2, we used two air dampers and two rotary dampers. In the model of SFS-HUS with TMD2, we used two air dampers adjusted to high damping mode and two rotary dampers. Dampers were decided only by the optimum damping ratio.

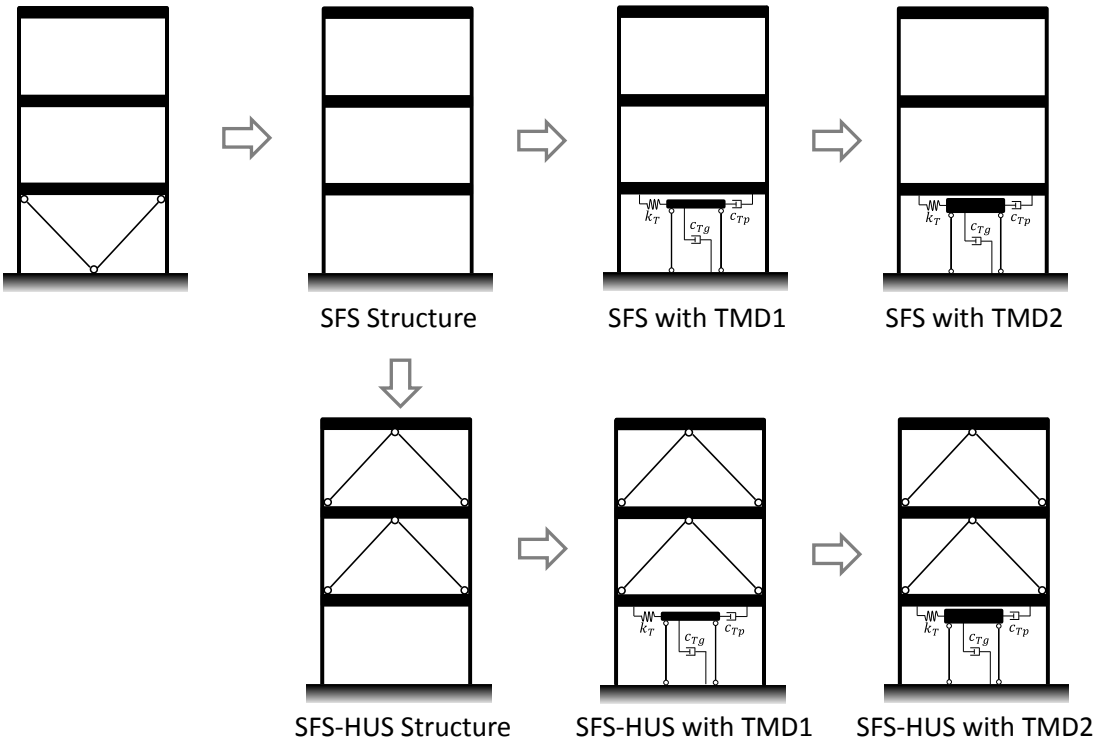

Figure 5.35 The retrofit system of pattern 2

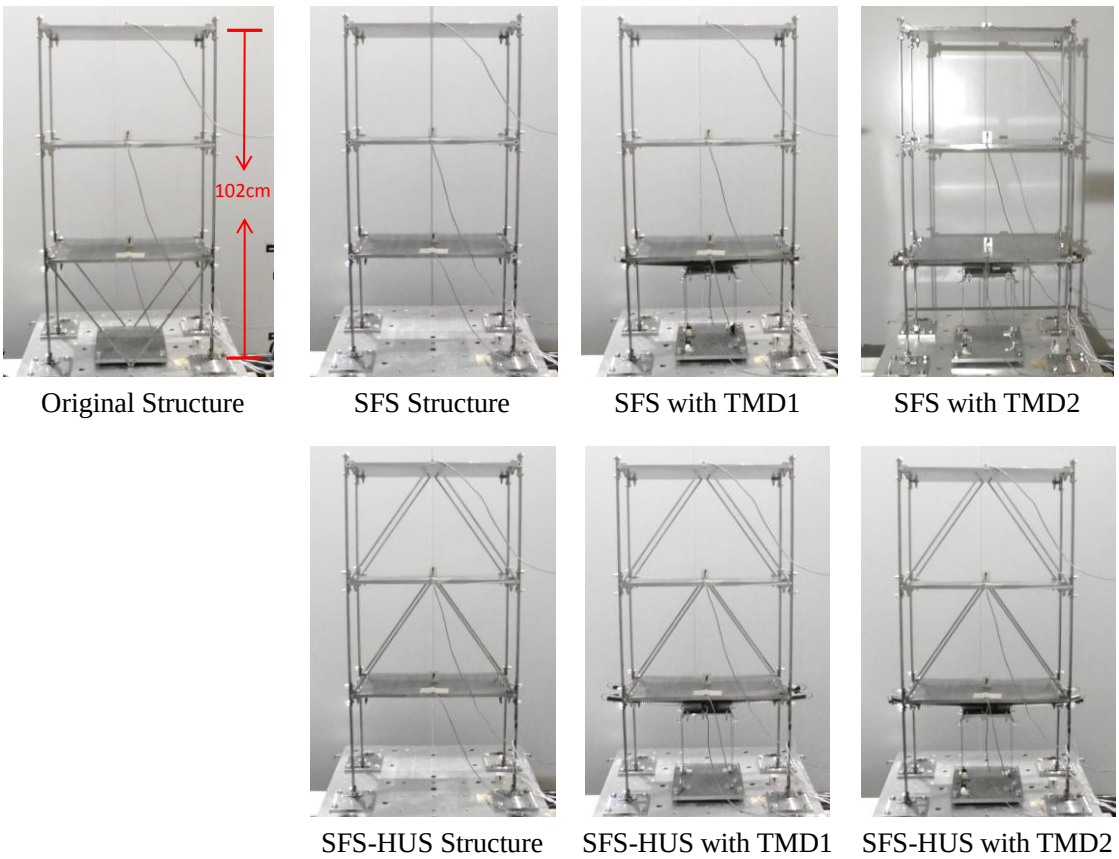

Figure 5.36 The test specimen of pattern 2

Table 5.6 Natural frequencies of the models without TMD

Model Type	Natural Frequency (Hz)		
	Mode 1	Mode 2	Mode 3
Original Structure	8.0	18.8	—
SFS Structure	5.3	14.8	22.1
SFS-HUS Structure	6.9	—	—

Table 5.7 Information of the TMD parameter of the seismic retrofit system

Model Type	Mass Ratio	Tuning Ratio	Damping Ratio	
			ξ_{Tg}	ξ_{Tp}
SFS with TMD1	0.0085	1.110	0.069	0
SFS-HUS with TMD1	0.024	1.096	0	0.099
SFS with TMD2	0.0187	1.010	0.023	0.064
SFS-HUS with TMD2	0.0528	0.968	0.019	0.098

The natural frequencies of the models of Original Structures, SFS Structures and SFS_HUS Structures are listed in Table 5.6. The information of the TMD parameters of the combined system, including mass ratio, tuning ratio and damping ratio, are listed in Table 5.7.

5.5.2 Test result

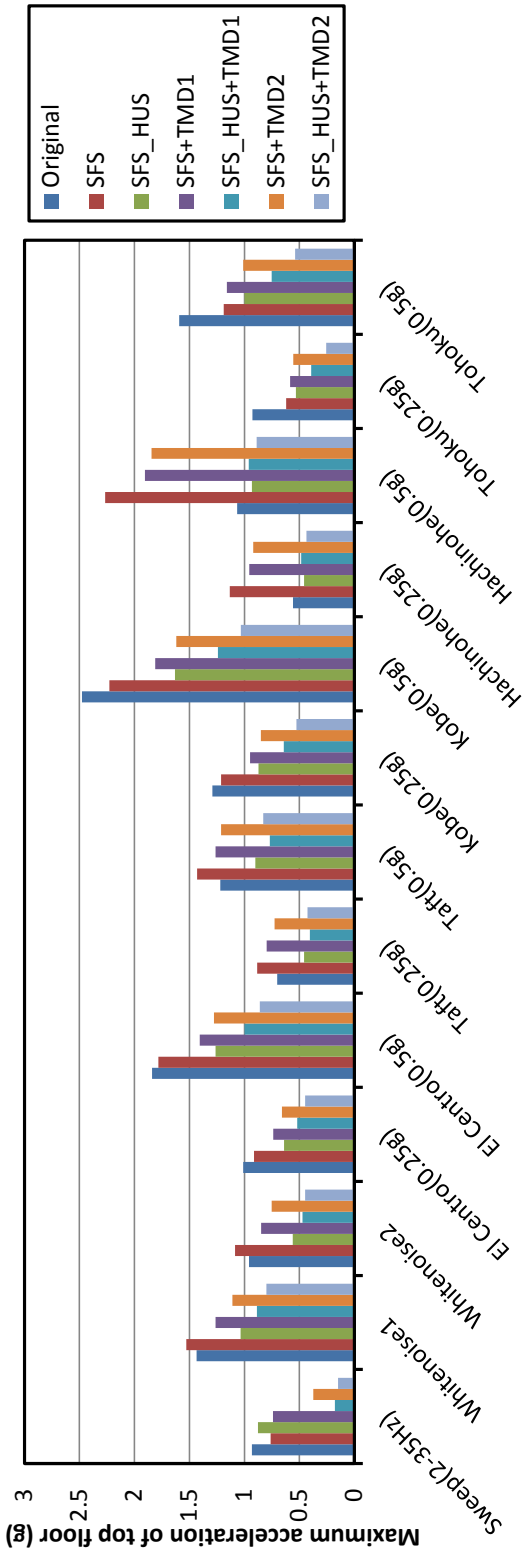

Figure 5.37 The maximum acceleration response of top floor

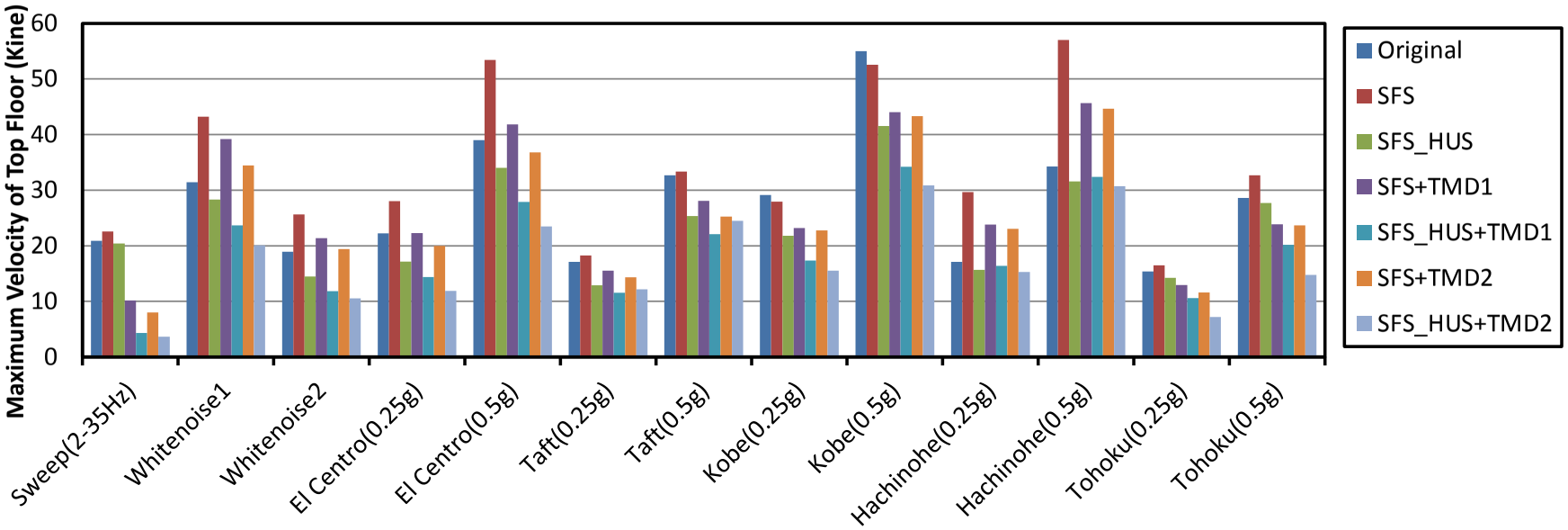

Figure 5.38 The maximum velocity response of top floor

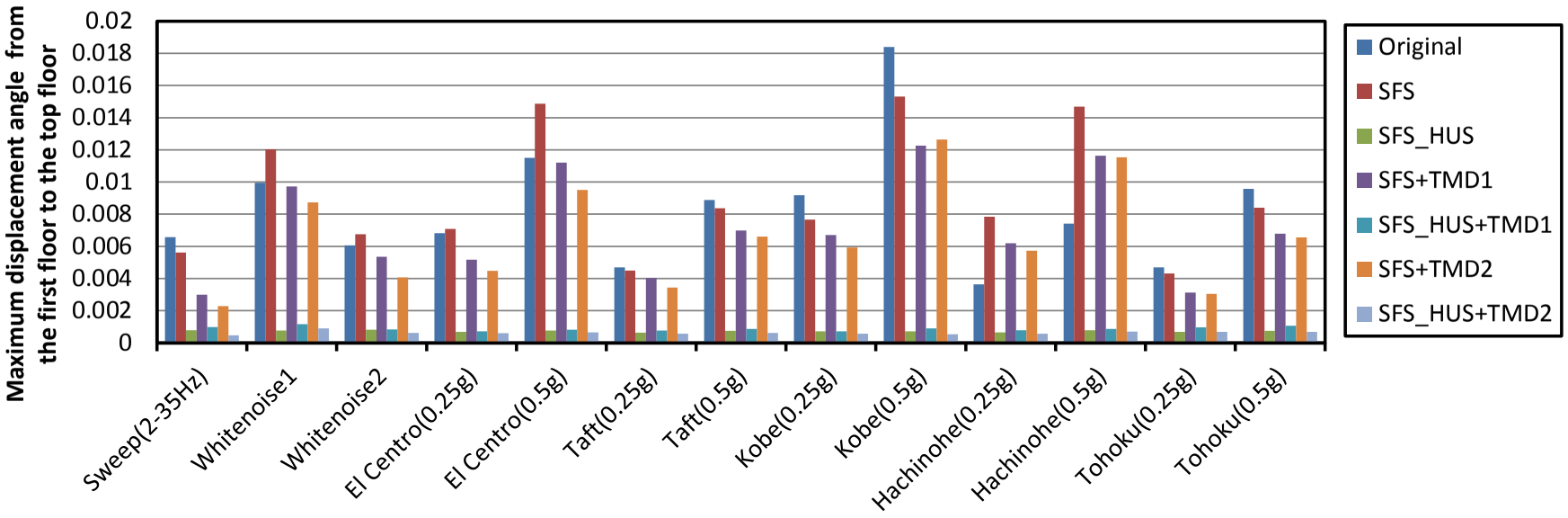

Figure 5.39 The maximum displacement angle from the second to the top floor

Fig. 5.37 shows the maximum acceleration response of top floor of the whole seven models subjected to 13 ground excitations including one sweep wave, two whitenoise and 10 earthquake inputs. From the result of the sweep input, where the peak response means the resonant response, the combined TMD system has the lowest acceleration response and the response of SFS_HUS with TMD is obviously smaller than that of SFS with TMD. Furthermore, for the systems with the same stiffness but different TMD, the one with a heavier TMD has a smaller peak response.

For the whitenoise input or earthquake input, we can get the same extend that the peak acceleration response could be reduced for the TMD combined system, especially for an SFS_HUS structure. The response of SFS_HUS with TMD is obviously smaller than that of SFS with TMD. Furthermore, for the systems with the same stiffness but different TMD, the one with a heavier TMD has a smaller peak response.

Fig. 5.38 shows the maximum velocity response of top floor of the whole seven models subjected to 13 ground excitations including one sweep wave, two whitenoise and 10 earthquake inputs. From the result of the sweep input, the combined TMD system has the lowest velocity response and the response of SFS_HUS with TMD is obviously smaller than that of SFS with TMD. Furthermore, for the systems with the same stiffness but different TMD, the one with a heavier TMD has a smaller peak response.

For the whitenoise input or earthquake input, we can get the same extend that the peak velocity response could be reduced for the TMD combined system, especially for an SFS_HUS structure. The response of SFS_HUS with TMD is obviously smaller than that of SFS with TMD. Furthermore, for the systems with the same stiffness but different TMD, the one with a heavier TMD has a smaller peak velocity response.

In order to confirm whether the frame especially the damper is still in a linear stage or not, two-stage GPA of earthquake was also adopted in this shaking table test the same as the test for Retrofit Pattern 1. The response of acceleration and velocity demonstrated that the system was still in a linear stage.

Fig. 5.39 shows the maximum displacement angle from the first to the top floor. From the result of the sweep input, we can see that the combined TMD system has the lowest acceleration response and the response of SFS_HUS with TMD is much

smaller than that of SFS with TMD.

For the whitenoise input or earthquake inputs, we can get the same extend that the peak displacement response of the SFS_HUS with TMD systems could be reduced to about less than 0.1 times of the original structure. Furthermore, for the systems with the same stiffness but different TMD, the one with a heavier TMD has a smaller peak response.

The acceleration spectrum of the input earthquake is showed in Fig. 5.40. This could be an important reference to explain why the vibration reduction effect is very good for some earthquakes and not so good for others. For example, the reduction effect of acceleration response showed in Fig.5.37 is better for Kobe than Hachinohe. It may be explained that the difference of spectrum value at the period for original structure to the value at the period for SFS or SFS_HUS structure for Kobe is much larger than that for Hachinohe.

Fig. 5.41 shows the maximum displacement angle of the first floor. From the result of the sweep input, we can see that the displacement of the first floor of the combined TMD system is much larger than that of the original structure.

Fig. 5.42 shows the maximum stroke of the TMD, and Fig. 5.43 shows the maximum acceleration of the TMD. From the result, we can conclude that, when a heavier TMD mass is adopted, the stroke length and the acceleration response of the TMD mass will become smaller.

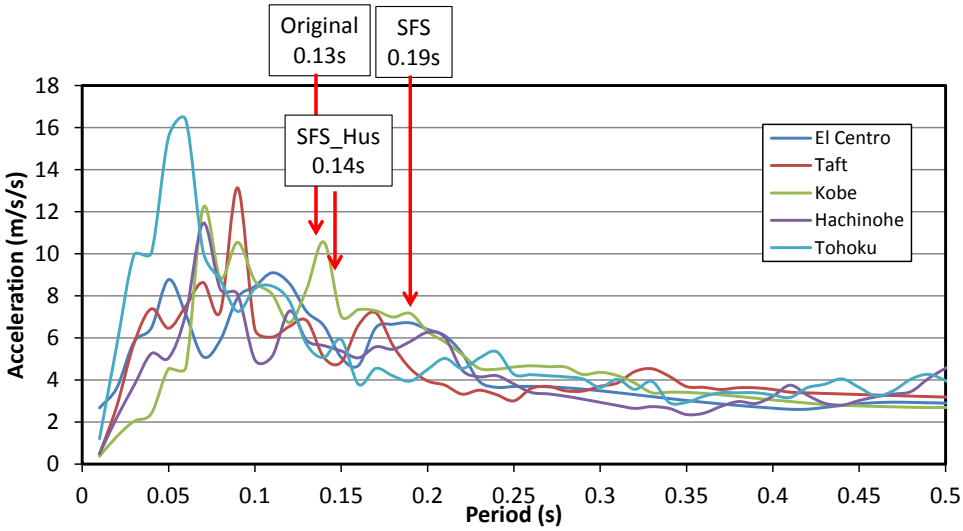

Figure 5.40 Acceleration spectrum of the input earthquake

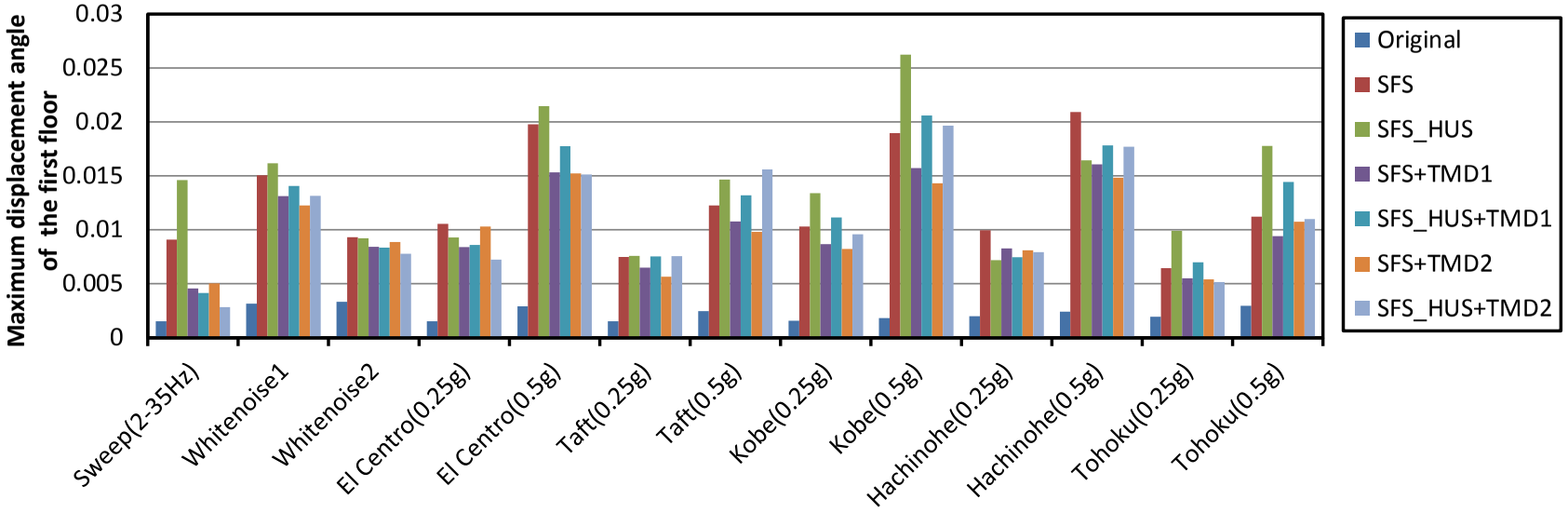

Figure 5.41 The maximum displacement angle of the first floor

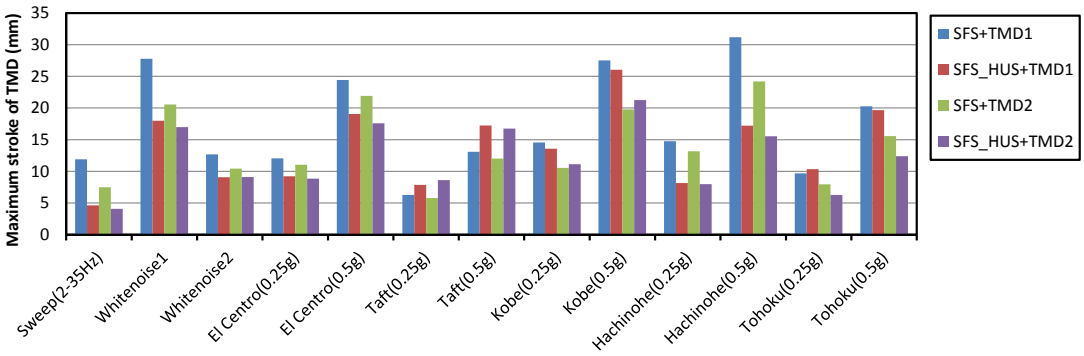

Figure 5.42 The maximum stroke length of the TMD

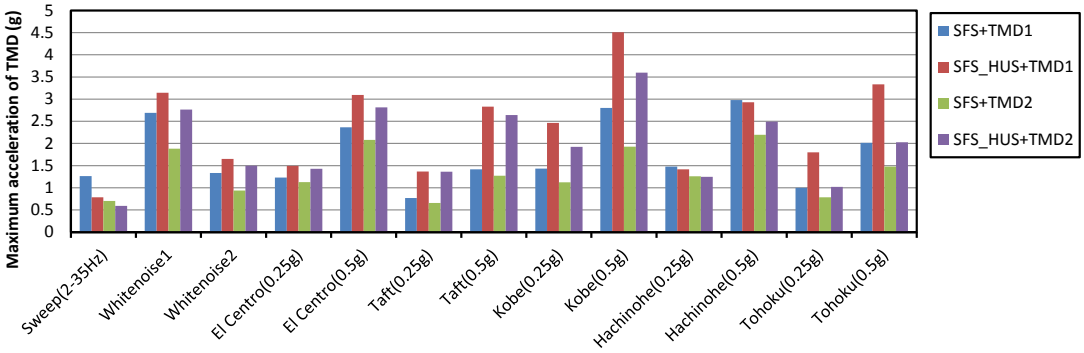

Figure 5.43 The maximum acceleration response of the TMD

5.5.3 Numerical simulation

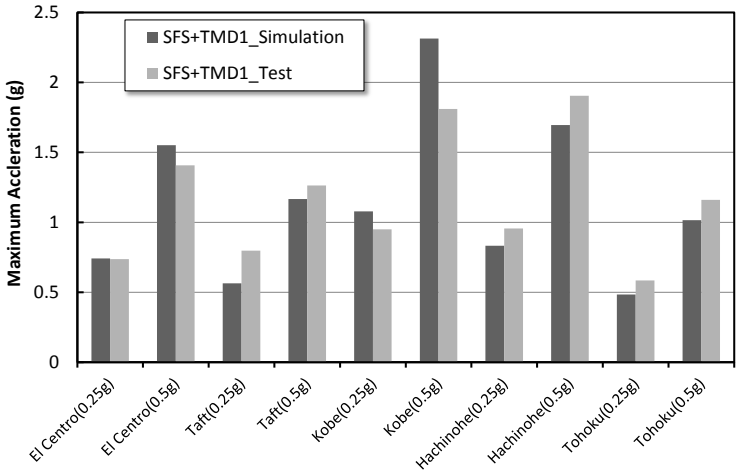

Figure 5.44 Maximum acceleration response for SFS with TMD1

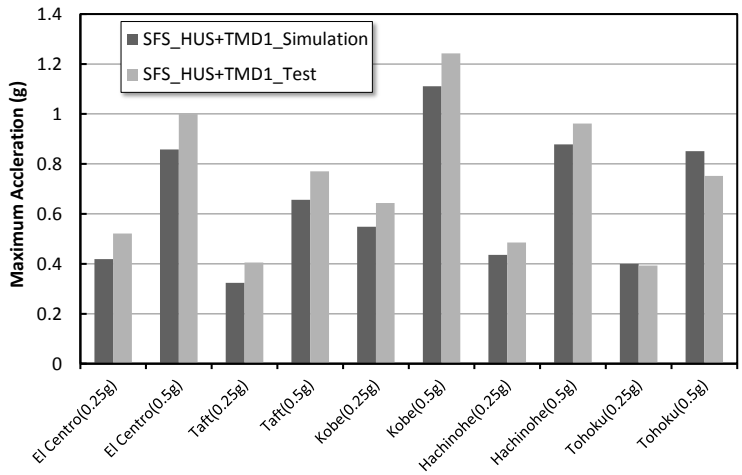

Figure 5.45 Maximum acceleration response for SFS_HUS with TMD1

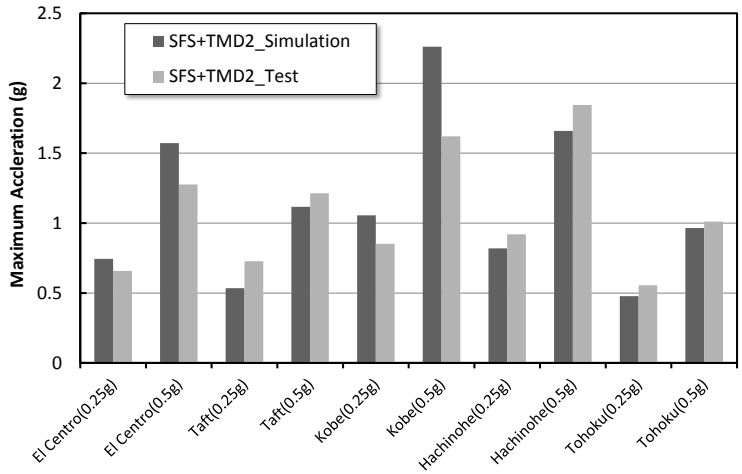

Figure 5.46 Maximum acceleration response for SFS with TMD2

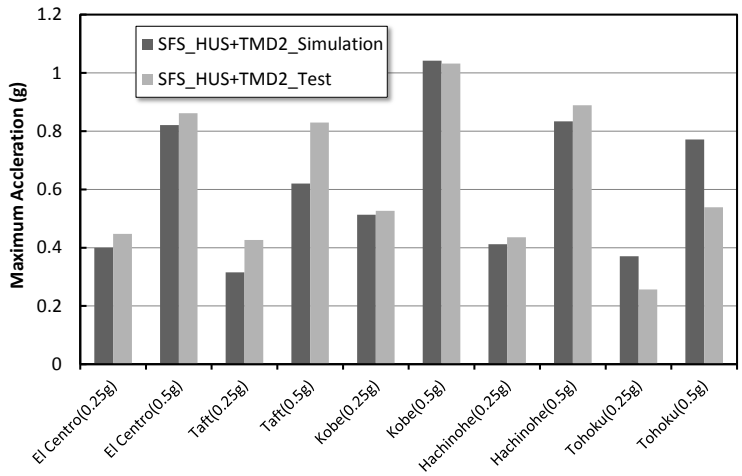

Figure 5.47 Maximum acceleration response for SFS_HUS with TMD2

A numerical simulation using the parameters totally from the test specimen, including the mass matrix (Eq.5.1), stiffness matrix (Eq. 5.2) and TMD parameters (Table 5.7), is carried out to comparing with the result from the shaking table test.

Maximum acceleration response for SFS with TMD1, SFS_HUS with TMD1, SFS with TMD2 and SFS_HUS with TMD2 is showed in Fig. 5.44~5.47, respectively. The result shows that the difference between numerical analysis and the test result is within an acceptable range.

But the difference between the result of simulation and the test for SFS with TMD is relatively large especially under the Kobe wave may possibly because the numerical itself, a shear model, is different from the test specimen when it is strengthened with brace. Meanwhile, the fix assumption of the connections between the columns and the floor slabs maybe another reason.

5.6 Conclusion

In this chapter, a shaking table test was carried out with a scale model in order to test the effectiveness of the proposed seismic retrofit system for steel structures. This 3 story steel frame model is based on a benchmark model for structure control. There are two types of retrofit patterns were considered here. It can be concluded as follows.

1) For the retrofit pattern 1, under the whitenoise input or earthquake input, the peak acceleration response of the TMD combined system could be reduced significantly to about 0.2~0.5 times of the original structure. And the peak displacement angle from the first floor to the top floor of the SFS with TMD systems could be reduced to about 0.4~0.8 times of the original structure. Furthermore, the peak response of SFS_HUS with TMD structure is about 50% smaller than that of SFS with TMD.

2) The maximum moment at the top of the column of the first floor will mostly be smaller than that of the original structure, while the peak displacement angle of the first floor of the combined TMD systems will be normally larger than that of the original structure.

3) When the predominant frequency of the input earthquake was close to the original structure, a better vibration control effect could be obtained for the proposed retrofit

system. For example, Kobe and Hachinohe both has a peak at about 0.2 Hz, which can be found from the response spectrum, which is very close to the structural natural frequency of the first mode. The vibration mitigation decrement of these two earthquake inputs were high up to about 80%.

4) For retrofit pattern 2, under the whitenoise input or earthquake input, the peak acceleration response of the top floor could be reduced for the TMD combined system, especially for a SFS_HUS structure. The peak displacement angle from the first floor to the top floor of the SFS_HUS with TMD system could be reduced to about less than 0.1 times of the original structure.

5) The vibration mitigation effect for pattern 2 is not as good as pattern 1, and this could be explained that firstly, the predominant of the input earthquake is far from the original structures. And secondly, the TMD virtual mass ratio of pattern 2 is smaller than that of pattern 1.

6) For the systems with the same stiffness but different TMD, the one with a heavier TMD has a smaller peak response. When the TMD mass ratio is larger, the stroke length and the acceleration response of the TMD mass itself will become smaller.

7) From the 1:10 length scaling, it can be calculated back to the original building that the TMD stroke will be 70mm~160mm when the PGA of the input earthquake is 0.1g.

Chapter 6

Practical Considerations

6.1 Additional Stiffness from Supporting Frame

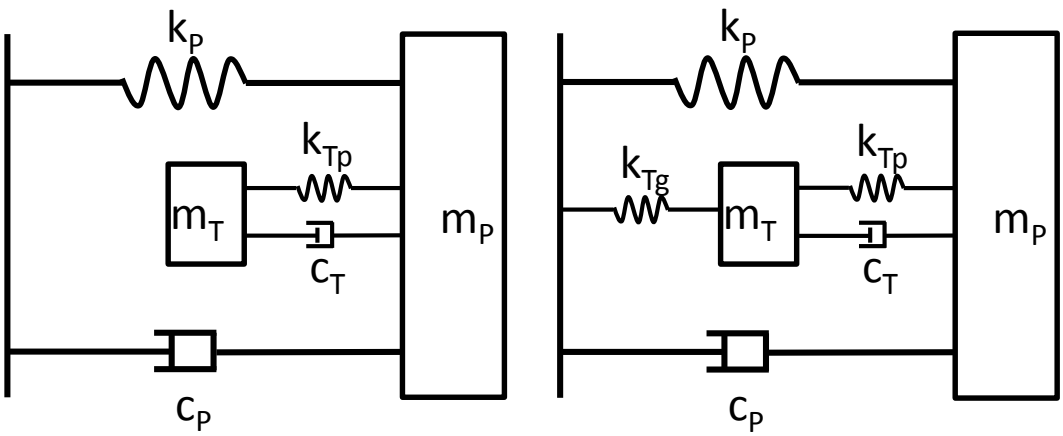

a) Traditional TMD b) Non-traditional stiffness considered

Figure 6.1 The model of TMD

For a real use of the proposed retrofit system, because the TMD mass is supported from ground, there is more or less lateral stiffness exists in the supporting structure. Especially, when a relatively heavy TMD mass was adopted, the additional stiffness k_{Tg} , named non-traditional stiffness here, brought by the supporting part could not be ignored. The influence of the additional stiffness from the supporting to the optimum parameters and vibration control effect is first studied here.

We first consider a common influence of the additional stiffness, so the parameter of stiffness ratio α is adopted here. αk_T and $(1-\alpha)k_T$ is expressed as the non-traditional stiffness which connects the TMD mass with ground, and the

traditional stiffness which connects the TMD mass with the primary structure. The range of α is from 0 to 1. When α equals to 0, the mixed system becomes a traditional TMD. When α equals to 1, the system becomes a pure dashpot system with a reaction force supporting.

6.1.1 Influence on optimum parameters

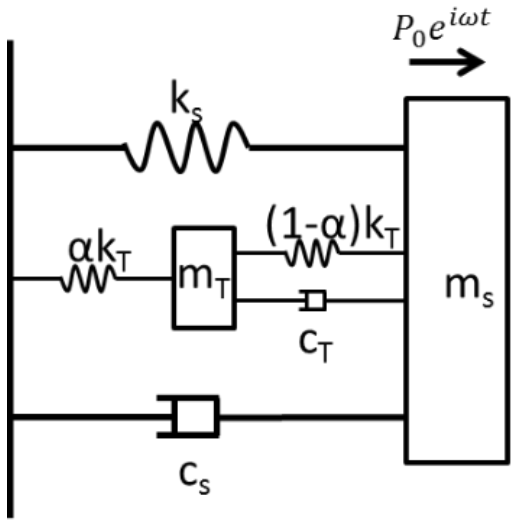

Figure 6.2 The simplified model

The motion equilibrium equation is as follows, here we ignored the damping in the primary structure.

$$\begin{bmatrix} m_s & \\ & m_T \end{bmatrix}\begin{Bmatrix} \ddot{x_P} \\ \ddot{x_T} \end{Bmatrix} + \begin{bmatrix} c_T & -c_T \\ -c_T & c_T \end{bmatrix}\begin{Bmatrix} \dot{x_P} \\ \dot{x_T} \end{Bmatrix} + \begin{bmatrix} k_P + (1-\alpha)k_T & -(1-\alpha)k_T \\ -(1-\alpha)k_T & k_T \end{bmatrix}\begin{Bmatrix} x_P \\ x_T \end{Bmatrix} = \begin{Bmatrix} P_0 e^{i\omega t} \\ 0 \end{Bmatrix} \qquad 6.1$$

We assumed $x_P = x_1 e^{i\omega t}$, and $x_T = x_2 e^{i\omega t}$, then Eq.6.2 could be obtained

$$\frac{x_1}{P_0} = \frac{\left(k_T - m_T\,\omega^2\right) + i\omega c_T}{\left[(-m_s\omega^2 + k_s)(-m_T\omega^2 + k_T) - m_T\omega^2(1-\alpha)k_T + \alpha(1-\alpha){k_T}^2\right] + i\omega c_T(-m_s\omega^2 + k_s - m_T\omega^2 + \alpha k_T)} \qquad 6.2$$

Nondimensionalize Eq. 6.2, it leads to

$$D = \sqrt{\frac{(1+\mu)^2(2\xi_T\beta\gamma)^2 + (\beta^2-\gamma^2-\mu(1-\alpha)\gamma^2)^2}{(2\xi_T\beta\gamma)^2(\beta^2-1+\mu\beta^2-\alpha\mu\gamma^2)^2 + [(1-\alpha)\mu\gamma^2\beta^2-\alpha(1-\alpha)\mu\gamma^4-(\beta^2-1)(\beta^2-\gamma^2)]^2}} \quad 6.3$$

Where, mass ratio $\mu = m_T/m_s$, tuning ratio $\gamma = \omega_T/\omega_P$, TMD damping ratio $\xi_T = c_T/2m_T\,\omega_T$, TMD circular frequency ${\omega_n}^2 = k_T/m_T$, circular frequency of primary system ${\omega_P}^2 = k_p/m_P$, force circular frequency ratio $\beta = \omega/\omega_P$, the dynamic response ratio $D = |\,x_1 k_s/P_0|$.

Figure 6.3 shows 5 response curves with different damping ratio under constant mass ratio $\mu = 0.1$, stiffness ratio $\alpha = 0.1$, and tuning ratio $\gamma = 1$. A useful phenomenon of these 5 curves is that they all pass through two fixed point P and Q. This provides the probability for using Fixed point method, proposed by Den Hartog, doing the optimization of the TMD parameters. As mentioned in Chapter 2, there are mainly two steps using this method. Firstly, calculate the optimum tuning ratio γ^{opt} in order to let the height of the two fixed point equals to each other. Then, calculate the optimum damping ratio ${\xi_T}^{opt}$ in order to make the curve passing through the two fixed points horizontally.

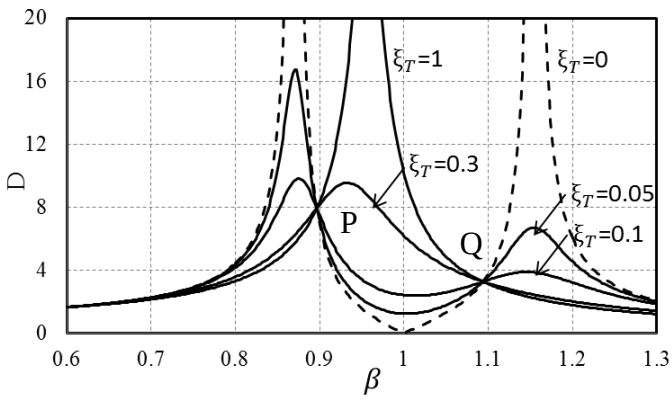

Figure 6.3 The influence of damping ratio

($\mu = 0.1\ \alpha = 0.1\ \gamma = 1$)

First, because the response curve is independent from damping ratio ξ_T at the two fixed point, using the condition that the ratio of items from numerator and denominator dependent from ξ_T and its coefficient be equaled to each other, Eq. 6.4 could be obtained.

$$\left(\frac{1}{\beta^2 - 1 + \mu\beta^2 + \alpha\mu\gamma^2}\right)^2$$
$$= \left(\frac{\beta^2 - \gamma^2}{(1-\alpha)\mu\gamma^2\beta^2 - \alpha(1-\alpha)\mu\gamma^4 - (\beta^2 - 1)(\beta^2 - \gamma^2)}\right)^2 \quad 6.4$$

It leads to

$$\beta^4 - 2\beta^2\frac{1 + \gamma^2 + \mu\gamma^2}{2 + \mu} + \frac{2\gamma^2 + (2\alpha - \alpha^2)\mu\gamma^4}{2 + \mu} = 0 \quad 6.5$$

In another hand, if $\xi_T \to \infty$, Eq. 6.6 could be obtained.

$$\beta_1{}^2 + \beta_2{}^2 = \frac{2 + 2\alpha\mu\gamma^2}{1 + \mu} \quad 6.6$$

Then, $\beta_1{}^2 + \beta_2{}^2$ could also be obtained from Eq. 6.5 showed as Eq. 8.7

$$\beta_1{}^2 + \beta_2{}^2 = \frac{2(1 + \gamma^2 + \mu\gamma^2)}{2 + \mu} \quad 6.7$$

Using the condition that the height of the two fixed point equals to each other, the optimum tuning ratio γ^{opt} could be obtained as Eq. 6.8.

$$\gamma^{opt} = \frac{1}{\sqrt{(1-\alpha)\mu^2 + 2(1-\alpha)\mu + 1}} \quad 6.8$$

Figure 6.4 shows 3 response curves with different tuning ratio under constant mass ratio $\mu = 0.1$, stiffness ratio $\alpha = 0.1$, and optimum damping ratio $\xi_T = 0.1665$. It can be found that the maximum of the response curve will change when tuning ratio changes. Where, $\gamma = 0.917$ is the optimum value from Eq. 6.8. The curve with the optimum value of $\gamma = 0.917$ shows the shape of lowest height.

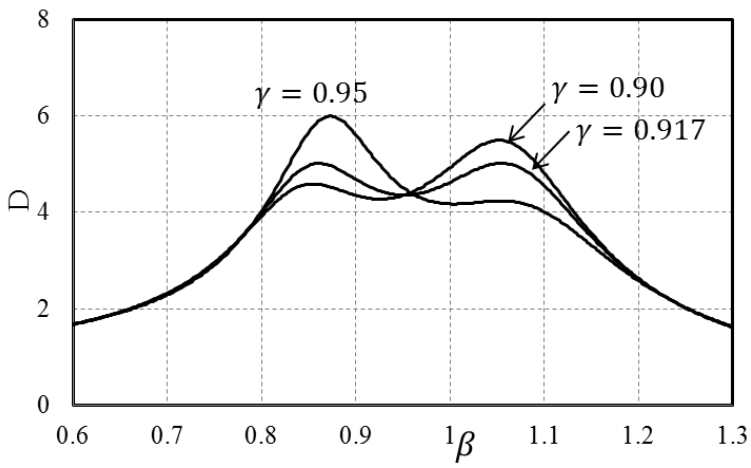

Figure 6.4 The influence of tuning ratio

$(\mu = 0.1\ \alpha = 0.1\ \xi_T = 0.1665)$

Then, calculate the optimum damping ratio $\xi_T{}^{opt}$ in order to make the curve passing through the two fixed points horizontally. However, it is impossible to make the curve pass through the two fixed points horizontally at the same time. So, the average value of the two optimum damping ratios calculated using the condition of each point is adopted as the TMD optimum damping ratio.

Here, the numerical method is used to search for the optimum damping ratio. The calculation flow is showed in Fig. 6.5, there are mainly four steps.

1) Calculate the optimum tuning ratio using Eq. 6.8, with assigned mass ratio μ, stiffness ratio α

2) Calculate the two values of force circle frequency β_1 and β_2, of the two fixed point.

3) Using the condition of $(\frac{\partial \mathrm{D}}{\partial \beta})_{\beta=\beta_1} = 0$ and $(\frac{\partial \mathrm{D}}{\partial \beta})_{\beta=\beta_2} = 0$, calculate the corresponding value of ξ_{T_1} and ξ_{T_2}.

4) Adopt the average value of ξ_{T_1} and ξ_{T_2} as the optimum damping ratio $\xi_T{}^{opt}$.

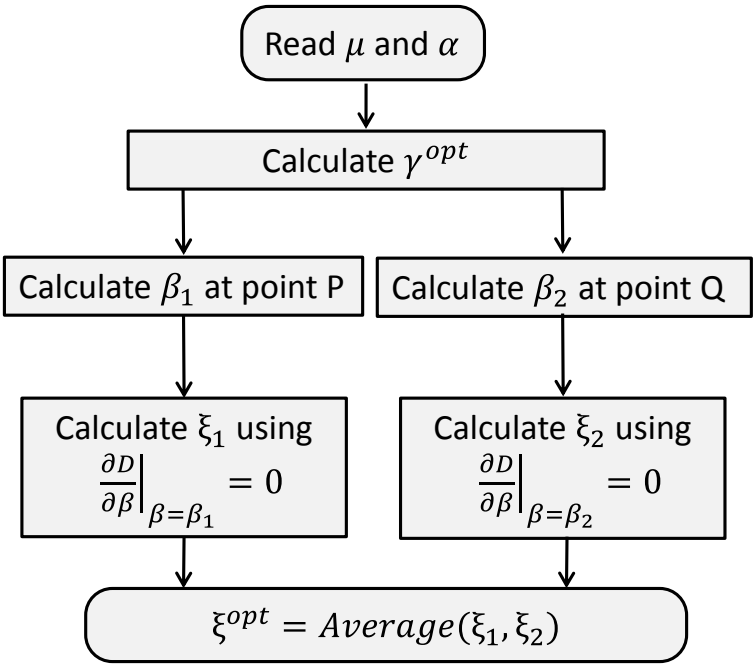

Figure 6.5 The calculation flow for the optimum damping ratio

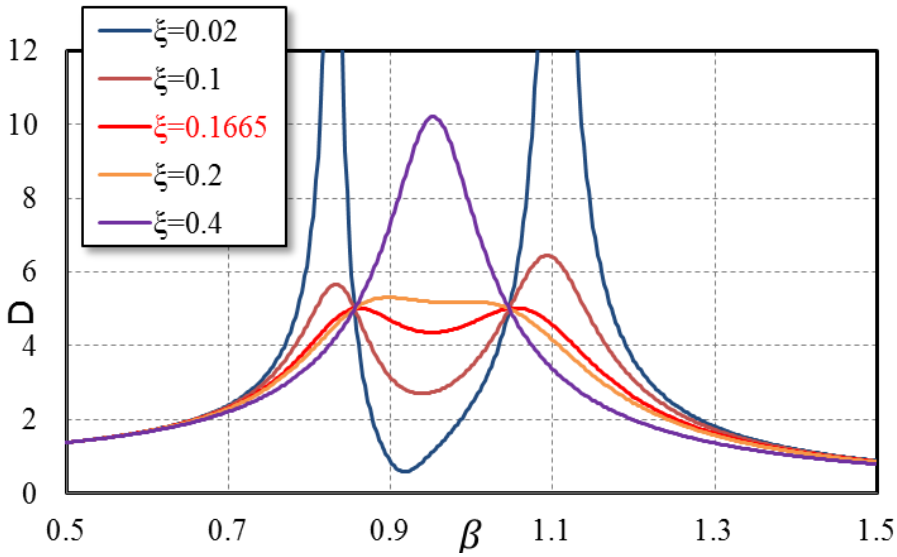

Figure 6.6 The influence of damping ratio under optimum tuning ratio (**μ**=0.1, $\alpha = 0.1$, $\gamma = 0.9171$)

Fig. 6.6 shows 5 response curves with different TMD damping ratio under constant mass ratio $\mu = 0.1$, stiffness ratio $\alpha = 0.1$, and optimum tuning ratio $\gamma = 0.9171$. Here, the optimum tuning ratio is obtained using Eq. 6.8, and the optimum damping ratio ($\xi_T = 0.1665$) is obtained by the numerical calculation showed in Fig. 6.5. The red curve shows the optimum curve by using optimum tuning ratio and optimum damping ratio.

Fig. 6.7 shows the optimum tuning ratio under various mass ratio μ and stiffness ratio α. When the mass ratio becomes larger, the optimum tuning ratio becomes smaller and goes close to 1. When the stiffness ratio becomes larger, the optimum tuning ratio also becomes larger. Further, the change of optimum tuning ratio caused by stiffness ratio will becomes larger as mass ratio gets larger.

Fig. 6.8 shows the optimum damping ratio under various mass ratio μ and stiffness ratio α. When the mass ratio becomes smaller, the optimum damping ratio becomes smaller and goes close to 0. When the stiffness ratio becomes larger, the optimum tuning ratio becomes smaller. Further, the change of optimum damping ratio caused by stiffness ratio will becomes larger as mass ratio gets larger.

Fig. 6.9 shows the maximum response D, showed in Eq. 6.3, of the optimal system, under various mass ratio μ and stiffness ratio α. As the mass ratio gets larger, the response ratio becomes smaller; a better TMD effect could be obtained. When the stiffness ratio becomes larger, the response ratio becomes larger; TMD will lose its effect.

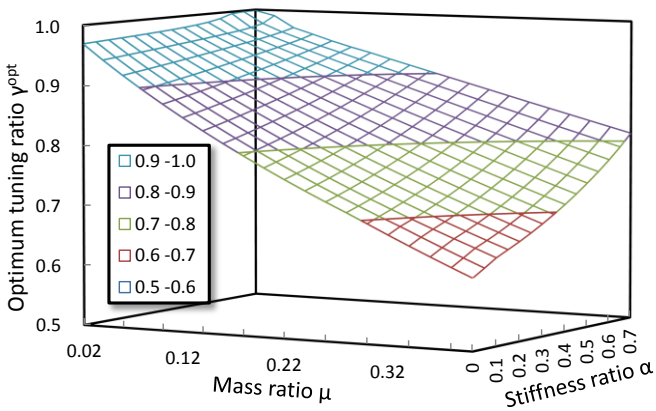

Figure 6.7 The relationship between the optimum tuning ratio with the mass ratio and stiffness ratio

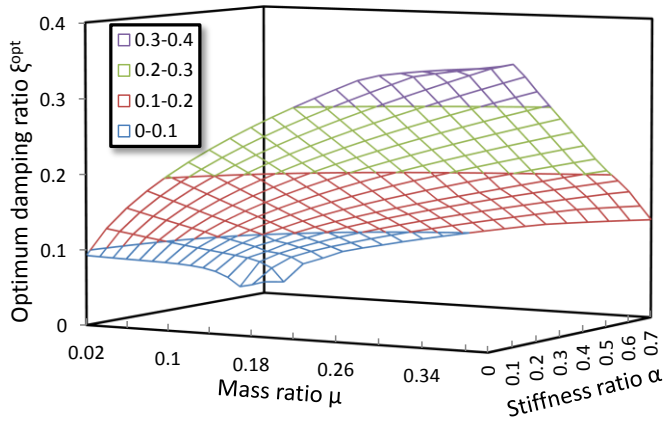

Figure 6.8 The relationship between the optimum damping ratio with the mass ratio and stiffness ratio

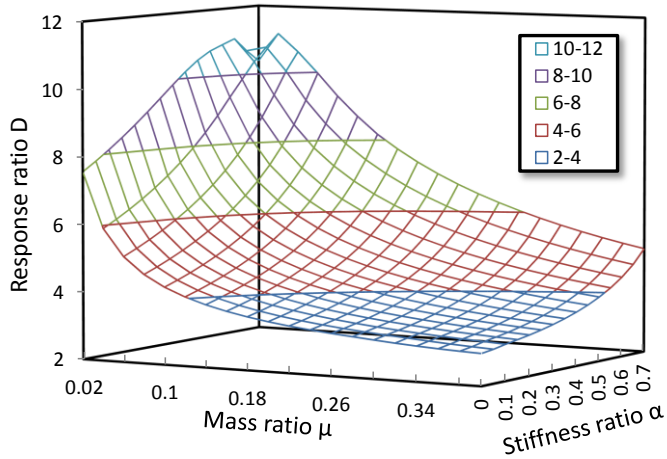

Figure 6.9 The relationship between the maximum response ratio of the optimal system with the mass ratio and stiffness ratio

Then, we consider the situation that the tuning ratio γ becomes super large. From the response equation Eq. 6.3, we can find when tuning ratio γ gets to infinite, the response ratio will becomes close to 0. This means that the TMD mass can't be moved. Especially, when the stiffness ratio is 1, the system becomes to a pure dashpot system. In order to illustrate this property, Fig. 6.10 is provided. The figure above shows the relationship between the frequency ratios of the fixed point with the tuning ratio. The figure below shows the relationship between the response ratios of the fixed point with the tuning ratio. The tuning ratio of the cross point of the dash line and the solid line is the optimum tuning ratio. As tuning ratio gets more than 1, the response ratio of point of Q becomes smaller quickly. Furthermore, when the stiffness ratio gets larger, the tuning ratio becomes larger, and the response ratio of point of P will become smaller quickly.

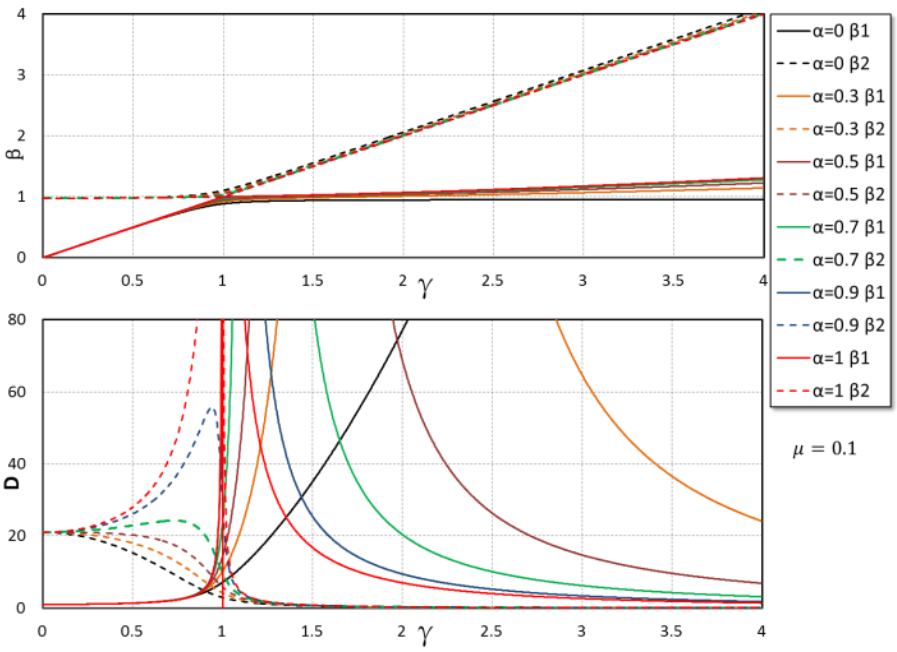

Figure 6.10 Above: Relationship between the frequency ratios of the fixed point with the tuning ratio; Below: Relationship between the response ratios of the fixed point with the tuning ratio

Theoretically, this kind of system can also be optimized. As mentioned above, the optimum system is depended on the condition that the response ratio of the point of P was minimized. Fig. 6.11 shows the optimum flow of this system, which is listed as follows.

1) Determine the value of tuning ratio γ

2) Calculate the frequency ratio of the point of P.

3) Using the condition of $(\frac{\partial D}{\partial \beta})_{\beta=\beta_1} = 0$, ${\xi_T}^{opt}$ could be obtained.

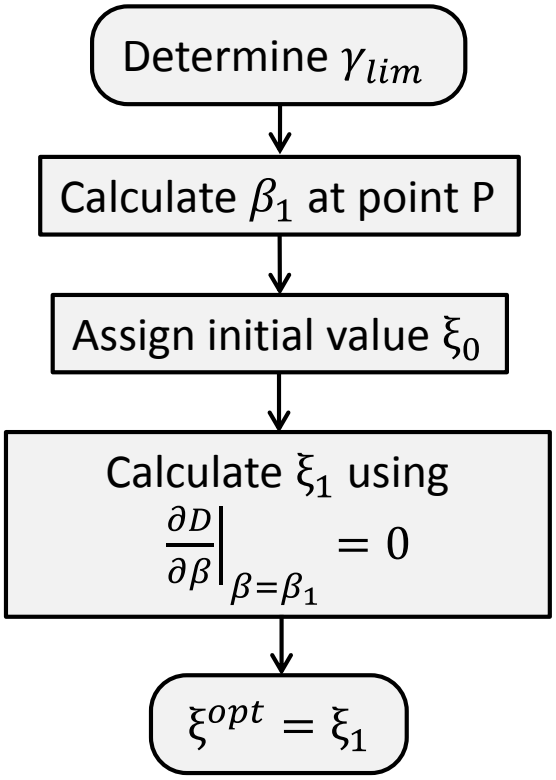

Figure 6.11 The optimization flow when γ is super large

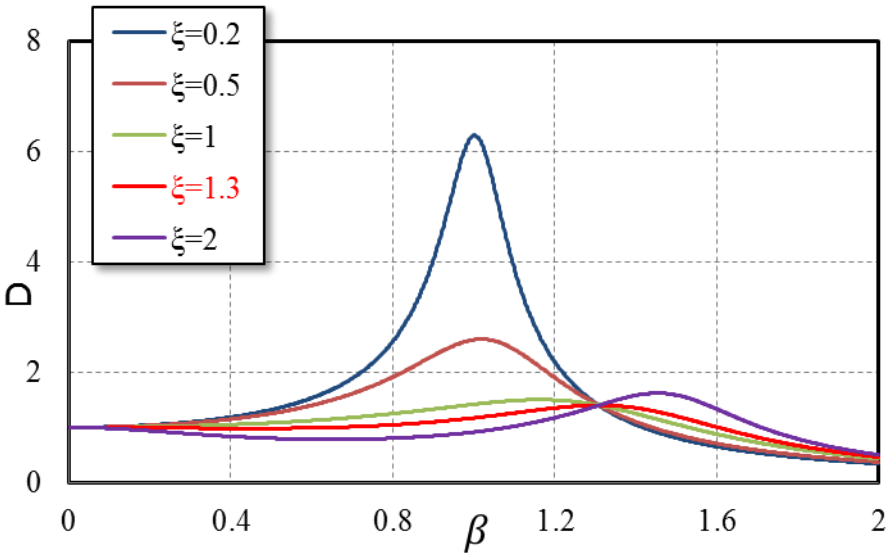

Figure 6.11 The influence of damping ratio when γ is super large.
（μ=0.1, $\alpha = 1$, $\gamma = 4$）

Fig. 6.11 shows the response of the situation that stiffness ratio is 1, which is a pure dashpot system. Where, the damping ratio of 1.3 is the optimum damping ratio calculated by the method showed in Fig. 6.11.

6.1.2 Proposal of double adjustment method

From the result above, it is clear that when the stiffness α is small, the influence to the response ratio is also small and can be ignored. Oppositely, here we proposed a better use of the additional stiffness from the supporting structure, which is so called Double adjustment method

6.1.2.1 Undamped primary structure

Firstly, from the motion equilibrium equation of Eq. 6.1, the equation of response ratio subjected to harmonious force excitation could be deduced as Eq. 6.9.

$$D = \sqrt{\frac{\left(2\xi_T\beta\gamma_{Tp}\right)^2 + (\beta^2 - {\gamma_{Tp}}^2 - {\gamma_{Tg}}^2)^2}{\left(2\xi_T\beta\gamma_{Tp}\right)^2\left(\beta^2 - 1 + \mu\beta^2 - \mu{\gamma_{Tg}}^2\right)^2 + [\mu{\gamma_{Tp}}^4 - (\beta^2 - 1 - \mu{\gamma_{Tp}}^2)(\beta^2 - {\gamma_{Tp}}^2 - {\gamma_{Tg}}^2)]^2}} \qquad 6.9$$

Where, traditional tuning ratio $\gamma_{Tp} = \omega_{Tp}/\omega_p$,non-traditional tunig ratio $\gamma_{Tg} = \omega_{Tg}/\omega_p$,traditionl TMD circular frequency ${\omega_{Tp}}^2 = k_{Tp}/m_T$, non-traditional TMD circular frequency ${\omega_{Tg}}^2 = k_{Tg}/m_T$,TMD damping ratio $\xi_T = c_T/2m_T\,\omega_{Tp}$ and response ratio $D = |\,x_1 k_p/P_0|$.

Then the Fixed point method could be used to do the optimization. First, we can get the equation that

$$\frac{\beta^2 - {\gamma_{Tp}}^2 - {\gamma_{Tg}}^2}{\mu{\gamma_{Tp}}^4 - (\beta^2 - 1 - \mu{\gamma_{Tp}}^2)(\beta^2 - {\gamma_{Tp}}^2 - {\gamma_{Tg}}^2)} = \pm\frac{1}{\beta^2 - 1 + \mu\beta^2 - \mu{\gamma_{Tg}}^2} \qquad 6.10$$

At the condition of '+', it leads to

$${\beta_1}^2 + {\beta_2}^2 = \pm\frac{(2 + 2\mu){\gamma_{Tp}}^2 + (2 + 2\mu){\gamma_{Tg}}^2 + 2}{2 + \mu} \qquad 6.11$$

On the other hand, when $\xi_T \to \infty$, Eq. 6.12 could be obtained.

$$\beta_1{}^2 - 1 + \mu\beta_1{}^2 - \mu\gamma_{Tg}{}^2 = -\left(\beta_2{}^2 - 1 + \mu\beta_2{}^2 - \mu\gamma_{Tg}{}^2\right) \qquad 6.12$$

Which leads to

$$\beta_1{}^2 + \beta_2{}^2 = \frac{2 + 2\mu\gamma_{Tg}{}^2}{1 + \mu} \qquad 6.13$$

Let Eq. 6.11 equals to Eq. 6.13, the optimum express could be obtained.

$$\gamma_{Tp}{}^{opt} = \frac{\sqrt{1 - \gamma_{Tg}{}^2}}{1 + \mu} \qquad 6.14$$

$$\gamma_{Tg}{}^{opt} = \sqrt{1 - (1 + \mu)^2\gamma_{Tp}{}^2} \qquad 6.15$$

Then, we do a similar work to deduce the optimum tuning ratio subjected to harmonious ground excitations. First, the equation of response ratio could be obtained from Eq.6.1 by substitute the force item for $\begin{Bmatrix} -m_p A_0 e^{i\omega t} \\ -m_T A_0 e^{i\omega t} \end{Bmatrix}$.

$$D = \sqrt{\frac{(1 + \mu)^2\left(2\xi_T\beta\gamma_{Tp}\right)^2 + (\beta^2 - \gamma_{Tp}{}^2 - \gamma_{Tg}{}^2 - \mu\gamma_{Tp}{}^2)^2}{\begin{array}{c}\left(2\xi_T\beta\gamma_{Tp}\right)^2\left(\beta^2 - 1 + \mu\beta^2 - \mu\gamma_{Tg}{}^2\right)^2 + \\ [\mu\gamma_{Tp}{}^4 - (\beta^2 - 1 - \mu\gamma_{Tp}{}^2)(\beta^2 - \gamma_{Tp}{}^2 - \gamma_{Tg}{}^2)]^2\end{array}}} \qquad 6.16$$

Then the Fixed point method could be used to do the optimization. First, we can get the equation that

$$\frac{\beta^2 - \gamma_{Tp}{}^2 - \gamma_{Tg}{}^2 - \mu\gamma_{Tp}{}^2}{\mu\gamma_{Tp}{}^4 - (\beta^2 - 1 - \mu\gamma_{Tp}{}^2)(\beta^2 - \gamma_{Tp}{}^2 - \gamma_{Tg}{}^2)} = \pm\frac{1 + \mu}{\beta^2 - 1 + \mu\beta^2 - \mu\gamma_{Tg}{}^2} \qquad 6.17$$

At the condition of '+', it leads to

$$\beta_1{}^2 + \beta_2{}^2 = \pm\frac{2(1 + \mu)^2\gamma_{Tp}{}^2 + (2 + 3\mu)\gamma_{Tg}{}^2 + 2 + \mu}{2(1 + \mu)} \qquad 6.18$$

On the other hand, when $\xi_T \to \infty$, Eq. 6.19 could be obtained.

$$\beta_1{}^2 - 1 + \mu\beta_1{}^2 - \mu\gamma_{Tg}{}^2 = -\left(\beta_2{}^2 - 1 + \mu\beta_2{}^2 - \mu\gamma_{Tg}{}^2\right) \qquad 6.19$$

Which leads to

$$\beta_1{}^2 + \beta_2{}^2 = \frac{2 + 2\mu\gamma_{Tg}{}^2}{1 + \mu} \qquad 6.20$$

Let Eq. 6.18 equals to Eq. 6.20, the optimum express could be obtained.

$$\gamma_{Tp}{}^{opt} = \frac{\sqrt{(1 - \frac{\mu}{2})(1 - \gamma_{Tg}{}^2)}}{1 + \mu} \qquad 6.21$$

$$\gamma_{Tg}{}^{opt} = \sqrt{1 - \frac{(1 + \mu)^2\gamma_{Tp}{}^2}{1 - \mu/2}} \qquad 6.22$$

Here, the so called Double adjustment method means that either of γ_{Tg} or γ_{Tp} is known, the corresponding optimum value $\gamma_{Tp}{}^{opt}$ or $\gamma_{Tg}{}^{opt}$ can be obtained. For a traditional TMD system, even if the tuning ratio is adjusted as the optimum value, the spring or the frequency of the primary structure will change with time. Once the tuning ratio is different from the optimum value, the vibration control effect of TMD will decrease quickly. So, the adjustment of the stiffness at the supporting structure provides one more chance to keep the TMD system at an optimum level. Furthermore, if the adjustment for the stiffness at the supporting structure is easier than the adjustment for the stiffness of the traditional spring, this double adjustment method becomes a significant advantage.

By the way, it should be noted here that, for the adjustment of the stiffness from the supporting structure, there is an existing condition for γ_{Tp}, that γ_{Tp} should be smaller than $(\gamma_{Ts}{}^{opt})_{\gamma_{Tg}=0}$. Otherwise, there is only one way as reducing γ_{Tp} to keep the system optimal. The conditions for Eq. 6.14 and 6.15 of force excitation and Eq. 6.21 and 6.22 of ground excitation is showed as Eq. 6.23 and 6.24, respectively.

$$\gamma_{Tg} < \frac{1}{1+\mu} \qquad 6.23$$

$$\gamma_{Tg} < \frac{\sqrt{1-\mu/2}}{1+\mu} \qquad 6.24$$

6.1.2.2 Damped primary structure

If we take the damping of the primary structure into consideration, the closed form of the expressions of optimum value becomes impossible to be deduced. A numerical method is adopted here to obtain the optimum values.

Eq. 6.23 and 6.24 is the response ratio of the combined system considering of primary damping ratio subjected to force excitation and ground excitation, respectively.

$$D = \sqrt{\frac{\left(2\xi_T\beta\gamma_{Tp}\right)^2 + (\beta^2 - {\gamma_{Ts}}^2 - {\gamma_{Tg}}^2)^2}{\begin{array}{l}(2\beta)^2[\left(\beta^2 - 1 + \mu\beta^2 - \mu{\gamma_{Tg}}^2\right)\xi_T\gamma_{Tp} + (\beta^2 - {\gamma_{Tp}}^2 - {\gamma_{Tg}}^2)\xi_p]^2 \\ +[\left(\beta^2 - 1 - \mu{\gamma_{Tp}}^2\right)\left(\beta^2 - {\gamma_{Tp}}^2 - {\gamma_{Tg}}^2\right) - \mu{\gamma_{Tp}}^4 - 4\xi_T\xi_p\gamma_{Tp}\beta^2\end{array}}} \qquad 6.23$$

$$D = \sqrt{\frac{(1+\mu)^2\left(2\xi_T\beta\gamma_{Tp}\right)^2 + (\beta^2 - {\gamma_{Tp}}^2 - {\gamma_{Tg}}^2 - \mu{\gamma_{Tp}}^2)^2}{\begin{array}{l}(2\beta)^2[\left(\beta^2 - 1 + \mu\beta^2 - \mu{\gamma_{Tg}}^2\right)\xi_T\gamma_{Tp} + (\beta^2 - {\gamma_{Tp}}^2 - {\gamma_{Tg}}^2)\xi_p]^2 \\ +[\left(\beta^2 - 1 - \mu{\gamma_{Tp}}^2\right)\left(\beta^2 - {\gamma_{Tp}}^2 - {\gamma_{Tg}}^2\right) - \mu{\gamma_{Tp}}^4 - 4\xi_T\xi_p\gamma_{Tp}\beta^2\end{array}}} \qquad 6.24$$

Where, the response ratio function D is $|x_1 k_p/P_0|$ and $|x_1{\omega_p}^2/A_0|$, respectively. And the purpose function is to minimize the maximum of D. Fig. 6.12 shows the calculation flow of the optimization. γ_T represents for γ_{Tp} or γ_{Tg} depends on which of them is decided.

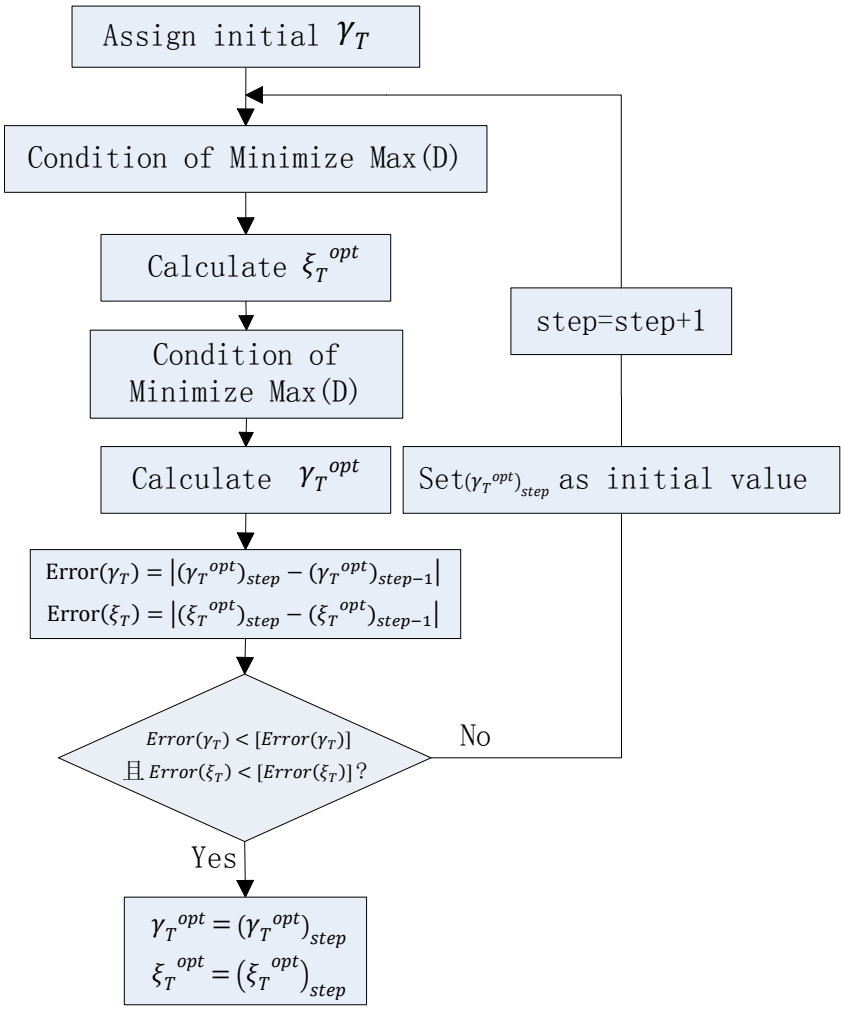

Figure 6.12 The computing flow

As showed in Fig. 6.12, when adopt the double adjustment method, there are mainly three steps.

1) The assignment of the initial value for γ_T. It can be done by Eq. 6.14 or Eq.6.15 when subjected to force excitation or by Eq. 6.21 or Eq. 6.22 when subjected to ground excitation, which could reduce the amount of looping.

2) Loop computing. First, calculate the maximum value of D with an initial value of ξ_T, using the assigned initial value of γ_T. Searching for local optimum value of ξ_T to make the maximum value of D minimized. Then, use the obtained ξ_T as the initial value to searching for local optimum value of γ_T. Assign the obtained value of γ_T as the initial value, repeat the calculation above.

3) Stop the computing when the loop condition is satisfied. From the work above, the optimum tuning ratio ${\gamma_T}^{opt}$, optimum damping ratio ${\xi_T}^{opt}$ and the corresponding maximum response ratio could be obtained

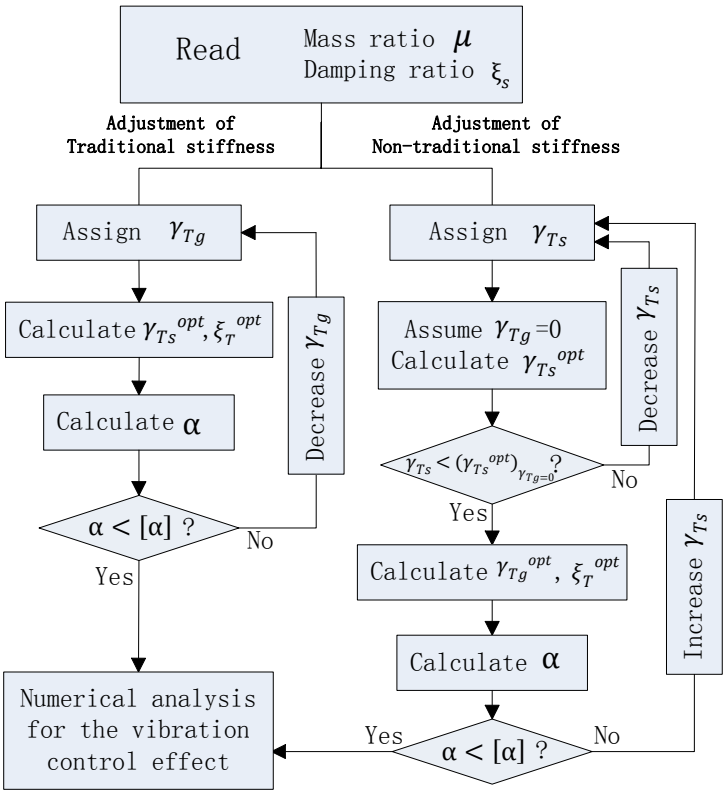

Figure 6.13 The design flow for double adjustment method

As showed in Fig. 6.13, the design procedure of the double adjustment method is summarized here. The procedure is composed by two parts: the traditional stiffness adjustment and the non-traditional stiffness adjustment.

The $[\alpha]$ in Fig. 6.13 is the allowable stiffness ratio. From section 6.1.1, it can be concluded that when α becomes larger, TMD will lose its effect and also lose its robustness, which will be introduced in the next section 6.1.3. So, an allowable stiffness ratio is necessary for the design of double adjustment method. α can be calculated from Eq. 6.25.

$$\alpha = \frac{{\gamma_{Tg}}^2}{{\gamma_{Tg}}^2 + {\gamma_{Ts}}^2} \qquad 6.25$$

6.1.3 Conclusion

In this section, the property of additional stiffness is considered from the supporting frame. It can be concluded that:

1) When the stiffness ratio α is small, such as less than 0.1, the influence on the vibration control effect is also small and can be ignored. But, if the stiffness ratio α becomes larger, TMD will lose its effect. So, considering of an allowable stiffness ratio $[\alpha]$ is recommended here.

2) When the mass ratio becomes larger, the vibration control effect will expectedly increase, and the influence from the change of the stiffness ratio will become smaller.

3) The double adjustment method is proposed here, in order to make better use of the additional stiffness from the TMD supporting frame. The numerical method is also introduced here for the TMD optimization of damped primary structure.

6.2 Introduction of System Robustness

The equivalent additional damping ratio is studied here which is seemed as an important index for the robustness of the TMD combined system. It is obtained using Eq. 6.25, and is independent from the optimum tuning ratio and optimum damping ratio [6-1].

$$\xi_{eff} = \frac{1}{2D_{max}} - \xi_P \qquad 6.25$$

Fig. 6.13 shows the equivalent additional damping ratio for TMD combined system under various mass ratio μ and stiffness ratio α. From the result, it is clear that the equivalent damping ratio is sensitive to the changing of tuning ratio and damping ratio. When TMD is applied for a real use, the non-sensitivity property between the equivalent damping ratio of the TMD combined system with the TMD tuning ratio and TMD damping ratio is adopted as the robustness of the vibration control effect of TMD. The TMD robustness should be considered during its design process [6-2].

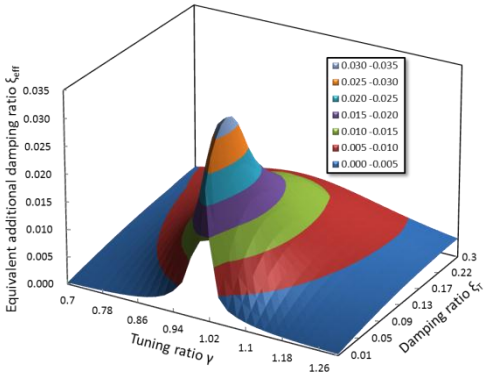

a-1) μ=0.01, α=0

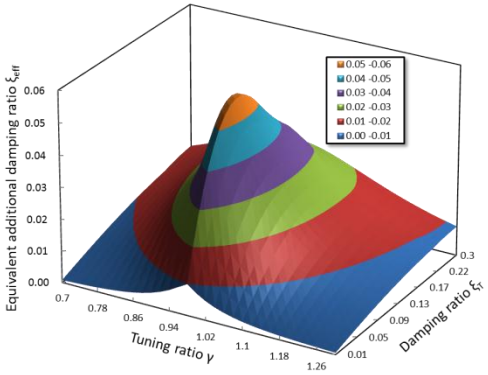

b-1) μ=0.03, α=0

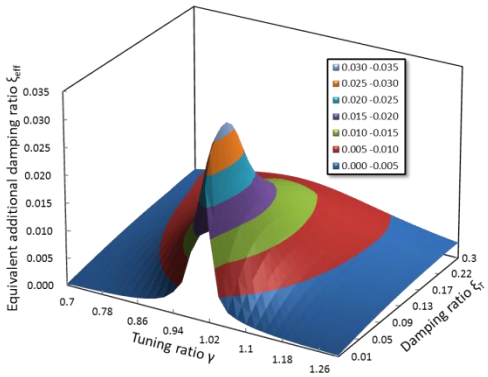

a-2) μ=0.01, α=0.05

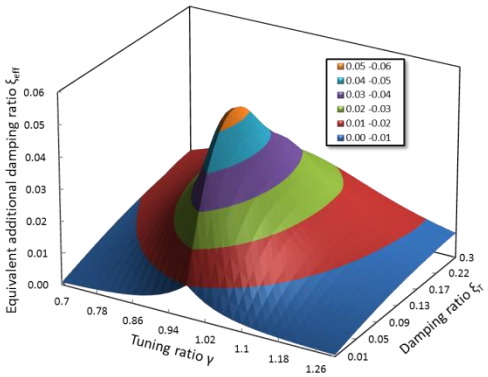

b-2) μ=0.03, α=0.05

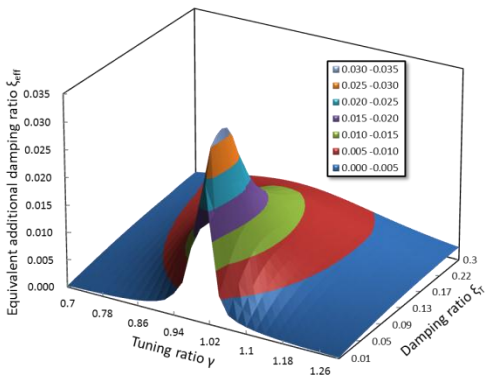

a-3) μ=0.01, α=0.1

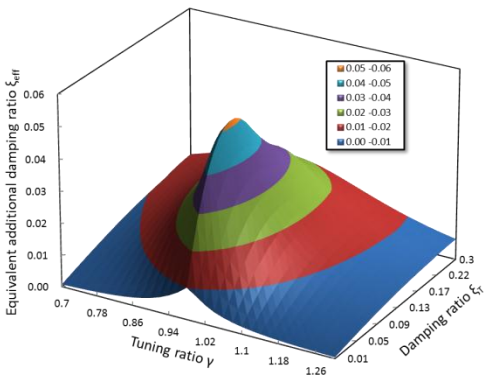

b-3) μ=0.03, α=0.1

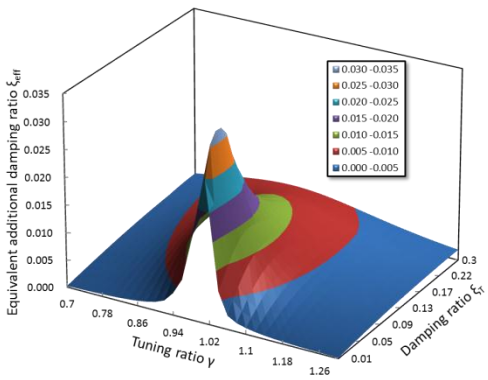

a-4) μ=0.01, α=0.15

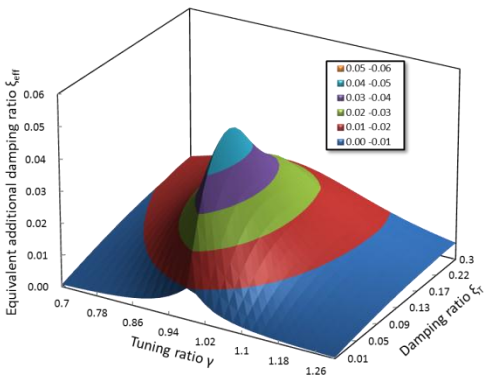

b-4) μ=0.03, α=0.15

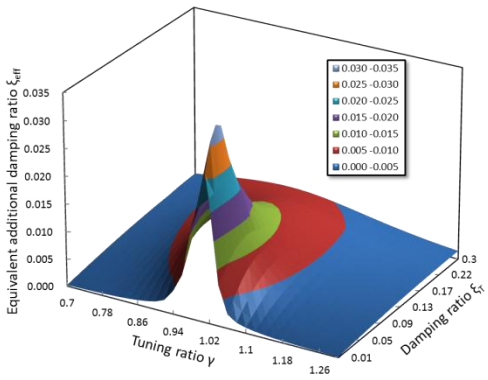

a-5) μ=0.01, α=0.2

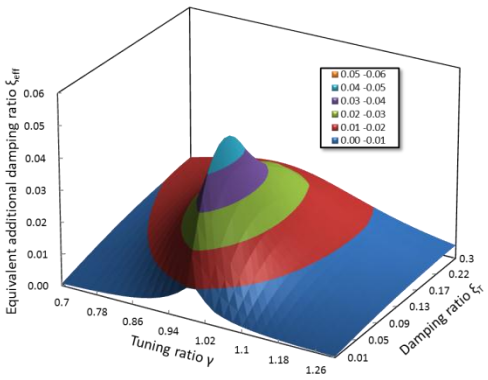

b-5) μ=0.03, α=0.2

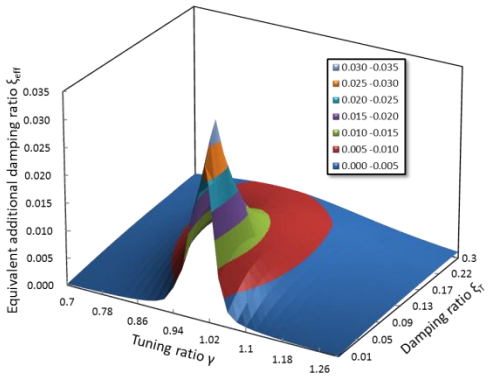

a-6) μ=0.01, α=0.25

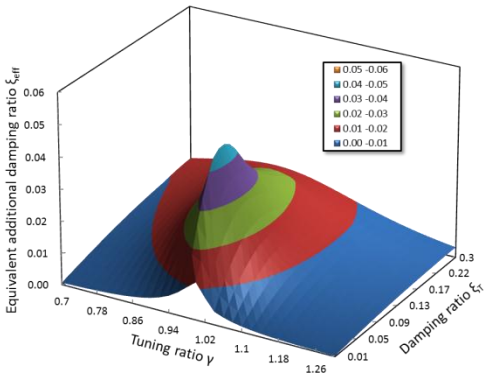

b-6) μ=0.03, α=0.25

Figure 6.13 Equivalent additional damping ratio

From Fig. 6.13, it can be found that the equivalent additional damping ratio is more sensitive to the change of tuning ratio than the damping ratio. When the mass ratio becomes larger the robustness will become better.

The stiffness ratio α is also considered here, it can be concluded from the result that, when the stiffness ratio α becomes larger, the TMD will lose its robustness. But

when α is relatively small, such as smaller than 0.1, the influence on the robustness is quite small thus can be ignored. And, expectedly, when the mass ratio becomes larger, the robustness will become better under the same stiffness ratio α. So, the allowable value of stiffness ratio α is recommended here.

6.3 Introduction of Initial Displacement Method

It is well known that TMD is quite effective in reducing vibrations when subjected to stationary excitations, and it will lose its effects for the earthquake excitations [6-3][6-4][6-5]. Because of the TMD mass is initially at rest, it needs some time interval before it becomes effective. In order to improve the reliability of the TMD combined system, an initial TMD displacement has been proposed and studied by some researchers [6-6][6-7][6-8]. The concept of this method is giving the TMD an initial displacement and it will be released when the response reached the defined conditions.

It has been demonstrated that the TMD systems with an initial displacement has a better effect than the one without an initial displacement by numerical simulation and experiments [6-6]. The design formula for tuning ratio, damping ratio and initial displacement, has been proposed by Abe in order to improving the vibration control effect for impulse excitations [6-7]. The effect was illustrated by numerical simulations using 1DOF model subjected to El Centro (1940NS) input [6-9]. Tanaka explained why the normal TMD under an optimal design still could not get a vibration mitigation effect to an impact force excitation. He proposed a design formula of the TMD with initial displacement for the impact force excitation and verified the effect of so designed TMD [6-10]. Furthermore, Yoshinaka extended this method for MDOF models [6-8].

Based on the previous study, when the TMD was applied to a real structure, especially when it is designed controlling the seismic response, an adoption of initial displacement method might improve the system reliability.

6.4 Some Discussions for Realization

First, consider the feasibility of the TMD mass with an overall mass ratio of 0.1, which has been used several times for the comparison in Chapter 4. For example, if

the building has four stories and the area of 10m*10m, the overall mass should be 72000kg when the gravity load is assumed as 180kg/m^2. Then the TMD mass will be 7200kg, and 0.91m^3 of volume for the material of iron, which is entirely possible to be placed at the ground floor.

Then, consider the stiffness softening rate of 0.25 for the first story and stiffness hardening rate of 3 for upper stories, which were commonly used for the simulation result comparison in Chapter 4. For the softening rate of 0.25, using the pin connection for the column with the foundation can easily realize it. To realize the stiffness hardening rate of 3 for the upper stories, a simplified calculation could be done as follows. If the number of column is N in each floor with square section of a*a, the side length of brace should be $b = \frac{a^2}{h}\sqrt{\frac{N}{M}}$, h is the story height, when the number of brace is M in each floor with the angle of 45°. For example, if the number of braces equals to that of columns, h=4m, a=0.2m, the section area of brace is 1% of that of column. Although, the buckling problem will surely be considered in a detailed design and the real section of columns or braces will probably be I or H section, the hardening rate of 3 could be realized by using less quantity of braces comparing to the existing columns.

Because of the retrofit system will experience a larger displacement of the first story comparing to the original structure, the lateral mobility of pipes or elevators should be taken into consideration. Actually, this kind of technique has been developed enough as appeared in Middle-floor seismic isolation buildings [6-11]. The applied methods about the mobility of pipes and elevators in middle-floor seismic isolation buildings could be an important reference for the design of proposed hybrid seismic retrofit systems.

6.5 Conclusion

In this chapter, we considered some practical problems when the proposed retrofit system is applied to a real use. First, the additional stiffness from the TMD supporting frame has been considered and analyzed. Then, a Double adjustment method is proposed when make use of the additional stiffness. The system robustness has been introduced with various mass ratio and additional stiffness. Finally, an initial displacement method is introduced which is considered can improve the system

reliability. The following conclusions could be obtained.

1) When the stiffness ratio α is small, such as less than 0.1, the influence on the vibration control effect is also small and can be ignored. But, if the stiffness ratio α becomes larger, TMD will lose its effect and robustness.

2) The double adjustment method is proposed here, in order to make better use of the additional stiffness from the TMD supporting frame. The numerical method is also introduced here for the TMD optimization of damped primary structure.

Chapter 7

Vision Based Measuring Method

7.1 Research Background

Lots of steel structures had experienced an intense and long transient response caused by the great earthquake motion during the Great East Japan Earthquake on 11th March 2011 [7-1][7-2]. As same as the recent large earthquakes, there were rarely damage reports about structural component. However, according to the damage report of Special Investigation Committee of Architectural Institute of Japan (AIJ), lots of non-structural damages such as ceiling fallen, glass broken, etc. are the main damage characteristics of steel structures, especially the large response of the top floor [7-3]. Furthermore, with the popularity of digital equipment, a lot of videos about the process of building vibrations during the earthquake had been recorded by portable video equipment at different locations which been shared each other through the internet.

In order to know the seismic behavior of the steel structures under the actual situation more clearly or provide some useful references for the further research, in this study, we summarized some opened seismic record of steel structures, and moreover, a vision based method was adopted to obtain the seismic response of high-rise steel buildings at Shinjuku, Tokyo, through a video of TV broadcasting.

Normally, acceleration and velocity signals can be easily acquired by installing corresponding devices such as accelerometers and velocimeters. However, displacement measurement of existing building is quite difficult because traditional displacement sensors, such as linear variable differential transformers (LVDTs) and dial gauges, requires stationary fixed position as the measurement reference. The difficulty of providing reference point has become the crucial problem for displacement

measurement. Although, displacement can be obtained by double integration of acceleration data using acceleration-based technique, the result is not stable because of the bias especially in low-frequency contents [7-4].

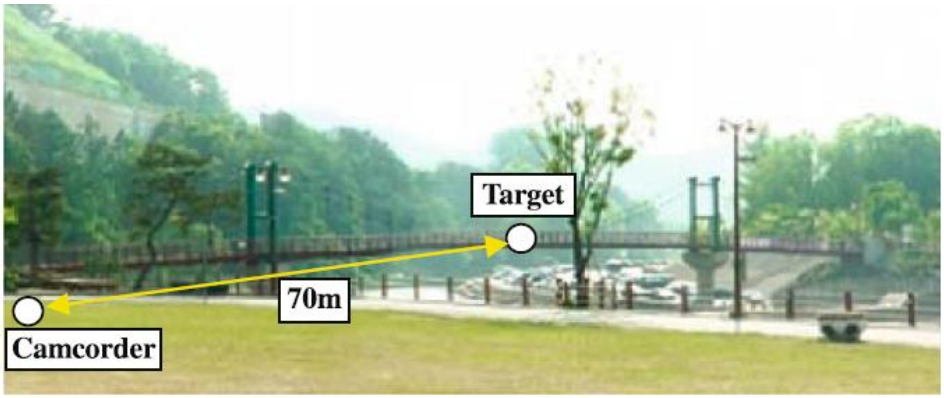

Figure 7.1 An image used displacement measuring system for flexible bridge [7-8]

To overcome this problem, the vision-based method has been developed and studied by researchers through decades especially in bridge measurement. Stephen [7-5] proposed a visual tracking system in the measurement of deck displacement of the Humber Bridge in the UK. A transputer network was adopted to realize parallel tracking which can deal with multiple moving objects in real-time. User-selected templates are extracted from the initial frame and a template matching operation applied repeatedly to track the motion of multiple, independent objects at video frame rate. Using visual tracking system can effectively observe the very low frequency movement of the bridge.

Olaszek [7-6] has developed a viewing system for investigation of the dynamic characteristic of bridges with an additional reference system. The reference point can be used to exclude the effect of translational movement at image capturing camera but not rotational movements. It was possible to measure the displacement of typical bridge structure spans under dynamic and static loads.

Wahbeh [7-7] proposed a vision-based approach for obtaining direct measurements of the absolute displacement time history at Vincent Thomas Bridge using a highly accurate camera with a resolution of 520 lines and a capacity of 450digital zoom. Two high-resolution red lights (LED) are adopted as the targets mounted on a black steel sheet with 28 inches high and 32 inches wide. Optical data reduction and a nonlinear Gaussian regression curve fit were used to obtain the highest intensity of the red spot

and determine the center of the spot, respectively.

Lee [7-8] proposed a digital image processing techniques used for the real-time measurement of dynamic displacement of flexible bridges (Fig. 7.1). A target panel of known geometry was used as the measurement point whose displacement is calculated using the image processing techniques using texture recognition algorithm. Two field tests showed that this method can be successfully utilized to measure the displacement of a flexible bridge, and also highly cost effective and easy to implement.

Park [7-9] supposed a vision-based displacement measurement method for high-rise building structures using partitioning approach. The whole structure is divided into several parts to overcome the visibility range of optical devices. The test results showed that the displacement measurement error is less than 0.5%.

In the previous studies, the camera is all seemed as fixed thus difficult to be used in the seismic response measurement. Even if an additional reference point [7-6] can exclude the rotational movements, the camera with a large zoom concentrating at the target point may lose the target when suffering a strong ground vibration.

With the development of camera industry, highly accurate camera becomes possible thus can provide certain precision in a full-view image. On the other hand, the seismic investigation showed that a quite large response in structures had been occurred during a big earthquake such as the Off Pacific Coast Tohoku Earthquake [7-10]. Especially, the high-rise buildings experienced a long period vibration with big displacement amplitude for a long time. The large displacement can give us the possibility that even if the precision is relatively low in the full-view image, the displacement is also identifiable. These two reasons above provide the theoretical feasibility of the application of the full-view image into seismic response measurement.

In this study, a novel displacement measurement method based on a full-view image is proposed for investigation of seismic response of flexible structures such as high-rise buildings. The whole size of the building is shot in one image while the ground part is seemed as the reference in order to exclude the vibration of the camera including the translational and rotational movement.

7.2 Proposal of Full-view Image Method

7.2.1 Introduction

Figure 7.2 adopted the high-rise building as an example shows the image of the proposed method. The black circle is chosen as the basic template point. Two reference points on the ground floor are used as the reference system to record the vibration of the camera from the earthquake including translational and rotational movement. Several target points which mounted on the floor whose displacement is in interested are used for calculating the relative displacement between the target floor and the ground floor by excluding the camera movement recorded by the two reference points.

7.2.2 Camera movement excluding method

Figure 7.3 shows the camera movement represented by the two reference points. The translational movements of the midpoint of the two reference points are adopted as the camera translational movements. The change of the angle of the straight line connecting the two reference points is adopted as the camera rotational movements.

We assume the coordinates of the two reference point and the ith target point as (x_{R1}, y_{R1}), (x_{R2}, y_{R2}) and (x_{Ti}, y_{Ti}), respectively. And use superscript "0" as the initial position, "k" as the kth frame of the recorded video. So the camera movement of each frame can be calculated as follows.

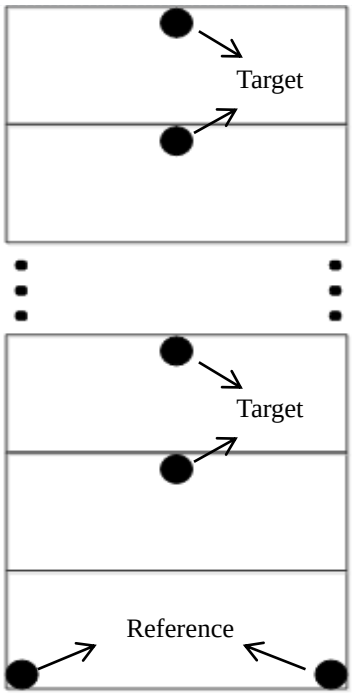

Figure 7.2 Full view image of building

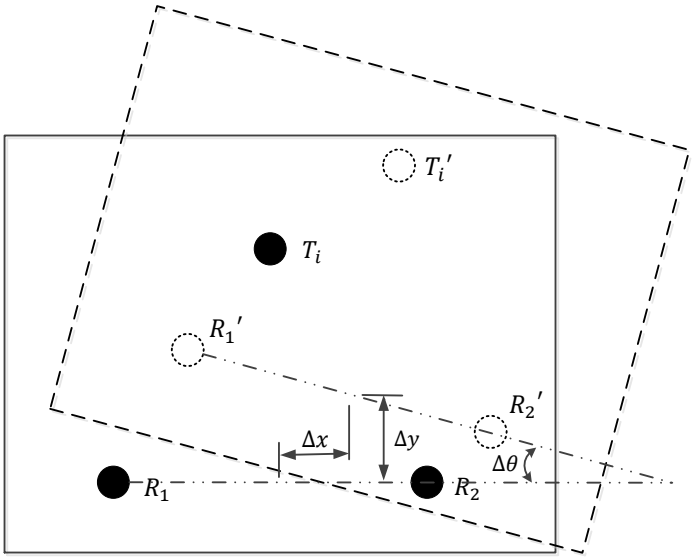

Figure 7.3 Frame movement

$$\Delta x^k = x_m^k - x_m^0 \qquad 7.1$$

$$\Delta y^k = y_m^k - y_m^0 \qquad 7.2$$

$$\Delta\theta^k = \arctan\left\{\frac{\tan\alpha^k - \tan\alpha^0}{1 + \tan\alpha^k \tan\alpha^0}\right\} \quad 7.3$$

Where, Δx^k, Δy^k and $\Delta\theta^k$ are the horizontal displacement, vertical displacement and angle movement at the kth frame, respectively. x_m^k and y_m^k are the coordinates of the midpoint of the two reference points. $\tan\alpha$ and $\tan\beta$ are the inclination angle of the straight line connecting the two reference points at the initial position and the kth frame, respectively. It can be calculated by the following formula.

$$\tan\alpha^0 = \frac{y_{R2}^0 - y_{R1}^0}{x_{R2}^0 - x_{R1}^0} \quad 7.4$$

$$\tan\alpha^k = \frac{y_{R2}^k - y_{R1}^k}{x_{R2}^k - x_{R1}^k} \quad 7.5$$

Then, the excluding of the camera movement for the target point can be done as follows.

$$x_{Ti}^{k\,\prime} = \left(x_{Ti}^k - \Delta x^k - x_m^0\right)\cos\left(-\Delta\theta^k\right) - \left(y_{Ti}^k - \Delta y^k - y_m^0\right)\sin\left(-\Delta\theta^k\right) + x_m^0 \quad 7.6$$

$$y_{Ti}^{k\,\prime} = \left(y_{Ti}^k - \Delta y^k - y_m^0\right)\cos\left(-\Delta\theta^k\right) + \left(x_{Ti}^k - \Delta x^k - x_m^0\right)\sin\left(-\Delta\theta^k\right) + y_m^0 \quad 7.7$$

Where, $x_{Ti}^{k\,\prime}$ and $y_{Ti}^{k\,\prime}$ are the coordinate of target point whose camera movement has been excluded. Finally, the relative displacement of each target point to the ground floor can be calculated by the following formula.

$$dx^k = x_{Ti}^{k\,\prime} - x_{Ti}^0 \quad 7.8$$

$$dy^k = y_{Ti}^{k\,\prime} - y_{Ti}^0 \quad 7.9$$

7.2.3 Implementing procedure

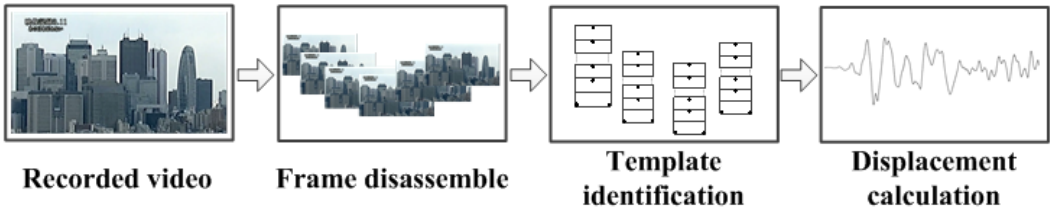

Figure 7.4 Procedure of proposed measuring method

Figure 7.4 shows the procedure of this vision-based measuring method. There are mainly three steps:

Firstly, the recorded video should be disassembled frame by frame, and normally, the frame rate is 25 FPS for PAL standard and 30 FPS for NTSC standard. The frame rate of a normal digital video can reach about 100 FPS, and a high-speed camera can reach up to 1000~10000 FPS. However, a high-speed frame rate device will increase the cost and the difficulty of data storage. Thus a normal speed less than 100 FPS is considered highly cost-effective and high enough to obtain the structural dynamic properties from the result because of the long period of the high rise buildings.

Secondly, the so called template identification is implemented to each image. The black spots located in the white background can be identified from the black-and-white image. Then the coordinate of the center of each spot can be determined using a nonlinear Gaussian regression curve fit as Wahbeh [7-7] did.

Finally, the displacement response can be calculated using formula 8.1~8.9 above. If the precision is good enough, a time history result can be obtained. Otherwise, we can get part of the response or only the peak amplitude which will be illustrated later.

7.3 Validation of the Full-view Image Method by Shaking Table Test

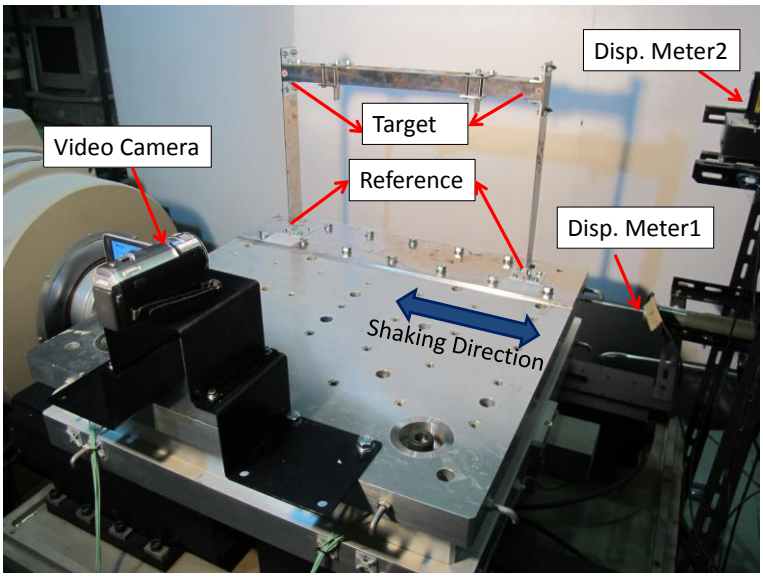

Figure 7.5 Test setup

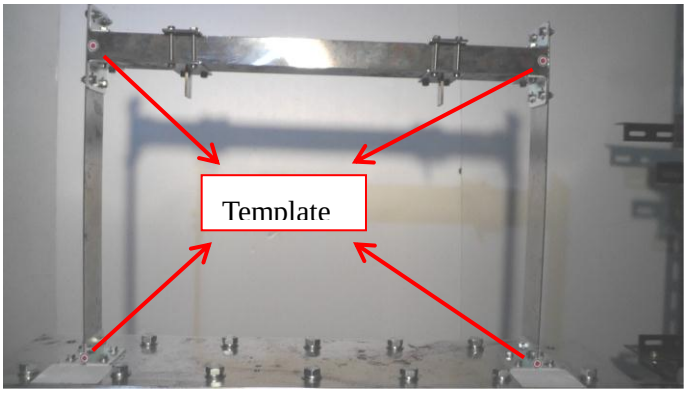

Figure 7.6 The full view image of the specimen

A shaking table test is carried out in order to demonstrate the feasibility of the proposed full-view image method, especially to explore the possibility of the obtainment of time history response. Fig. 7.5 shows the picture of the test setup, which includes a steel frame, the same frame used in the test of Chapter 3.3.4, a video camera, which is placed at on the shaking table. The displacement of the frame would be recorded by a laser displacement meter. Fig. 7.6 shows the full view image shoot by the video camera. There are four templates in the specimen used for the identification of the target point and reference point.

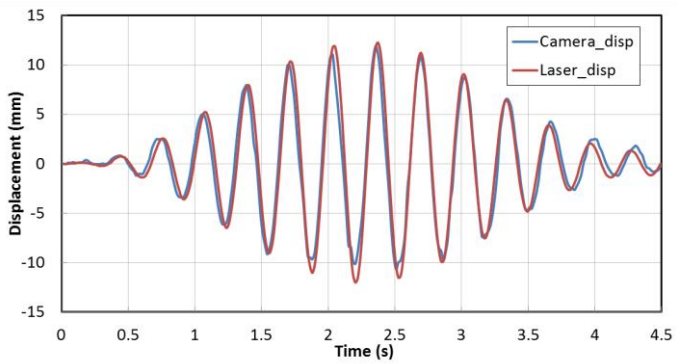

Figure 7.7 The result of Sine wave

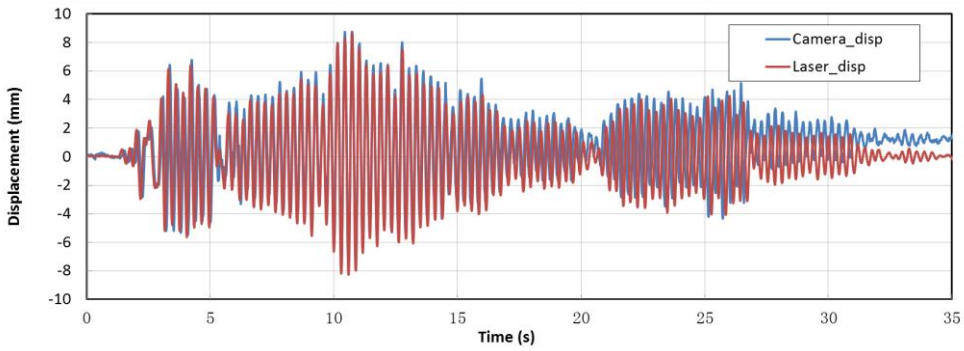

Figure 7.8 The result of El Centro wave

Fig. 7.7 shows the result comparison between the displacement result from the proposed vision method and the displacement result from the laser displacement meter, under a sine wave input. The result showed that a time history displacement response could be obtained using the proposed vision based method. The difference between the results from two measuring methods has an error within 5% at the peak point.

Fig. 7.8 shows the result comparison between the displacement result from the proposed vision method and the displacement result from the laser displacement meter, under an El Centro wave input. The result showed that a time history displacement response of an earthquake input could be obtained using the proposed vision based method. The difference between the results from two measuring methods has an error within 5% at the peak point. But the response from the vision based method has a little bias from the result from laser displacement meter, which is considered caused by the out-of-plane rotation of the specimen.

7.4 Application to a Video of Surveillance Camera

The vibration of the high-rise buildings at Shinjuku (Figure 7.9) during the Great East Japan Earthquake on 11th March 2011 had been recorded by a surveillance camera of Japan Broadcasting Corporation (Nippon Housou Kyoukai) at NHK Broadcasting Center in Shibuya, Tokyo [7-11]. The high-rise buildings had been recorded as full-view image in the video and we analyzed 10 buildings whose vibration was relatively large enough to be identified.

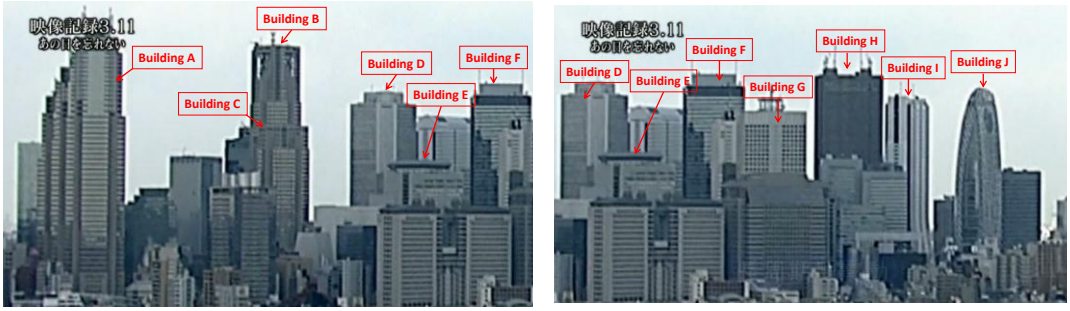

a) **b)**

Figure 7.9 The high-rise building group at Shinjuku, Tokyo

Because the camera which shot this video is used for the temperature observation, the pixel of the image is low (856×480), the frame rate is 3 FPS, and also we had not set the template on the structure. The proposed method in this study can't be applied on this video analysis completely. The following simplifications had been taken into this analysis. Firstly, use the existing remarkable components on the structures such as windows, edge of the wall, as the template of the reference point and target point.

Secondly, because the camera movement had been extruded by handwork, only two point, top and bottom of the building, are adopted to only extrude small residual translational movement and obtain the displacement at the top of the building. Thirdly, only the peak displacements within this video time are resulted instead of time history result because it is quite difficult to recognize the displacement frame by frame without prior template setup under a low pixel.

Table 7.1 The response of the high-rise buildings at Shinjuku

Name	Height (m)	Floors	Structural Style	From Video		From Accelerometer	
				Period(s)	Peak-to-peak Amplitude(m)	Period(s)	Peak-to-peak Amplitude(m)
Building A	235	52 B5	Steel ; BG: SRC, RC	6.9	2.0	—	—
Building B	243	48 B3	Steel ; BG: SRC	5.5	1.6	5.4	1.3
Building C	163	34 B3	Steel ; BG: SRC	4.1	1.0	4.0	1.22
Building D	210	52 B4	Steel ; BG: SRC, RC	4.9	1.9	5.0	—
Building E	122	30 B3	Steel ; BG: SRC	4.4	0.7	—	—
Building F	210	55 B3	Steel ; BG: SRC	6.2	1.2	—	—
Building G	165	32 B3	Steel ; BG: SRC	4.5	1.8	—	—
Building H	216	54 B4	Steel ; BG: SRC, RC	5.5	0.8	5.2	0.98
Building I	193	43 B6	Steel ; BG: SRC, RC	4.8	1.0	—	—
Building J	204	50 B3	Steel ; BG: SRC, RC	4.4	1.0	—	—

Table 7.1 shows the result of this video analysis, the displacement response of the high-rise buildings at Shinjuku. In which, the period and peak-to-peak displacement amplitude of building B and C from the response record has been opened by Tokyo Local Finance Bureau [7-12], as 5.4s, 1.3m and 4s, 1.22m, respectively. The period and peak-to-peak displacement amplitude of Building H was also published [7-13], as 5.2s and 0.98m, respectively. Furthermore, the natural period of Building D was also reported as 5.0s [7-14].

The opened information is also listed in Table 7.1, where, the natural frequency obtained from accelerometer can be seemed has a relatively high precision; however, the displacement information is not so accurate. From the comparison with the opened information, it can be concluded that the natural frequency recognized from the video still has a good precision. Otherwise, the difference of the displacement is not so high, but at the present stage, it is still difficult to judge the accuracy about the displacement recognition. We hope this vision based method could provide a better precision, especially when a high accurate camera was used.

7.5 Earthquake Response Simulation

The earthquake response simulation has been implemented adopted lumped mass

MDOF model. Because of the high precise of the detected natural period of the vision based method, the value of natural period is adopted in modeling process.

7.5.1 Information of the Numerical Model

In this section, a numerical simulation is carried out to explore the response amplitude comparing to the result from the vision based method. As mentioned in the last section, the natural frequency of the buildings recognized by the vision based method has a very small difference from the recorded result. So, the natural frequencies from the vision based method are adopted in the modeling for the numerical simulation.

10 models of the buildings in Table 7.1 have been set up using the lumped mass model, showed in Fig. 7.10. The number of floors of the model is the same as the real building, and the natural frequencies of the first mode from the vision based method is adopted as the first mode of the model. The mass of each floor is assumed as 180kg/m^2 [7-15]. The stiffness of each floor is distributed as $k_N = k_1 \frac{1}{N^{2/3}}$ [7-16], where N means the Nth floor. The damping ratio of the first and second mode is assumed as 1.5%, and Rayleigh damping matrix is used here. The Newmark method is used to solve the motion equilibrium equation.

The input earthquake wave is the record of the 3.11 Great East Japan Earthquake at Shinjuku, as showed in Fig. 7.11. The acceleration time history and the velocity spectrum are showed in Fig. 7.12 and 7.13, respectively.

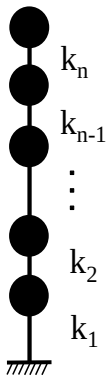

Figure 7.10 The lumped mass model

Figure 7.11 The earthquake record location (modified from google map: https://maps.google.co.jp)

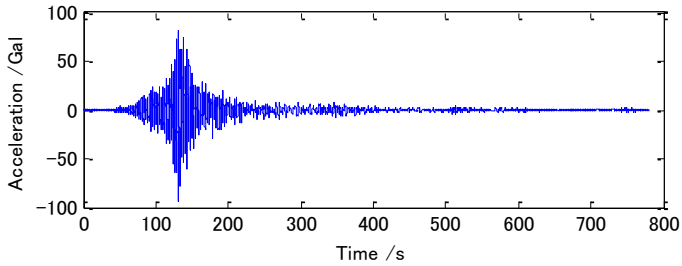

Figure 7.12 Time history of the input earthquake record

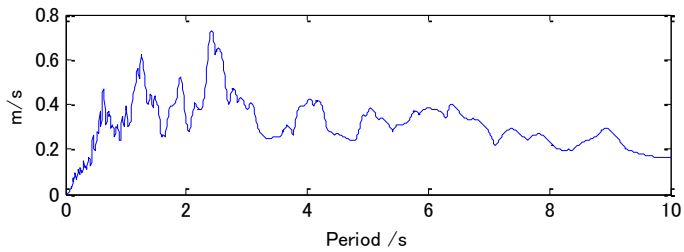

Figure 7.13 The velocity response spectrum of the input earthquake record

7.5.2 Result

The comparison of the numerical simulation and the earthquake record is showed in Fig. 7.14, Fig. 7.15 and Fig. 7.16 for Building B, C and H, respectively. And table 7.2 shows the periods and the peak-to-peak displacement response amplitude from numerical simulation and vision based method.

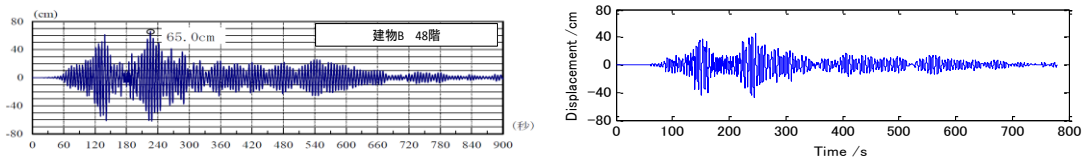

a) Result from record b) Result from simulation

Figure 7.14 Displacement response of the 48th floor of building B

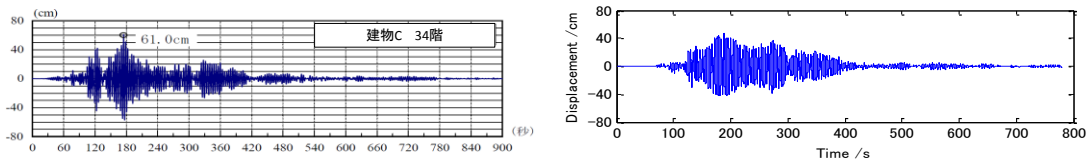

a) Result from record b) Result from simulation

Figure 7.15 Displacement response of the 34th floor of building C

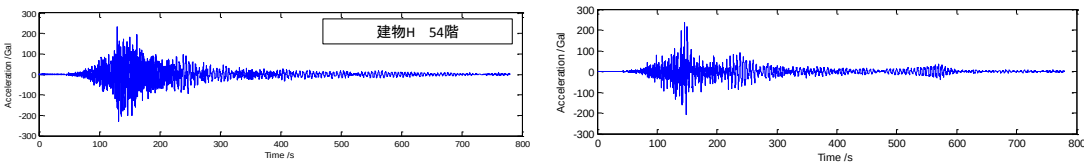

a) Result from record b) Result from simulation

Figure 7.16 Acceleration response of the 54th floor of building H

Table 7.2 The comparison between the peak-to-peak amplitude of the displacement response from the vision based method and that from numerical simulation

Building		A	B	C	D	E	F	G	H	I	J
Period (s)	Mode 1	6.9	5.5	4.1	4.9	4.4	6.2	4.5	5.5	4.8	4.4
	Mode 2	2.8	2.2	1.6	2.0	1.8	2.5	1.8	2.2	1.9	1.8
	Mode 3	1.7	1.4	1.0	1.2	1.1	1.6	1.1	1.4	1.2	1.1
Peak-to-Peak Amplitude (m)	Vision based method	2.0	1.6	1.0	1.9	0.7	1.2	1.8	0.8	1.0	1.0
	Numerical simulation	1.2	0.9	0.9	0.9	0.7	1.5	0.6	0.9	0.6	0.7

From the Fig. 7.13 (a) and (b), we can find that the shape of the response is similar to each other; the amplitude of the numerical one is a little smaller than the record one. Furthermore, from the result in Table 7.2, the difference of the result from vision based method and the numerical simulation is more than 30% for building A, B, D, G and I, and less than 30% for building C, E, F, H and J.

For example, the natural period of Building F is 2.5s, for it is close to the predominant period 2.0s~3.0s of the input earthquake record, the amplitude of the numerical simulation is larger than that from vision based method. The reason for this difference is considered as the natural period of the first mode is assumed as the same to the result from vision based method, but the periods of a higher mode may be far from the real value. Furthermore, the assumed model may possibly different from the real structure. For example, the plane view of building D is a shape of triangle with a hollowed center, which will make the mass matrix and stiffness distribution huge different from the actual structure. These detailed modeling is considered as the future study.

As the popularity and low costly of the smart phone and memory media, the video record could be obtained easier and faster. It is expected that, the higher mode could be identified using a better video with high pixel to improve the precise of this vision based method. It could be a valuable research area in a near future.

7.6 Conclusion

In this chapter, a new vision based displacement measuring method is proposed and discussed. It is appropriate to be applied for structures with large displacement such as high-rise building, structures with soft story or isolated story. First, the basic calculation equations and analysis flow was introduced. Then, a shaking table test has been carried out to test the feasibility for obtaining an historical displacement response. Finally, an application has been implemented into a video from a surveillance camera which recorded the response of the high-rise buildings at Shinjuku during the Great East Japan Earthquake. The conclusions could be obtained as follows.

1) A new vision based displacement measuring method is proposed. It is considered

having great meaning in the earthquake field measurement.

2) The result of the shaking table test demonstrates the feasibility for obtaining a historical displacement response when the camera was suffering earthquake excitations in the same field as the structure.

3) An application for obtaining the displacement response of the high-rise buildings at Shinjuku during the Great East Japan Earthquake illustrated that this measuring method has a high practical value and could be expected doing more contribution.

Chapter 8

Conclusion

8.1 Conclusions of This Thesis

A hybrid seismic retrofit system using TMD and soft-first story principle is proposed. In order to explore the dynamic properties and vibration mitigation effectiveness of the proposed system, mainly 3 parts of works has been done and shown in this thesis. Firstly, the basic theory of optimization methods for TMD was studied and some popular optimum methods were summarized and analyzed. Then, a numerical simulation, including frequency response analysis and earthquake response analysis, has been done and studied. Finally, a shaking table test was carried out to explore the feasibility and effectiveness of the proposed retrofit system. The conclusions can be summarized as follows.

1) The hybrid seismic retrofit systems using TMD and soft-first story principle is proposed for existing medium and low-rise steel buildings in order to reduce their large earthquake response especially at the top floor.

2) It has been demonstrated theoretically that, the softening of the lateral stiffness of the first floor and the hardening of the upper floors could enlarge the TMD virtual mass ratio.

3) From the comparison analysis using 60 earthquake records among three optimum methods, Fixed point method, Minimal variance method and Equal damping method, it can be seen that Fixed point method has the best performance among these three in the respect of the response mitigation effect.

4) The closed-form optimum expressions (Eq. 3.21, 3.24, 3.31, 3.32, 3.39 and 3.40)

for tuning ratio and damping ratio have been formulated for Non-traditional TMD combined with viscous damper or friction damper. And the results from shaking table test for Non-traditional TMD illustrate that this TMD system either combined with viscous damper or friction damper can significantly reduce the resonant vibration for the controlled structure.

5) The Hybrid TMD, which can make the TMD design more freely thus promote the feasibility of the proposed retrofit system, is proposed. A numerical optimum process was proposed for the Hybrid TMD subjected to ground excitation with various mass ratios.

6) The frequency analysis showed that the softening of the lateral stiffness of the first floor and the hardening of the lateral stiffness of the upper floors will reduce the resonant acceleration response of the top floor and the peak drift response from the first floor to the top floor comparing to the original structure.

7) The earthquake response analysis showed that, 4 story model and 8 story model has the best vibration mitigation effect including the control of acceleration response of the top floor and the drift from the first floor to the top floor. And, they have the best stability among those six models according to the result of the coefficient of variation of the response rate.

8) From the shaking table test, for the retrofit pattern 1, it can be concluded that both the peak acceleration response of the top floor and the peak displacement angle from the first floor to the top floor for the TMD combined system could be reduced significantly comparing to the original structure.

9) The effect of the TMD combined system is related to the predominant frequency of the input earthquake. When it is close to the original structure, a better vibration control effect could be obtained.

10) The peak displacement angle of the first floor of the combined TMD systems will be normally larger than that of the original structure. But the maximum moment at the top of the column of the first floor will still be smaller or could keep at a same level to that of the original structure.

11) When the TMD mass ratio is larger, the vibration mitigation effect will be better, the stroke length and the acceleration response of the TMD mass itself will become smaller.

12) A new vision based displacement measuring method is proposed, and its feasibility for obtaining a displacement response history is demonstrated by data analysis of a shaking table test and a real record of the Great East Japan Earthquake, 3.11, 2011.

8.2 Future Work

The author considers the following items should be taken into account as the future study.

1) Considering the P-δ effect into the numerical simulation especially when structure gets higher, and an appropriate evaluation method for the large response of the first story.

2) Because of the effect of the TMD is related to the predominant frequency of the input earthquake, it would be practical to consider the ground property.

3) A limit stroke design method and the numerical simulation of its influence on the vibration mitigation effect should be considered.

4) The design strategy for an extremely large earthquake should be considered probably with fail-safe approach.

5) Further development of practical joints and other structural parts and devices in order to utilize the proposed hybrid seismic retrofit system.

6) The excluding of the out-of-plane rotation of the camera when using full-view image method should be considered.

Reference

Reference of Chapter 1

[1-1] Midorikawa, M., Hasegawa, T., Mukai, A., Nishiyama, I., Fukuta, T. & Yamanouchi, Y. : Damage investigation of steel buildings in specific areas due to the 1995 Hyogoken-Nanbu Earthquake. *J. Struct. Constr. Eng., AIJ*, No. 493, 115-120, 1997 (in Japanese: 1995 年兵庫県南部地震における特定地域の鉄骨造建物被害調査)

[1-2] Hasegawa T.: Estimation of earthquake input level based on damage of steel gymnasiums due to the 2004 Mid Niigata Prefecture Earthquake. J. Struct. Constr. Eng., AIJ, Vol. 73 No. 625, 457-464, Mar., 2008 (in Japanese: 2004 年新潟県中越地震における鉄骨造体育館の被害状況に基づく地震入力レベル推定)

[1-3] National Institute for Land and Infrastructure Management, Ministry of Land, Infrastructure, Transport and Tourism, Japan. & Building Research Institute, Incorporated Administrative Agency, Japan. : Report of field survey of building damages on the Niigataken Chuetsu-oki Earthqukae in 2007, 2007 (in Japanese: 平成 16 年新潟県中越地震建築物被害調査)

[1-4] Architectural Institute of Japan: Preliminary reconnaissance report of the 2011 Tohoku-Chiho Taiheiyo-Oki Earthquake, 2011 (in Japanese: 2011 年東北地方太平洋沖地震災害調査速報)

[1-5] National Institute for Land and Infrastructure Management, Ministry of Land, Infrastructure, Transport and Tourism, Japan. & Building Research Institute, Incorporated Administrative Agency, Japan. : Quick report of the field survey and research on “The 2011 off the Pacific coast of Tohoku Earthquake”(the Great East Japan Earthquake) , 2011 (in Japanese: 平成 23 年(2011 年)東北地方太平洋沖地震(東日本大震災)調査研究(速報))

[1-6] Cheng, C. & Kawaguchi, K. : Preliminary research on the response of steel structures during Off Pacific Coast Tohoku Earthquake, *Summaries of Technical Papers of Annual Meeting, AIJ, Nagoya, Japan*, No.21013, 25-26, 2012 (in Japanese: 東北地方太平洋沖地震における鉄骨造建物の挙動の基礎的調査)

[1-7] Institute of Technology, Shimizu Corporation. : Investigation report of the 1995 Hyogoken-Nanbu Earthquake, 1995 (in Japanese: 1995 年兵庫県南部地震調査報告書)

[1-8] Editorial Committee for the Report on the Hanshin-Awaji Earthquake Disaster.: Report on the Hanshin-Awaji Earthquake Disaster, 1997

[1-9] Architectural Institute of Japan: Guidelines for prevention of fallings of non-structural components, 2013.3 (in Japanese: 天井等の非構造材の落下事故防止ガイドライン)

[1-10] Tsuchimoto, Building damages by earthquake. National Institute for Land and Infrastructure Management, General Research Center for Technological Policy. (in Japanese: 建物の地震動による被害)

[1-11] Kato M.: Prior works in Shinjuku preventing long-period earthquakes for high-rise buildings. Eco Conscious and Human Oriented City, Vol.027, pp.24-27, 2014 (in Japanese: 超高層の長周期地震動対策先行する新宿副都心の事情)

[1-12] The Asahi Shimbun: Shinjuku Center Building, 13 minutes of vibratio – Strengthening of Seismic criterion. 2011.4 (in Japanese: 新宿センタービル、13 分揺れた　国の耐震基準強化へ)

[1-13] Yamamura S.: Sympathy to the Great Earthquake. Home page of Wada Y., The message corner, http://wadaphoto.jp/otayori.htm

[1-14] Fintel M., Khan F. R.: Shock-absorbing soft story concept for multistorey earthquake structures. ACIJ, 66:381-390, 1969

[1-15] Arnold, C. : Soft first stories: truths and myths. Proc 8th WCEE, Vol V:943-949, 1984

[1-16] Chen, Y. Q. & Constantinou, M. C. : Use of Teflon sliders in a modification of the concept of soft first storey. Construction & Building materials, Vol. 6 No. 2:97-105, 1992

[1-17] Boardman, P. R., Wood, B. J. and Carr., A. J. : Union House - a cross braced structure with energy dissipaters. Bull N Z Nat Soc Earthquake Engng, New Zealand, Vol 2:377-388, 1987

[1-18] Charleson, A. Q., Wright, P. D. & Skinner, R. I. : Wellington Central Police Station, Base isolation of an essential facility. Proc. Pacific Conf. Earthquake Engng. New Zealand, V2:377-388, 1987

[1-19] Taisei Corporation. : Vibration control structure using soft first story. http://www.taisei.co.jp/index.html

[1-20] Matsuo K., Yamasaki R., Takehara Y. : Home building of Yachiyo Bank. Building Equipment, pp. 9-15, 2012.5 (in Japanese: 八千代銀行本店)

[1-21] Yamaguchi H.G.: Structural Vibration & Control, 1996 (in Japanese: 構造振動・制御)

[1-22] Frahm H.: Device for damping vibration of bodies. U.S. Patent 989985, 1911

[1-23] Housner, G.W., Bergman, L.A., Caughey, T.K., Chassiakos, A.G., Claus, R.O., Masri, S.F., etc.: Structural control: past, present, future, J. Eng. Mech. 123:897-971, 1997

[1-24] Aly M.A.: Proposed robust tuned mass damper for response mitigation in buildings exposed to multidirectional wind, Struct. Design Tall Spec. Build. DOI: 10.1002/tal. 1068, 2012

[1-25] Kremer E.: Examining the Citicorp case: ethical paragon or chimera, Cross Currents, Vol.52, No 3. 2002

[1-26] Suryawanshi Y. R., Rahane D.T., Dyposoe P.: Study of Tuned Mass Dampers system as vibration controller multistoried buildings, International Journal of Advanced and Innovative research , pp.280-284, 2012

[1-27] Kitamura H., Fujita T., Teramoto T., Kihara H.: Design and analysis of a tower structure with a tuned mass damper, Proceedings of Ninth World Conference on Earthquake Engineering, Tokyo-Kyoto, 1988

[1-28] Lu X., Chen J.: Mitigation of wind-induced response of Shanghai Center Tower by tuned mass damper, Strut. Design Tall Spec. Build. 20, 435-452, 2011

[1-29] Ioannis K.: Structural systems and tuned mass dampers of super-tall buildings: case study of Taipei 101. Master Thesis, Dept. of Civil and Environmental Engineering, Massachusetts Institute of Technology, 2007

[1-30] Ghorbani-Tanha A.K., Noorzad A., Rahimian M.: Mitigation of wind-induced motion of Milad tower by tuned mass damper. Strut. Design Tall Spec. Build. 18: 371-385, Doi: 10.1002/tal. 421

[1-31] Yoshinaka S.: Vibration control of large-span architectural structures using spatially distributed MTMDs. Doctor thesis, 2007 (in Japanese: 分散型 MTMD による大スパン建築構造の振動制御に関する研究)

[1-32] Melkumyan, M.G. : The state-of-the-art in structural control in Armenia and proposal on application of the dynamic dampers for seismically isolated building. Proceedings of the third international workshop on structural control for civil and infrastructure engineering, 2000

[1-33] Melkumyan, M.G. : First application of the dynamic damper in the design of seismically isolated dwelling house. Proceeding of the third European conference on structural control. Vol. I, Mini symposium M6, 2004

[1-34] Taniguchi, T., Kiureghian, A.D., Melkumyan, M.G. : Effect of tuned mass damper on displacement demand of base-isolated structures. Engineering Structures, 30:3478-3488, 2008

Reference of Chapter 2

[2-1] Housner G.W., Bergman L.A., Caughey T.K., Chassiakos A.G., Claus R.O., Masri S.F., etc.: Structural control: past, present, future, J. Eng. Mech. 123:897-971, 1997

[2-2] James M.K., Aseismic base isolation: review and bibliography, Soil Dynamics and Earthquake Engineering, Vol. 5, No. 3:202-216, 1986

[2-3] Yamaguchi H.G.: Structural Vibration & Control, 1996 (in Japanese: 構造振動・制御)

[2-4] Sato K.: Dynamic vibration absorbers and its application, 2010 (in Japanese: 動吸振器とその応用)

[2-5] Sarno L.D., Elnashai A.S.: Bracing systems for seismic retrofitting of steel frames, Journal of Constructional Steel Research, Vol. 65, pp.452-465, 2009

[2-6] Sakamoto J., Kohama Y., Yamazaki T.: On the dynamic behaviour of braced steel frames, Summaries of Technical Papers of AIJ., No. 270, pp.43-52, 1978 (in Japanese: 鉄骨筋かい付ラーメン架構の動的応答性状に関する考察)

Reference of Chapter 3

[3-1] Brock J.E., A note on the damped vibration absorber, Transactions of the American Society of Mechanical Engineers, A-28, 1946

[3-2] Den Hartog, J. P., Mechanical Vibrations, McGraw-Hill, Inc., New York, N.Y.

[3-3] Housner, G.W., Bergman, L.A., Caughey, T.K., Chassiakos, A.G., Claus, R.O., Masri, S.F., etc. Structural control: past, present, future, J. Eng. Mech. 123:897-971, 1997

[3-4] Villaverde R.: Seismic control of structures with damped resonant appendages. Proc., First World Conf. on Struct. Control, Vol. 1, WP4-113-WP4-112, 1999

[3-5] Gupta Y.P.: Chandrasekaren, Absorber system for earthquake excitation, Proc. 4th world conf. on earthquake engineering. Santiago, Chile, Vol. II, pp. 139-148, 1969

[3-6] Kaynia A.M., Veneziano D., Biggs J.M.: Seismic effectiveness of tuned mass dampers. J. Struct. div. ASCE 107, 1465-1484, 1981

[3-7] Sladek J.R., Klingner R.E.: Effect of tuned-mass damper on seismic response. J. struct. div. ASCE 109, 2004-2009, 1983

[3-8] Wirsching P.H., Yao J.T.P.: Safety design concepts for seismic structures. Comput. struct. 3, 809-826, 1973

[3-9] Wirsching P.H., Campbell G.W.: Minimal structural response under random excitation using vibration absorber. Earthquake eng. struct. dyn. 2, 303-312

[3-10] Dong R.G.: Vibration-absorbing effect under seismic excitation, J. struct. div. ASCE 102, 2021-2031, 1976

[3-11] Ohno S., Watari A., Sano I.: Optimum tuning of the dynamic damper to control response of structures to earthquake ground motion. Proc. 6th world conf. on earthquake engineering, New Delhi, India, Vol. 3, pp. 157-161, 1977

[3-12] Jagadish K.S., Prasad B.K.R., Rao P.V.: The inelastic vibration absorber subjected to earthquake gournd motions. Earthquake eng. struct. dyn. 7, 317-326, 1979

[3-13] Sadek F., Mohraz B., Taylor A.W., Chung R.M.: A method of estimating the parameters of tuned mass dampers for seismic applications. Earthquake Engineering and Structural Dynamics, Vol. 26, 617-635, 2007

[3-14] Warburton G.B.: Optimum absorber parameters for various combinations of response and excitation parameters. Earthquake Engineering and Structural Dynamics, Vol. 10, 381-401, 1982

[3-15] Neubert V.H.: Dynamic absorbers applied to a bar that has solid damping, J. acoust. soc. Am. 37, 673-680, 1964

[3-16] Sauer F.M., Garland C.F.: Performance of the viscously damped vibration absorber applied to systems having frequency squared excitation, J. appl. mech. ASME 16, 109-117, 1949

[3-17] Bakre S.V., Jangid R.S.: Optimum parameters of tuned mass damper for damped main system. Struct. Control Health Monit. 14: 448-470, 2007

[3-18] Ghosh A., Basu B.: A closed-form optimal tuning criterion for TMD in damped structures, Struct. Control Health Monit. 14: 681-692, 2007

[3-19] Crandall S.H., Mark W.D.: Random Vibration in Mechanical Systems. Academic Press, New York, 1963

[3-20] Ayorinde E.O., Warburton G.B.: Minimizing structural vibrations with absorbers. Earthquake eng. strut. dyn. 8, 219-236, 1980

[3-21] Villaverde R.: Reduction in seismic response with heavily-damped vibration absorbers, Earthquake eng. struct. dyn. 13, 33-42, 1985

[3-22] Villaverde R.: Seismic control of structures with damped resonant appendages. Proc. 1st world conf. on structural control, 3-5, August, Los Angeles, California, USA, pp. WP4-113-119, 1994

[3-23] Villaverde R., Koyama L.A.: Damped resonant appendages to increase inherent damping in buildings. Earthquake eng. strut. dyn. 22, 491-507, 1993

[3-24] Villaverde R., Martin S.C.: Passive seismic control of cable-stayed bridges with damped resonant appendages, Earthquake eng. struct. dyn. 24, 233-246, 1995

[3-25] Sadek F., Mohraz B., Taylor A.W., Chung R.M.: A method of estimating the parameters of tuned mass dampers for seismic applications. Earthquake eng. struct. dyn. Vol. 26, 617-635, 1997

[3-26] Ren M.Z.: A variant design of the dynamic vibration absorber. Journal of Sound and Vibration , 245(4): 762-770, 2001

[3-27] Liu K.F., Liu J.: The damped dynamic vibration absorbers: revisited and new result. Journal of Sound and Vibration, 284: 1181-189, 2005

[3-28] Wong W.O., Cheung Y.L.: Optimal design of a damped dynamic vibration absorber for vibration control of structure excited by ground motion. Engineering Structures, 30: 282-286, 2008

[3-29] Liu K.F., Coppola G.: Optimal design of damped dynamic vibration absorber for damped primary system. Transactionof the Canadian Society for Mechanical Engineering, 34(1): 119-135, 2010

[3-30] Cheung Y.L., Wong W.O.: H2 optimization of a non-traditional dynamic vibration absorber for vibration control of structures under random force excitation. Journal of Sound and Vibration, 330: 1039-1044, 2011

[3-31] Xiang P., Nishitani A.: Optimum design for more effective tuned mass damper system and its application to base-isolated buildings. Structural Control and Health Monitoring, 2013

[3-32] Pennestri E.: An application of Chebyshev's min-max criterion to the optimum design of a damped dynamic vibration absorber. Journal of Sound and Vibration, Vol. 217, pp. 757-765, 1998

[3-33] Belegundu A., Chandrupatla T.: Optimization Concepts and Applications in Engineering, Prentice-Hall, Inc. Upper Saddle River, New Jersey, 1999

[3-34] Ricciardelli F., Vickery B.J.: Tuned vibration absorbers with dry friction damping. Earthquake Engng. Struct. Dyn. 28, 707-723, 1999

[3-35] Inaudi J.A., Kelly J.M.: Mass damper using friction-dissipating devices. J. Engng. Mech. ASCE 121, pp. 142-149, 1995

Reference of Chapter 4

[4-1] Esteva L.: Nonlinear seismic response of soft-first-story buildings subjected to narrow-band accelerograms. Earthquake Spectra, Vol. 8, No. 3, 1992

[4-2] Saito Y.: Natural period and dynamic property of low-and medium-rise steel structure, Journal of structure engineering, Vol.46B, pp.609-617, 2000 (in Japanese: 中低層鉄骨造建築物の固有周期と動特性)

[4-3] Hurty W.C., Rubinstein M.F.: Dynamics of structures, Prentice-Hall, Inc. Englewood Cliffs, New Jersey, 1964

Reference of Chapter 5

[5-1] Spencer Jr. B.F., Dyke S.J., Deoskar H.S.: Benchmark problems in structural control Part I: Active mass drive system. Proceeding of the 1997ASCE Structural Congress, Portland, Oregon, April 13-16, 1997

[5-2] Spencer Jr. B.F., Dyke S.J., Deoskar H.S.: Benchmark problems in structural control Part II: Active tendon system. Earthquake Engineering & Structural Dynamics, Vol. 27, pp.1141-1147, 1998

[5-3] Soong T.T.: Active structural control: theory and practice. Longman Scientific and Technical, Essex, England, 1990

[5-4] Housner G.W., Soong T.T., Masri S.: Second generation of active structural control in civil engineering. Proc. First World Conference on Structural Control, Pasadena, California, Vol. 1, pp. Panel:3-18, August3-5, 1994

[5-5] Fujino Y., Soong T.T., Spencer Jr. B.F.: Structural control: basic concepts and applications. Proceedings of the ASCE Structures Congress XIV, Chicago, Illinois, April 15-18, 1996

[5-6] Chung L.L., Lin R.C., Soong T.T., Reinborn A.M.: Experiments on active control for MDOF seismic structures. J. of Engrg. Mech., ASCE, Vol. 115, No. 8, pp.1609-1627, 1989

[5-7] Fuji Latex Co. Ltd.: Rotary damper, Catalogue, pp.11, http://jp.c.misumi-ec.com/book/FUL1_01/digitalcatalog.html

[5-8] Takigen: General Catalogue, pp.890, www.takigen.co.jp

[5-9] Chopra A.K.: Dynamics of structures: Theory and applications to earthquake engineering, 2nd Edition, Pearson Education, Inc., 2001

Reference of Chapter 6

[6-1] Fujino Y.: The latest achievement of Tuned Mass Damper, KATAYAMA Technical Report, No. 13, Page: 2-10, 1993 (in Japanese: 同調質量ダンパー(TMD)に関して:最近の成果をまじえて)

[6-2] Yamaguchi H.G.: Structural Vibration & Control, 1996 (in Japanese: 構造振動・制御)

[6-3] Kaynia A.M., Veneziano D., Biggs J.M.: Seismic effectiveness of tuned mass dampers. J. struct. div. ASCE 107, 1465-1484, 1981

[6-4] Sladek J.R., Klingner R.E.: Effect of tuned mass dampers on seismic response. J. strut. eng. ASCE 109, 2004-2009, 1983

[6-5] Sinha R., Igusa T.: Response of primary-secondary systems to short-duration, wide-band input. J. sound vib. 185, 119-137, 1995

[6-6] Ohrui S., Koshika N., Mizuno T., Kobori T., Sakamoto M., Nishimura I., Sasaki K.: Study in pulse type seismic control by initial stroke appended TMD. Proc. 1st int. condf. on motion and vibration control, Yokohama, Japan, 267-272, 1992

[6-7]Abe M.: Semi-active tuned mass dampers for seismic protection of civil structures. Earthquake Engineering and Structural Dynamics, Vol. 25, 743-749, 1996

[6-8] Yoshinaka S., Taniguchi Y.: Vibration control of transient response for spatial structures by using tuned mass dampers with initial displacement-Fundamental investigation about design formulas with initial displacement. J. Struct. Constr. Eng., AIJ, Vol. 75 No. 653, 1299-1308, Jul., 2010 (in Japanese: 初期変位付与型 TMD を用いた空間構造の過渡応答の振動制御―初期変位設計式に関する基礎的検討)

[6-9] Abe M.: Semi-active tuned mass dampers for seismic protection of civil structures. Earthquake Engineering and Structural Dynamics, Vol. 25, pp. 743-749, 1996

[6-10] Tanaka S.: Vibration Control, 3.3 The method for mass adjustment (Semi-active damper with ability for vibration control of impact vibration), 2008.9 (in Japanese: 振動制御、3.3 質量を調整する方式)

[6-11] Sekiya Y., Shigeta M., Ueda N., Miyata K.: Elevators compatible with middle-floor seismic isolation buildings. The Japan Society of Mechanical Engineers, Proceeding of technical conference, 2004.1 (in Japanese: 中間層免震建物対応エレベーター)

Reference of Chapter 7

[7-1] Architectural Institute of Japan: Damage investigation quick report of the Great East Japan Earthquake, 2011.7(in Japanese: 2011 年東北地方太平洋沖地震災害調査速報)

[7-2] National Institute for Land and Infrastructure Management, Building Research Institute: Damage investigation report of the Great East Japan Earthquake, 2012.3 (in Japanese: 平成 23 年東北地方太平洋沖地震被害調査報告)

[7-3] Architectural Institute of Japan: For the prevention of the frequent ceiling failure, Proceeding of the research seminar of department of social needs in 2012, 2012.9 (in Japanese: 頻発する天井の落下事故防止に向けて)

[7-4] Park, K.T., Kim, S.H., Park, H.S. and Lee, K.W.: The determination of bridge displacement using measured acceleration. Engineering Structures, Vol.27, 371-378, 2005

[7-5] Stephen, G.A., Brownjohn, J.M.W. and Taylor C.A.: Measurements of static and dynamic displacement from visual monitoring of the Humber Bridge. Engineering Structures, Vol.15, 197-208, 1993

[7-6] Olaszek, P.: Investigation of the dynamic characteristic of bridge structures using a computer vision method. Measurement, Vol.25, 227-236, 1999

[7-7] Wahheh, A.M., Caffrey J.P. and Masri, S.F.: A vision-based approach for the direct measurement of displacements in vibrating systems. Smart Mater Struct 12, 785-794, 2003

[7-8] Lee, J.J. and Shinozuka, M. Real-time displacement measurement of a flexible bridge using digital image processing techniques. Experimental Mechanics, Vol.46, 105-114, 2006

[7-9] Park, J.W., Lee, J.J., Jung, H.J. and Myung, H.: Vision-based displacement measurement method for high-rise building structures using partitioning approach. NDT&E International, 43, 642-647, 2010

[7-10] Cheng, C. and Kawaguchi, K.: Preliminary research on the response of steel structures during Off Pacific Coast Tohoku Earthquake. Summaries of Technical Papers of Annual Meeting of Architectural Institute of Japan, pp. 25-26 , 2012 (in Japanese: 東北地方太平洋沖地震における鉄骨造建物の挙動の基礎的調査)

[7-11] NHK Channel: NHK Special video record of 3.11-Can't forget that day, Time.20:00-20:58, 2012.3.4 (in Japanese: NHK スペシャル 映像記録 3.11~あの日を忘れない~)

[7-12] Tokyo Local Finance Bureau: The seismic strategies of the first and second Metropolitan Government central government office building from long-period ground motions, 2011.5 (in Japanese: 都庁第一本庁舎・第二本庁舎における長周期時振動対策への取組)

[7-13] Hosozawa N: Earthquake resistant upgrade of Shinjuku Center Building and its effect to long-period ground motions, Symposium of steel structures about the Great East Japan Earthquake, 2011.11.17 (in Japanese: 新宿センタービルの耐震グレードアップと長周期時振動にタイル効果)

[7-14] Yano K, Abe H, Suitsu H: Research about the structure of the Shinjuku Sumitomo Building, Summaries of Technical Papers of Annual Meeting of Architectural Institute of Japan, pp.1527-1528, 1972.10 (in Japanese: 新宿住友ビルの構造に関する研究（その１）構造計画)

[7-15] Committee of Kanto Brand, Architectural Institute of Japan.: Design of steel structures, 1982 (in Japanese: 鋼構造の設計)

[7-16] Esteva L.: Nonlinear seismic response of soft-first-story buildings subjected to narrow-band accelerograms. Earthquake Spectra, Vol. 8, No. 3, 1992

Published Papers

Journal Paper

*[1] Chun CHENG and Ken'ichi KAWAGUCHI: Preliminary research on a seismic retrofit method using Tuned Mass Damper and Soft-first story principle for medium and low-rise existing steel buildings, Engineering Structures (Submit)

*[2] Chun CHENG and Ken'ichi KAWAGUCHI: A preliminary study on the response of steel structures using surveillance camera image with vision-based method during the Great East Japan Earthquake, Measurement (Submit)

*[3] CHENG Chun and KAWAGUCHI Ken'ichi: Preliminary Research on the Response of Steel Structures During Off Pacific Coast Tohoku Earthquake on 11th March 2011 Using a Weather Camera, The Journal of JAEE, Vol.14, No.1, Feb. 2014.02, pp.25-33 (in Japanese)

*[4] Chun CHENG and Ken'ichi KAWAGUCHI: Fundamental research on a seismic retrofit system using TMD and Soft-first story principle: Shaking table test, SEISAN KENKYU, Vol.65, No.6, pp.181-183 (in Japanese)

*[5] Chun CHENG and Ken'ichi KAWAGUCHI: A preliminary study on investigation of seismic response of high-rise buildings using a vision-based method based on full-view image, Bulletin of Earthquake Resistant Structure Research Center, No. 46, March 2013, pp. 99-104

[6] Tao Wang, Chun Cheng and Xun Guo, Model-based predicting and correcting algorithms for substructure online hybrid tests, Earthquake Engng Stuct. Dyn. 2012; 41:2331-2349

[7] Wang Tao, CHENG Chun, A Non-iterative distributed substructure online hybrid test method, Engineering Mechanics, March 2013 (in Chinese)

[8] WANG Tao, CHENG Chun, DU Yufeng, A Non-Iterative Distributed Online Hybrid Test Method, Structural Engineers, Vol.28, No.6, Dec. 2012 (in Chinese)

[9] Liguo Dong, Guo Xun, Cheng Chun. Experimental study on the mechanical behavior of a spatial truss. World Earthquake Engineering. 2010, 26(9), 201-206. (in Chinese)

[10] LIU Hong-biao, HUANG Si-ning, GUO Xun, LI Guo-dong, ZHANG He, CHENG Chun, LI Zhi-xing. A preliminary study on structural damage detection method based on sound wave. Journal of Harbin University of Commerce : Natural Sciences Edition. 2010, 26(1), 81-84 (in Chinese)

Conference Paper

*[11] C. Cheng and K. Kawaguchi: Scale model experiments for the hybrid seismic retrofit system using TMD and Soft-first story principle, Summaries of Technical Papers of Annual Meeting, AIJ, Kinki, Japan, Sep. 12-14, 2014 (in Japanese)

*[12] Chun CHENG and Ken'ichi KAWAGUCHI: A research on hybrid seismic retrofit system using TMD and Soft-first story principle, Proceedings of the 13th World Conference on Seismic Isolation, Energy Dissipation and Active Vibration Control of Structures, Commemoration JSSI 20th Anniversary, Sep. 24-27 2013, Sendai, Japan, No.865257

*[13] C. Cheng and K. Kawaguchi: Preliminary Research on the Response of Steel Structures During Off Pacific Coast Tohoku Earthquake, Summaries of Technical Papers of Annual Meeting, AIJ, Nagoya, Japan, Sep. 12-14, 2012, No.21013, pp. 25-26 (in Japanese)

*[14] CHENG Chun and KAWAGUCHI Ken'ichi: Preliminary Research on the hybrid seismic retrofit system using TMD and Soft-first story principle for buildings with moderate heights, Summaries of Technical Papers of Annual Meeting, AIJ, Hokaido, Japan, Aug. 2012, No.21517, pp. 1033-1034 (in Japanese)

[15] Tao WANG, Chun CHENG, A Model-based Predictor-Corrector Algorithm for

Substructure Hybrid Test System, Proceedings of the Ninth Pacific Conference on Earthquake Engineering, Building an Earthquake-Resilient Society, 14-16 April, 2011, Auckland, New Zealand

[16] Chun CHENG, Tao WANG, Chenshou DUAN, Xun GUO. A model based predictor-corrector algorithm for substructure hybrid test system. Proceedings of the 11th International Symposium on Structural Engineering, 2010, pp. 1948-1954

Note: papers with * are related to this thesis.

Appendix A

Equivalent mass of Fundamental Mode

First, the mode method [2-4] for obtaining equivalent mass is introduced here. For an MDOF dynamic system with N degrees of freedom, the *i*th mode which is aimed to be controlled can be written as Eq. A.1.

$$\{x_1 \ \dots \ x_j \ \dots \ x_N\}^T \qquad \text{A.1}$$

The velocity for each mass point for this mode ($\omega = \omega_i$) should be

$$\rho x_1, \dots, \rho x_j, \dots, \rho x_N \ \ (\rho \ \text{ is the factor}) \qquad \text{A.2}$$

The total kinetic energy T_{total} of the whole system is as follows

$$T_{total} = \frac{1}{2}\rho^2(m_1{x_1}^2 + m_2{x_2}^2 + \cdots + m_j{x_j}^2 + \cdots + m_N{x_N}^2) \qquad \text{A.3}$$

Use 1DOF equivalent mass M_{ji} taking place of the MDOF system at the place of *j*th mass, the kinetic energy T_j is as follows

$$T_j = \frac{1}{2}M_{ji}(\rho x_j)^2 \qquad \text{A.4}$$

The equivalent mass could be obtained letting $T_{total} = T_j$, it can be expressed as follows

$$M_{ji} = m_1\left(\frac{x_1}{x_j}\right)^2 + m_2\left(\frac{x_2}{x_j}\right)^2 + \cdots + m_j\left(\frac{x_j}{x_j}\right)^2 + \cdots + m_N\left(\frac{x_N}{x_j}\right)^2 \qquad \text{A.5}$$

Then, consider the 2DOF system in Chapter 2, the mode shape of the fundamental mode can be obtained as Eq. A.6

$$\Phi_1 = \begin{Bmatrix} 1 \\ 1 \\ \hline 1 - \dfrac{A - \sqrt{A^2 - B}}{2k_2 m_1} \end{Bmatrix} \qquad \text{A.6}$$

Where $= k_1 m_2 + k_2 m_1 + k_2 m_2$ $B = 4k_1 k_2 m_1 m_2$, Then, we can get the equivalent mass of fundamental mode as Eq. A.7

$$M_1{}^* = \Phi_1{}^T M \Phi_1 = m_1 + \frac{m_2}{\left(1 - \dfrac{A - \sqrt{A^2 - B}}{2k_2 m_1}\right)^2} \qquad \text{A.7}$$

Obviously, the following relationship could be found from Eq. A.7

$$M_1{}^* > m_1 + m_2 \qquad \text{A.8}$$

Then, the partial differential of $M_1{}^*$ to k_1 could be obtained

$$\frac{\partial M_1{}^*}{\partial k_1} = \frac{m_2{}^2}{k_2 m_1} \frac{1}{\left(1 - \dfrac{A - \sqrt{A^2 - B}}{2k_2 m_1}\right)^3} \left(1 - \frac{A - 2k_2 m_1}{\sqrt{A^2 - B}}\right) \qquad \text{A.9}$$

Because of

$$\left(\frac{A - 2k_2 m_1}{\sqrt{A^2 - B}}\right)^2 = \frac{A^2 + 4k_2{}^2 m_1{}^2 - 4k_2 m_1 A}{A^2 - B} = \frac{A^2 - B - 4k_2{}^2 m_1 m_2}{A^2 - B} < 1 \qquad \text{A.10}$$

It can be concluded that

$$1-\frac{A-2k_2m_1}{\sqrt{A^2-B}}>0 \qquad \text{A.11}$$

And because

$$\frac{{m_2}^2}{k_2m_1}\frac{1}{\left(1-\frac{A-\sqrt{A^2-B}}{2k_2m_1}\right)^3}>0 \qquad \text{A.12}$$

It can be finally obtained that

$$\frac{\partial {M_1}^*}{\partial k_1}>0 \qquad \text{A.13}$$

The partial differential of ${M_1}^*$ to k_2 could be obtained

$$\begin{aligned}\frac{\partial {M_1}^*}{\partial k_2}&=\frac{m_2}{m_1{k_2}^2}\frac{1}{\left(1-\frac{A-\sqrt{A^2-B}}{2k_2m_1}\right)^3}\left(\frac{A^2-\frac{1}{2}B-k_2m_1A-k_2m_2A}{\sqrt{A^2-B}}-k_1m_2\right)\\&=\frac{m_2}{m_1{k_2}^2}\frac{1}{\left(1-\frac{A-\sqrt{A^2-B}}{2k_2m_1}\right)^3}\left(k_1m_2\frac{k_1m_2+k_2m_2-k_2m_1}{\sqrt{A^2-B}}-k_1m_2\right)\end{aligned} \qquad \text{A.14}$$

Because of

$$\frac{(k_1m_2+k_2m_2-k_2m_1)^2}{A^2-B}=\frac{A^2-B-4{k_2}^2m_1m_2}{A^2-B}<1 \qquad \text{A.15}$$

It can be concluded that

$$k_1m_2\frac{k_1m_2+k_2m_2-k_2m_1}{\sqrt{A^2-B}}-k_1m_2<0 \qquad \text{A.16}$$

And because

$$\frac{m_2}{m_1 {k_2}^2} \frac{1}{\left(1 - \frac{A - \sqrt{A^2 - B}}{2k_2 m_1}\right)^3} > 0 \qquad \text{A.17}$$

It can be finally obtained that

$$\frac{\partial {M_1}^*}{\partial k_2} < 0 \qquad \text{A.18}$$

Let $a = \frac{k_1}{k_2}$, The partial differential of ${M_1}^*$ to a could be obtained

$$\frac{\partial {M_1}^*}{\partial \frac{k_1}{k_2}} = \frac{\partial {M_1}^*}{\partial a} = \frac{m_2}{\left(1 - \frac{A - \sqrt{A^2 - B}}{2k_2 m_1}\right)^3} \left(1 - \frac{a m_1 + m_1 - m_2}{\sqrt{(a m_1 + m_1 + m_2)^2 - 4 a m_1 m_2}}\right) \qquad \text{A.19}$$

Because of

$$\left(\frac{a m_1 + m_1 - m_2}{\sqrt{(a m_1 + m_1 + m_2)^2 - 4 a m_1 m_2}}\right)^2 = \frac{(a+1){m_1}^2 + {m_2}^2 - 2 a m_1 m_2 - 2 m_1 m_2}{(a+1){m_1}^2 + {m_2}^2 - 2 a m_1 m_2 + 2 m_1 m_2} < 1 \qquad \text{A.20}$$

The following equation could be obtained

$$1 - \frac{a m_1 + m_1 - m_2}{\sqrt{(a m_1 + m_1 + m_2)^2 - 4 a m_1 m_2}} > 0 \qquad \text{A.21}$$

It can be finally concluded that

$$\frac{\partial {M_1}^*}{\partial \frac{k_1}{k_2}} > 0 \qquad \text{A.22}$$

Appendix B

Optimization for Non-traditional TMD Subjected to Ground Excitation

The absolute value of the transfer function is showed as follows.

$$|H(\beta)| = \frac{1}{\omega_P{}^2}\sqrt{\frac{(\beta^2-\gamma^2-\mu\gamma^2)^2+(2\xi_T\beta\gamma)^2}{[(-\beta^2+1+\mu\gamma^2)(-\beta^2+\gamma^2)-\mu\gamma^4]^2+(-\beta^2+1+\mu\gamma^2)^2(2\xi_T\beta\gamma)^2}} \qquad \text{B.1}$$

We could found that the transfer function of the non-traditional TMD has the same property as the conventional TMD, as Den Hartog found, that the function will pass through two fixed points whatever the TMD damping is if the frequency ratio is seemed as the independent variable. Therefore, the Fixed point method can be used in this optimization problem.

Firstly, choose the optimum tuning ratio which will let the two fixed points have the same height. Because the value of the fixed point has no relationship with the TMD damping ratio, the following formula could be obtained.

$$\frac{\beta^2-\gamma^2-\mu\gamma^2}{(-\beta^2+1+\mu\gamma^2)(-\beta^2+\gamma^2)-\mu\gamma^4} = \pm\frac{1}{-\beta^2+1+\mu\gamma^2} \qquad \text{B.2}$$

Which leads to

$$2\beta^4-(2+3\mu\gamma^2+2\gamma^2)\beta^2-\mu\gamma^4+(2\gamma^2+\mu\gamma^2)(1+\ \mu\gamma^2)=0 \qquad \text{B.3}$$

On the other hand, when $\xi_T \to \infty$, we can get

$$\frac{1}{-{\beta_1}^2 + 1 + \mu\gamma^2} = -\frac{1}{-{\beta_2}^2 + 1 + \mu\gamma^2} \qquad \text{B.4}$$

Which leads to

$${\beta_1}^2 + {\beta_2}^2 = 2 + 2\mu\gamma^2 \qquad \text{B.5}$$

From, Eq. B.3, the sum of two roots can be obtained as

$${\beta_1}^2 + {\beta_2}^2 = \frac{2 + 3\mu\gamma^2 + 2\gamma^2}{2} \qquad \text{B.6}$$

Let Eq. B.5 equals to Eq. B.6, the optimum tuning ratio and the frequency ratio at the two fixed points could be obtained.

$$\gamma^{opt} = \frac{1}{\sqrt{1 - \frac{\mu}{2}}} \qquad \text{B.7}$$

Furthermore, substitute Eq. B.7 to Eq. B.3, the roots of can be obtained as

$${\beta_{1,2}}^2 = \frac{2 + \mu \mp \sqrt{2\mu}}{2 - \mu} \qquad \text{B.8}$$

Then, the second step is to choose the optimum damping ratio which will let the response function curve pass the fixed points horizontally. Define R as

$$\begin{aligned} R^2 &= \frac{A}{B} = (|H(\omega)|{\omega_P}^2)^2 \\ &= \frac{(\beta^2 - \gamma^2 - \mu\gamma^2)^2 + \left(2\xi_T\beta\gamma\right)^2}{[(-\beta^2 + 1 + \mu\gamma^2)(-\beta^2 + \gamma^2) - \mu\gamma^4]^2 + (-\beta^2 + 1 + \mu\gamma^2)^2\left(2\xi_T\beta\gamma\right)^2} \end{aligned} \qquad \text{B.9}$$

where

$$A = (\beta^2 - \gamma^2 - \mu\gamma^2)^2 + \left(2\xi_T\beta\gamma\right)^2 \qquad \text{B.10}$$

$$B = [(-\beta^2 + 1 + \mu\gamma^2)(-\beta^2 + \gamma^2) - \mu\gamma^4]^2 + (-\beta^2 + 1 + \mu\gamma^2)^2\left(2\xi_T\beta\gamma\right)^2 \qquad \text{B.11}$$

So, the problem is to obtain the root of its differential equation.

$$\frac{\partial R^2}{\partial(\beta^2)} = 0 \qquad \text{B.12}$$

Which leads to

$$\frac{\partial A}{\partial(\beta^2)}B - \frac{\partial B}{\partial(\beta^2)}A = 0 \qquad \text{B.13}$$

Where

$$\frac{\partial A}{\partial(\beta^2)} = 2(\beta^2 - \gamma^2 - \mu\gamma^2) + \left(2\xi_T\gamma\right)^2 \qquad \text{B.14}$$

$$\begin{aligned}\frac{\partial B}{\partial(\beta^2)} &= 2[(-\beta^2 + 1 + \mu\gamma^2)(-\beta^2 + \gamma^2) - \mu\gamma^4](2\beta^2 - \gamma^2 - 1 - \mu\gamma^2) \\ &- 2\left(2\xi_T\beta\gamma\right)^2(-\beta^2 + 1 + \mu\gamma^2) + \left(2\xi_T\gamma\right)^2(-\beta^2 + 1 + \mu\gamma^2)^2\end{aligned} \qquad \text{B.15}$$

Substituted by ${\beta_1}^2$ of Eq. B.8 and Eq. B.7, the following formula B.16~B.19 can be obtained

$$\beta^2 - \gamma^2 - \mu\gamma^2 = \frac{-\mu - \sqrt{2\mu}}{2 - \mu} \qquad \text{B.16}$$

$$-\beta^2 + \gamma^2 = \frac{-\mu + \sqrt{2\mu}}{2 - \mu} \qquad \text{B.17}$$

$$-\beta^2 + 1 + \mu\gamma^2 = \frac{\sqrt{2\mu}}{2 - \mu} \qquad \text{B.18}$$

$$2\beta^2 - \gamma^2 - 1 - \mu\gamma^2 = \frac{\mu - \sqrt{2\mu}}{2 - \mu} \qquad \text{B.19}$$

And, substituted by ${\beta_2}^2$ of Eq. B.8 and Eq. B.7, the following formula B.20~B.23 can be obtained

$$\beta^2 - \gamma^2 - \mu\gamma^2 = \frac{-\mu + \sqrt{2\mu}}{2 - \mu} \qquad \text{B.20}$$

$$-\beta^2 + \gamma^2 = \frac{-\mu - \sqrt{2\mu}}{2 - \mu} \qquad \text{B.21}$$

$$-\beta^2 + 1 + \mu\gamma^2 = \frac{-\sqrt{2\mu}}{2 - \mu} \qquad \text{B.22}$$

$$2\beta^2 - \gamma^2 - 1 - \mu\gamma^2 = \frac{\mu + \sqrt{2\mu}}{2 - \mu} \qquad \text{B.23}$$

Let $\frac{\partial R}{\partial(\beta^2)}$ equals to zero at point P, substitute Eq. B.16~Eq. B.19 to Eq. B.13, ξ_T can be calculated. This is a long and tedious job, which leads to the result

$$\xi_{T,1}{}^2 = \frac{6\mu\sqrt{2\mu} - \mu^2\sqrt{2\mu} + 4\mu^2}{16\sqrt{2\mu} + 8\mu\sqrt{2\mu} - 16\mu} \qquad \text{B.24}$$

Then, let $\frac{\partial R}{\partial(\beta^2)}$ equals to zero at point Q, substitute Eq. B.20~Eq. B.23 to Eq. B.13, which leads to

$$\xi_{T,2}{}^2 = \frac{6\mu\sqrt{2\mu} - \mu^2\sqrt{2\mu} - 4\mu^2}{16\sqrt{2\mu} + 8\mu\sqrt{2\mu} + 16\mu} \qquad \text{B.25}$$

Finally, the optimum damping ratio is determined as the average of the results, showed in Eq. B.16 and Eq. B.17, of the two fixed points P and Q.

$$\xi_T{}^{opt} = \sqrt{\mu\frac{12 + 8\mu - \mu^2}{32 + 16\mu + 8\mu^2}} \qquad \text{B.26}$$

Appendix C

Optimization for Non-traditional TMD with Friction Damper Subjected to Force Excitation

The equilibrium equations of motion for non-traditional TMD subjected to force excitation is as follows

$$\begin{bmatrix} m_P & \\ & m_T \end{bmatrix}\begin{Bmatrix} \ddot{x_P} \\ \ddot{x_T} \end{Bmatrix} + \begin{bmatrix} c_P & \\ & c_T \end{bmatrix}\begin{Bmatrix} \dot{x_P} \\ sgn(\dot{x_T}) \end{Bmatrix} + \begin{bmatrix} k_P + k_T & -k_T \\ -k_T & k_T \end{bmatrix}\begin{Bmatrix} x_P \\ x_T \end{Bmatrix} = \begin{Bmatrix} q(t) \\ 0 \end{Bmatrix} \qquad \text{C.1}$$

$$q(t) = q_0 sin\omega t$$

$$x_P = x_1 \sin(\omega t + \varphi_1)$$

$$x_T = x_2 \sin(\omega t + \varphi_2)$$

If there was relative friction, the following motion equation could be obtained

$$m_P \ddot{x_1} + c_P \dot{x_1} + (k_P + k_T) x_1 = q(t) \qquad \text{C.2}$$

Then, x_1 could be solved as follows

$$x_1 = \frac{q_0}{k_1} \frac{1}{-\beta^2 + 1 + \mu\gamma^2 + 2\xi_1 \beta i}$$

$$|x_1| = \frac{q_0}{k_P} \frac{1}{\sqrt{(-\beta^2 + 1 + \mu\gamma^2)^2 + (2\xi_1 \beta)^2}} \qquad \text{C.3}$$

If the relative motion was triggered, the following relationship could be obtained

$$k_T x_1 = c_0$$

$$|x_1| = \frac{c_0}{k_T} \qquad \text{C.4}$$

Let Eq. C.3 equals to Eq. C.4, $q_{0,lim}$ and ${\beta^2}_{lim}$ could be obtained respectively

$$q_{0,lim} = \frac{c_0}{\mu\gamma^2}\sqrt{(-\beta^2 + 1 + \mu\gamma^2)^2 + (2\xi_1\beta)^2} \qquad \text{C.5}$$

$${\beta^2}_{lim} = 1 + \mu\gamma^2 \pm \frac{q_0\mu\gamma^2}{c_0} \qquad \text{C.6}$$

If there was no friction damping, $|x_1|$ could be obtained using the first equation in Eq. C.1

$$|x_1| = \frac{q_0}{k_P}\frac{|-\beta^2 + \gamma^2|}{|(-\beta^2 + \gamma^2)(1 - \beta^2 + \mu\gamma^2) - \mu\gamma^4|} \qquad \text{C.7}$$

Let Eq. C.3 equals to Eq. C.7, which leads to

$$\beta^2 = \frac{B \pm \sqrt{B^2 - 8C}}{4} \qquad \text{C.8}$$

where

$$B = 2(1 + \mu\gamma^2 + \gamma^2) \qquad \text{C.9}$$

$$C = 2\gamma^2 + \mu\gamma^4 \qquad \text{C.10}$$

Let Eq. C.6 equals to Eq. C.8, which leads to

$$c_0 = q_0 \frac{\mu\gamma^2}{\pm\frac{B \pm \sqrt{B^2 - 8C}}{4} \mp (1 + \mu\gamma^2)} \qquad \text{C.11}$$

Let the two values equals to each other in Eq. C.11, which leads to

$$\gamma^{opt} = \frac{1}{\sqrt{1 - \mu}} \qquad \text{C.12}$$

Then, the optimum value of c_0 could be obtained by substitute Eq. C.12 into Eq. C.11

$${c_0}^{opt} = \sqrt{2\mu} q_0 \qquad \text{C.13}$$

Appendix D

Optimization for Non-traditional TMD with Friction Damper Subjected to Ground Excitation

The equilibrium equations of motion for non-traditional TMD subjected to ground excitation is as follows

$$\begin{bmatrix} m_P & \\ & m_T \end{bmatrix} \begin{Bmatrix} \ddot{x_P} \\ \ddot{x_T} \end{Bmatrix} + \begin{bmatrix} c_P & \\ & c_T \end{bmatrix} \begin{Bmatrix} \dot{x_P} \\ sgn(\dot{x_T}) \end{Bmatrix} + \begin{bmatrix} k_P + k_T & -k_T \\ -k_T & k_T \end{bmatrix} \begin{Bmatrix} x_P \\ x_T \end{Bmatrix} = \begin{Bmatrix} -m_P \ddot{u_g} \\ -m_T \ddot{u_g} \end{Bmatrix} \qquad \text{D.1}$$

$$q(t) = q_0 sin\omega t$$

$$x_P = x_1 \sin(\omega t + \varphi_1)$$

$$x_T = x_2 \sin(\omega t + \varphi_2)$$

If there was relative friction, the following motion equation could be obtained

$$m_P \ddot{x_1} + c_1 \dot{x_1} + (k_P + k_T) x_1 = -m_P \ddot{u_g} \qquad \text{D.2}$$

Then, x_1 could be solved as follows

$$x_1 = \frac{q_0}{k_P} \frac{m_P}{-\beta^2 + 1 + \mu\gamma^2 + 2\xi_1 \beta i}$$

$$|x_1| = \frac{q_0}{k_P} \frac{m_P}{\sqrt{(-\beta^2 + 1 + \mu\gamma^2)^2 + (2\xi_1 \beta)^2}} \qquad \text{D.3}$$

If the relative motion was triggered, the following relationship could be obtained

$$k_T x_1 = c_0$$

$$|x_1| = \frac{c_0}{k_T} \qquad \text{D.4}$$

Let Eq. C.3 equals to Eq. C.4, $q_{0,lim}$ and ${\beta^2}_{lim}$ could be obtained respectively

$$q_{0,lim} = \frac{c_0}{\mu\gamma^2 m_P}\sqrt{(-\beta^2 + 1 + \mu\gamma^2)^2 + (2\xi_1\beta)^2} \qquad \text{D.5}$$

$${\beta^2}_{lim} = 1 + \mu\gamma^2 \pm \frac{q_0\mu\gamma^2}{c_0} m_P \qquad \text{D.6}$$

If there was no friction damping, $|x_1|$ could be obtained using the first equation in Eq. C.1

$$|x_1| = \frac{q_0}{k_P}\frac{|-m_P(-\beta^2 + \gamma^2) - m_T\gamma^2|}{|(-\beta^2 + \gamma^2)(1 - \beta^2 + \mu\gamma^2) - \mu\gamma^4|} \qquad \text{D.7}$$

Let Eq. C.3 equals to Eq. C.7, which leads to

$$\beta^2 = \frac{B \pm \sqrt{B^2 - 8C}}{4} \qquad \text{D.8}$$

where

$$B = 2 + 3\,\mu\gamma^2 + 2\gamma^2 \qquad \text{D.9}$$

$$C = \gamma^2 + (\gamma^2 + \mu\gamma^2)(1 + \mu\gamma^2) \qquad \text{D.10}$$

Let Eq. C.6 equals to Eq. C.8, which leads to

$$c_0 = q_0 \frac{\mu\gamma^2 m_P}{\pm\frac{B \pm \sqrt{B^2 - 8C}}{4} \mp (1 + \mu\gamma^2)} \qquad \text{D.11}$$

Let the two values equals to each other in Eq. C.11, which leads to

$$\gamma^{opt} = \frac{1}{\sqrt{1 - \frac{\mu}{2}}} \qquad \text{D.12}$$

Then, the optimum value of c_0 could be obtained by substitute Eq. C.12 into Eq. C.11

$${c_0}^{opt} = \sqrt{2\mu} m_P q_0 \qquad \text{D.13}$$

Appendix E

Input Earthquake Record for Numerical Simulation

Table E.1 List of the input earthquake record

EQ No.	Description	Mag.	Epicentral Distance (km)	PGA (cm/sec^2)
01	FN Imperial Valley, 1940, El Centro	6.9	10.0	452.03
02	FP Imperial Valley, 1940, El Centro	6.9	10.0	662.88
03	FN Imperial Valley, 1979, Array #05	6.5	4.1	386.04
04	FP Imperial Valley, 1979, Array #05	6.5	4.1	478.65
05	FN Imperial Valley, 1979, Array #06	6.5	1.2	295.69
06	FP Imperial Valley, 1979, Array #06	6.5	1.2	230.08
07	FN Landers, 1992, Barstow	7.3	36.0	412.98
08	FP Landers, 1992, Barstow	7.3	36.0	417.49
09	FN Landers, 1992, Yermo	7.3	25.0	509.70
10	FP Landers, 1992, Yermo	7.3	25.0	353.35
11	FN Loma Prieta, 1989, Gilroy	7.0	12.0	652.49
12	FP Loma Prieta, 1989, Gilroy	7.0	12.0	950.93
13	FN Northridge, 1994, Newhall	6.7	6.7	664.93
14	FP Northridge, 1994, Newhall	6.7	6.7	644.49
15	FN Northridge, 1994, Rinaldi RS	6.7	7.5	523.30
16	FP Northridge, 1994, Rinaldi RS	6.7	7.5	568.58
17	FN Northridge, 1994, Sylmar	6.7	6.4	558.43
18	FP Northridge, 1994, Sylmar	6.7	6.4	801.44
19	FN North Palm Springs, 1986	6.0	6.7	999.43
20	FP North Palm Springs, 1986	6.0	6.7	967.61
21	FN 1995 Kobe	6.9	3.4	1258.00
22	FP 1995 Kobe	6.9	3.4	902.75
23	FN 1989 Loma Prieta	7.0	3.5	409.95
24	FP 1989 Loma Prieta	7.0	3.5	463.76
25	FN 1994 Northridge	6.7	7.5	851.62
26	FP 1994 Northridge	6.7	7.5	925.29
27	FN 1994 Northridge	6.7	6.4	908.70

28	FP 1994 Northridge	6.7	6.4	1304.10
29	FN 1974 Tabas	7.4	1.2	793.45
30	FP 1974 Tabas	7.4	1.2	972.58
31	FN Elysian Park	7.1	17.5	1271.20
32	FP Elysian Park	7.1	17.5	1163.50
33	FN Elysian Park	7.1	10.7	767.26
34	FP Elysian Park	7.1	10.7	667.59
35	FN Elysian Park	7.1	11.2	973.16
36	FP Elysian Park	7.1	11.2	1079.30
37	FN Palos Verdes	7.1	1.5	697.84
38	FP Palos Verdes	7.1	1.5	761.31
39	FN Palos Verdes	7.1	1.5	490.58
40	FP Palos Verdes	7.1	1.5	613.28
41	FN Coyote Lake, 1979	5.7	8.8	578.34
42	FP Coyote Lake, 1979	5.7	8.8	326.81
43	FN Imperial Valley 1979	6.5	1.2	140.67
44	FP Imperial Valley 1979	6.5	1.2	109.45
45	FN Kern, 1952	7.7	107.0	141.49
46	FP Kern, 1952	7.7	107.0	156.02
47	FN Landers, 1992	7.3	64.0	331.22
48	FP Landers, 1992	7.3	64.0	301.74
49	FN Morgan Hill, 1984	6.2	15.0	312.41
50	FP Morgan Hill, 1984	6.2	15.0	535.88
51	FN Parkfield, 1966, Cholame 5W	6.1	3.7	765.65
52	FP Parkfield, 1966, Cholame 5W	6.1	3.7	619.36
53	FN Parkfield, 1966, Cholame 8W	6.1	8.0	680.01
54	FP Parkfield, 1966, Cholame 8W	6.1	8.0	775.05
55	FN North Palm Springs, 1986	6.0	9.6	507.58
56	FP North Palm Springs, 1986	6.0	9.6	371.66
57	FN San Fernando, 1971	6.5	1.0	248.14
58	FP San Fernando, 1971	6.5	1.0	226.54
59	FN Whittier, 1987	6.0	17.0	753.70
60	FP Whittier, 1987	6.0	17.0	469.07

Appendix F

The Virtual Mass Ratio of Each Model

Table F.1 2-story model with overall mass ratio of 0.1

		Stiffness rate of the upper floor								
		1	1.25	1.5	1.75	2	2.25	2.5	2.75	3
Stiffness	1	0.03783	0.04640	0.05323	0.05870	0.06311	0.06673	0.06974	0.07227	0.07442
rate of	0.75	0.04885	0.05700	0.06311	0.06780	0.07147	0.07442	0.07684	0.07884	0.08054
the first	0.5	0.06311	0.06974	0.07442	0.07788	0.08054	0.08263	0.08432	0.08572	0.08689
floor	0.25	0.08054	0.08432	0.08689	0.08873	0.09013	0.09122	0.09209	0.09280	0.09340

Table F.2 4-story model with overall mass ratio of 0.1

		Stiffness rate of the upper floor								
		1	1.25	1.5	1.75	2	2.25	2.5	2.75	3
Stiffness	1	0.01130	0.01573	0.02015	0.02443	0.02849	0.03228	0.03580	0.03906	0.04206
rate of	0.75	0.01721	0.02303	0.02849	0.03349	0.03800	0.04206	0.04570	0.04897	0.05190
the first	0.5	0.02849	0.03580	0.04206	0.04738	0.05190	0.05577	0.05910	0.06199	0.06451
floor	0.25	0.05190	0.05910	0.06451	0.06871	0.07204	0.07474	0.07698	0.07886	0.08045

Table F.3 8-story model with overall mass ratio of 0.1

		Stiffness rate of the upper floor								
		1	1.25	1.5	1.75	2	2.25	2.5	2.75	3
Stiffness	1	0.00293	0.00435	0.00594	0.00766	0.00946	0.01133	0.01324	0.01515	0.01707
rate of	0.75	0.00486	0.00707	0.00946	0.01196	0.01451	0.01707	0.01959	0.02206	0.02446
the first	0.5	0.00946	0.01324	0.01707	0.02083	0.02446	0.02792	0.03117	0.03422	0.03707
floor	0.25	0.02446	0.03117	0.03707	0.04221	0.04668	0.05058	0.05398	0.05698	0.05963

Table F.4 12-story model with overall mass ratio of 0.1

		Stiffness rate of the upper floor								
		1	1.25	1.5	1.75	2	2.25	2.5	2.75	3
Stiffness	1	0.00129	0.00195	0.00272	0.00358	0.00451	0.00552	0.00657	0.00768	0.00881
rate of	0.75	0.00220	0.00328	0.00451	0.00586	0.00730	0.00881	0.01037	0.01196	0.01357
the first	0.5	0.00451	0.00657	0.00881	0.01117	0.01357	0.01600	0.01840	0.02076	0.02307
floor	0.25	0.01357	0.01840	0.02307	0.02748	0.03157	0.03534	0.03879	0.04195	0.04485

Table F.5 16-story model with overall mass ratio of 0.1

		Stiffness rate of the upper floor								
		1	1.25	1.5	1.75	2	2.25	2.5	2.75	3
Stiffness	1	0.00193	0.00228	0.00264	0.00072	0.00109	0.00154	0.00204	0.00260	0.00321
rate of	0.75	0.00315	0.00368	0.00423	0.00123	0.00187	0.00260	0.00342	0.00432	0.00529
the first	0.5	0.00595	0.00683	0.00771	0.00260	0.00386	0.00529	0.00683	0.00846	0.01016
floor	0.25	0.01435	0.01582	0.01720	0.00846	0.01190	0.01542	0.01892	0.02233	0.02559

Table F.6 20-story model with overall mass ratio of 0.1

		Stiffness rate of the upper floor								
		1	1.25	1.5	1.75	2	2.25	2.5	2.75	3
Stiffness	1	0.00045	0.00069	0.00098	0.00131	0.00168	0.00208	0.00252	0.00299	0.00349
rate of	0.75	0.00078	0.00120	0.00168	0.00223	0.00283	0.00349	0.00420	0.00494	0.00572
the first	0.5	0.00168	0.00252	0.00349	0.00457	0.00572	0.00695	0.00823	0.00956	0.01091
floor	0.25	0.00572	0.00823	0.01091	0.01366	0.01643	0.01917	0.02185	0.02444	0.02694

Appendix G

Results of Frequency Response Analysis

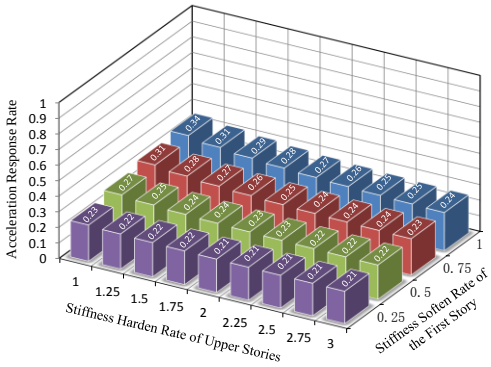

a1) 2 Story model with mass ratio of 0.01

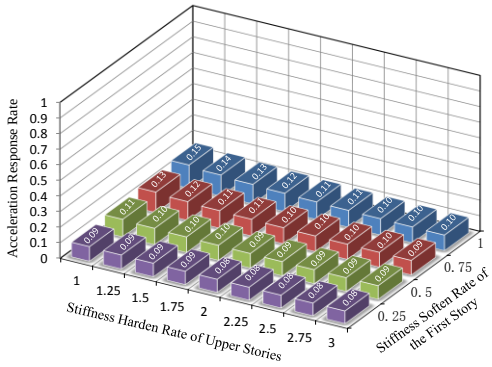

a2) 2 Story model with mass ratio of 0.1

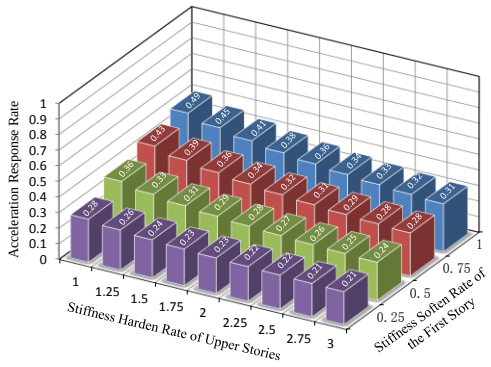

b1) 4 Story model with mass ratio of 0.01

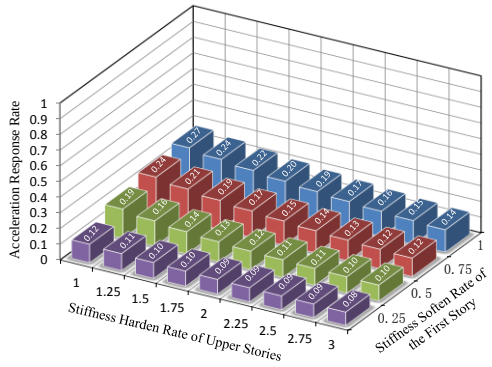

b2) 4 Story model with mass ratio of 0.1

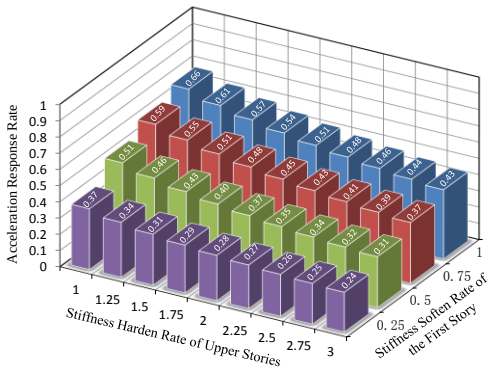

c1) 8 Story model with mass ratio of 0.01

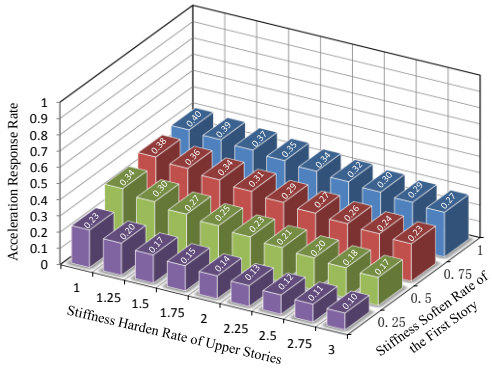

c2) 8 Story model with mass ratio of 0.1

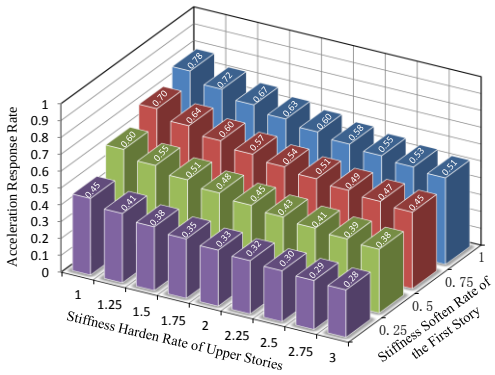

d1) 12 Story model with mass ratio of 0.01

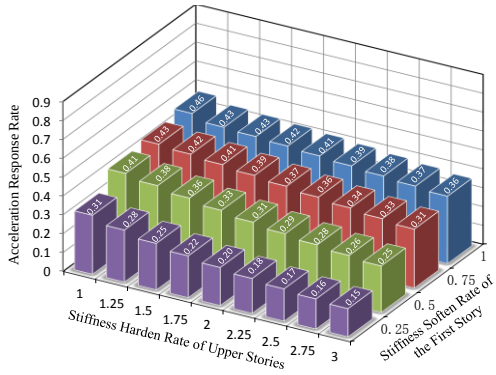

d2) 12 Story model with mass ratio of 0.1

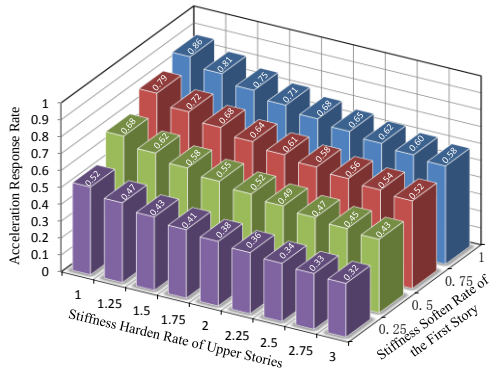

e1) 16 Story model with mass ratio of 0.01

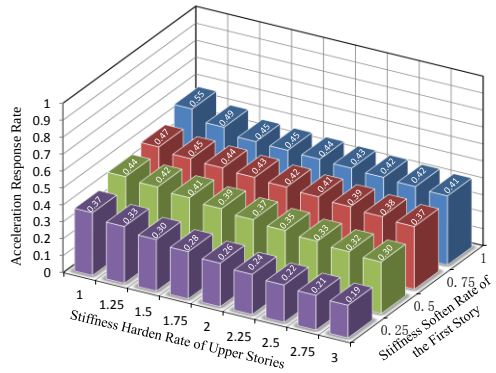

e2) 16 Story model with mass ratio of 0.1

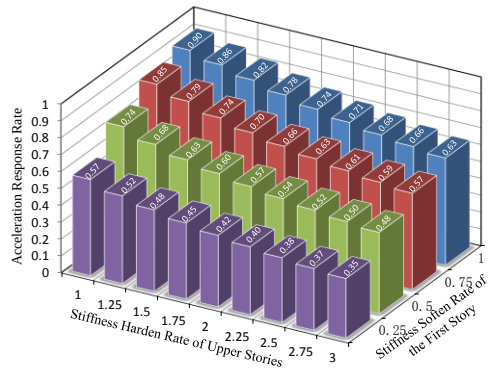

f1) 20 Story model with mass ratio of 0.01

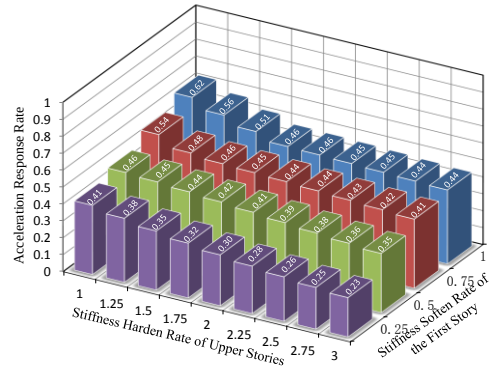

f2) 20 Story model with mass ratio of 0.1

Figure G.1 The rate of the maximum acceleration response of the top floor of the seismic retrofit structure to the original structure

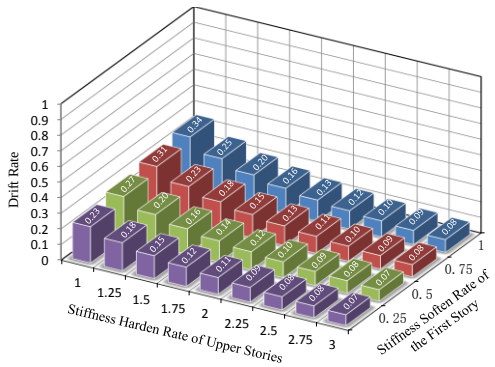

a1) 2 Story model with mass ratio of 0.01

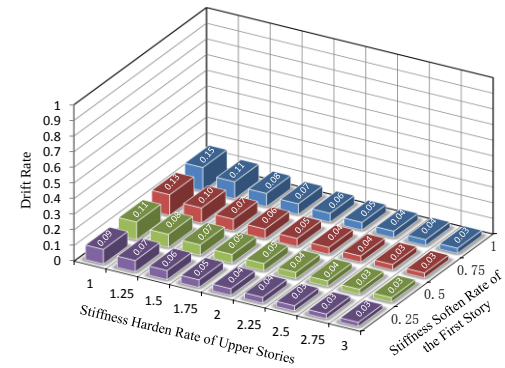

a2) 2 Story model with mass ratio of 0.1

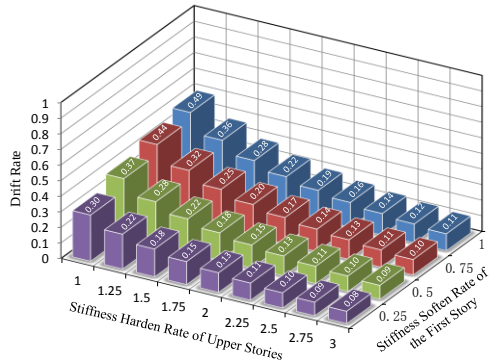

b1) 4 Story model with mass ratio of 0.01

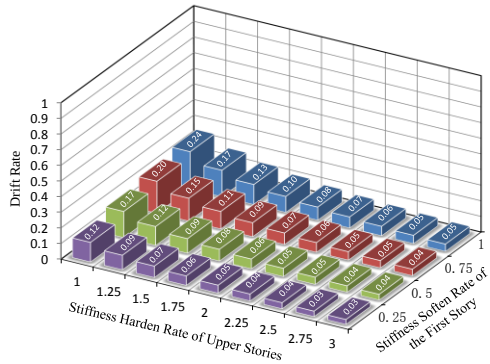

b2) 4 Story model with mass ratio of 0.1

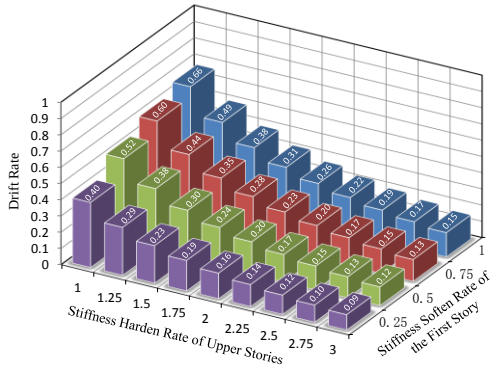

c1) 8 Story model with mass ratio of 0.01

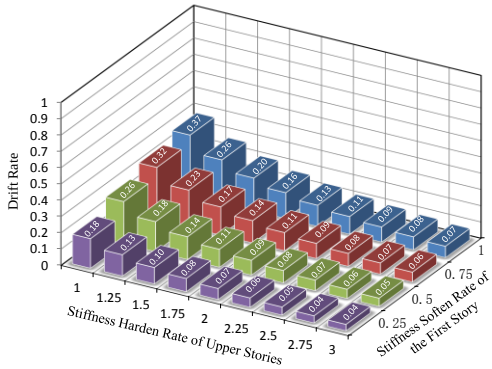

c2) 8 Story model with mass ratio of 0.1

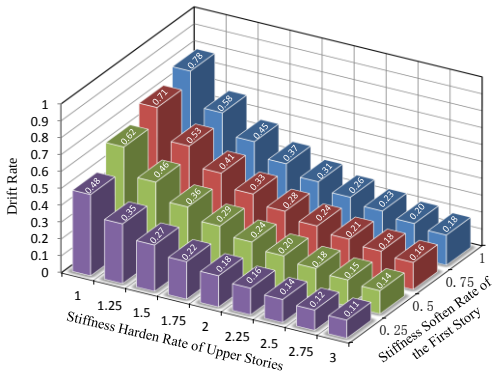

d1) 12 Story model with mass ratio of 0.01

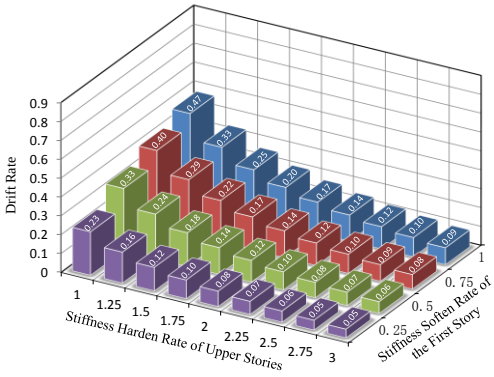

d2) 12 Story model with mass ratio of 0.1

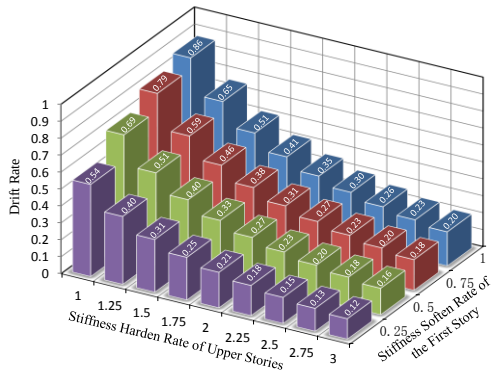

e1) 16 Story model with mass ratio of 0.01

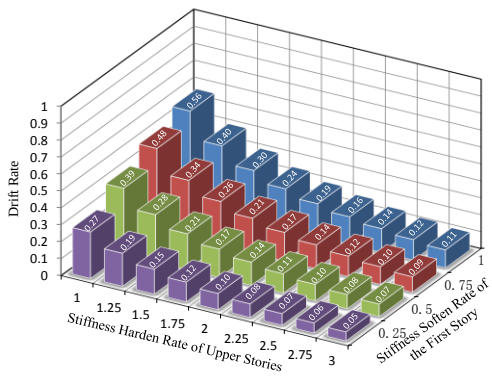

e2) 16 Story model with mass ratio of 0.1

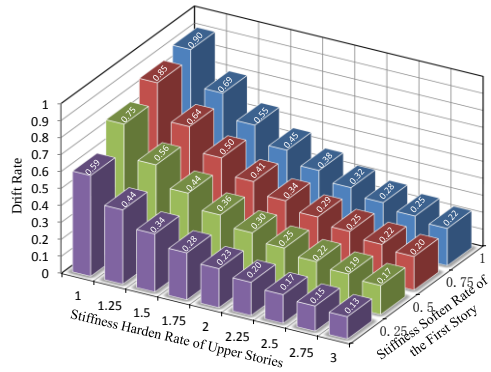

f1) 20 Story model with mass ratio of 0.01

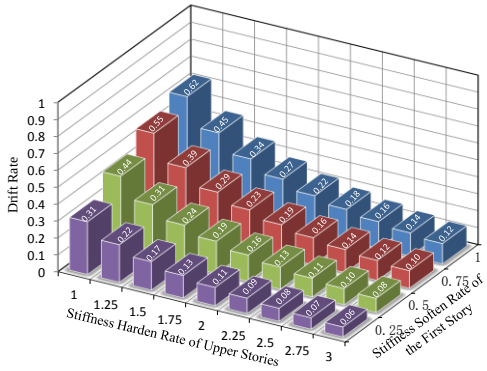

f2) 20 Story model with mass ratio of 0.1

Figure G.2 The rate of the maximum drift from the first floor to the top floor of the seismic retrofit structure to the original structure

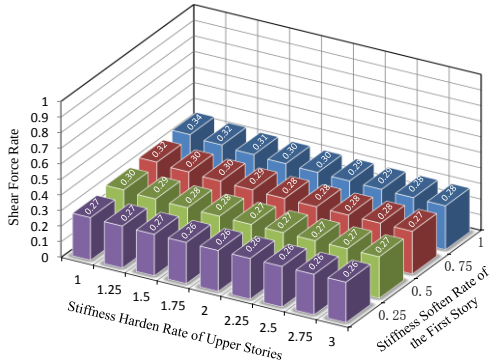

a1) 2 Story model with mass ratio of 0.01

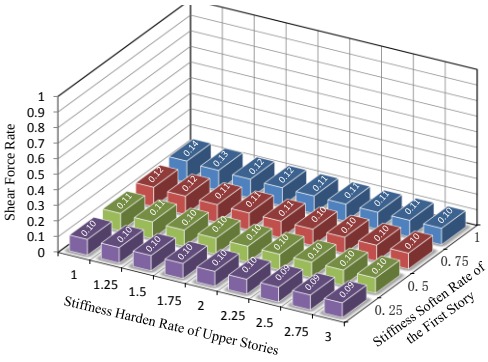

a2) 2 Story model with mass ratio of 0.1

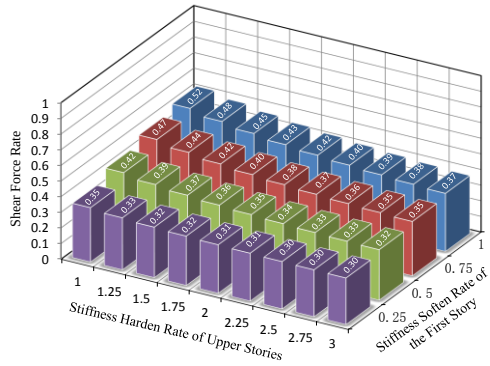

b1) 4 Story model with mass ratio of 0.01

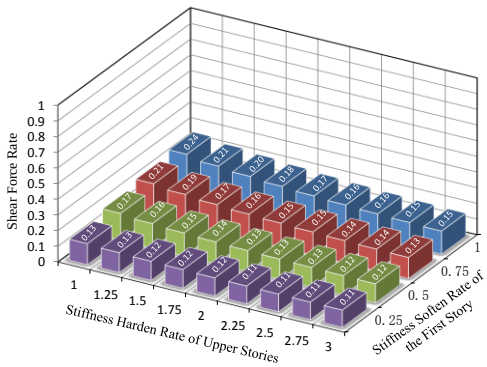

b2) 4 Story model with mass ratio of 0.1

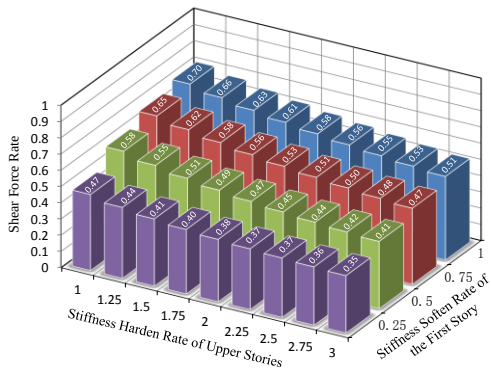

c1) 8 Story model with mass ratio of 0.01

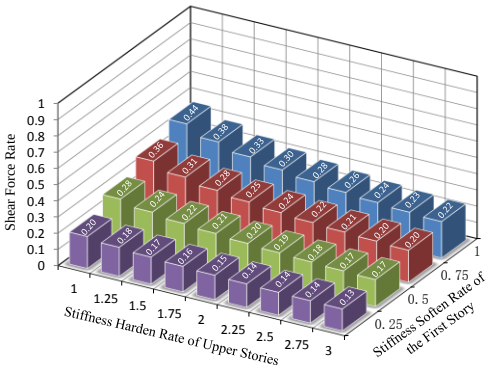

c2) 8 Story model with mass ratio of 0.1

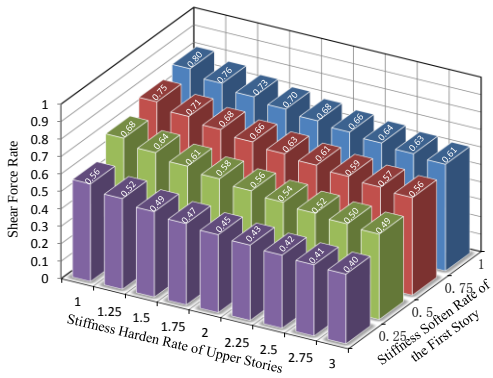

d1) 12 Story model with mass ratio of 0.01

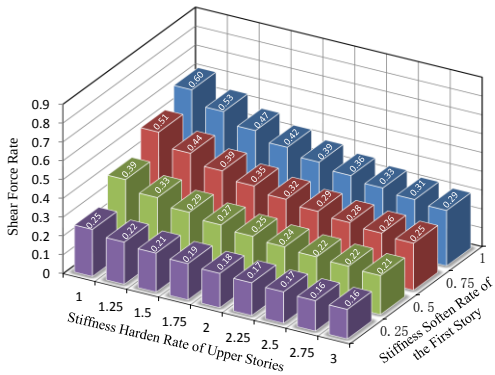

d2) 12 Story model with mass ratio of 0.1

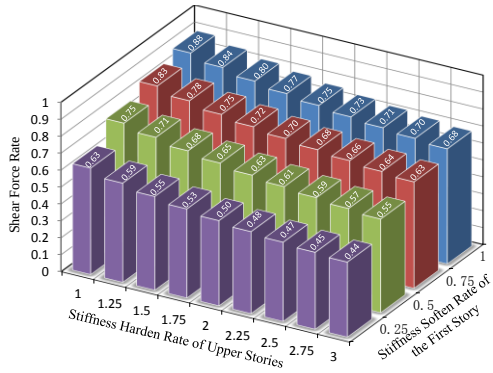

e1) 16 Story model with mass ratio of 0.01

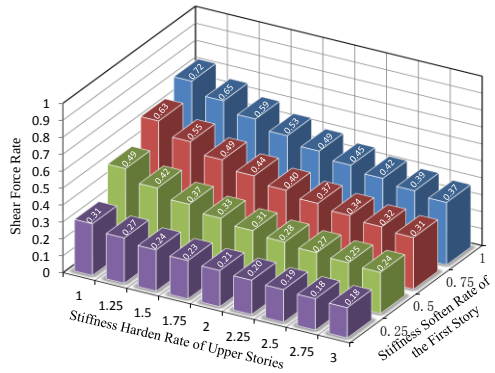

e2) 16 Story model with mass ratio of 0.1

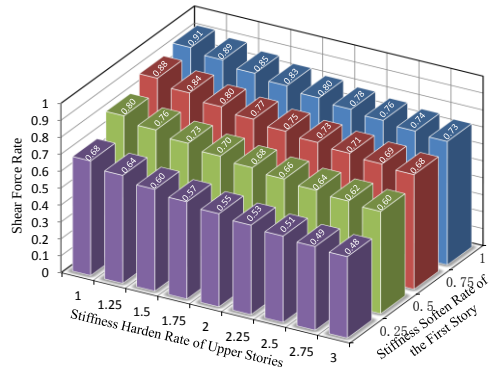

f1) 20 Story model with mass ratio of 0.01

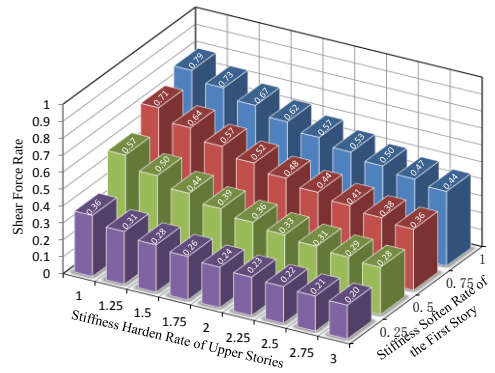

f2) 20 Story model with mass ratio of 0.1

Figure G.3 The rate of the maximum shear force of the first floor of the seismic retrofit structure to the original structure

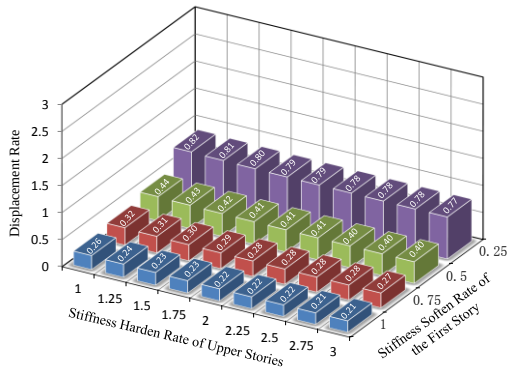

a1) 2 Story model with mass ratio of 0.01

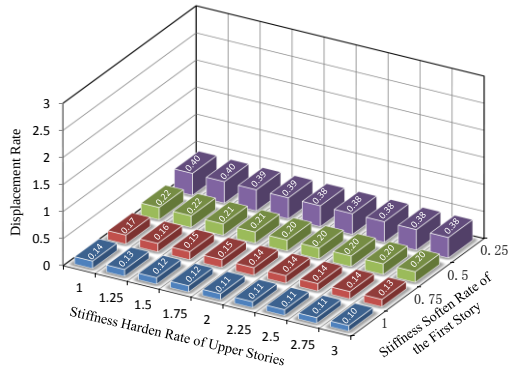

a2) 2 Story model with mass ratio of 0.1

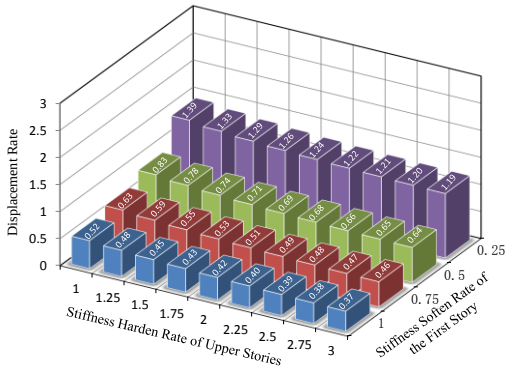

b1) 4 Story model with mass ratio of 0.01

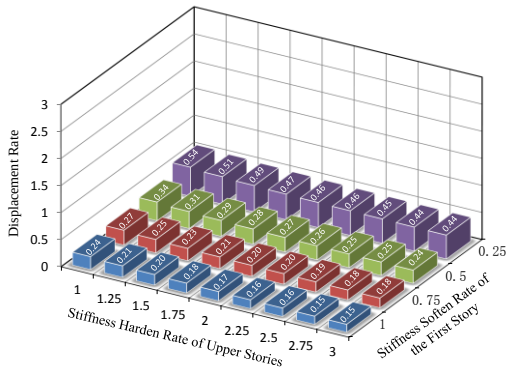

b2) 4 Story model with mass ratio of 0.1

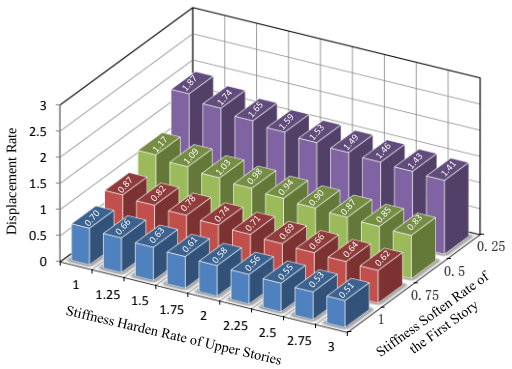

c1) 8 Story model with mass ratio of 0.01

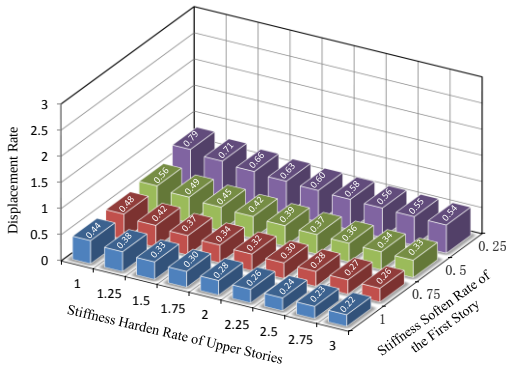

c2) 8 Story model with mass ratio of 0.1

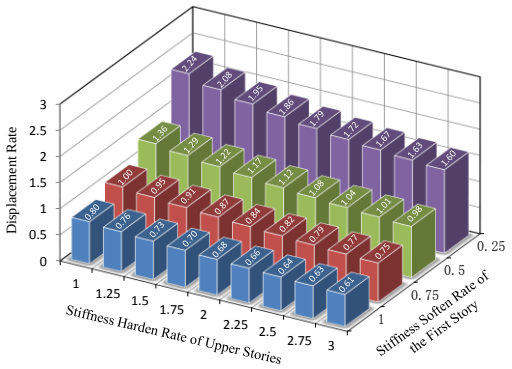

d1) 12 Story model with mass ratio of 0.01

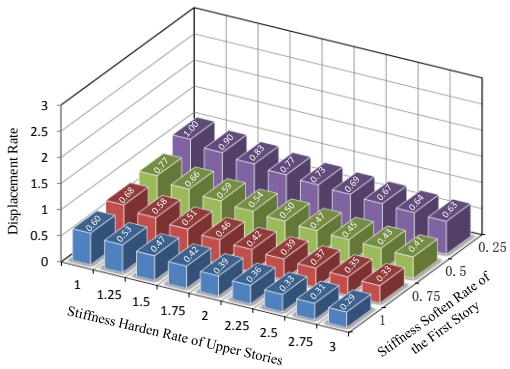

d2) 12 Story model with mass ratio of 0.1

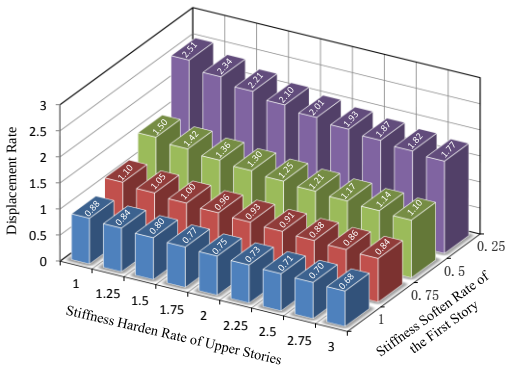

e1) 16 Story model with mass ratio of 0.01

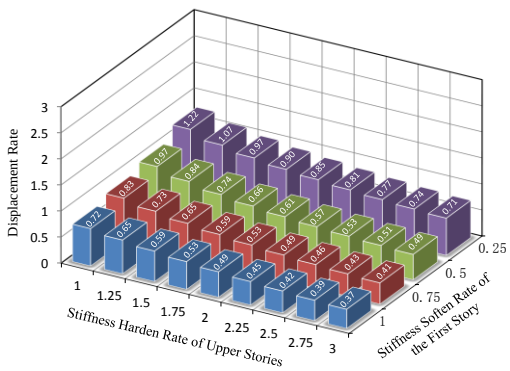

e2) 16 Story model with mass ratio of 0.1

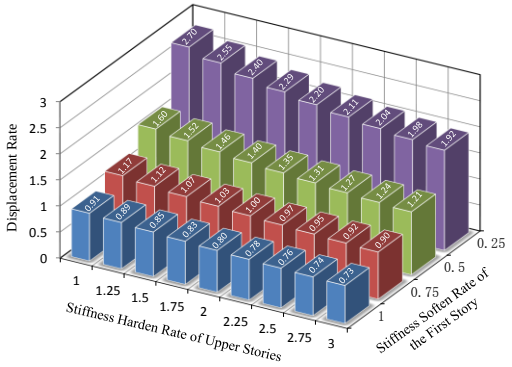

f1) 20 Story model with mass ratio of 0.01

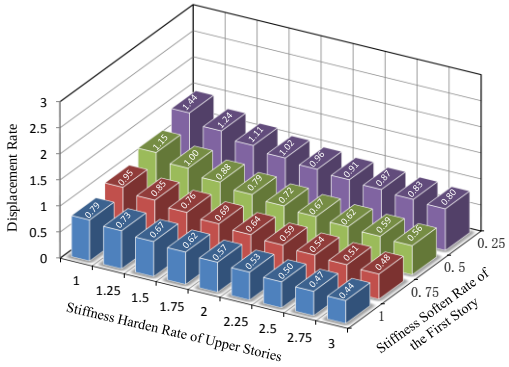

f2) 20 Story model with mass ratio of 0.1

Figure G.4 The rate of the maximum displacement response of the first floor of the seismic retrofit structure to the original structure

Appendix H

Results of Earthquake Response Analysis

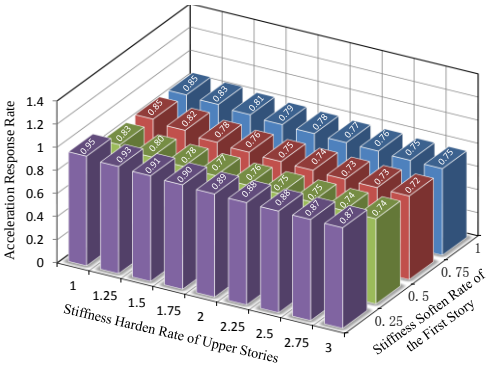

a1) 2 Story model with mass ratio of 0.01

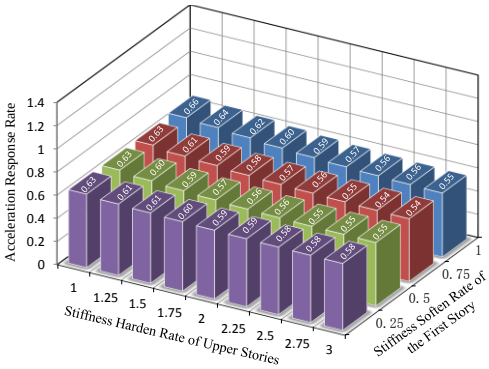

a2) 2 Story model with mass ratio of 0.1

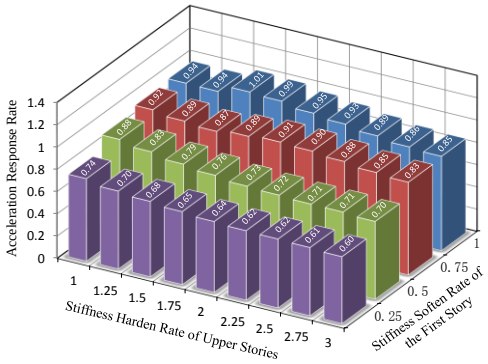

b1) 4 Story model with mass ratio of 0.01

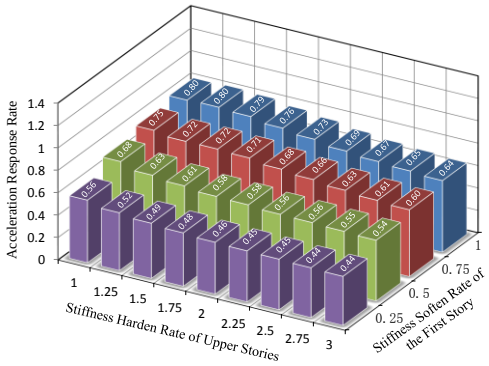

b2) 4 Story model with mass ratio of 0.1

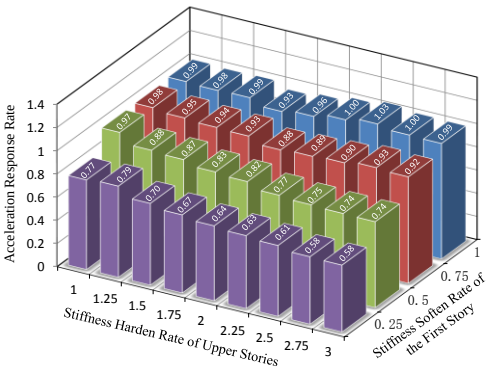

c1) 8 Story model with mass ratio of 0.01

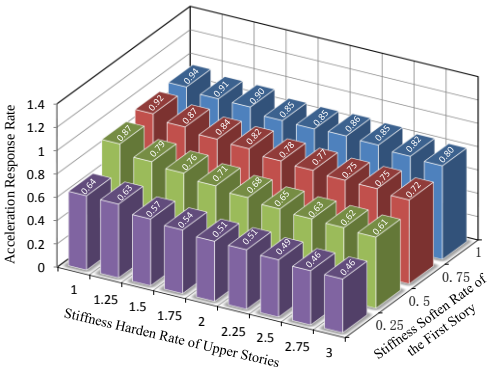

c2) 8 Story model with mass ratio of 0.1

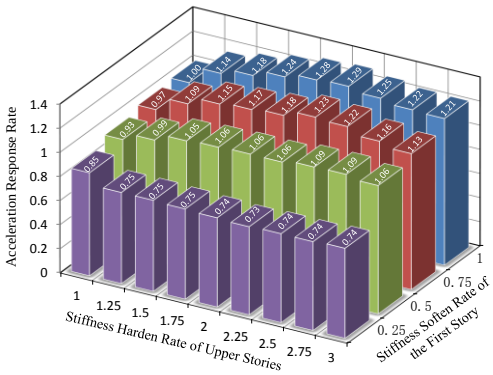

d1) 12 Story model with mass ratio of 0.01

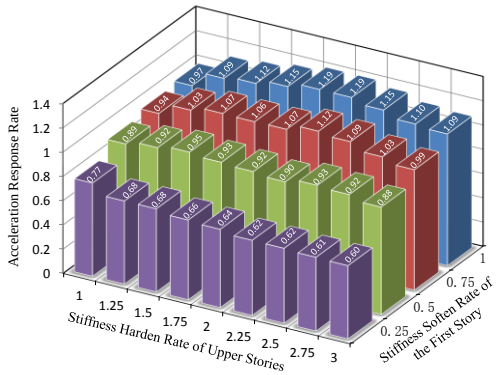

d2) 12 Story model with mass ratio of 0.1

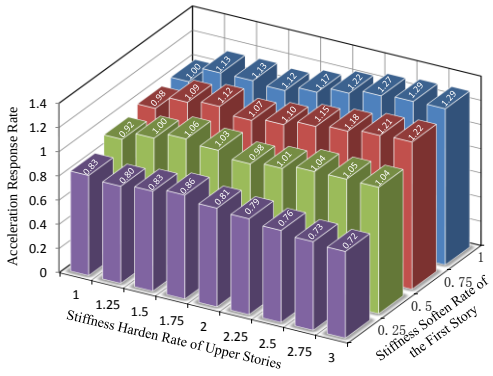

e1) 16 Story model with mass ratio of 0.01

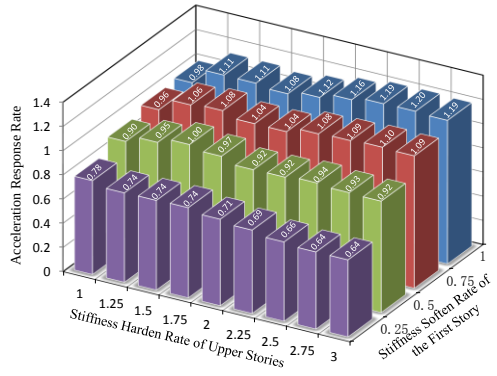

e2) 16 Story model with mass ratio of 0.1

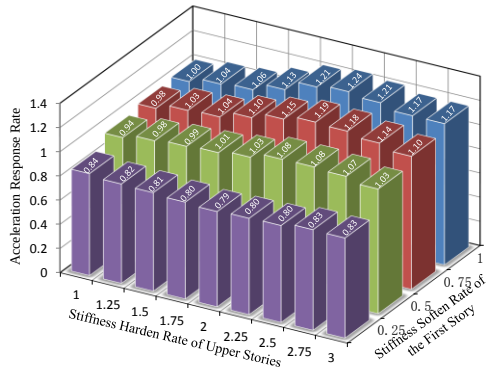

f1) 20 Story model with mass ratio of 0.01

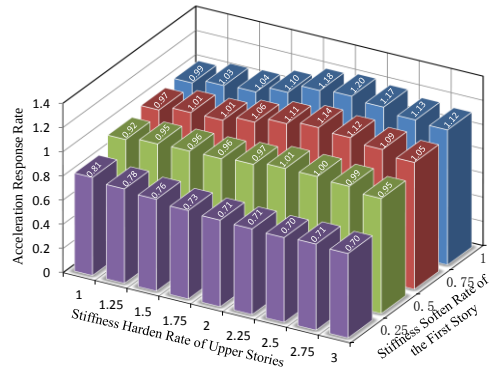

f2) 20 Story model with mass ratio of 0.1

Figure H.1 The mean rate of the maximum acceleration response of the top floor of the seismic retrofit structure to the original structure

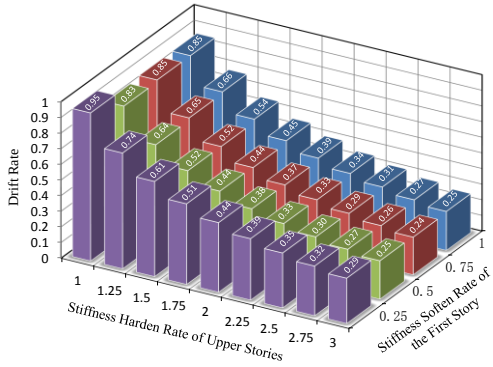

a1) 2 Story model with mass ratio of 0.01

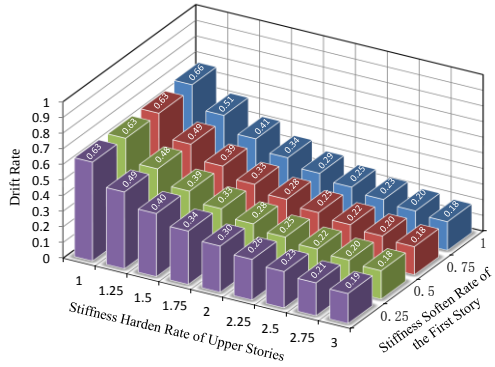

a2) 2 Story model with mass ratio of 0.1

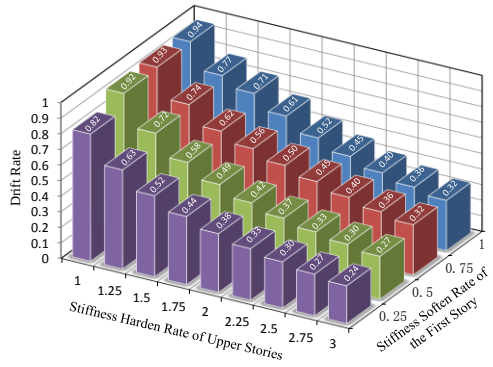

b1) 4 Story model with mass ratio of 0.01

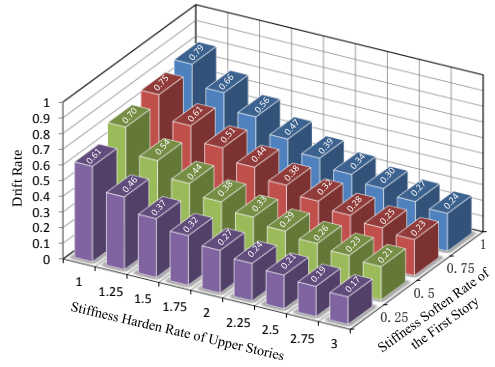

b2) 4 Story model with mass ratio of 0.1

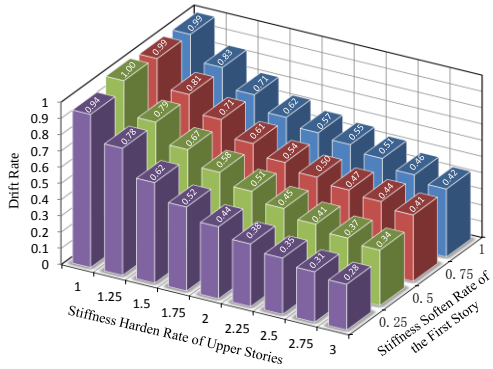

c1) 8 Story model with mass ratio of 0.01

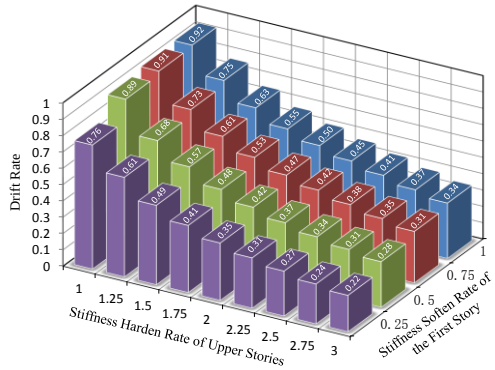

c2) 8 Story model with mass ratio of 0.1

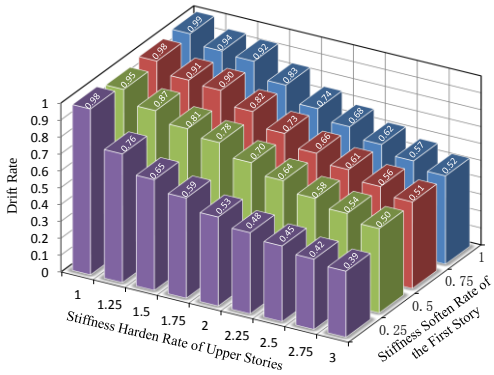

d1) 12 Story model with mass ratio of 0.01

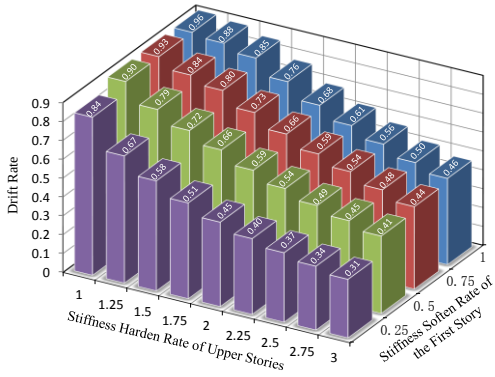

d2) 12 Story model with mass ratio of 0.1

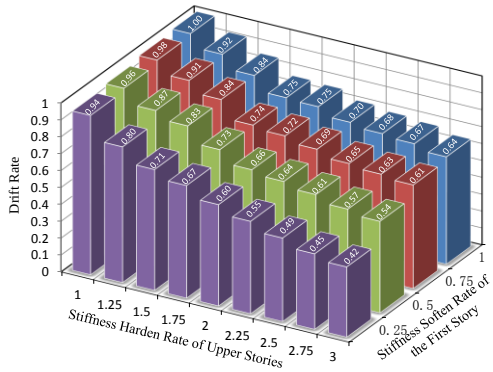

e1) 16 Story model with mass ratio of 0.01

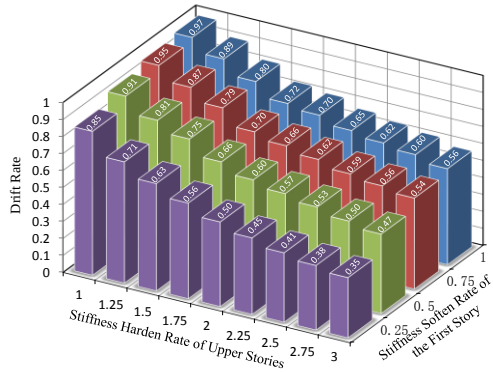

e2) 16 Story model with mass ratio of 0.1

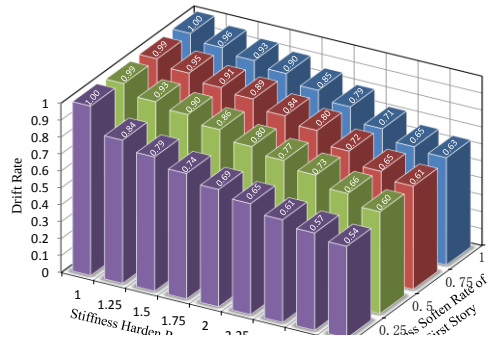

f1) 20 Story model with mass ratio of 0.01

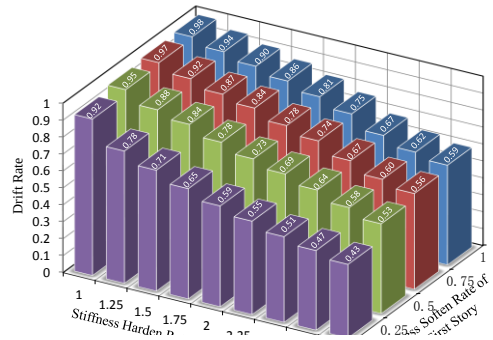

f2) 20 Story model with mass ratio of 0.1

Figure H.2 The mean rate of the maximum drift from the first floor to the top floor of the seismic retrofit structure to the original structure

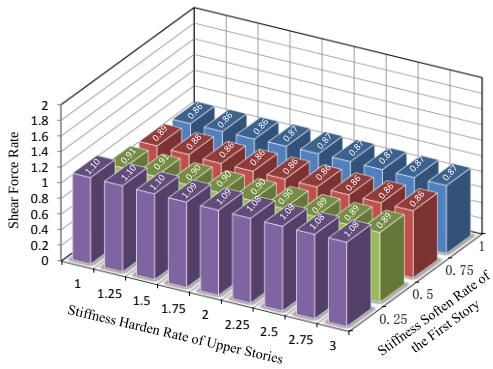

a1) 2 Story model with mass ratio of 0.01

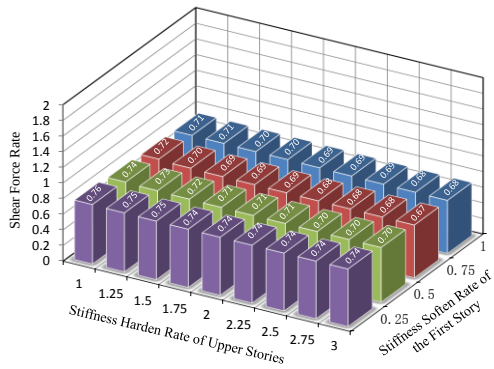

a2) 2 Story model with mass ratio of 0.1

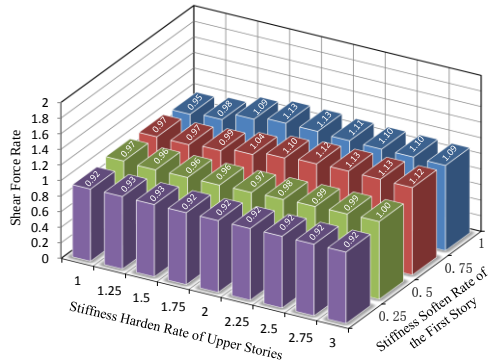

b1) 4 Story model with mass ratio of 0.01

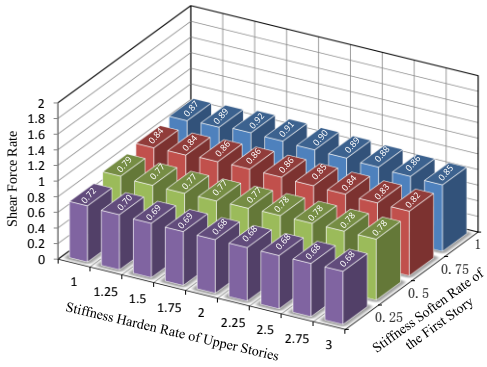

b2) 4 Story model with mass ratio of 0.1

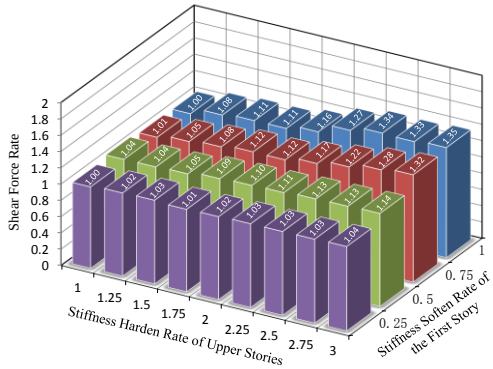

c1) 8 Story model with mass ratio of 0.01

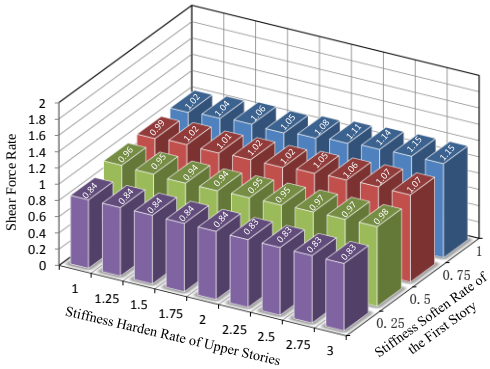

c2) 8 Story model with mass ratio of 0.1

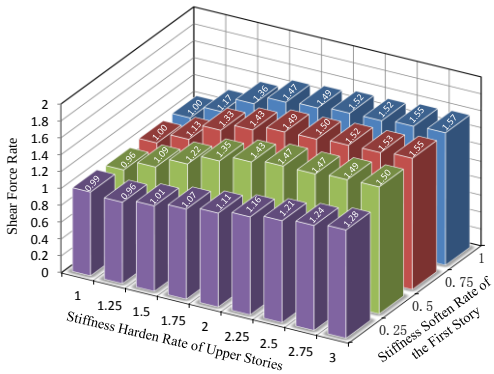

d1) 12 Story model with mass ratio of 0.01

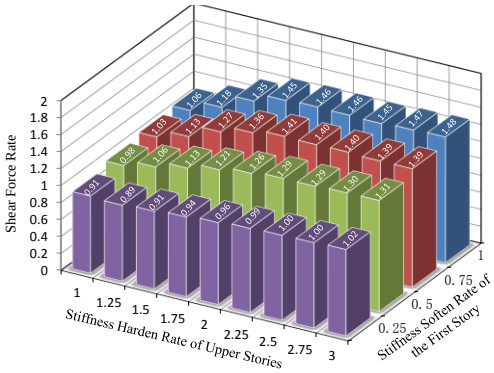

d2) 12 Story model with mass ratio of 0.1

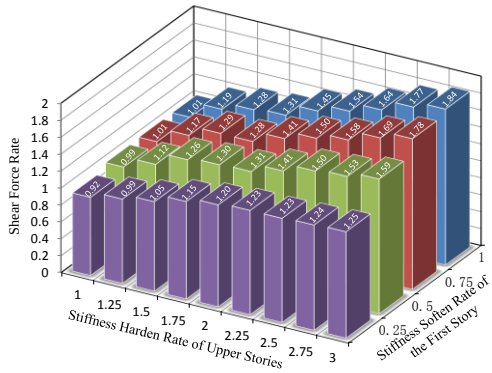

e1) 16 Story model with mass ratio of 0.01

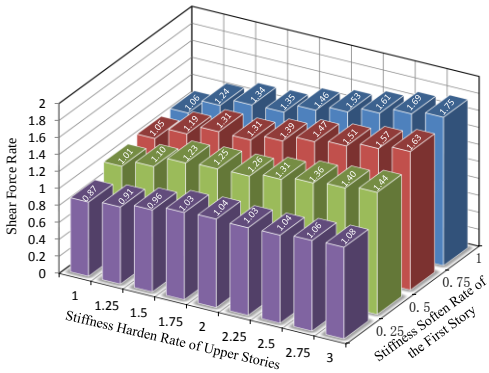

e2) 16 Story model with mass ratio of 0.1

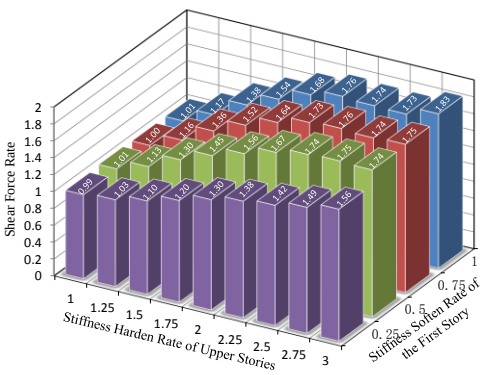

f1) 20 Story model with mass ratio of 0.01

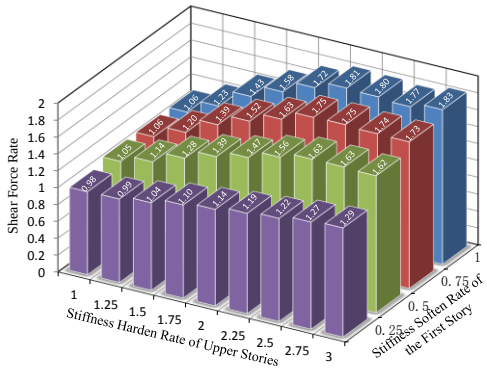

f2) 20 Story model with mass ratio of 0.1

Figure H.3 The mean rate of the maximum shear force of the first floor of the seismic retrofit structure to the original structure

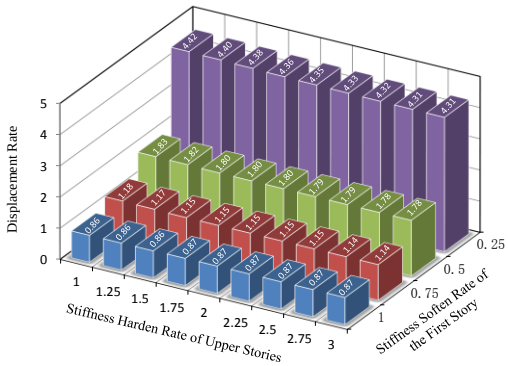

a1) 2 Story model with mass ratio of 0.01

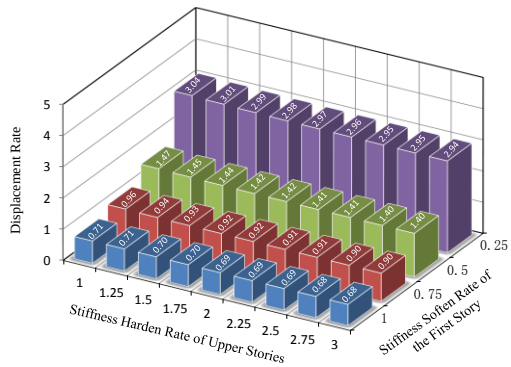

a2) 2 Story model with mass ratio of 0.1

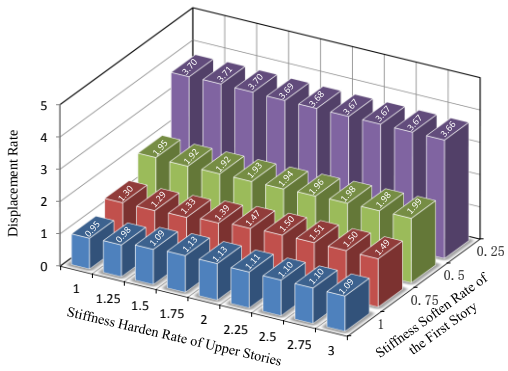

b1) 4 Story model with mass ratio of 0.01

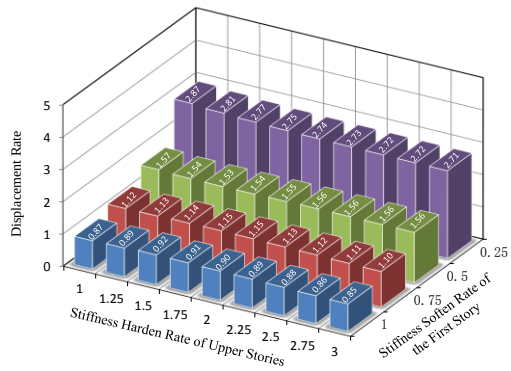

b2) 4 Story model with mass ratio of 0.1

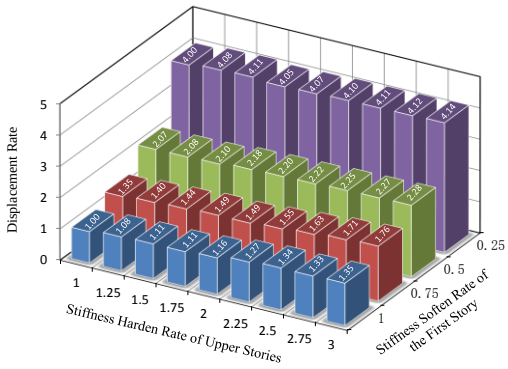

c1) 8 Story model with mass ratio of 0.01

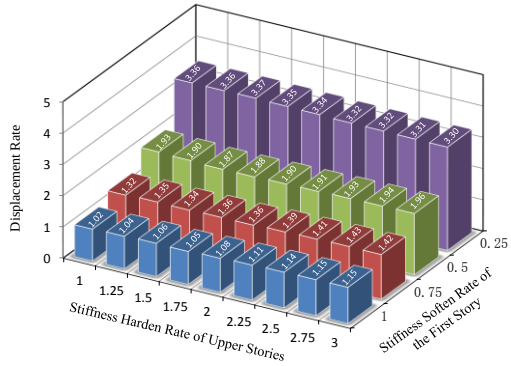

c2) 8 Story model with mass ratio of 0.1

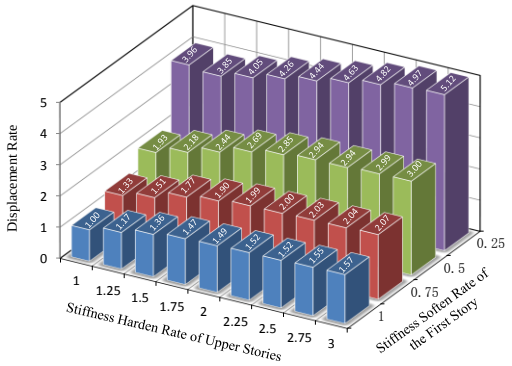

d1) 12 Story model with mass ratio of 0.01

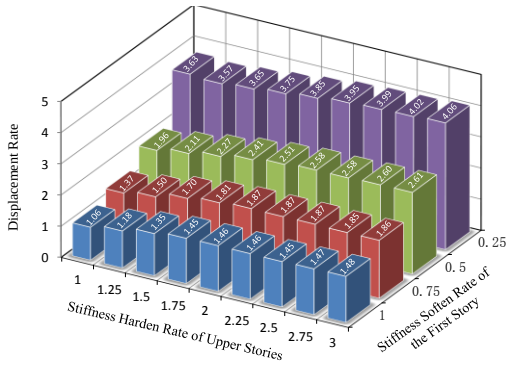

d2) 12 Story model with mass ratio of 0.1

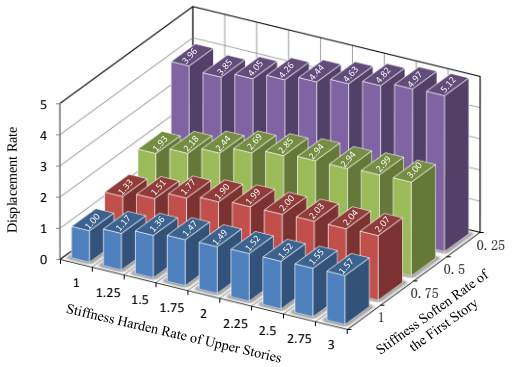

e1) 16 Story model with mass ratio of 0.01

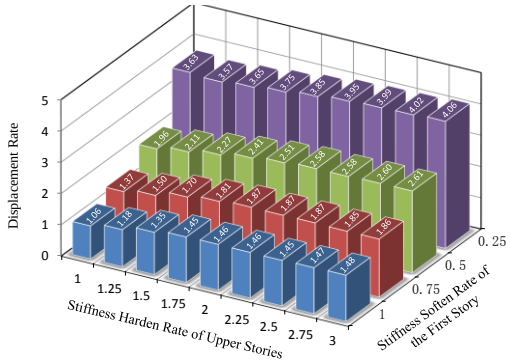

e2) 16 Story model with mass ratio of 0.1

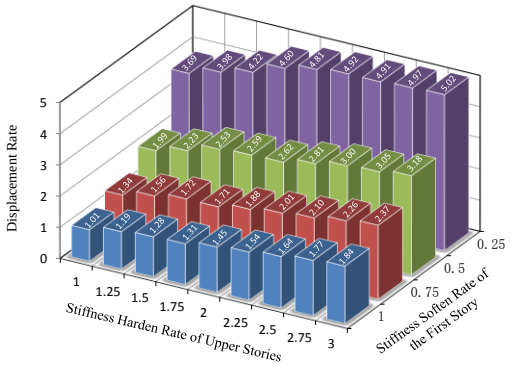

f1) 20 Story model with mass ratio of 0.01

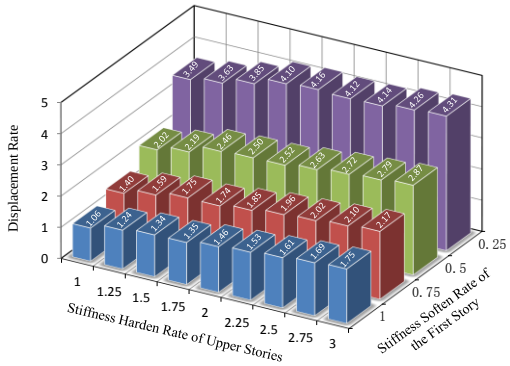

f2) 20 Story model with mass ratio of 0.1

Figure H.4 The mean rate of the maximum displacement response of the first floor of the seismic retrofit structure to the original structure

Appendix I

Acceleration Results of Earthquake Response Simulation

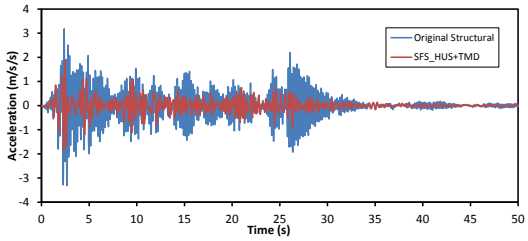

a) Response of 2 story model

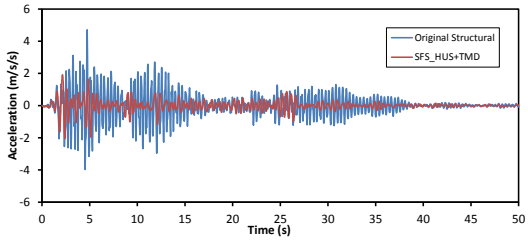

b) Response of 4 story model

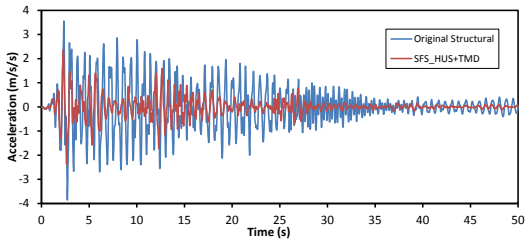

c) Response of 8 story model

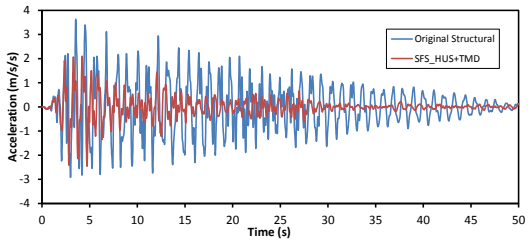

d) Response of 12 story model

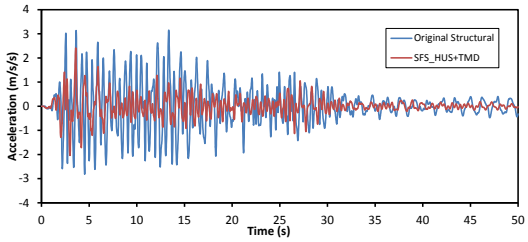

e) Response of 16 story model

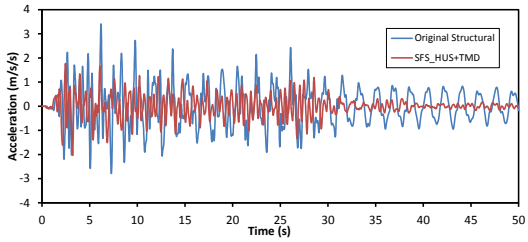

f) Response of 20 story model

Figure I.1 Acceleration response of the top floor under El Centro (NS 1940) record

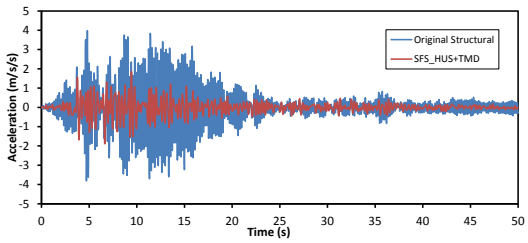

a) Response of 2 story model

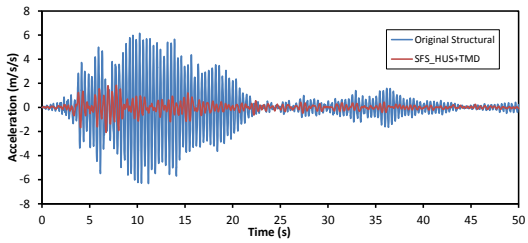

b) Response of 4 story model

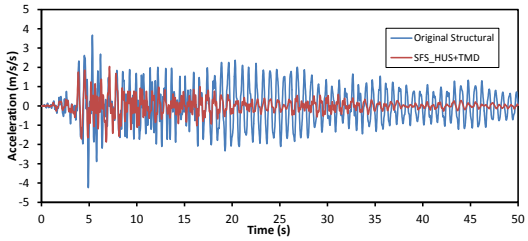

c) Response of 8 story model

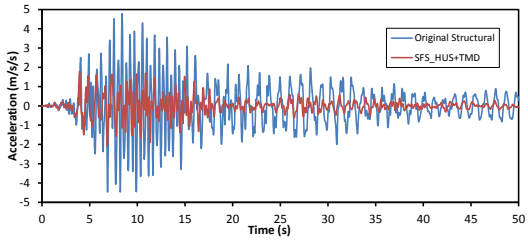

d) Response of 12 story model

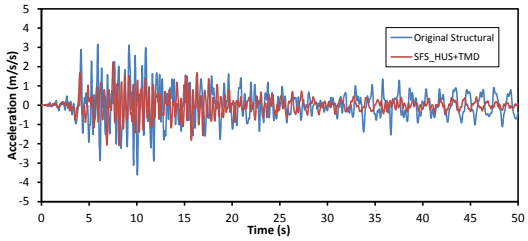

e) Response of 16 story model

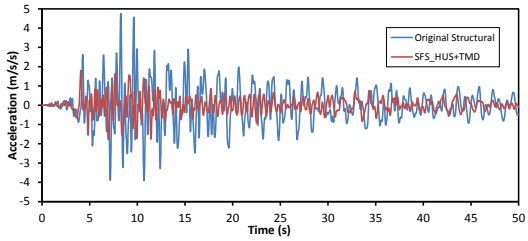

f) Response of 20 story model

Figure I.2 Acceleration response of the top floor under Taft (EW 1952) record

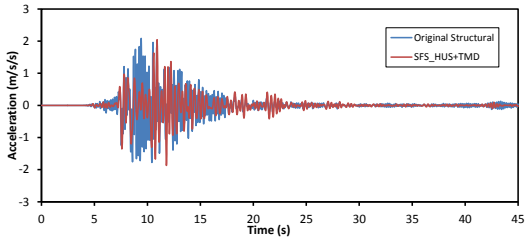

a) Response of 2 story model

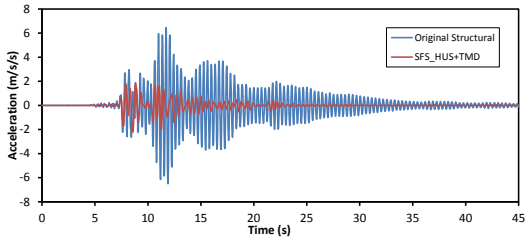

b) Response of 4 story model

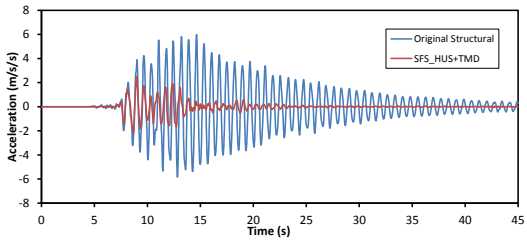

c) Response of 8 story model

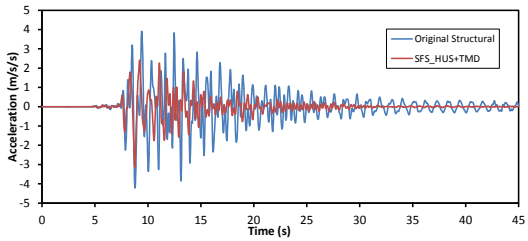

d) Response of 12 story model

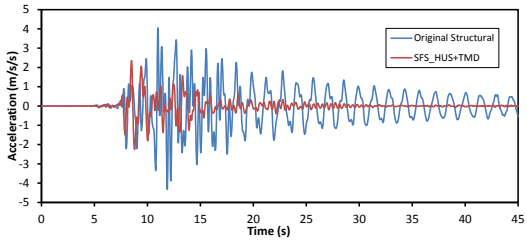

e) Response of 16 story model

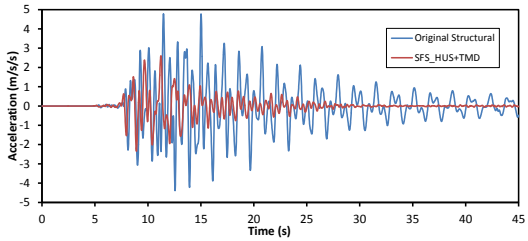

f) Response of 20 story model

Figure I.3 Acceleration response of the top floor under Kobe (EW 1952) record

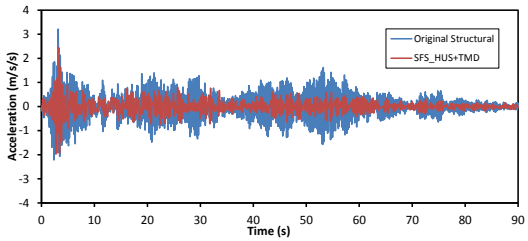

a) Response of 2 story model

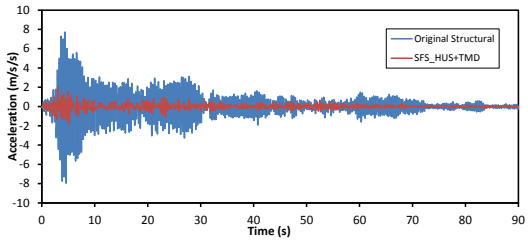

b) Response of 4 story model

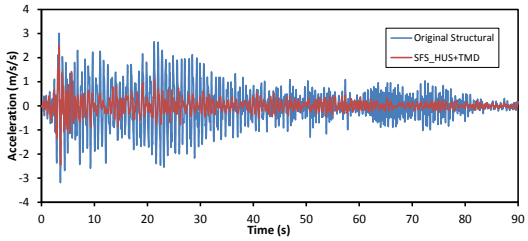

c) Response of 8 story model

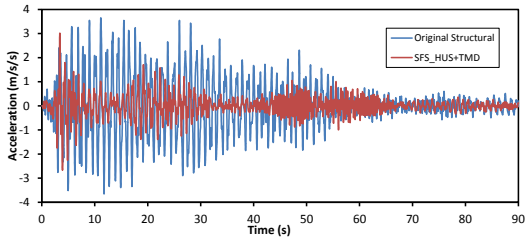

d) Response of 12 story model

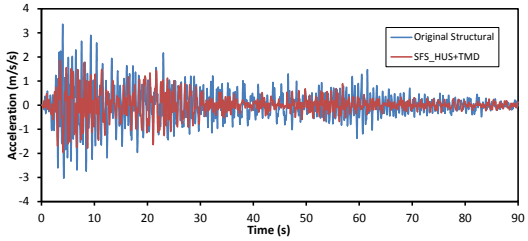

e) Response of 16 story model

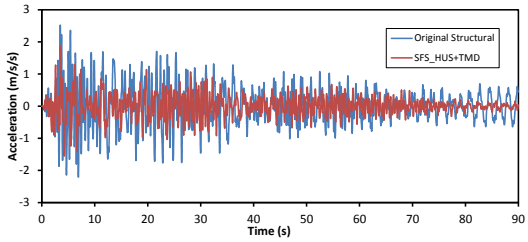

f) Response of 20 story model

Figure I.4 Acceleration response of the top floor under Hachinohe (NS 1968) record

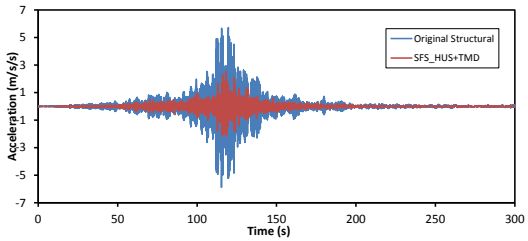

a) Response of 2 story model

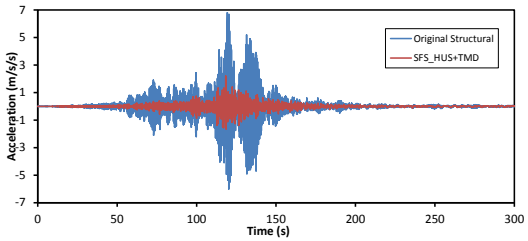

b) Response of 4 story model

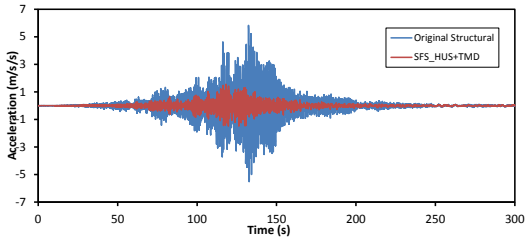

c) Response of 8 story model

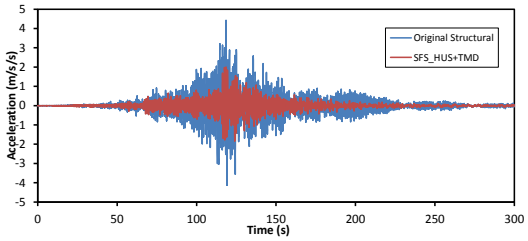

d) Response of 12 story model

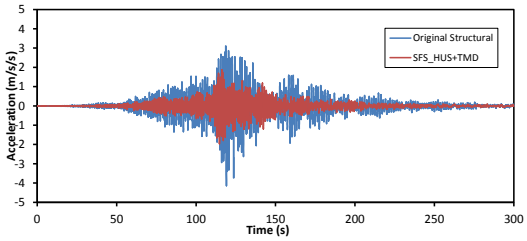

e) Response of 16 story model

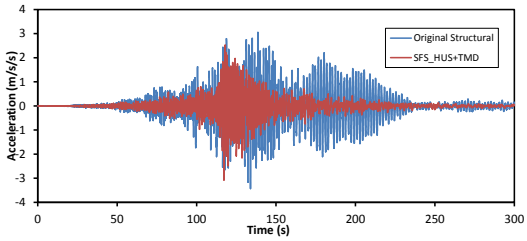

f) Response of 20 story model

Figure I.5 Acceleration response of the top floor under Tohoku (EW 2011) record

Appendix J

Results of Shaking Table Test for Retrofit Pattern 1

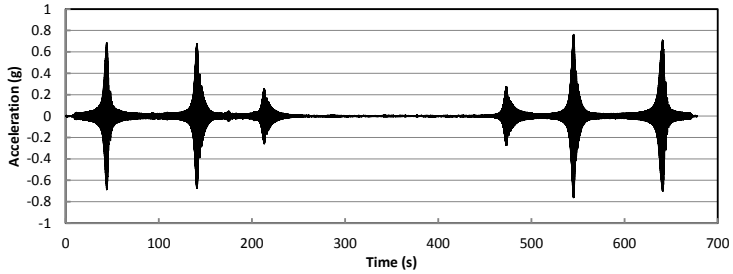

1) Acceleration response of the top floor of the original structure

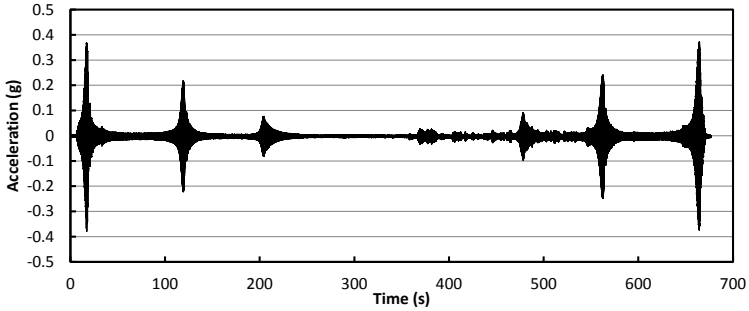

2) Acceleration response of the top floor of the SFS structure

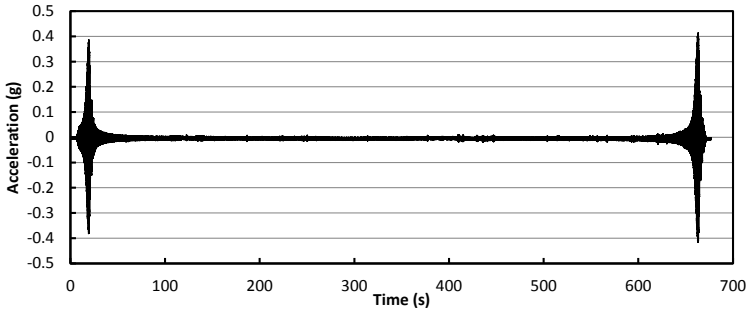

3) Acceleration response of the top floor of the SFS_HUS structure

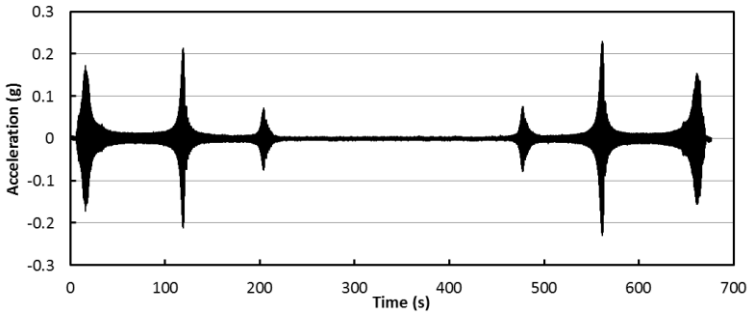

4) Acceleration response of the top floor of the SFS structure with TMD1

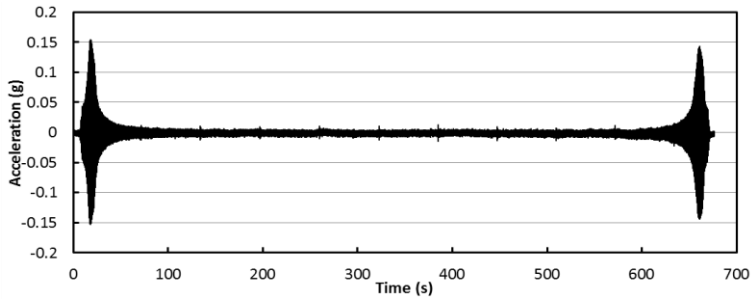

5) Acceleration response of the top floor of the SFS_HUS structure with TMD1

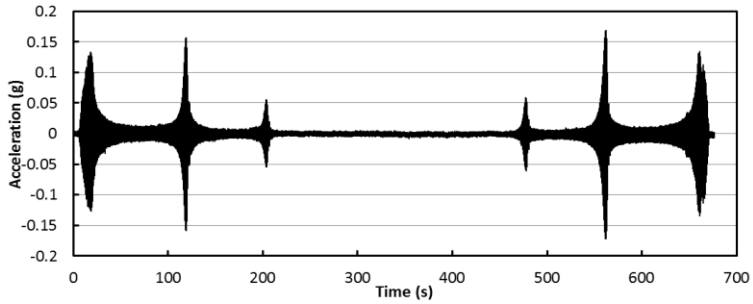

6) Acceleration response of the top floor of the SFS structure with TMD2

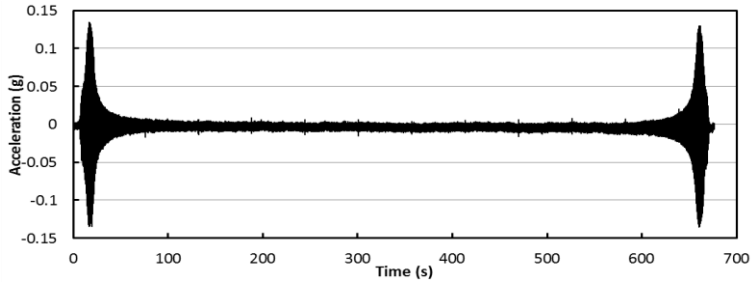

7) Acceleration response of the top floor of the SFS_HUS structure with TMD2

Figure J.1 Acceleration response of the top floor under sweep input

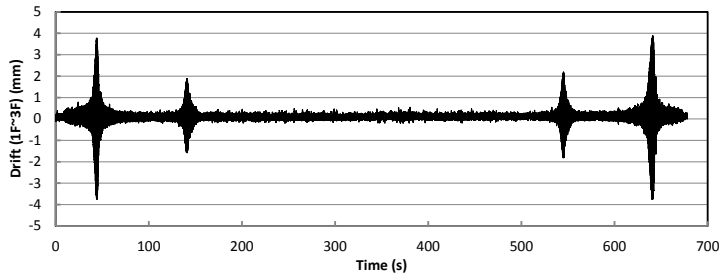

1) Drift from 1st floor to top floor of the original structure

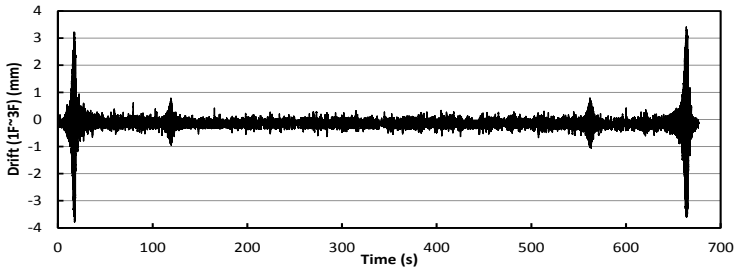

2) Drift from 1st floor to top floor of the SFS structure

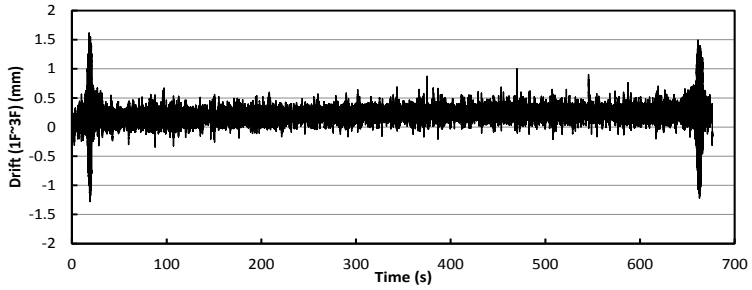

3) Drift from 1st floor to top floor of the SFS_HUS structure

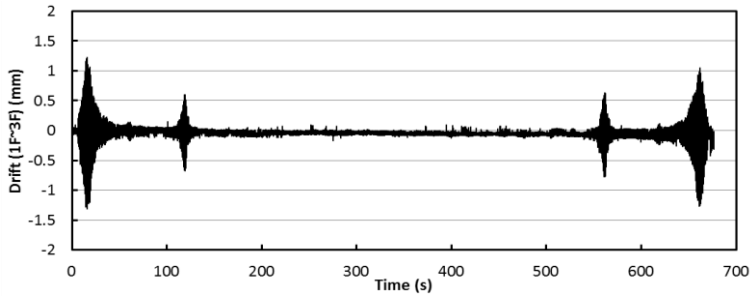

4) Drift from 1st floor to top floor of the SFS structure with TMD1

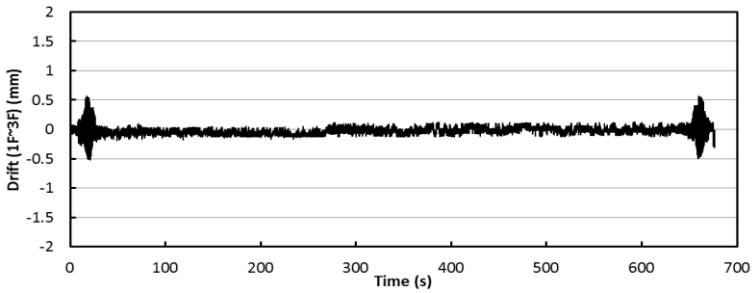

5) Drift from 1st floor to top floor of the SFS_HUS structure with TMD1

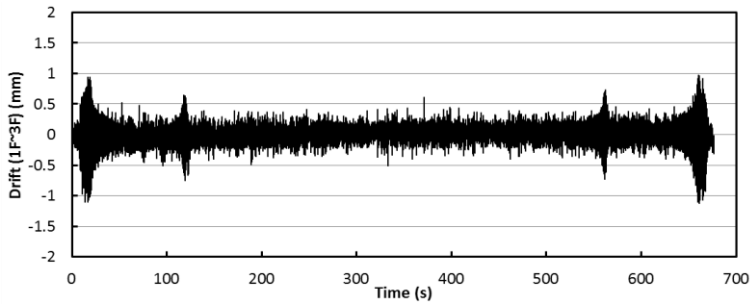

6) Drift from 1st floor to top floor of the SFS structure with TMD2

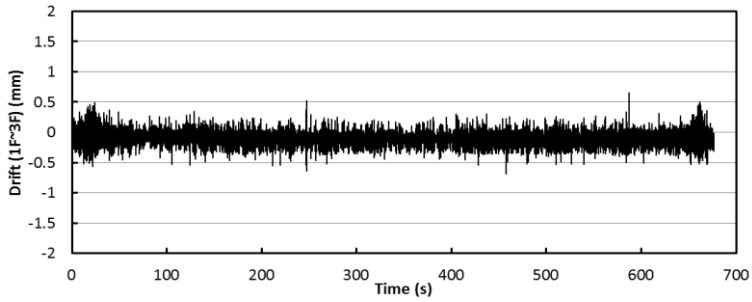

7) Drift from 1st floor to top floor of the SFS_HUS structure with TMD2

Figure J.2 Drift response from 1st floor to top floor under sweep input

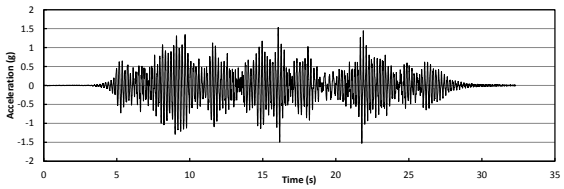

1) Original Structure

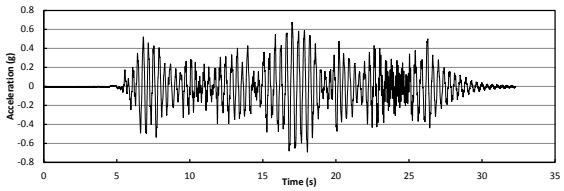

2) SFS Structure

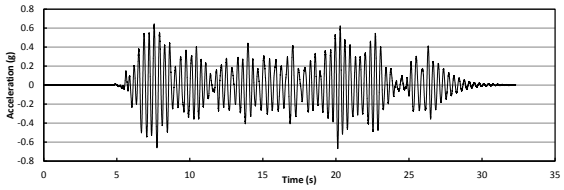

3) SFS_HUS Structure

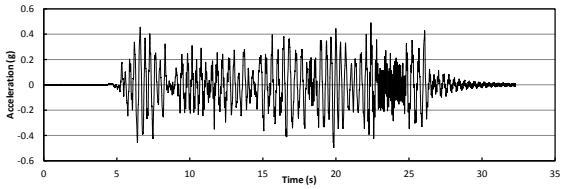

4) SFS Structure with TMD1

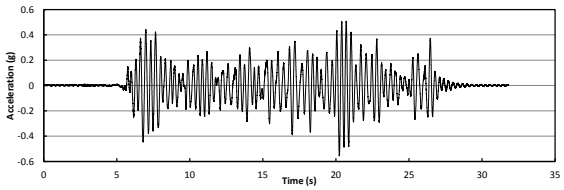

5) SFS_HUS Structure with TMD1

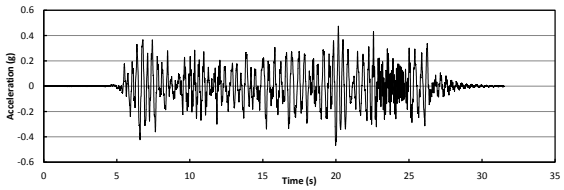

6) SFS Structure with TMD2

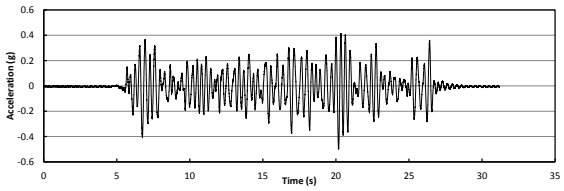

7) SFS_HUS Structure with TMD2

Figure J.3 Acceleration response of the top floor under input of Whitenoise1

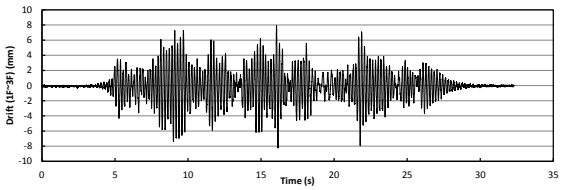

1) Original Structure

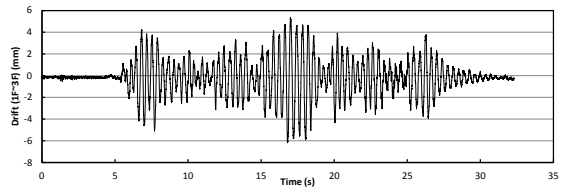

2) SFS Structure

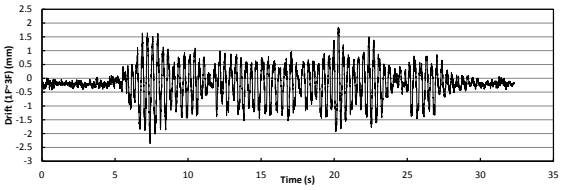

3) SFS_HUS Structure

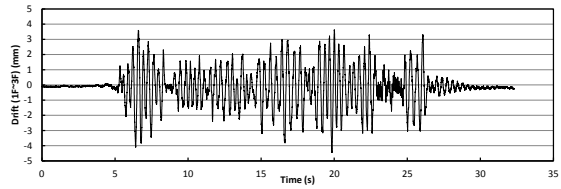

4) SFS Structure with TMD1

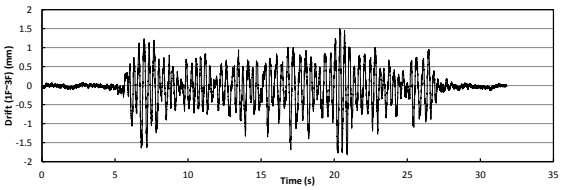

5) SFS_HUS Structure with TMD1

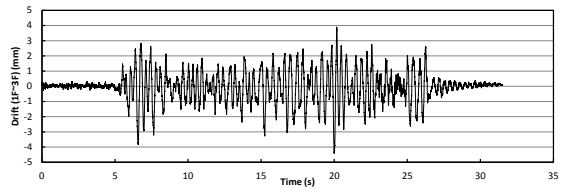

6) SFS Structure with TMD2

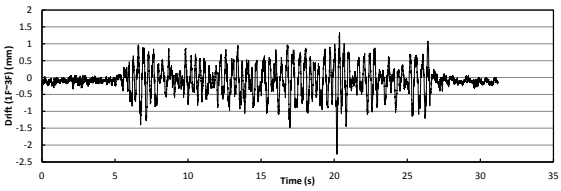

7) SFS_HUS Structure with TMD2

Figure J.4 Drift response from 1st floor to top floor under input of Whitenoise1

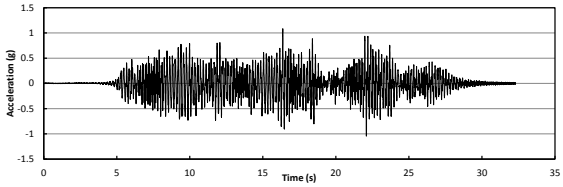

1) Original Structure

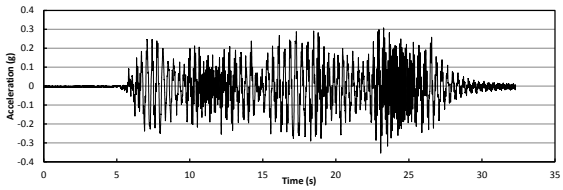

2) SFS Structure

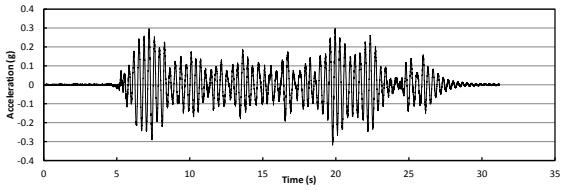

3) SFS_HUS Structure

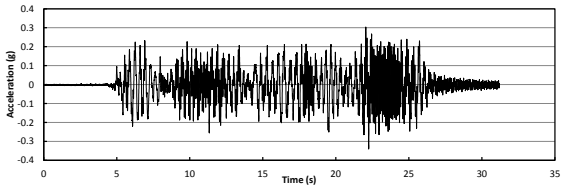

4) SFS Structure with TMD1

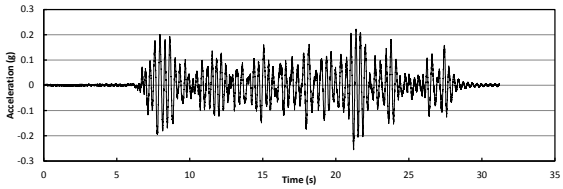

5) SFS_HUS Structure with TMD1

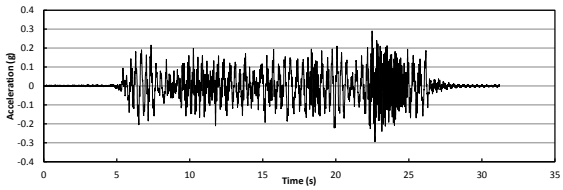

6) SFS Structure with TMD2

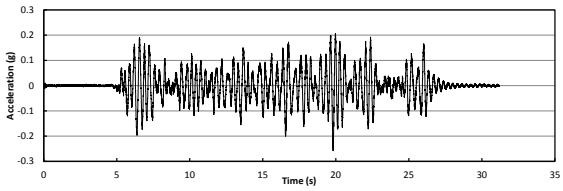

7) SFS_HUS Structure with TMD2

Figure J.5 Acceleration response of the top floor under input of Whitenoise2

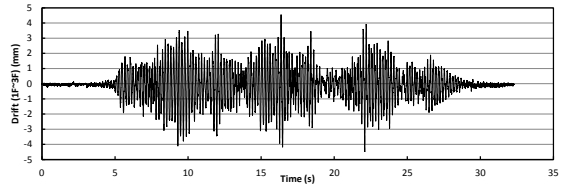

1) Original Structure

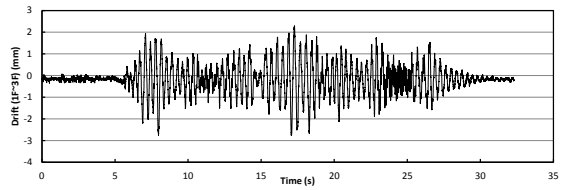

2) SFS Structure

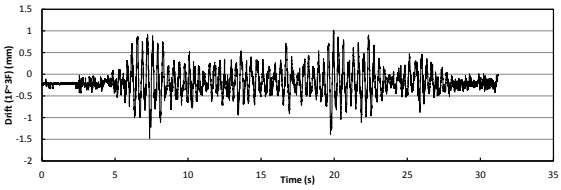

3) SFS_HUS Structure

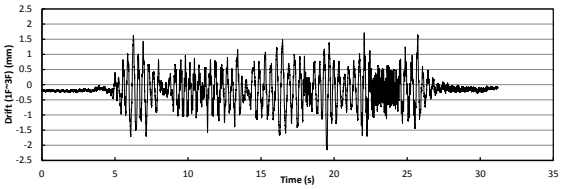

4) SFS Structure with TMD1

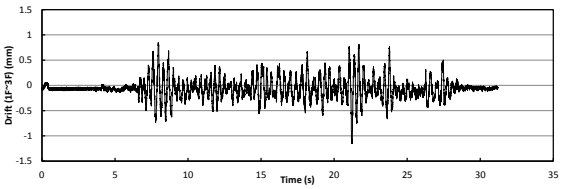

5) SFS_HUS Structure with TMD1

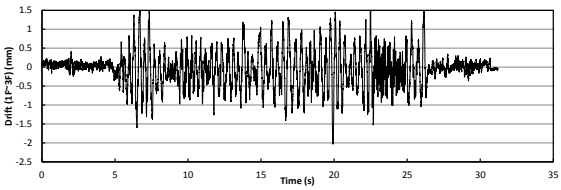

6) SFS Structure with TMD2

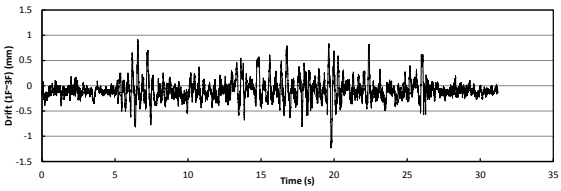

7) SFS_HUS Structure with TMD2

Figure J.6 Drift response from 1st floor to top floor under input of Whitenoise2

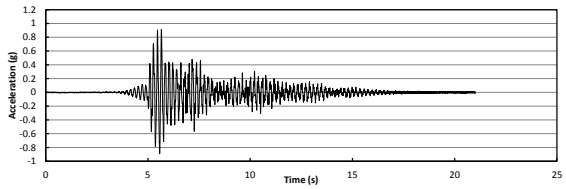

1) Original Structure

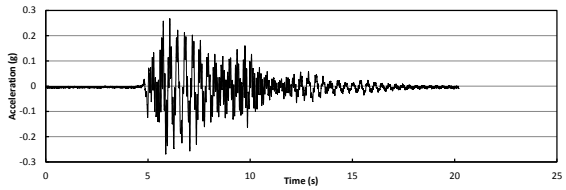

2) SFS Structure

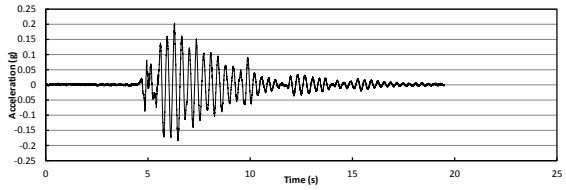

3) SFS_HUS Structure

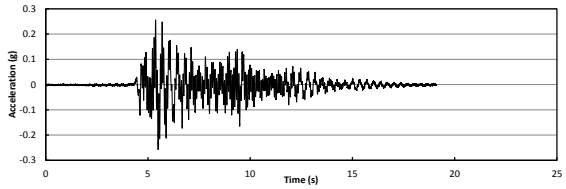

4) SFS Structure with TMD1

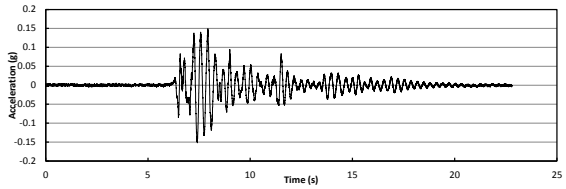

5) SFS_HUS Structure with TMD1

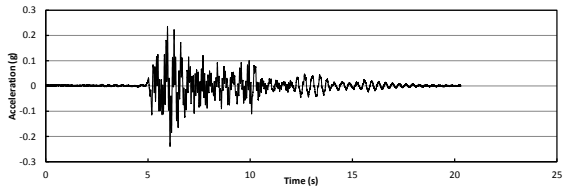

6) SFS Structure with TMD2

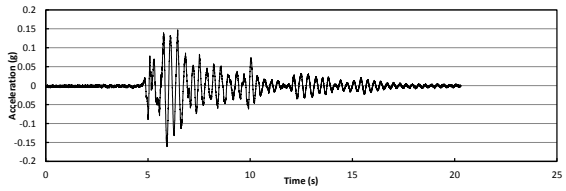

7) SFS_HUS Structure with TMD2

Figure J.7 Acceleration response of the top floor under input of El Centro (0.25g)

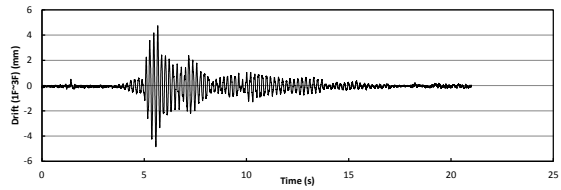

1) Original Structure

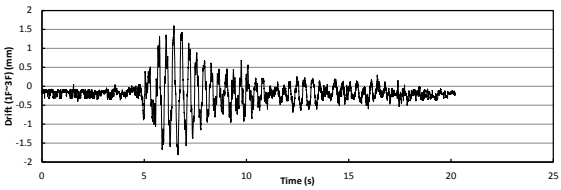

2) SFS Structure

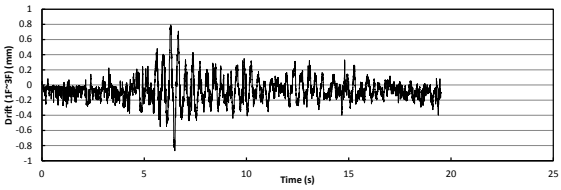

3) SFS_HUS Structure

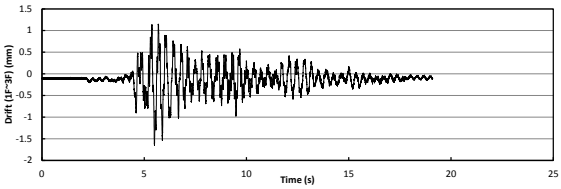

4) SFS Structure with TMD1

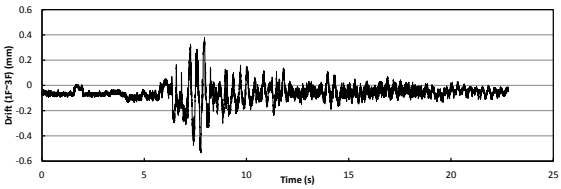

5) SFS_HUS Structure with TMD1

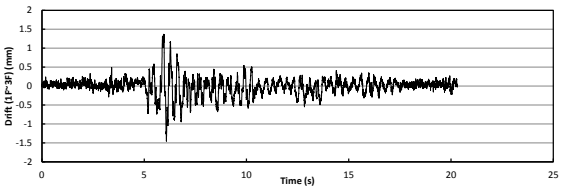

6) SFS Structure with TMD2

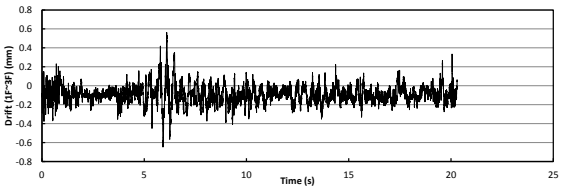

7) SFS_HUS Structure with TMD2

Figure J.8 Drift response from 1st floor to top floor under input of El Centro (0.25g)

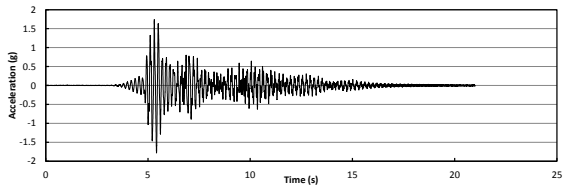

1) Original Structure

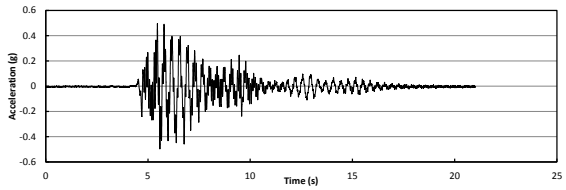

2) SFS Structure

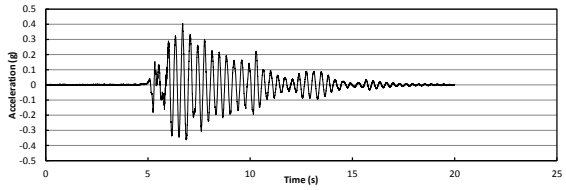

3) SFS_HUS Structure

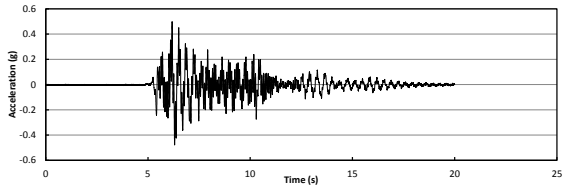

4) SFS Structure with TMD1

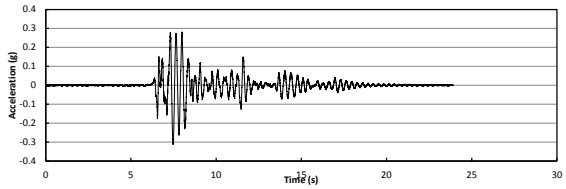

5) SFS_HUS Structure with TMD1

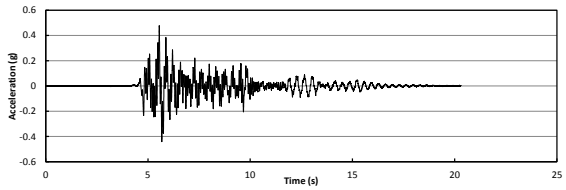

6) SFS Structure with TMD2

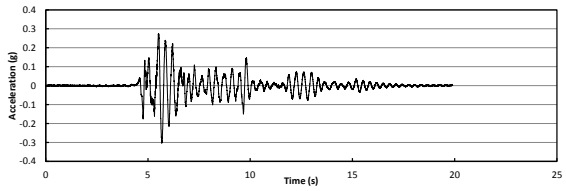

7) SFS_HUS Structure with TMD2

Figure J.9 Acceleration response of the top floor under input of El Centro (0.5g)

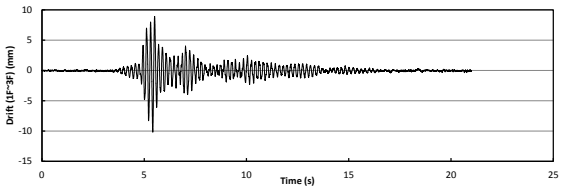

1) Original Structure

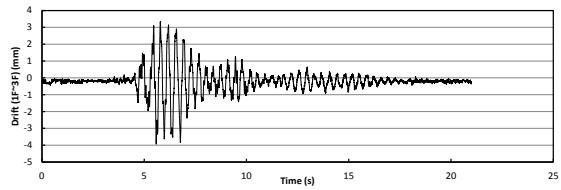

2) SFS Structure

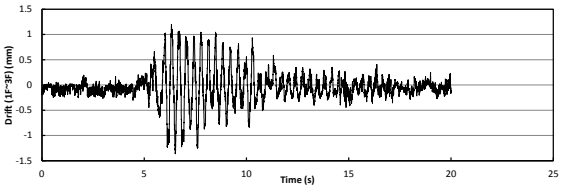

3) SFS_HUS Structure

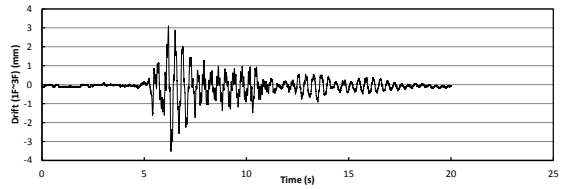

4) SFS Structure with TMD1

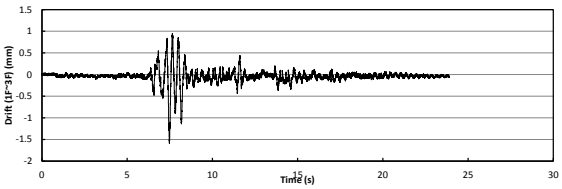

5) SFS_HUS Structure with TMD1

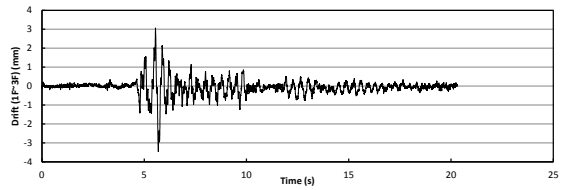

6) SFS Structure with TMD2

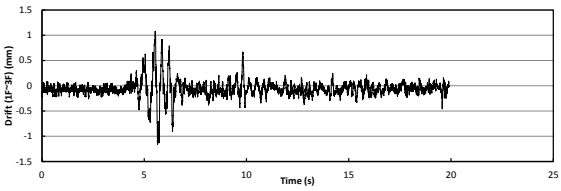

7) SFS_HUS Structure with TMD2

Figure J.10 Drift response from 1st floor to top floor under input of El Centro (0.5g)

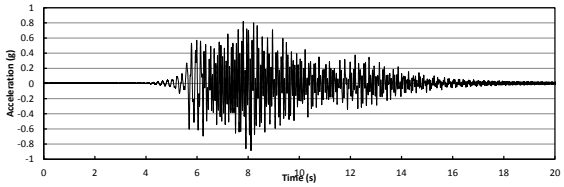

1) Original Structure

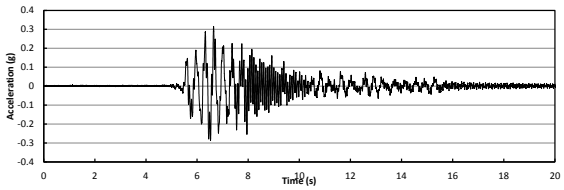

2) SFS Structure

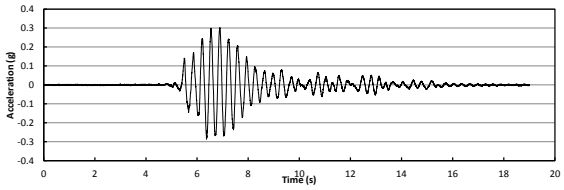

3) SFS_HUS Structure

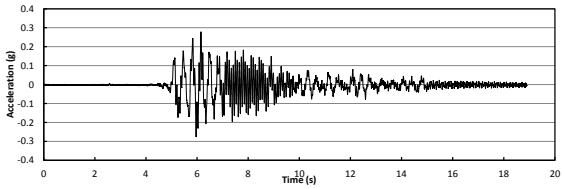

4) SFS Structure with TMD1

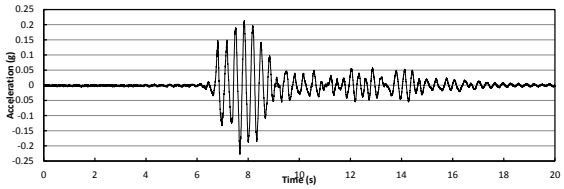

5) SFS_HUS Structure with TMD1

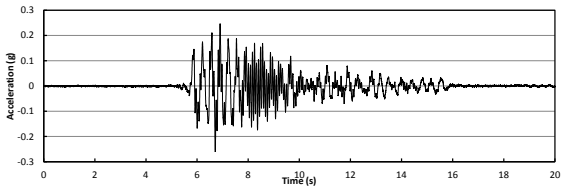

6) SFS Structure with TMD2

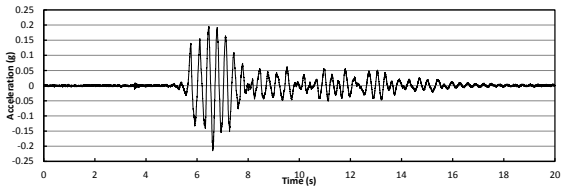

7) SFS_HUS Structure with TMD2

Figure J.11 Acceleration response of the top floor under input of Taft (0.25g)

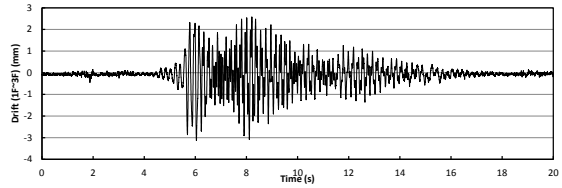

1) Original Structure

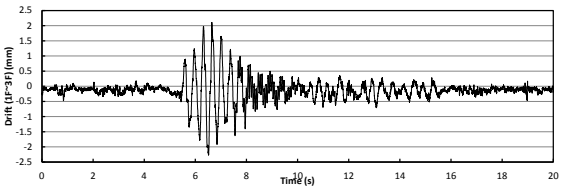

2) SFS Structure

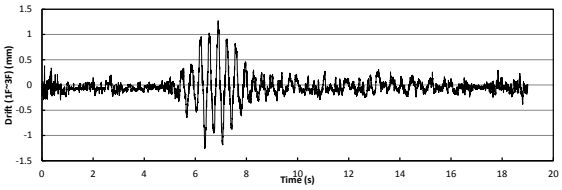

3) SFS_HUS Structure

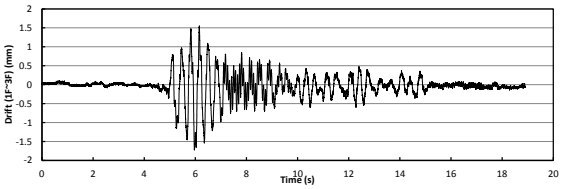

4) SFS Structure with TMD1

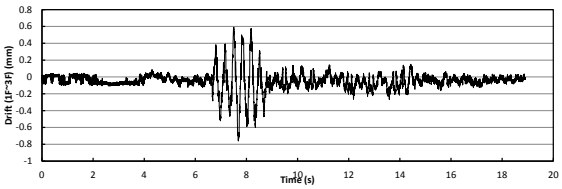

5) SFS_HUS Structure with TMD1

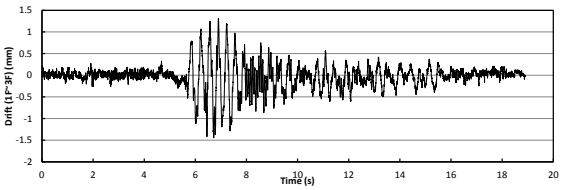

6) SFS Structure with TMD2

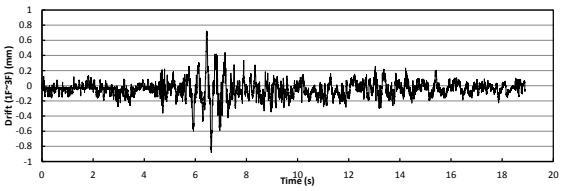

7) SFS_HUS Structure with TMD2

Figure J.12 Drift response from 1st floor to top floor under input of Taft (0.25g)

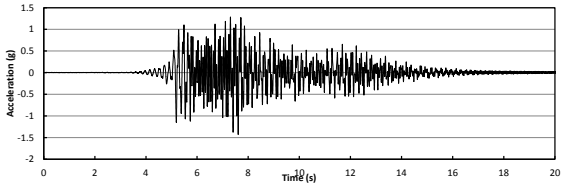

1) Original Structure

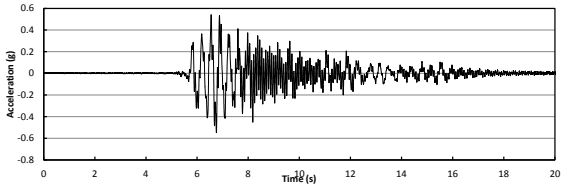

2) SFS Structure

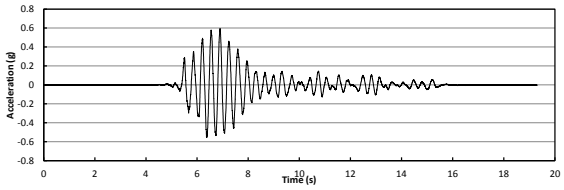

3) SFS_HUS Structure

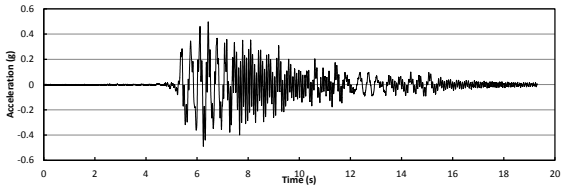

4) SFS Structure with TMD1

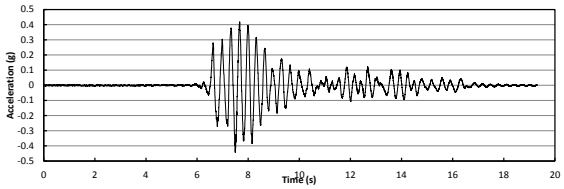

5) SFS_HUS Structure with TMD1

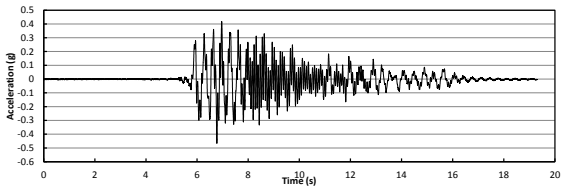

6) SFS Structure with TMD2

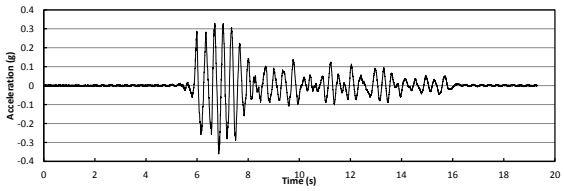

7) SFS_HUS Structure with TMD2

Figure J.13 Acceleration response of the top floor under input of Taft (0.5g)

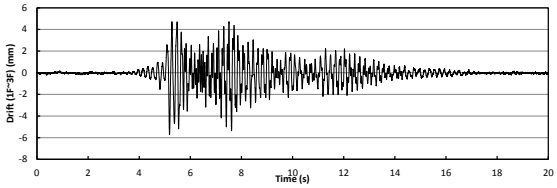

1) Original Structure

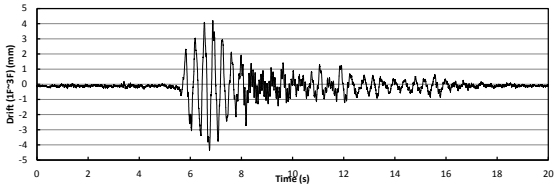

2) SFS Structure

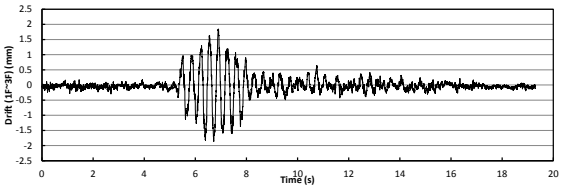

3) SFS_HUS Structure

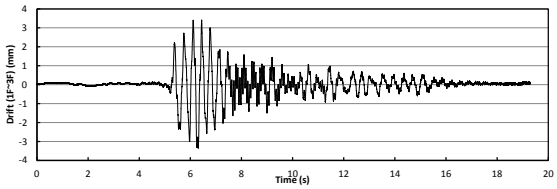

4) SFS Structure with TMD1

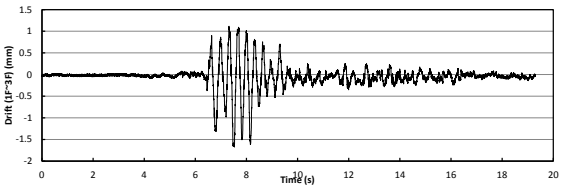

5) SFS_HUS Structure with TMD1

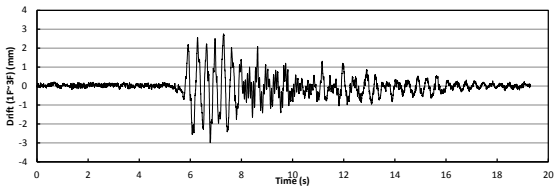

6) SFS Structure with TMD2

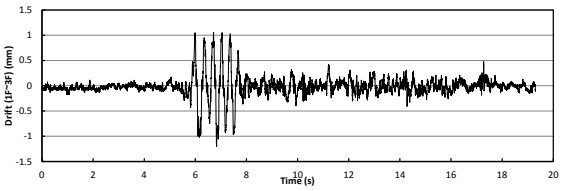

7) SFS_HUS Structure with TMD2

Figure J.14 Drift response from 1st floor to top floor under input of Taft (0.5g)

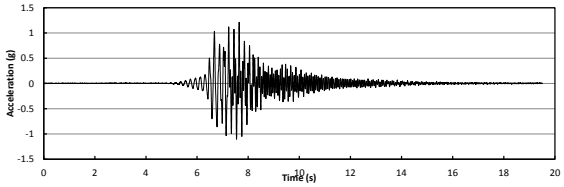

1) Original Structure

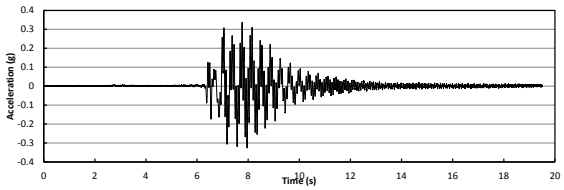

2) SFS Structure

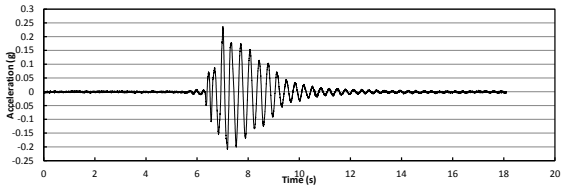

3) SFS_HUS Structure

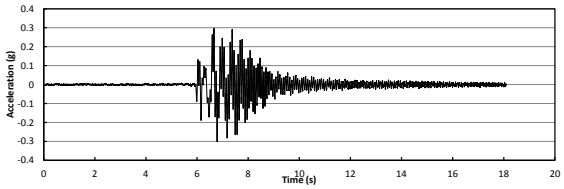

4) SFS Structure with TMD1

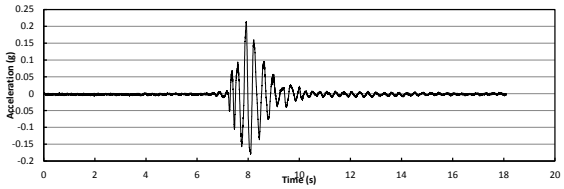

5) SFS_HUS Structure with TMD1

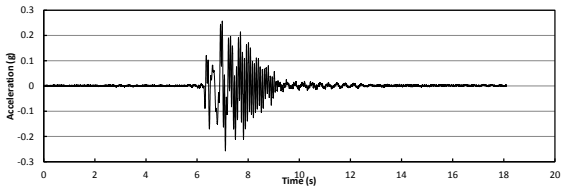

6) SFS Structure with TMD2

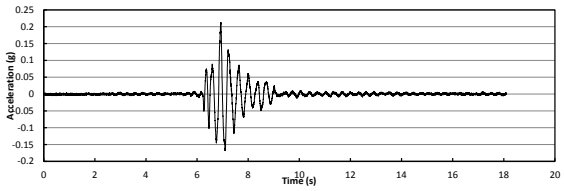

7) SFS_HUS Structure with TMD2

Figure J.15 Acceleration response of the top floor under input of Kobe (0.25g)

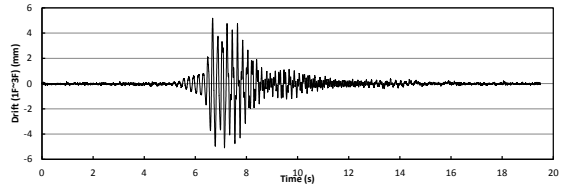

1) Original Structure

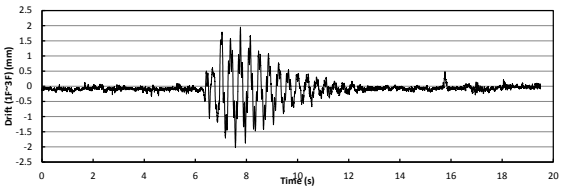

2) SFS Structure

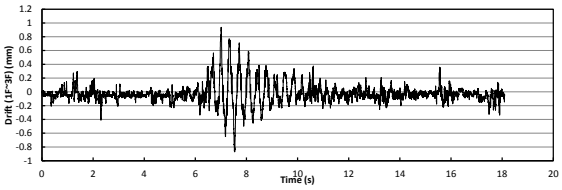

3) SFS_HUS Structure

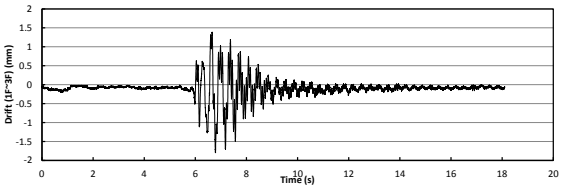

4) SFS Structure with TMD1

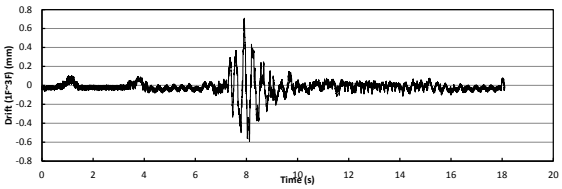

5) SFS_HUS Structure with TMD1

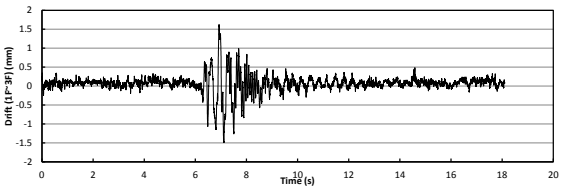

6) SFS Structure with TMD2

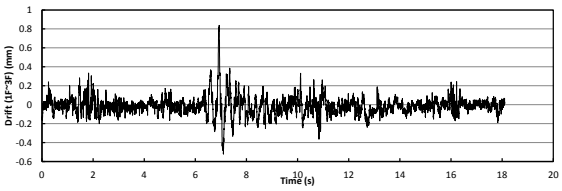

7) SFS_HUS Structure with TMD2

Figure J.16 Drift response from 1st floor to top floor under input of Kobe (0.25g)

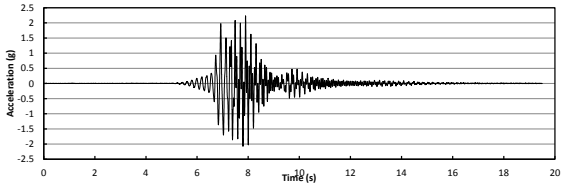

1) Original Structure

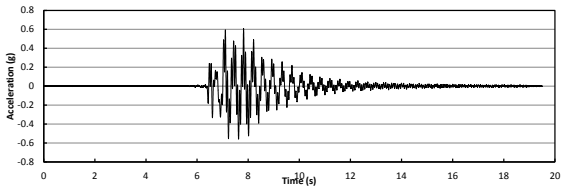

2) SFS Structure

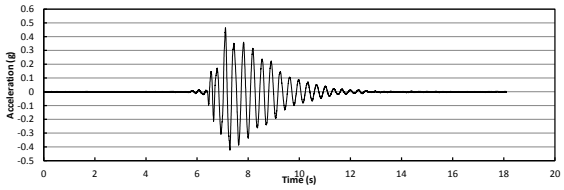

3) SFS_HUS Structure

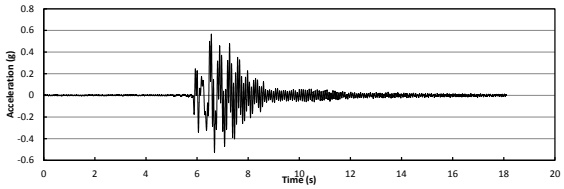

4) SFS Structure with TMD1

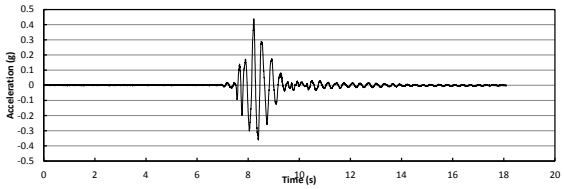

5) SFS_HUS Structure with TMD1

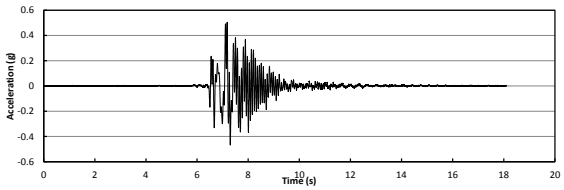

6) SFS Structure with TMD2

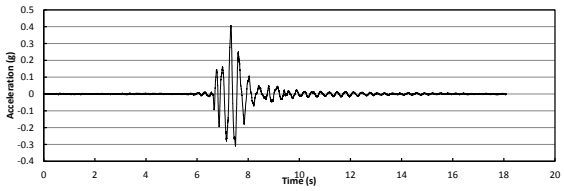

7) SFS_HUS Structure with TMD2

Figure J.17 Acceleration response of the top floor under input of Kobe (0.5g)

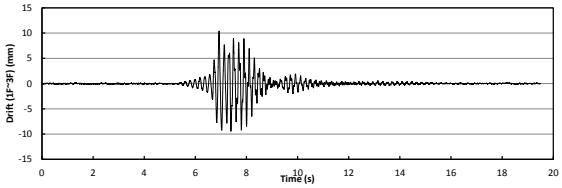

1) Original Structure

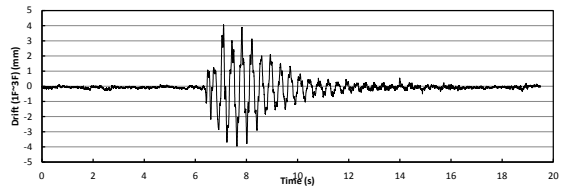

2) SFS Structure

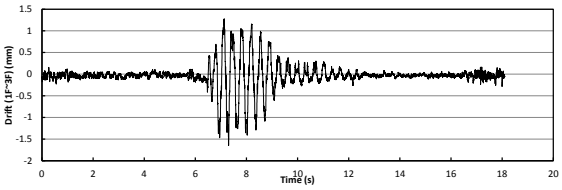

3) SFS_HUS Structure

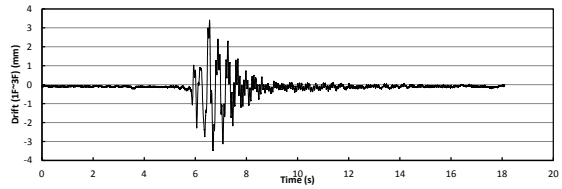

4) SFS Structure with TMD1

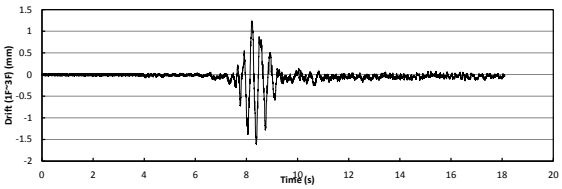

5) SFS_HUS Structure with TMD1

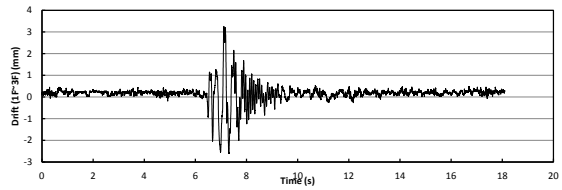

6) SFS Structure with TMD2

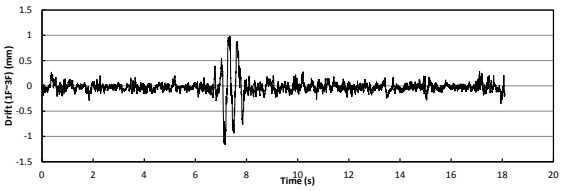

7) SFS_HUS Structure with TMD2

Figure J.18 Drift response from 1st floor to top floor under input of Kobe (0.5g)

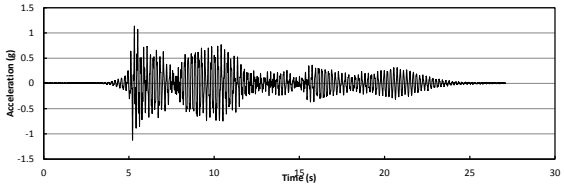

1) Original Structure

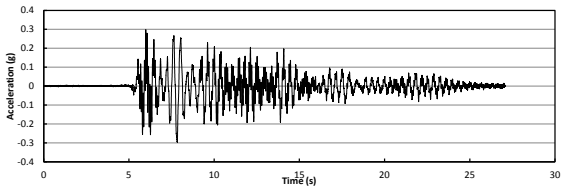

2) SFS Structure

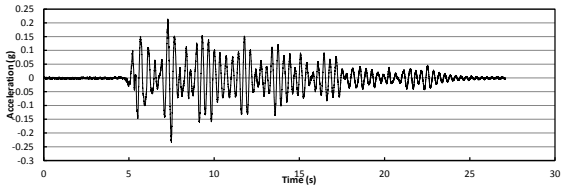

3) SFS_HUS Structure

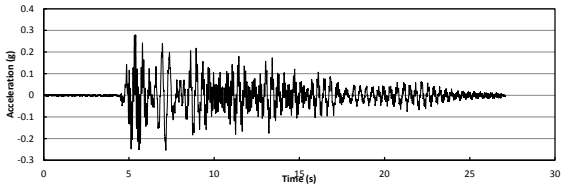

4) SFS Structure with TMD1

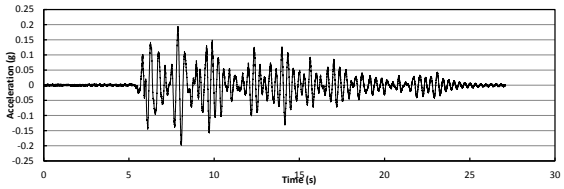

5) SFS_HUS Structure with TMD1

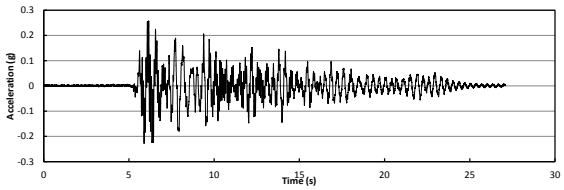

6) SFS Structure with TMD2

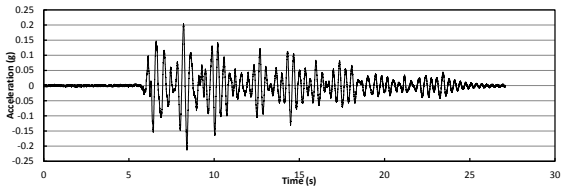

7) SFS_HUS Structure with TMD2

Figure J.19 Acceleration response of the top floor under input of Hachinohe (0.25g)

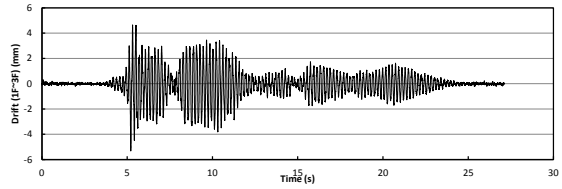

1) Original Structure

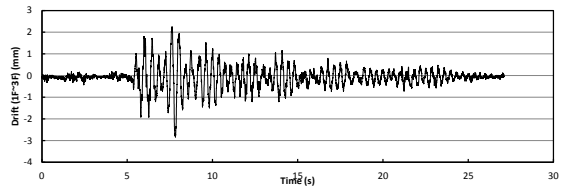

2) SFS Structure

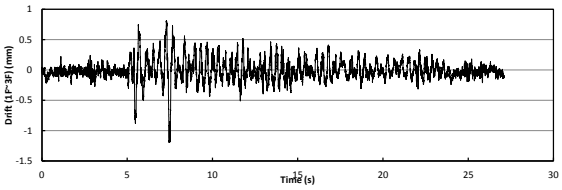

3) SFS_HUS Structure

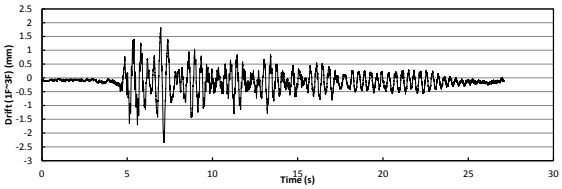

4) SFS Structure with TMD1

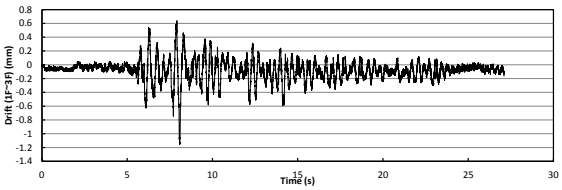

5) SFS_HUS Structure with TMD1

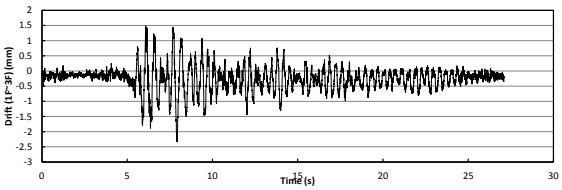

6) SFS Structure with TMD2

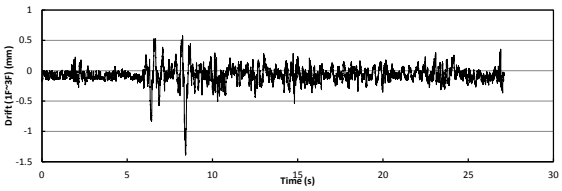

7) SFS_HUS Structure with TMD2

Figure J.20 Drift response from 1st floor to top floor under input of Hachinohe (0.25g)

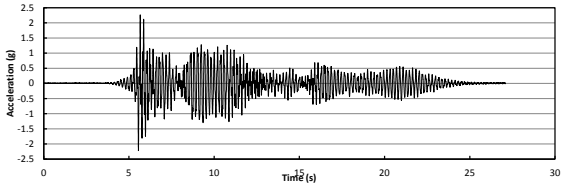

1) Original Structure

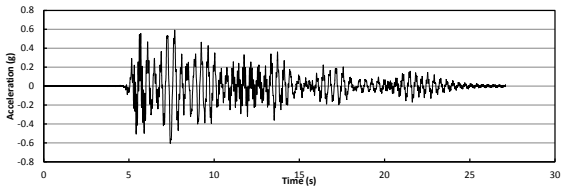

2) SFS Structure

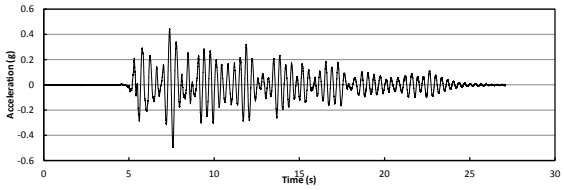

3) SFS_HUS Structure

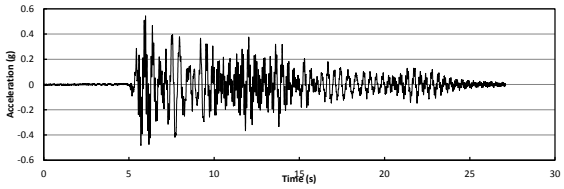

4) SFS Structure with TMD1

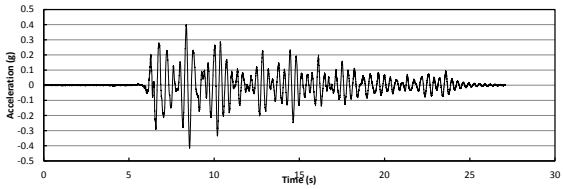

5) SFS_HUS Structure with TMD1

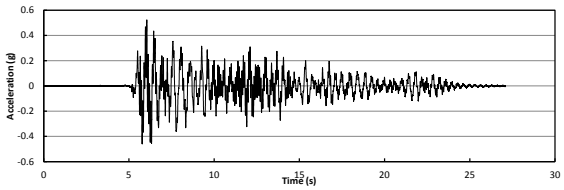

6) SFS Structure with TMD2

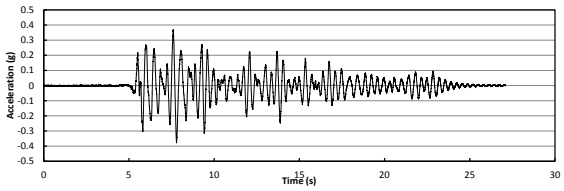

7) SFS_HUS Structure with TMD2

Figure J.21 Acceleration response of the top floor under input of Hachinohe (0.5g)

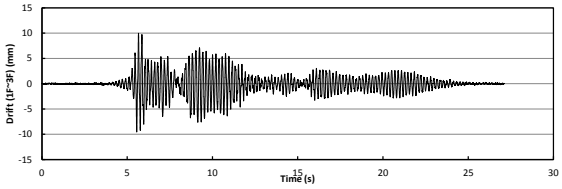

1) Original Structure

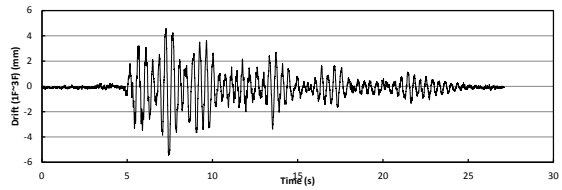

2) SFS Structure

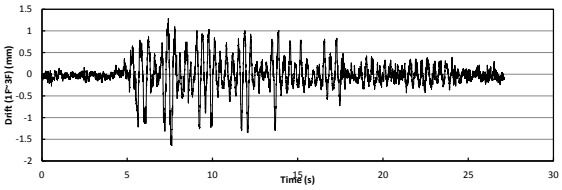

3) SFS_HUS Structure

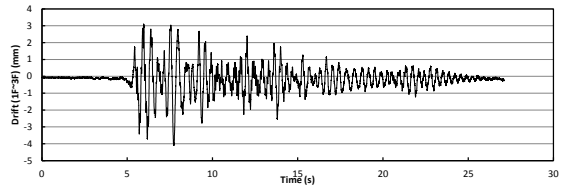

4) SFS Structure with TMD1

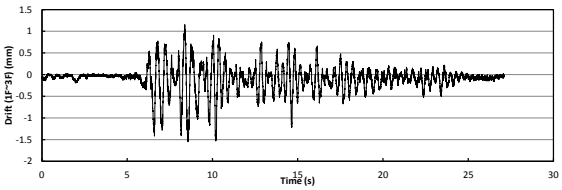

5) SFS_HUS Structure with TMD1

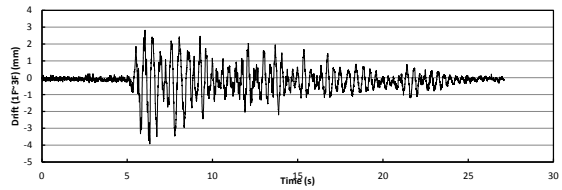

6) SFS Structure with TMD2

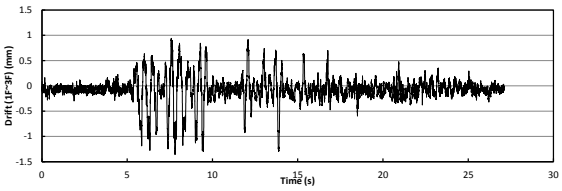

7) SFS_HUS Structure with TMD2

Figure J.22 Drift response from 1st floor to top floor under input of Hachinohe (0.5g)

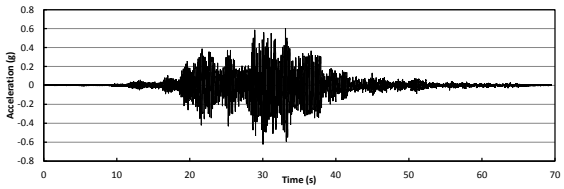

1) Original Structure

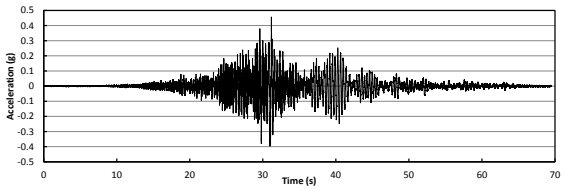

2) SFS Structure

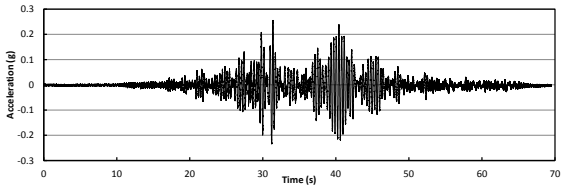

3) SFS_HUS Structure

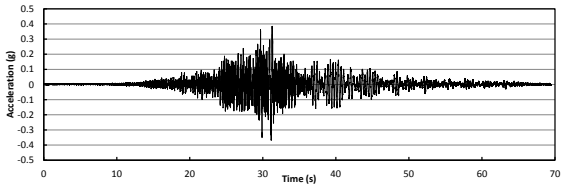

4) SFS Structure with TMD1

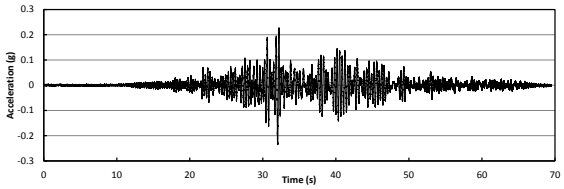

5) SFS_HUS Structure with TMD1

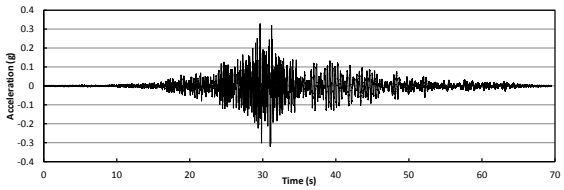

6) SFS Structure with TMD2

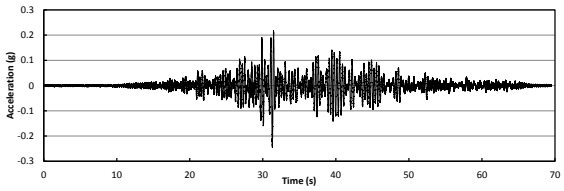

7) SFS_HUS Structure with TMD2

Figure J.23 Acceleration response of the top floor under input of Tohoku (0.25g)

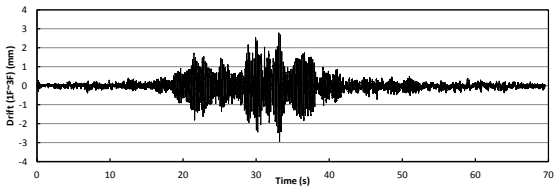

1) Original Structure

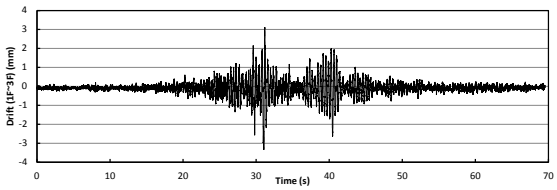

2) SFS Structure

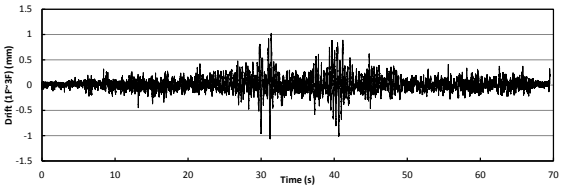

3) SFS_HUS Structure

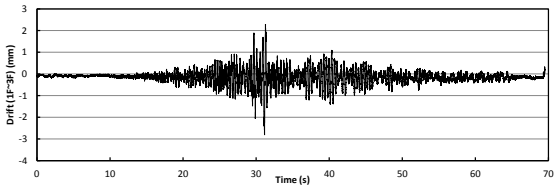

4) SFS Structure with TMD1

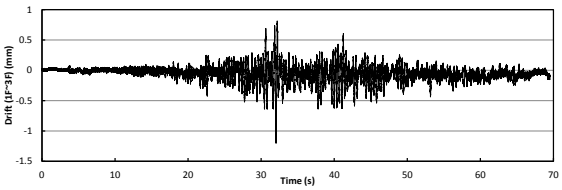

5) SFS_HUS Structure with TMD1

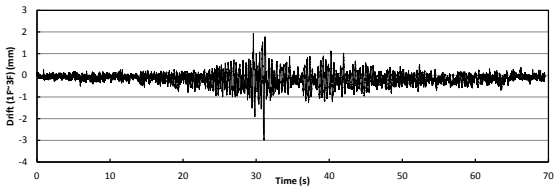

6) SFS Structure with TMD2

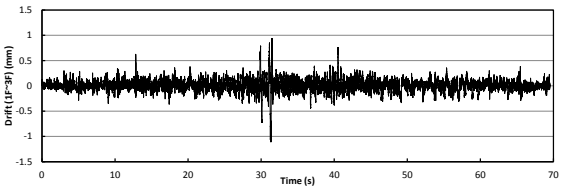

7) SFS_HUS Structure with TMD2

Figure J.24 Drift response from 1st floor to top floor under input of Tohoku (0.25g)

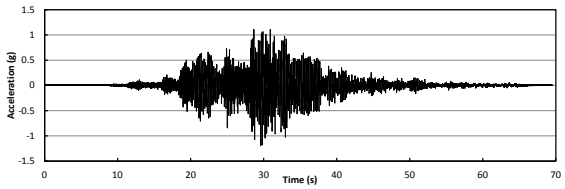

1) Original Structure

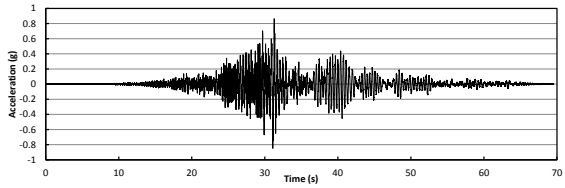

2) SFS Structure

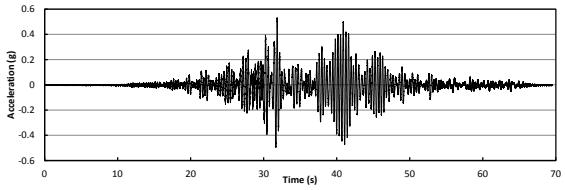

3) SFS_HUS Structure

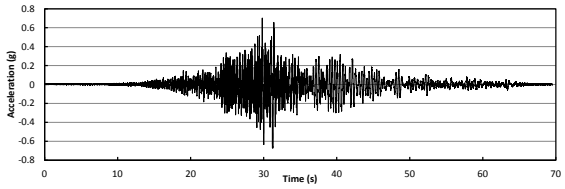

4) SFS Structure with TMD1

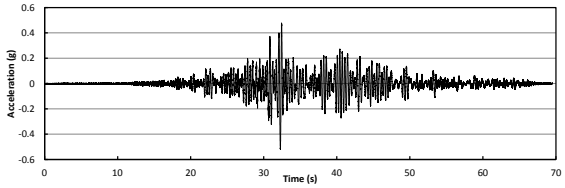

5) SFS_HUS Structure with TMD1

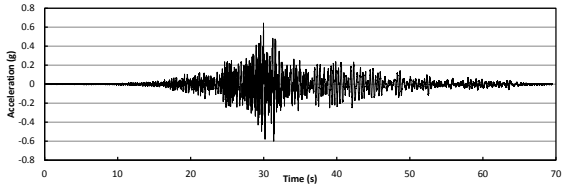

6) SFS Structure with TMD2

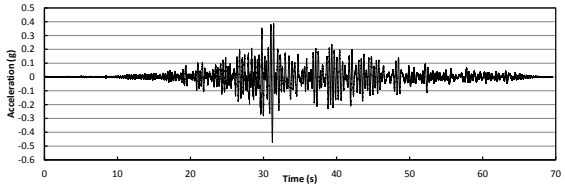

7) SFS_HUS Structure with TMD2

Figure J.25 Acceleration response of the top floor under input of Tohoku (0.5g)

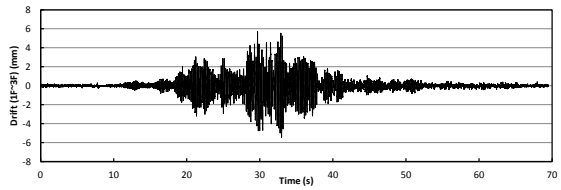

1) Original Structure

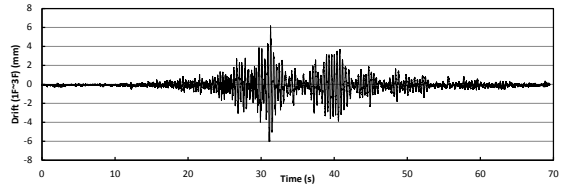

2) SFS Structure

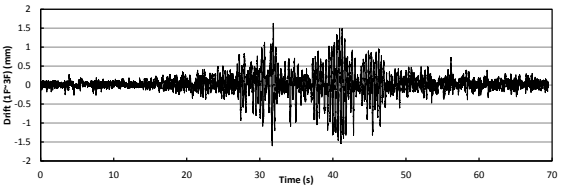

3) SFS_HUS Structure

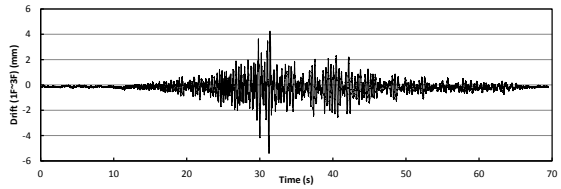

4) SFS Structure with TMD1

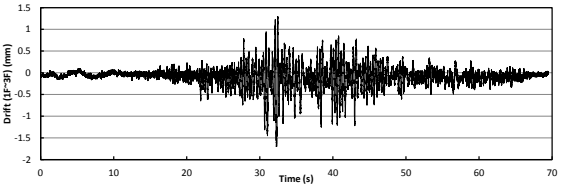

5) SFS_HUS Structure with TMD1

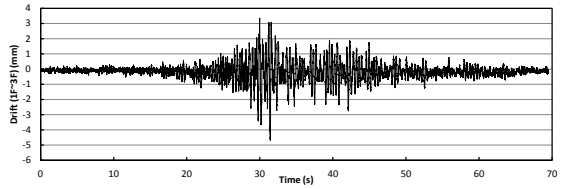

6) SFS Structure with TMD2

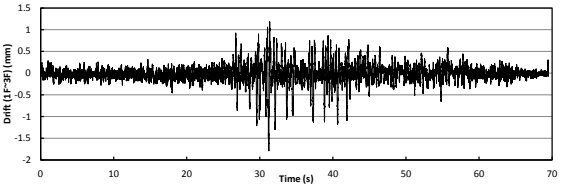

7) SFS_HUS Structure with TMD2

Figure J.26 Drift response from 1st floor to top floor under input of Tohoku (0.5g)

Appendix K

Results of Shaking Table Test for Retrofit Pattern 2

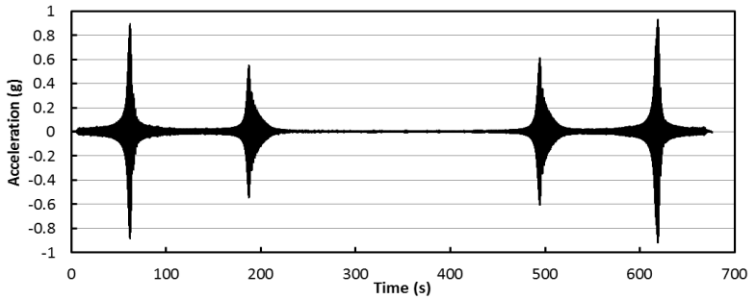

1) Acceleration response of the top floor of the original structure

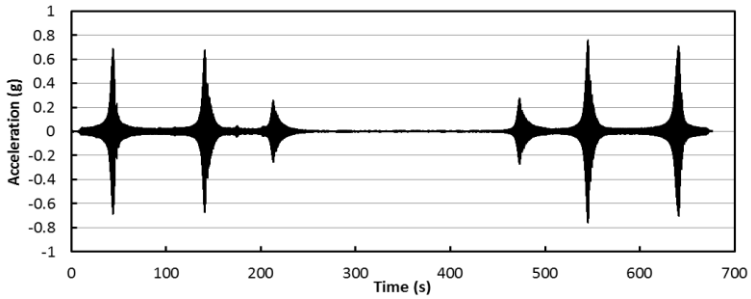

2) Acceleration response of the top floor of the SFS structure

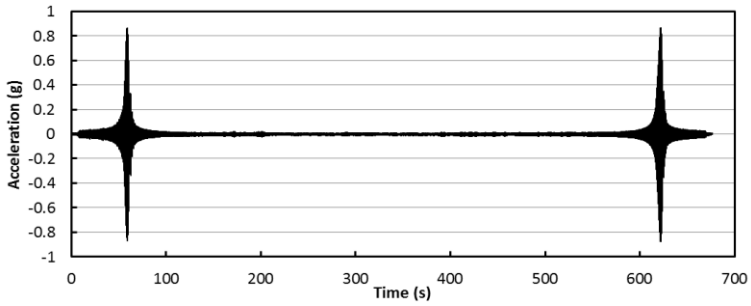

3) Acceleration response of the top floor of the SFS_HUS structure

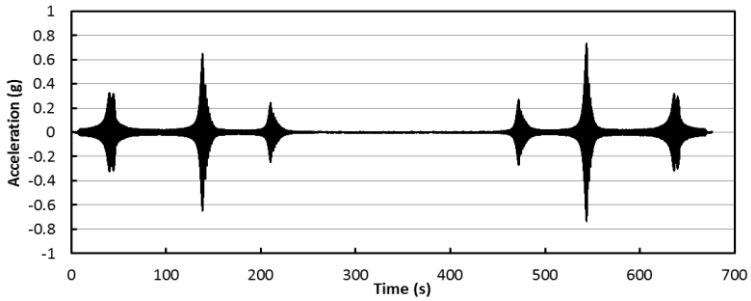

4) Acceleration response of the top floor of the SFS structure with TMD1

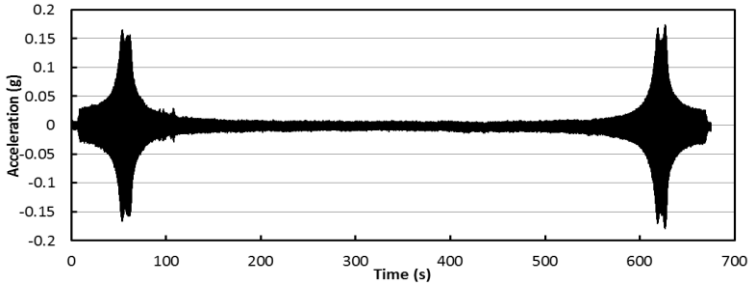

5) Acceleration response of the top floor of the SFS_HUS structure with TMD1

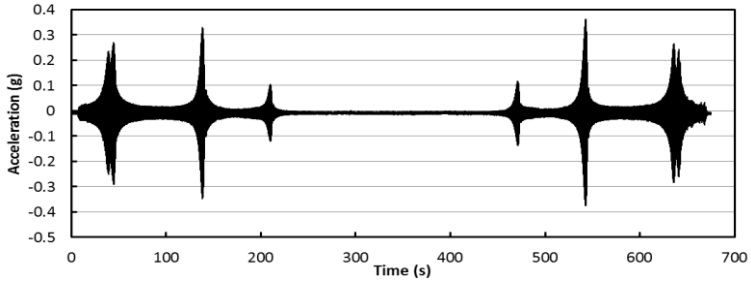

6) Acceleration response of the top floor of the SFS structure with TMD2

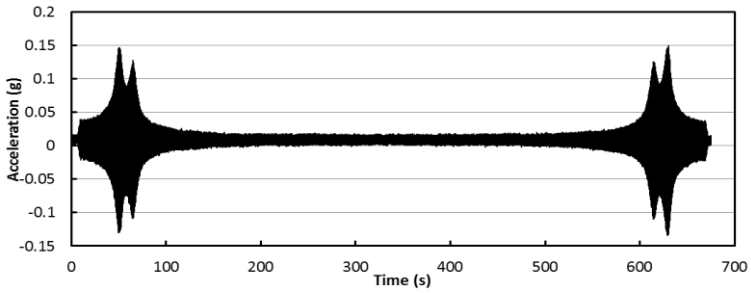

7) Acceleration response of the top floor of the SFS_HUS structure with TMD2

Figure K.1 Acceleration response of the top floor under sweep input

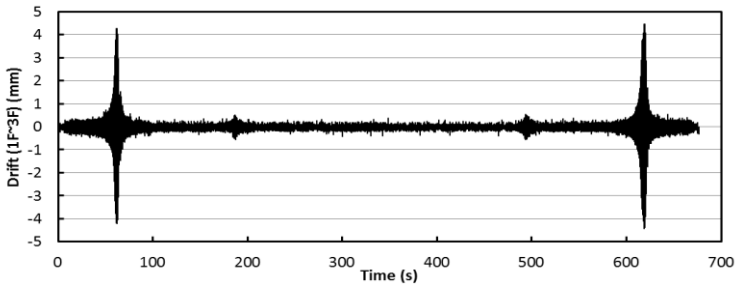

1) Drift from 1st floor to top floor of the original structure

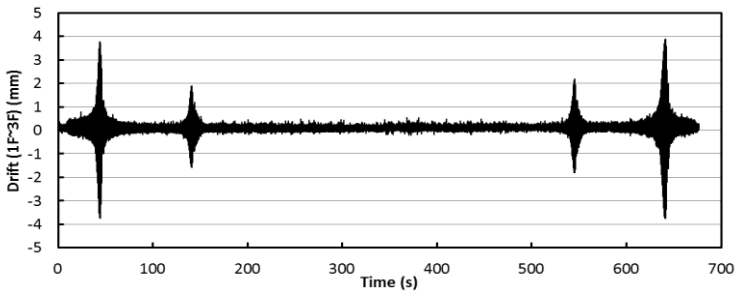

2) Drift from 1st floor to top floor of the SFS structure

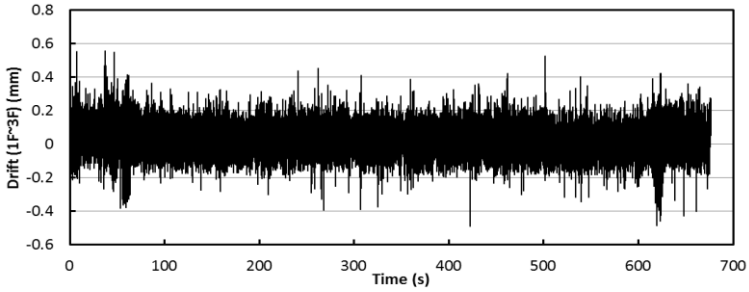

3) Drift from 1st floor to top floor of the SFS_HUS structure

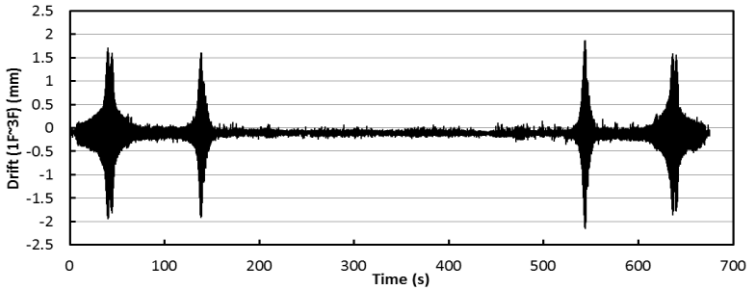

4) Drift from 1st floor to top floor of the SFS structure with TMD1

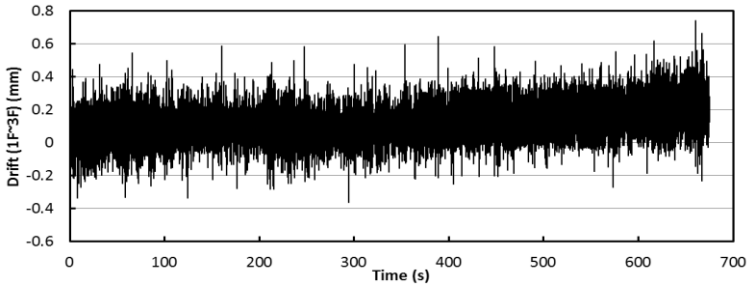

5) Drift from 1st floor to top floor of the SFS_HUS structure with TMD1

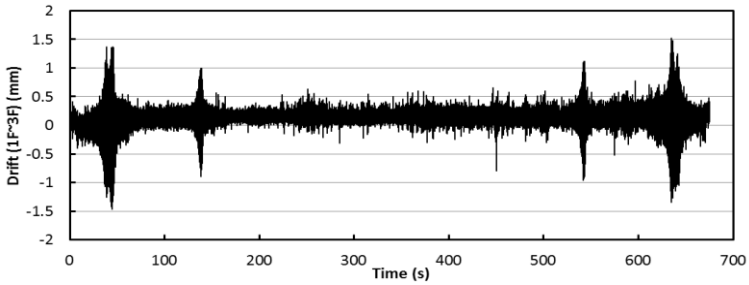

6) Drift from 1st floor to top floor of the SFS structure with TMD2

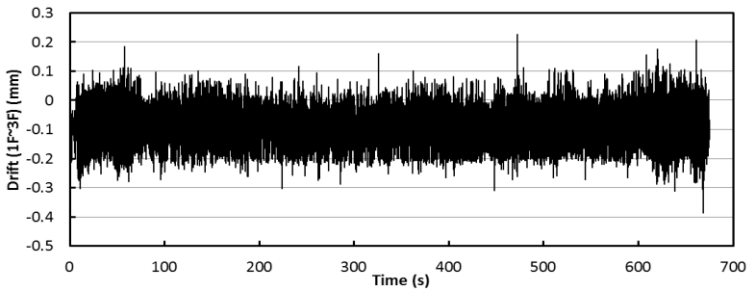

7) Drift from 1st floor to top floor of the SFS_HUS structure with TMD2

Figure K.2 Drift response from 1st floor to top floor under sweep input

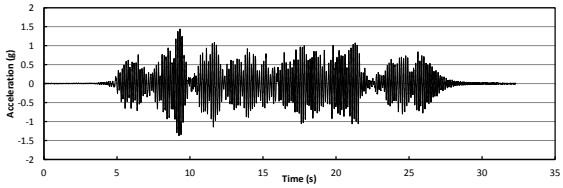

1) Original Structure

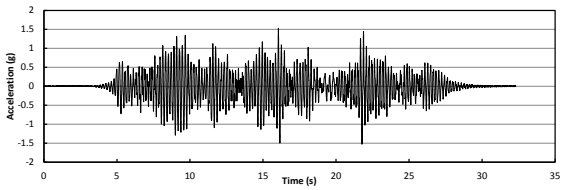

2) SFS Structure

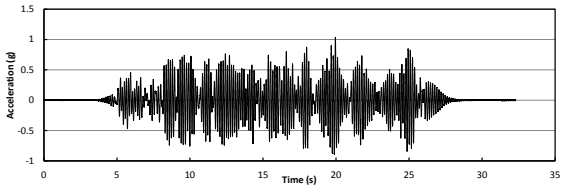

3) SFS_HUS Structure

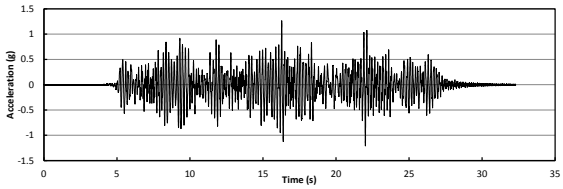

4) SFS Structure with TMD1

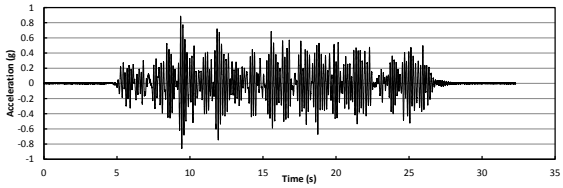

5) SFS_HUS Structure with TMD1

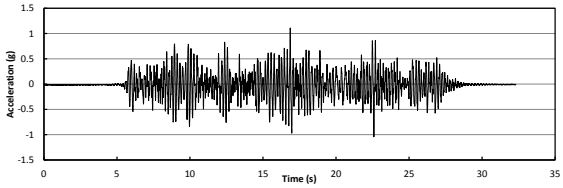

6) SFS Structure with TMD2

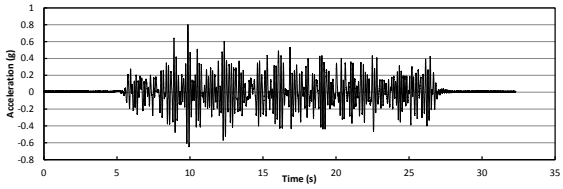

7) SFS_HUS Structure with TMD2

Figure K.3 Acceleration response of the top floor under input of Whitenoise1

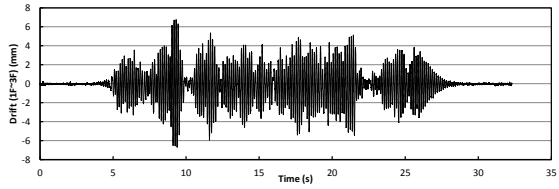

1) Original Structure

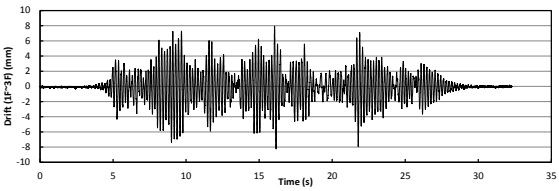

2) SFS Structure

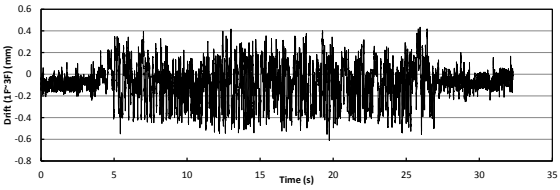

3) SFS_HUS Structure

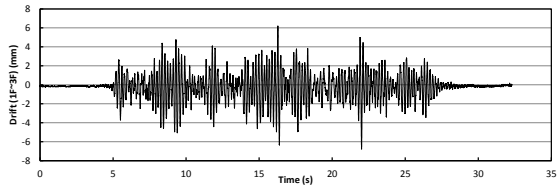

4) SFS Structure with TMD1

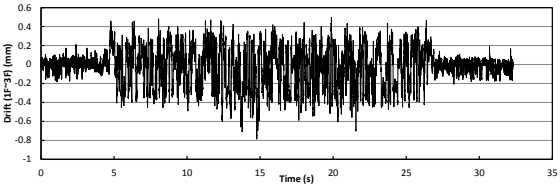

5) SFS_HUS Structure with TMD1

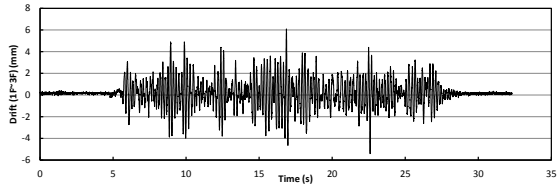

6) SFS Structure with TMD2

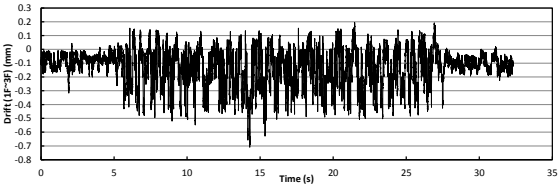

7) SFS_HUS Structure with TMD2

Figure K.4 Drift response from 1st floor to top floor under input of Whitenoise1

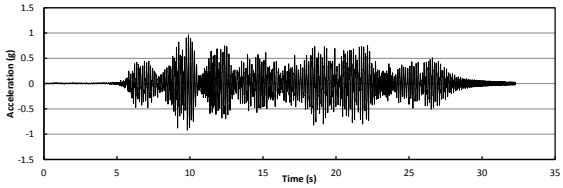

1) Original Structure

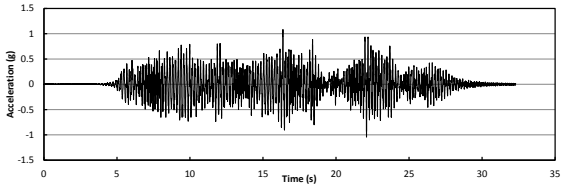

2) SFS Structure

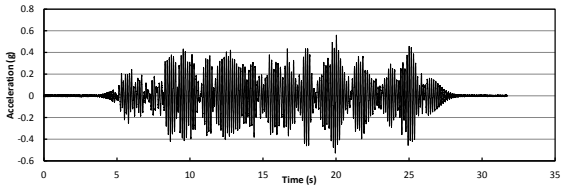

3) SFS_HUS Structure

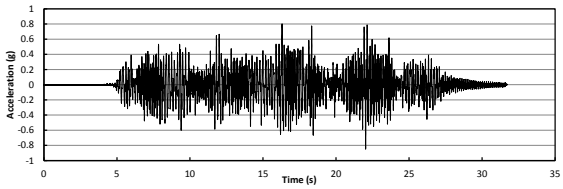

4) SFS Structure with TMD1

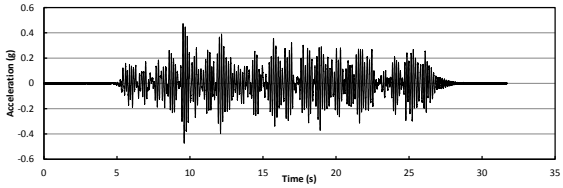

5) SFS_HUS Structure with TMD1

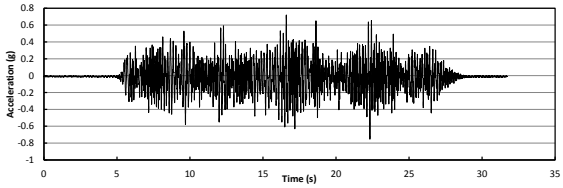

6) SFS Structure with TMD2

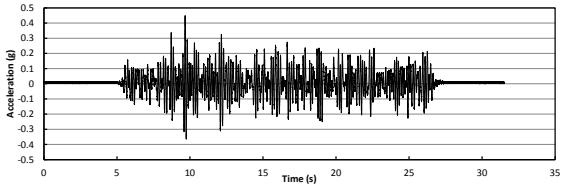

7) SFS_HUS Structure with TMD2

Figure K.5 Acceleration response of the top floor under input of Whitenoise2

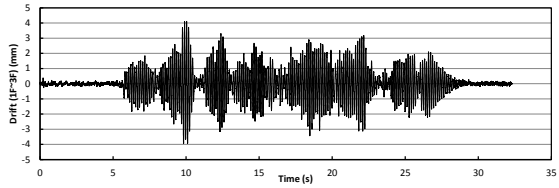

1) Original Structure

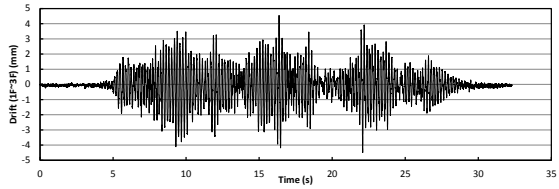

2) SFS Structure

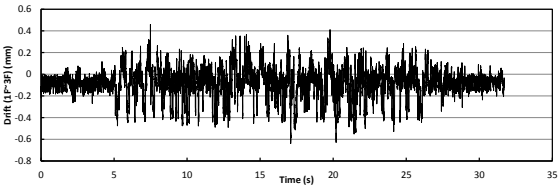

3) SFS_HUS Structure

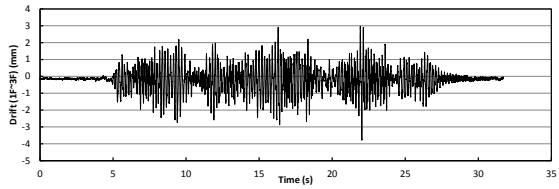

4) SFS Structure with TMD1

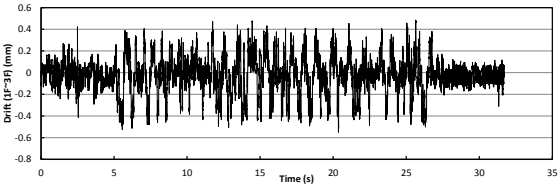

5) SFS_HUS Structure with TMD1

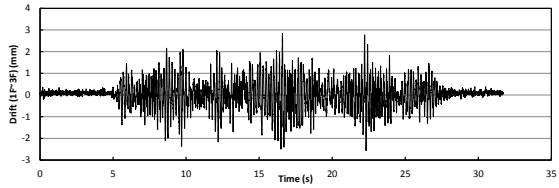

6) SFS Structure with TMD2

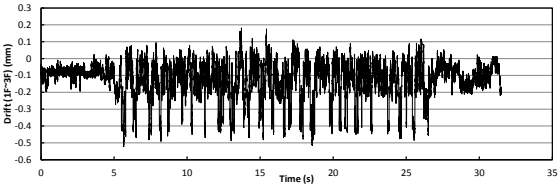

7) SFS_HUS Structure with TMD2

Figure K.6 Drift response from 1st floor to top floor under input of Whitenoise2

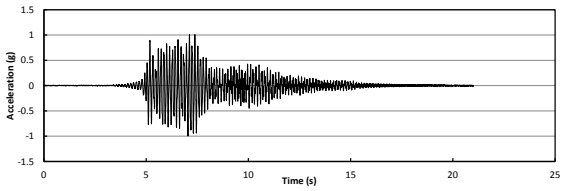

1) Original Structure

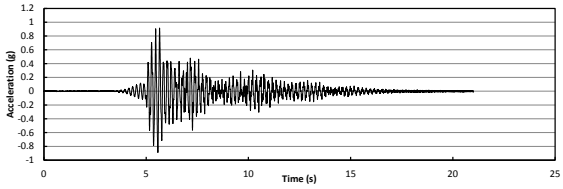

2) SFS Structure

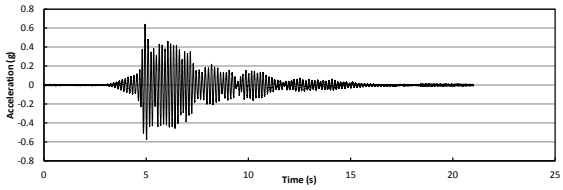

3) SFS_HUS Structure

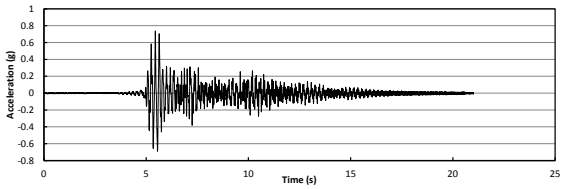

4) SFS Structure with TMD1

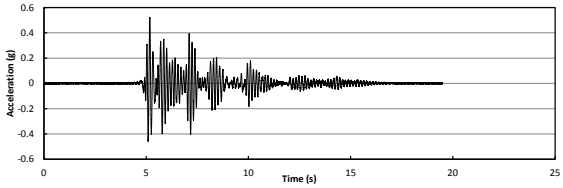

5) SFS_HUS Structure with TMD1

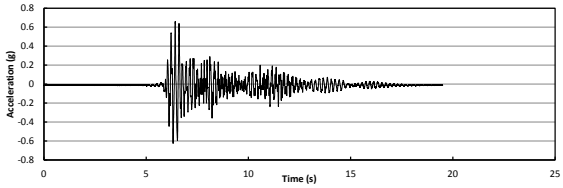

6) SFS Structure with TMD2

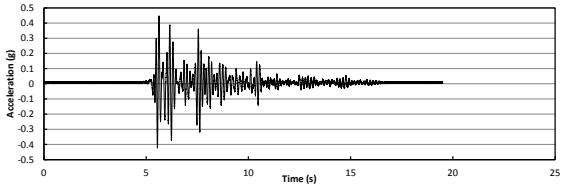

7) SFS_HUS Structure with TMD2

Figure K.7 Acceleration response of the top floor under input of El Centro (0.25g)

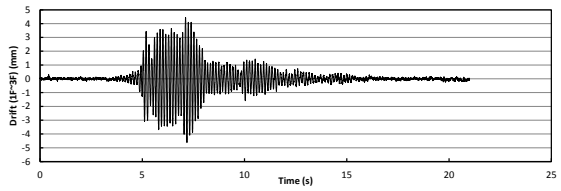

1) Original Structure

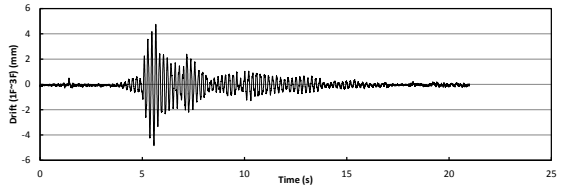

2) SFS Structure

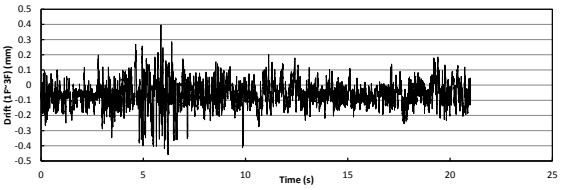

3) SFS_HUS Structure

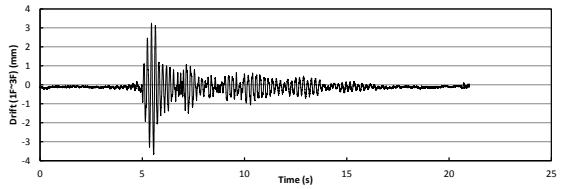

4) SFS Structure with TMD1

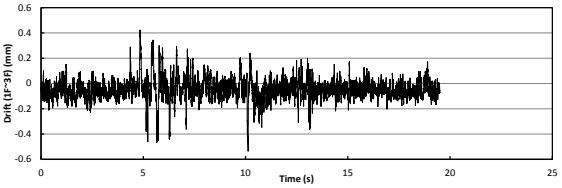

5) SFS_HUS Structure with TMD1

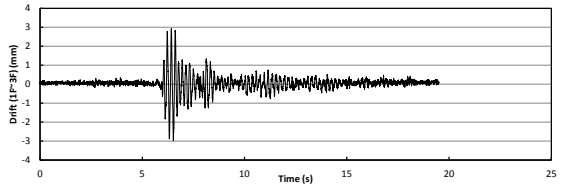

6) SFS Structure with TMD2

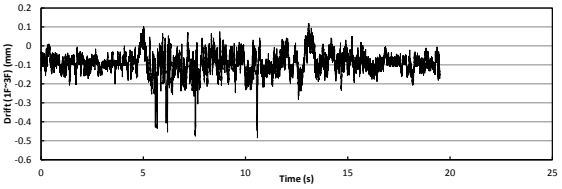

7) SFS_HUS Structure with TMD2

Figure K.8 Drift response from 1st floor to top floor under input of El Centro (0.25g)

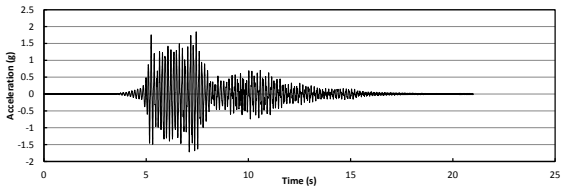

1) Original Structure

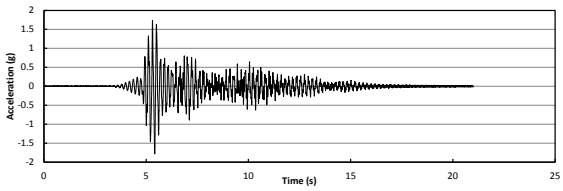

2) SFS Structure

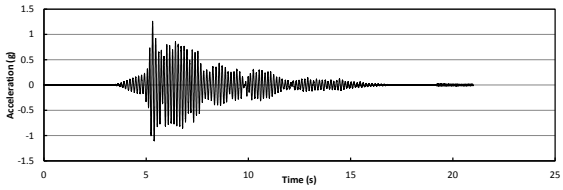

3) SFS_HUS Structure

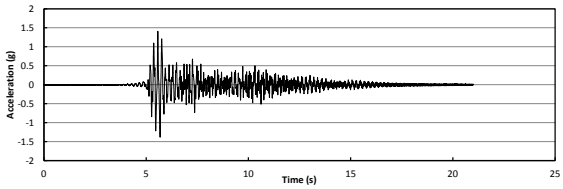

4) SFS Structure with TMD1

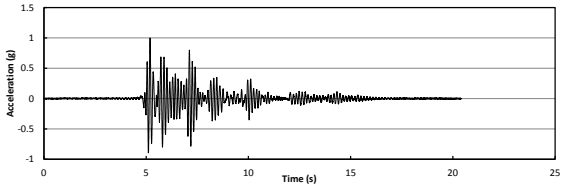

5) SFS_HUS Structure with TMD1

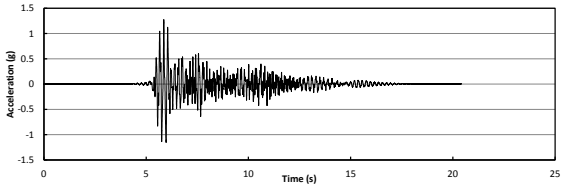

6) SFS Structure with TMD2

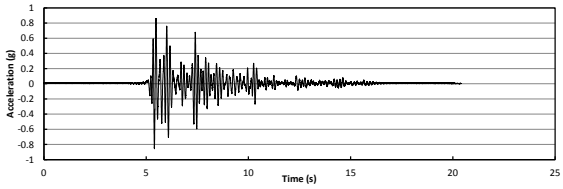

7) SFS_HUS Structure with TMD2

Figure K.9 Acceleration response of the top floor under input of El Centro (0.5g)

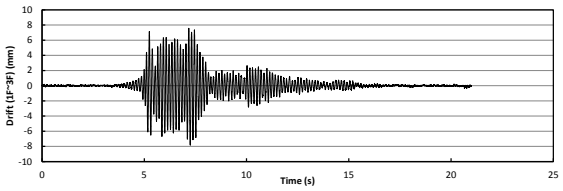

1) Original Structure

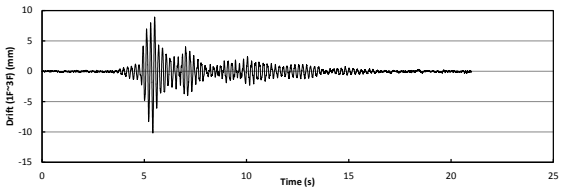

2) SFS Structure

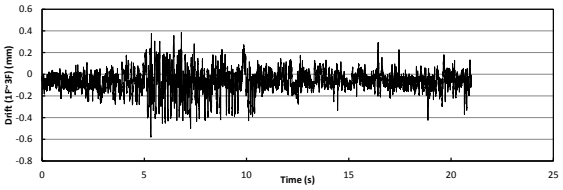

3) SFS_HUS Structure

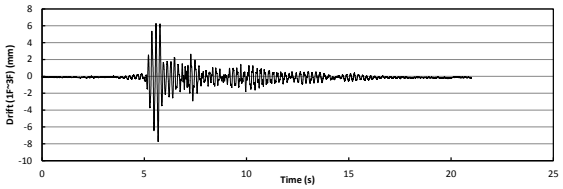

4) SFS Structure with TMD1

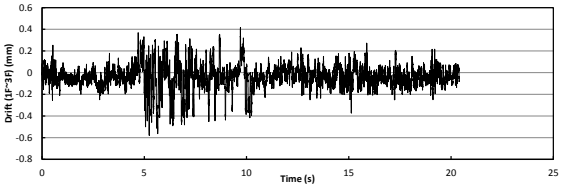

5) SFS_HUS Structure with TMD1

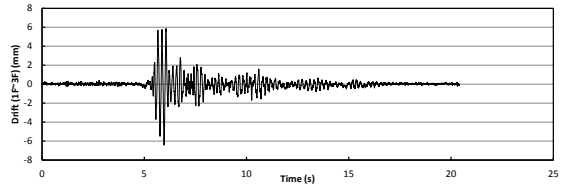

6) SFS Structure with TMD2

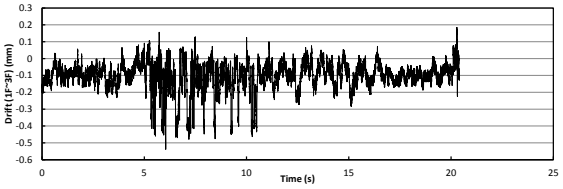

7) SFS_HUS Structure with TMD2

Figure K.10 Drift response from 1st floor to top floor under input of El Centro (0.5g)

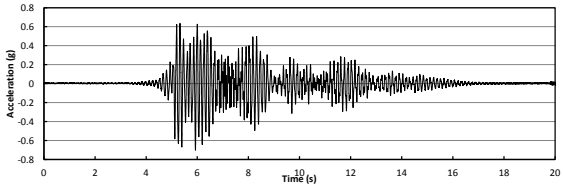

1) Original Structure

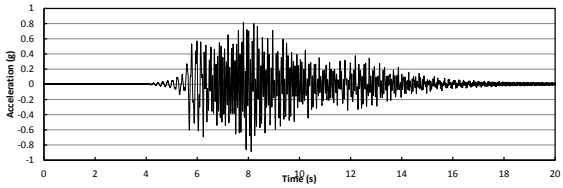

2) SFS Structure

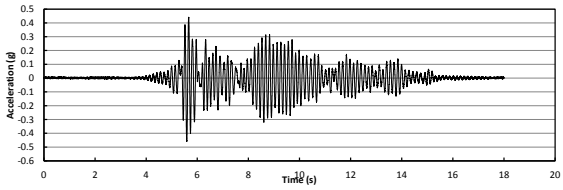

3) SFS_HUS Structure

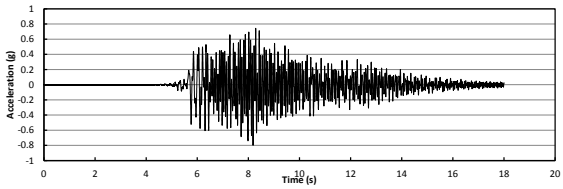

4) SFS Structure with TMD1

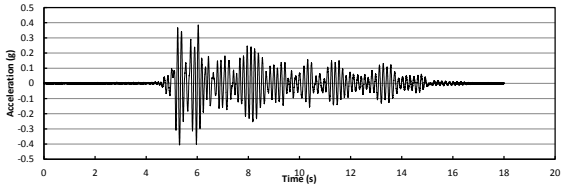

5) SFS_HUS Structure with TMD1

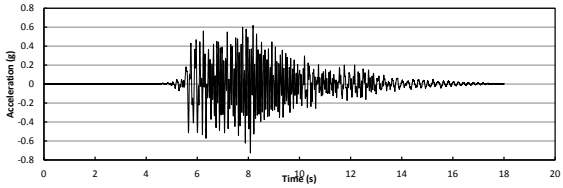

6) SFS Structure with TMD2

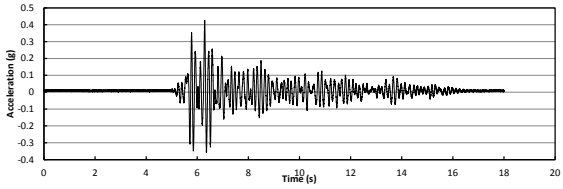

7) SFS_HUS Structure with TMD2

Figure K.11 Acceleration response of the top floor under input of Taft (0.25g)

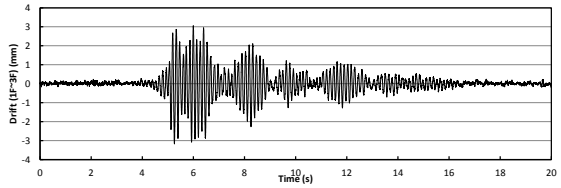

1) Original Structure

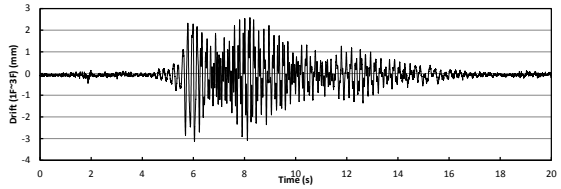

2) SFS Structure

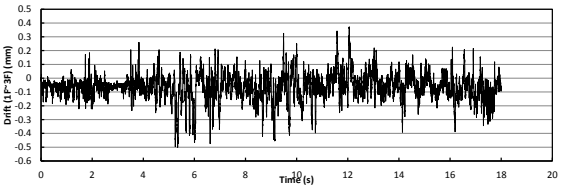

3) SFS_HUS Structure

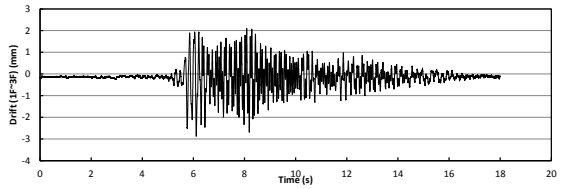

4) SFS Structure with TMD1

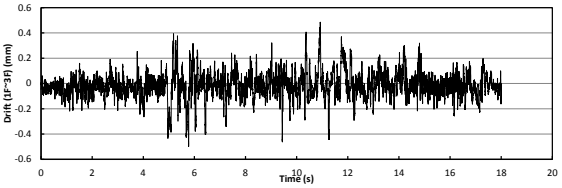

5) SFS_HUS Structure with TMD1

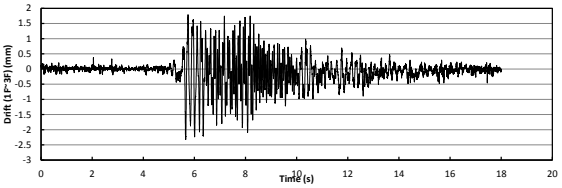

6) SFS Structure with TMD2

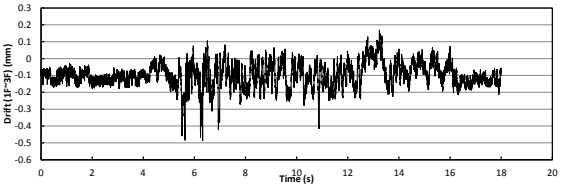

7) SFS_HUS Structure with TMD2

Figure K.12 Drift response from 1st floor to top floor under input of Taft (0.25g)

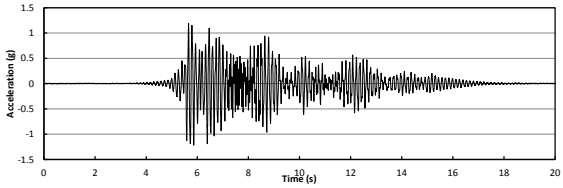

1) Original Structure

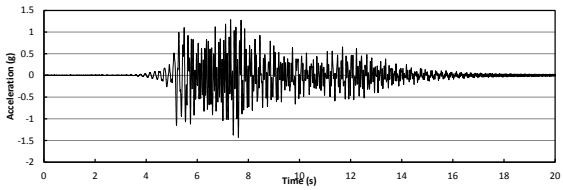

2) SFS Structure

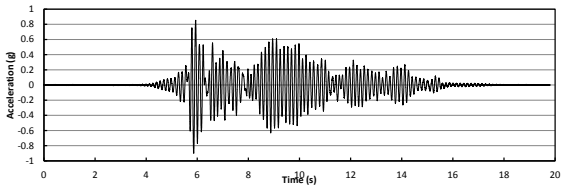

3) SFS_HUS Structure

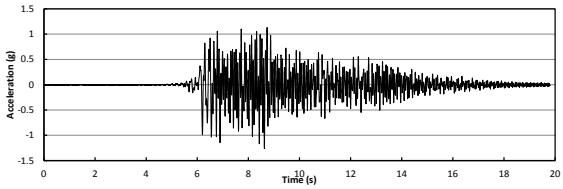

4) SFS Structure with TMD1

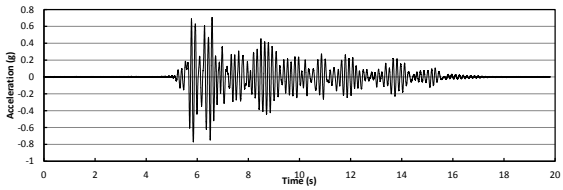

5) SFS_HUS Structure with TMD1

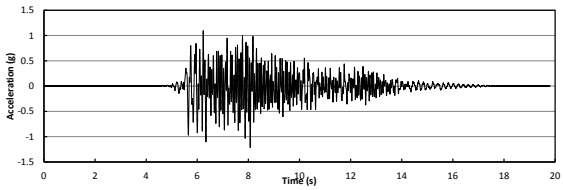

6) SFS Structure with TMD2

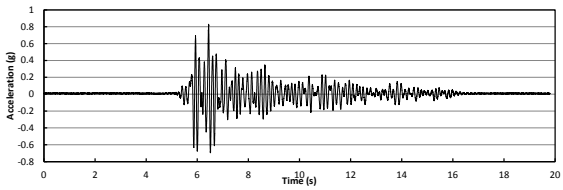

7) SFS_HUS Structure with TMD2

Figure K.13 Acceleration response of the top floor under input of Taft (0.5g)

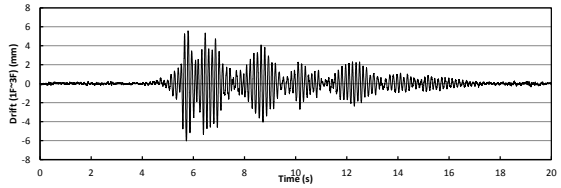

1) Original Structure

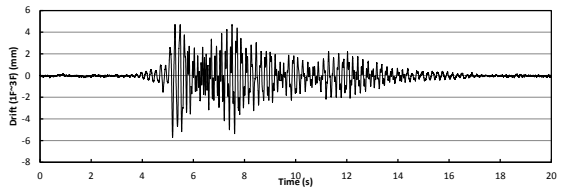

2) SFS Structure

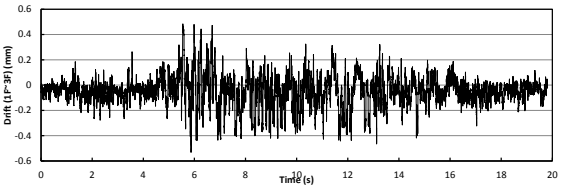

3) SFS_HUS Structure

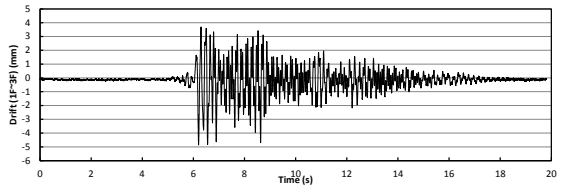

4) SFS Structure with TMD1

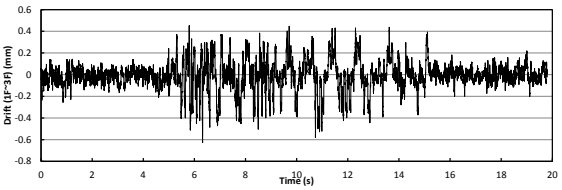

5) SFS_HUS Structure with TMD1

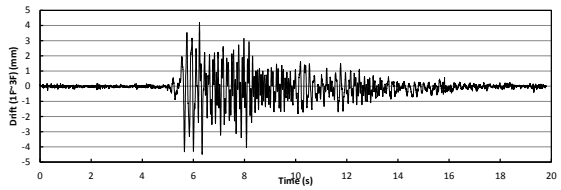

6) SFS Structure with TMD2

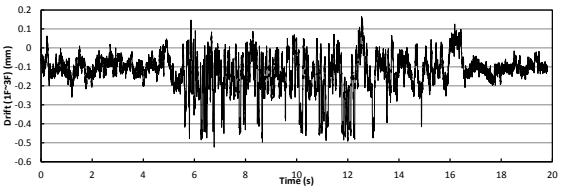

7) SFS_HUS Structure with TMD2

Figure K.14 Drift response from 1st floor to top floor under input of Taft (0.5g)

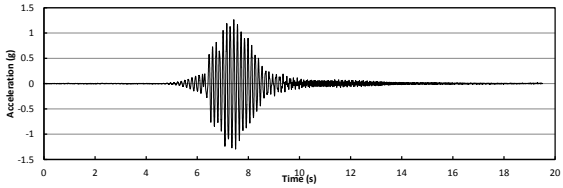

1) Original Structure

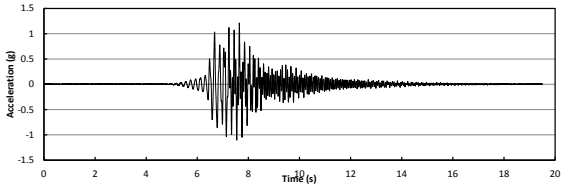

2) SFS Structure

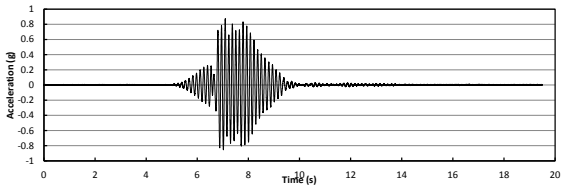

3) SFS_HUS Structure

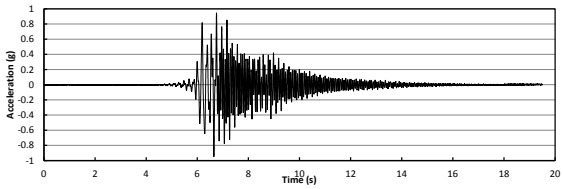

4) SFS Structure with TMD1

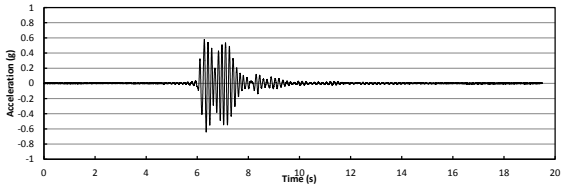

5) SFS_HUS Structure with TMD1

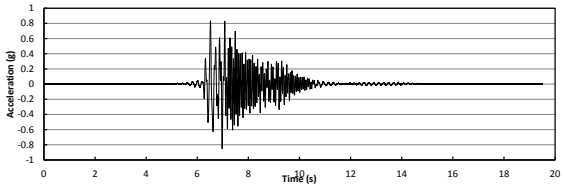

6) SFS Structure with TMD2

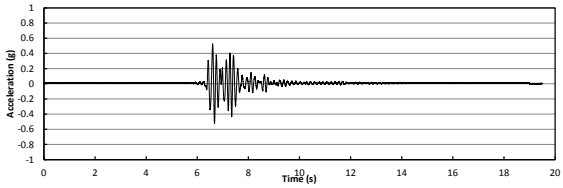

7) SFS_HUS Structure with TMD2

Figure K.15 Acceleration response of the top floor under input of Kobe (0.25g)

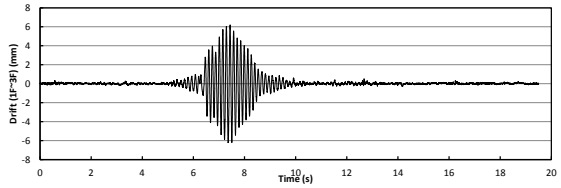

1) Original Structure

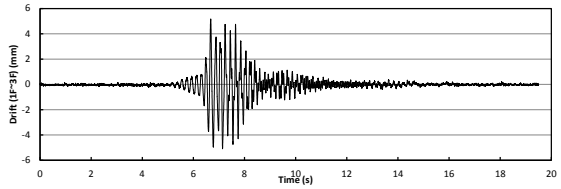

2) SFS Structure

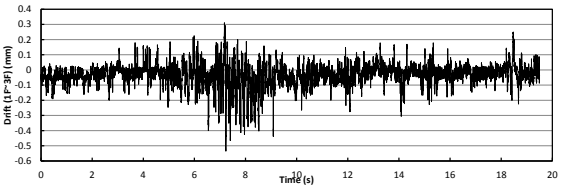

3) SFS_HUS Structure

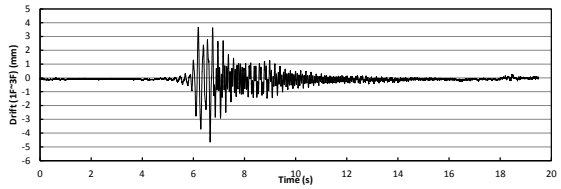

4) SFS Structure with TMD1

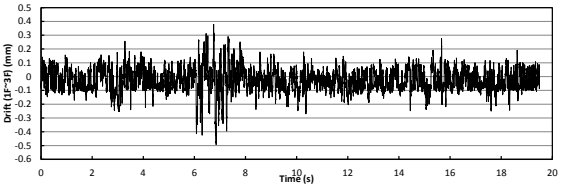

5) SFS_HUS Structure with TMD1

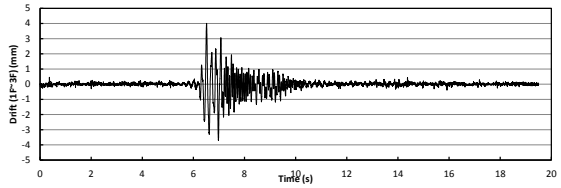

6) SFS Structure with TMD2

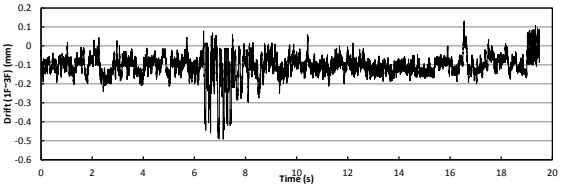

7) SFS_HUS Structure with TMD2

Figure K.16 Drift response from 1st floor to top floor under input of Kobe (0.25g)

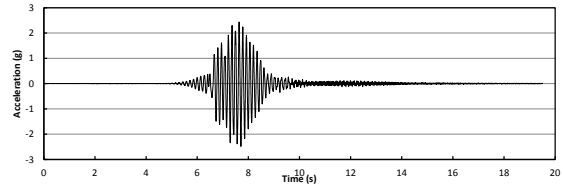

1) Original Structure

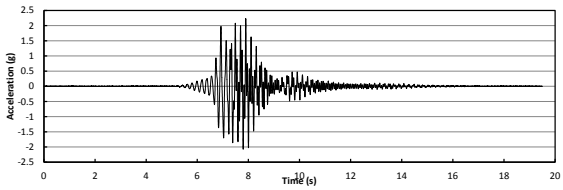

2) SFS Structure

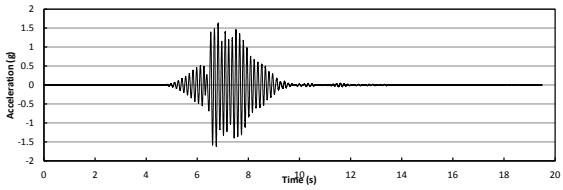

3) SFS_HUS Structure

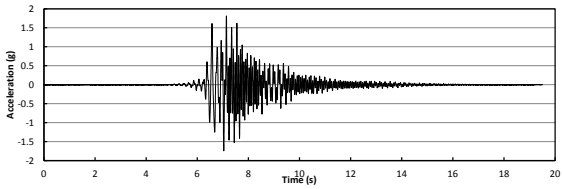

4) SFS Structure with TMD1

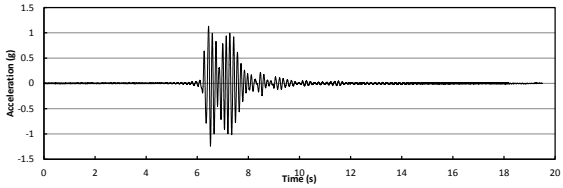

5) SFS_HUS Structure with TMD1

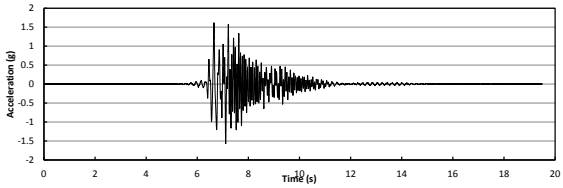

6) SFS Structure with TMD2

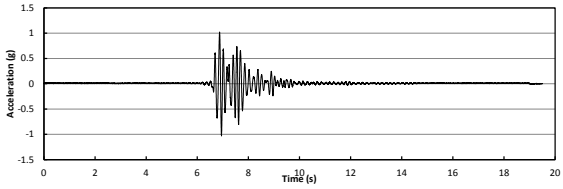

7) SFS_HUS Structure with TMD2

Figure K.17 Acceleration response of the top floor under input of Kobe (0.5g)

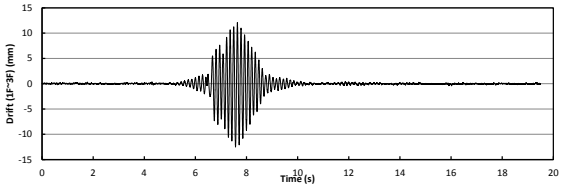

1) Original Structure

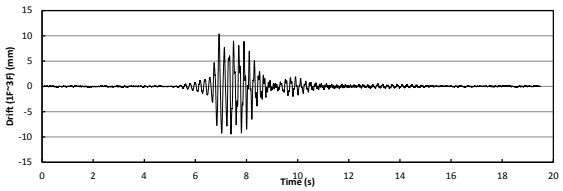

2) SFS Structure

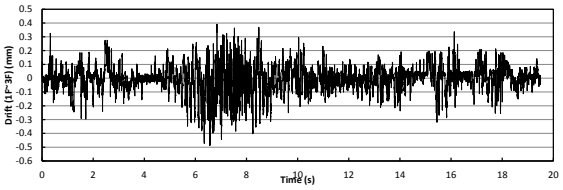

3) SFS_HUS Structure

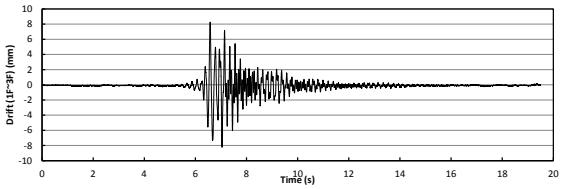

4) SFS Structure with TMD1

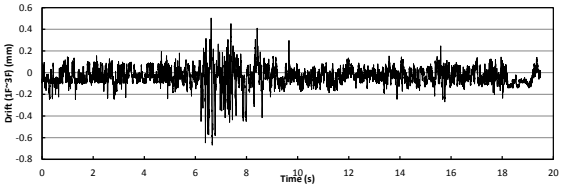

5) SFS_HUS Structure with TMD1

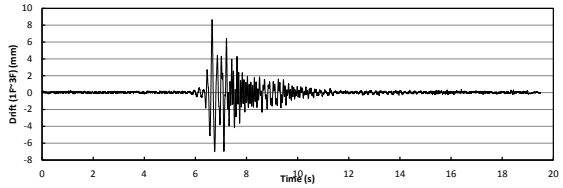

6) SFS Structure with TMD2

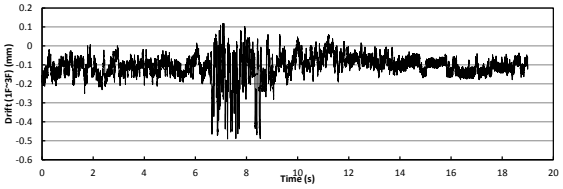

7) SFS_HUS Structure with TMD2

Figure K.18 Drift response from 1st floor to top floor under input of Kobe (0.5g)

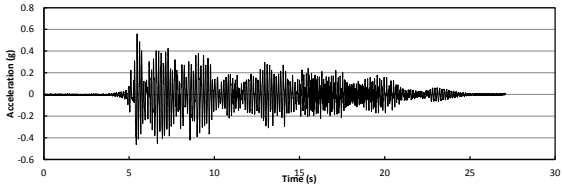

1) Original Structure

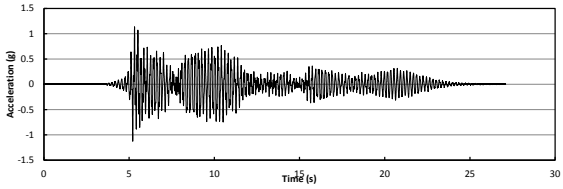

2) SFS Structure

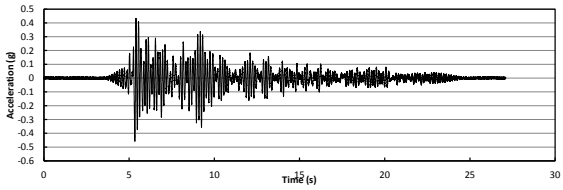

3) SFS_HUS Structure

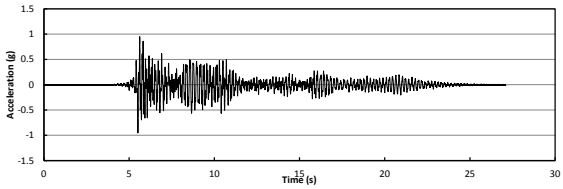

4) SFS Structure with TMD1

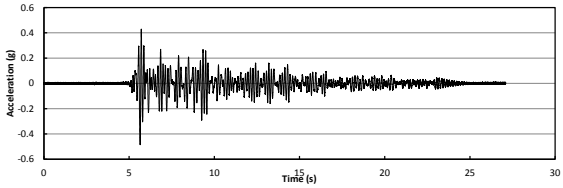

5) SFS_HUS Structure with TMD1

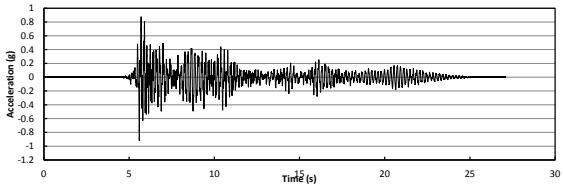

6) SFS Structure with TMD2

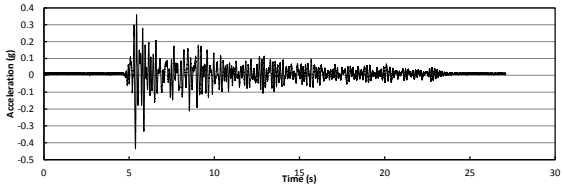

7) SFS_HUS Structure with TMD2

Figure K.19 Acceleration response of the top floor under input of Hachinohe (0.25g)

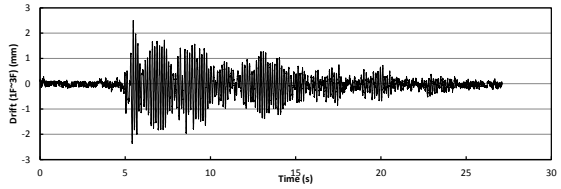

1) Original Structure

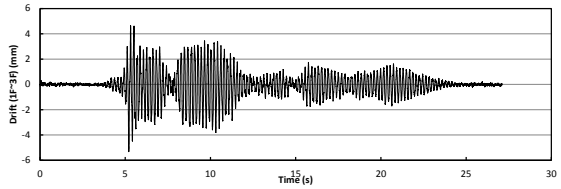

2) SFS Structure

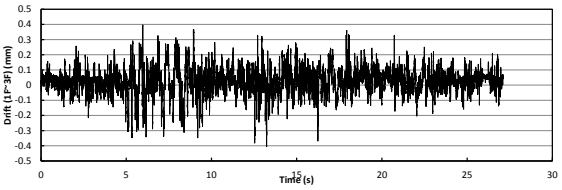

3) SFS_HUS Structure

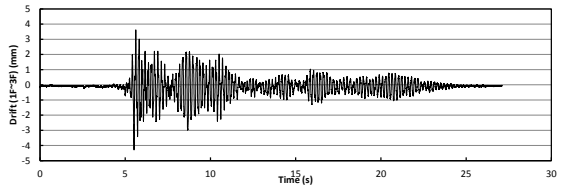

4) SFS Structure with TMD1

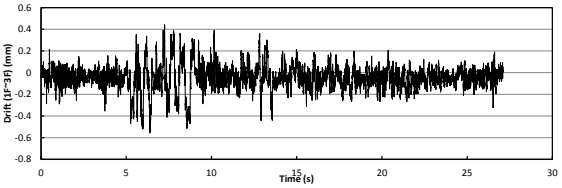

5) SFS_HUS Structure with TMD1

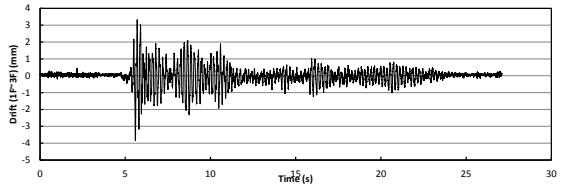

6) SFS Structure with TMD2

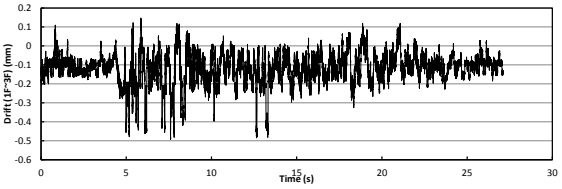

7) SFS_HUS Structure with TMD2

Figure K.20 Drift response from 1st floor to top floor under input of Hachinohe (0.25g)

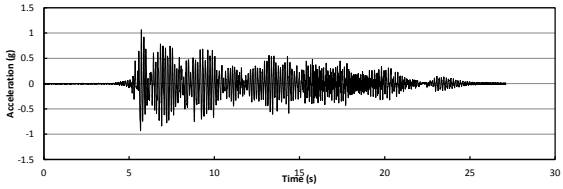

1) Original Structure

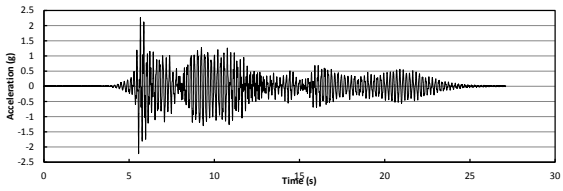

2) SFS Structure

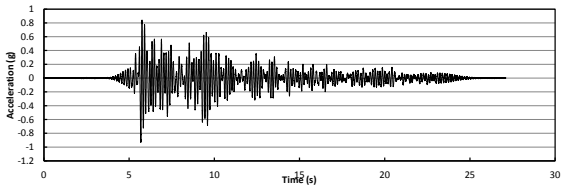

3) SFS_HUS Structure

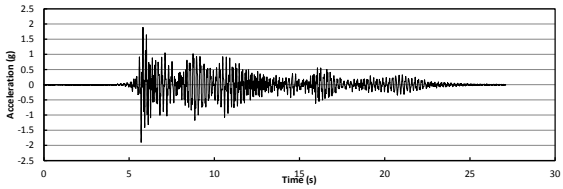

4) SFS Structure with TMD1

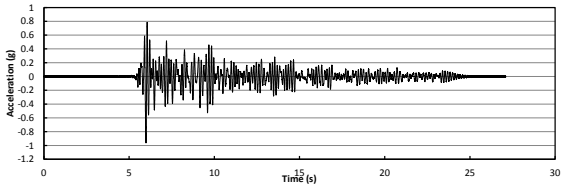

5) SFS_HUS Structure with TMD1

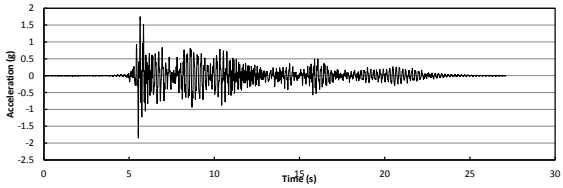

6) SFS Structure with TMD2

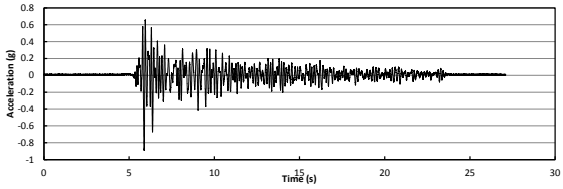

7) SFS_HUS Structure with TMD2

Figure K.21 Acceleration response of the top floor under input of Hachinohe (0.5g)

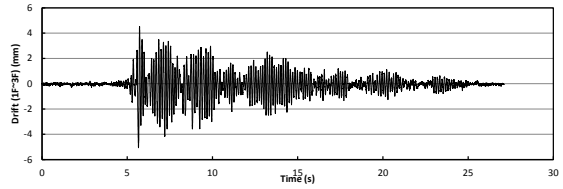

1) Original Structure

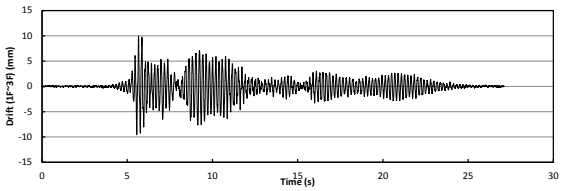

2) SFS Structure

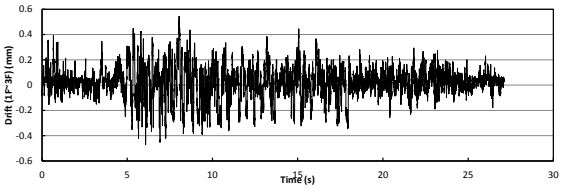

3) SFS_HUS Structure

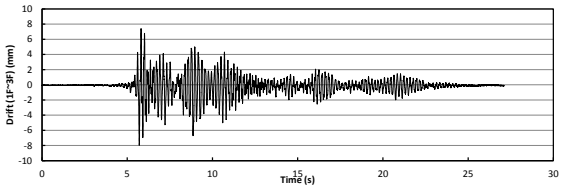

4) SFS Structure with TMD1

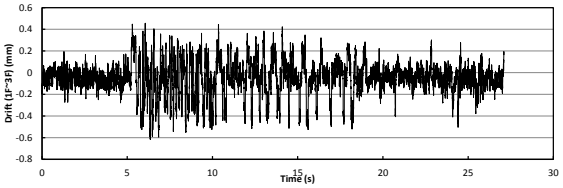

5) SFS_HUS Structure with TMD1

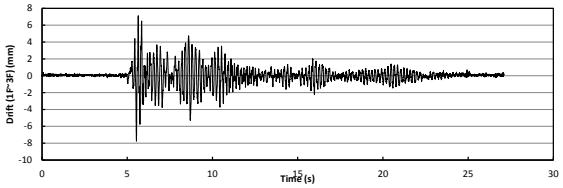

6) SFS Structure with TMD2

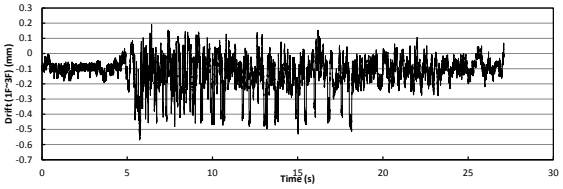

7) SFS_HUS Structure with TMD2

Figure K.22 Drift response from 1st floor to top floor under input of Hachinohe (0.5g)

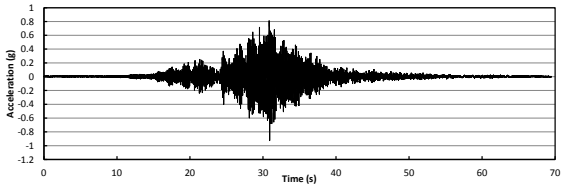

1) Original Structure

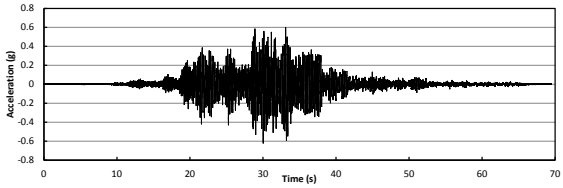

2) SFS Structure

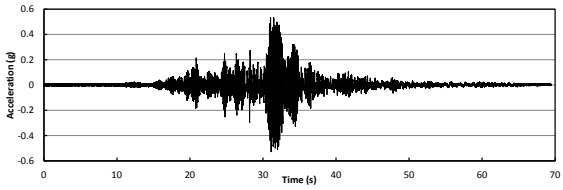

3) SFS_HUS Structure

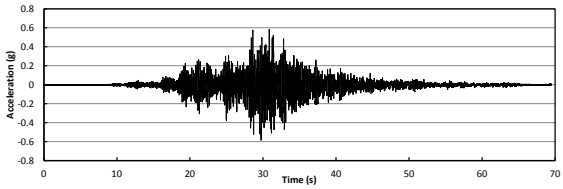

4) SFS Structure with TMD1

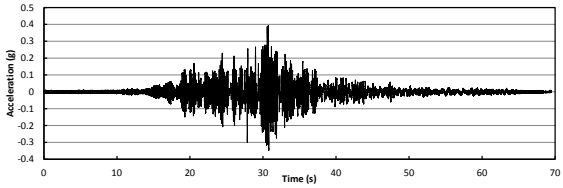

5) SFS_HUS Structure with TMD1

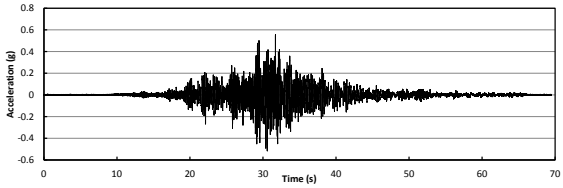

6) SFS Structure with TMD2

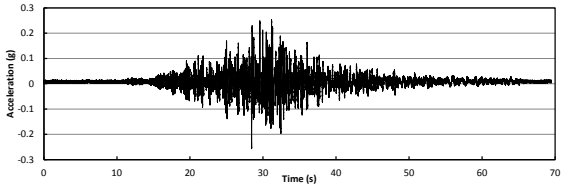

7) SFS_HUS Structure with TMD2

Figure K.23 Acceleration response of the top floor under input of Tohoku (0.25g)

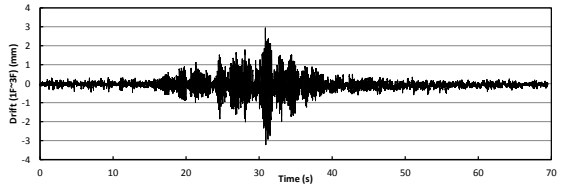

1) Original Structure

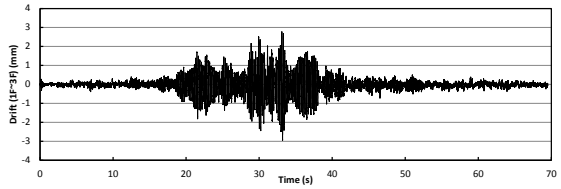

2) SFS Structure

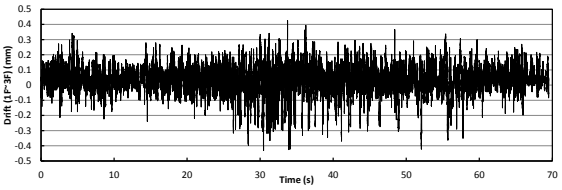

3) SFS_HUS Structure

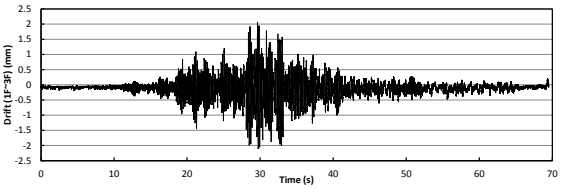

4) SFS Structure with TMD1

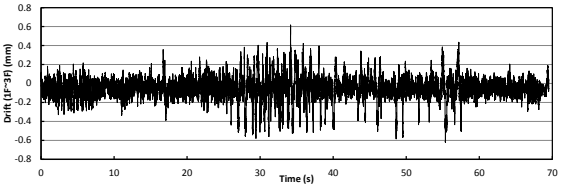

5) SFS_HUS Structure with TMD1

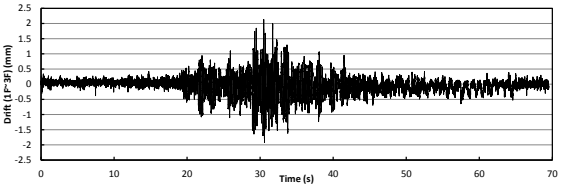

6) SFS Structure with TMD2

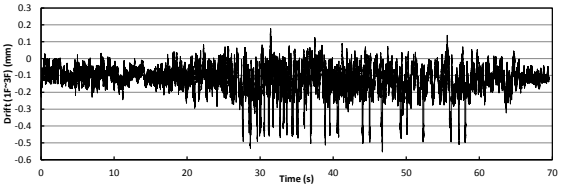

7) SFS_HUS Structure with TMD2

Figure K.24 Drift response from 1st floor to top floor under input of Tohoku (0.25g)

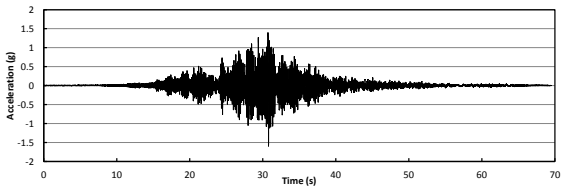

1) Original Structure

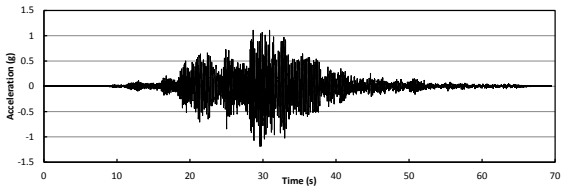

2) SFS Structure

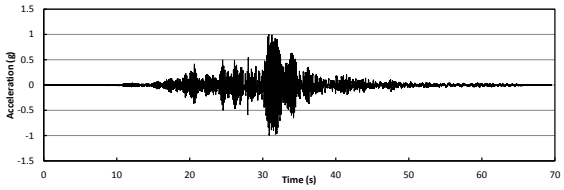

3) SFS_HUS Structure

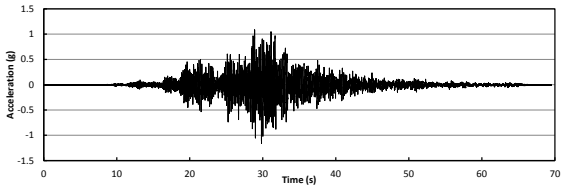

4) SFS Structure with TMD1

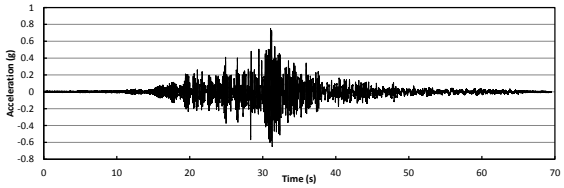

5) SFS_HUS Structure with TMD1

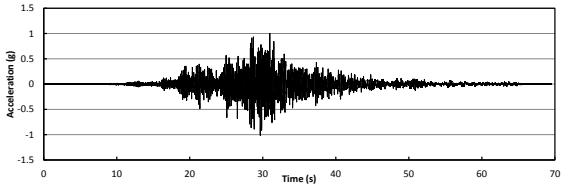

6) SFS Structure with TMD2

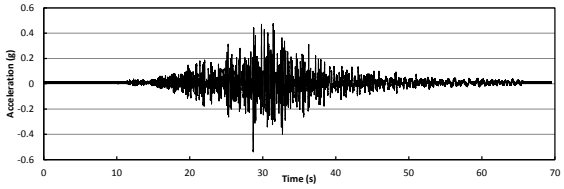

7) SFS_HUS Structure with TMD2

Figure K.25 Acceleration response of the top floor under input of Tohoku (0.5g)

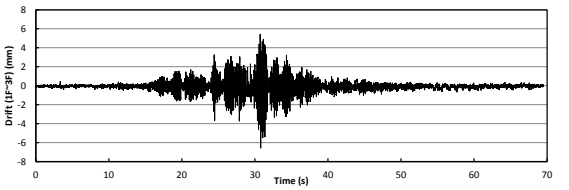

1) Original Structure

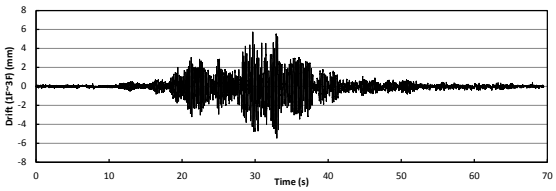

2) SFS Structure

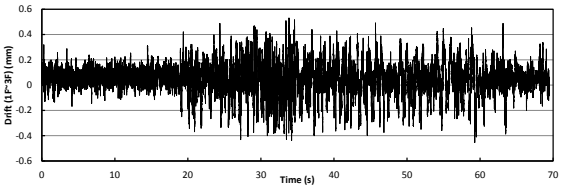

3) SFS_HUS Structure

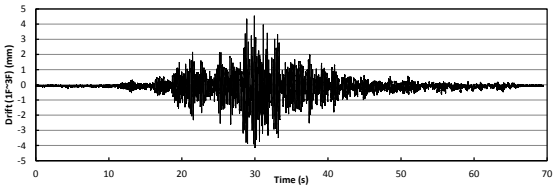

4) SFS Structure with TMD1

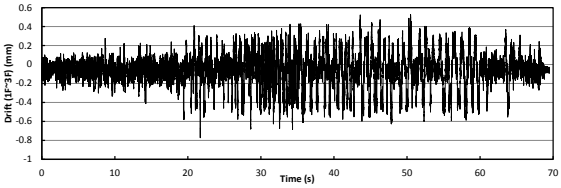

5) SFS_HUS Structure with TMD1

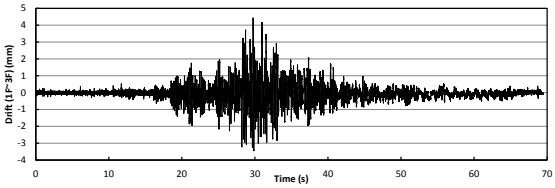

6) SFS Structure with TMD2

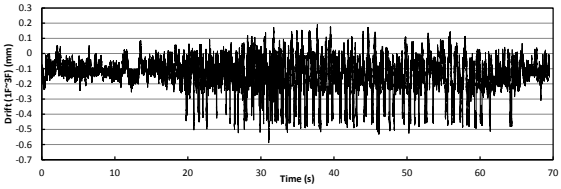

7) SFS_HUS Structure with TMD2

Figure K.26 Drift response from 1st floor to top floor under input of Tohoku (0.5g)

Acknowledgements

First and foremost, I would like to give my deepest gratitude to Prof. Ken'ichi Kawaguchi, my supervisor, for his continuous supervision during my doctoral study. He always gives me constant encouragement and constructive advices when I faced difficulties or got confused. Without his consistent and illuminating instruction, this thesis could not have reached its present form.

I would like to thank Prof. Tsuyoshi Takada, my vice supervisor, for his kindly instruction and valuable advices during our discussions semi-annually, and the reviewing of this thesis. I would like to thank the meaningful comments and the reviews by Prof. Hitoshi Shiohara, Associate Prof. Jun Iyama from the University of Tokyo and Prof. Akira Nishitani from Waseda University.

Further, I would like to thank Lecture Dr. Yshiro Ogi, Assistant Prof. Daisuke Akita for their advices during laboratory meetings. I also acknowledge Technical Staff Mr. Shunji Oya for his help and cooperation during the shaking table test. I would like to express my gratitude to Prof. Tao Wang, who is from Institute of Engineering Mechanics, China Earthquake Administration, for his frequently greetings and valuable advices.

I also would like to thank Secretaries of Kawaguchi Laboratory Ms. Yasuko Uhara, Ms. Mitsuyo Kakimoto and Ms. Yoko Kondo for their concern and help not only for the research but daily life. I would like to thank Ph.D candidates Mr. Yosuke Nakaso for his time consuming work revising my Japanese papers and some other academic materials. I would like to express my gratitude to another two Chinese Ph.D candidates Mr. Junbin Ma and Mr. Kun Chen for their help and important comments and also the happy time we spent together. I would like to thank Mr. Shunsuke Sadakane for his guidance and introduction in helping me accustom the daily life in Japan smoothly.

I also enjoyed the time spent together with the students from Kawaguchi Laboratory, Mr. Shota Nonaka, Mr. Genki Honda, Mr. Takuto Sato, and graduated Master students, Mr. Ken'ichi Inoue, Mr. Namil Seo, Mr Ryota Hosomi, Mr. Takuya Hirotama, Ms. Ikuyo Honda, Mr. Shiuhe Furuichi, Mr. Afra and Mr. Wenhan Hong, in Tokyo. Thanks so much to all the members in Kawaguchi Laboratory

At last, I would like to thank my family members. I would like to extend my deep

thanks to my parents for their persistent supporting not only materially but more spiritually. Finally, I would like to express my deepest appreciation to my beloved wife Lifang. She keeps fully supporting me, doing housework and taking good care of our lovely daughter when she is also doing Ph.D course at the same time, which gave me a strong reassurance letting me concentrate to finish this dissertation.